Integral representations for semiclassical dynamics

A dissertation by

Gabriel Mousinho Lando

Advisor:
Alfredo M. Ozorio de Almeida
Centro Brasileiro de Pesquisas Físicas

Co-advisor:
Gert-Ludwig Ingold
Universität Augsburg

Centro Brasileiro de Pesquisas Físicas
Rio de Janeiro - Rio de Janeiro, Brazil
December 2019

"INTEGRAL REPRESENTATIONS FOR SEMICLASSICAL DYNAMICS"

GABRIEL MOUSINHO LANDO

Tese de Doutorado em Física apresentada no Centro Brasileiro de Pesquisas Físicas do Ministério da Ciência Tecnologia e Inovação. Fazendo parte da banca examinadora os seguintes professores:

Alfredo Miguel Ozorio de Almeida – Presidente/Orientador/CBPF

Fernando Antonio Nazareth Nicacio - UFRJ

Caio Henrique Lewenkopf - UFF

Tobias Micklitz - UFRJ

Raúl Oscar Vallejos - CBPF

Rio de Janeiro, 17 de dezembro de 2019.

Abstract

In this work we employed Integral Representations to calculate the semiclassical evolution of coherent states using both Wigner functions and wavefunctions. In phase space, the propagator used was the Final Value Representation for Wigner evolution, which was put to the test for the first time and shown to successfully reproduce the intricate quantum evolution of the Wigner function of a coherent state in the homogeneous Kerr system – an integrable system that is exact both quantum and classical mechanically. For the semiclassical evolution of wavefunctions we used the Herman-Kluk propagator, analyzing both the Kerr system and a new softly chaotic planar map that we called the "coserf system", which is also exactly solvable in both the quantum and the classical regimes. After attesting for the accuracy of the Herman-Kluk propagator, we devised a procedure to obtain effective regular trajectories from the Baker-Hausdorff-Campbell series, capable of erasing the chaotic orbits in any planar hamiltonian map and replace them by regular ones. We then evolved a coherent state using two distinct HK propagators: One using the coserf system's true chaotic trajectories, and the other the effective regular ones. The results show that the quantum propagation of a coherent state in a chaotic system can be semiclassically reproduced without any reference to chaos, and its erasing produces a better and longer-lasting approximation.

Resumo

Neste trabalho empregamos Representações Integrais para o cálculo da evolução semiclássica de estados coerentes utilizando tanto funções de Wigner quanto funções de onda. No espaço de fase o propagador escolhido foi a Representação de Valor Final para a evolução da função de Wigner, demonstradamente capaz de reproduzir a intricada evolução quântica da função de Wigner de um estado coerente sob a ação do hamiltoniano de Kerr homogêneo – um sistema integrável que é exatamente solúvel tanto classicamente quanto quanticamente. Para a evolução semiclássica de funções de onda foi utilizado o propagador de Herman-Kluk, empregando como modelos tanto o hamiltoniano de Kerr quanto um mapa planar caótico e exatamente quantizável, apelidado de "mapa coserf". Atestada a precisão do propagador de Herman-Kluk, demos continuidade ao trabalho criando um procedimento para definir trajetórias regulares efetivas a partir de séries de Baker-Hausdorff-Campbell, capazes de substituir as órbitas caóticas de um mapa hamiltoniano no plano por órbitas regulares. Finalmente, comparamos a evolução de estados coerentes para o mapa coserf usando dois propagadores de Herman-Kluk distintos: Um baseado nas trajetórias verdadeiras do mapa (caóticas), e outra nas trajetórias efetivas (regulares). A comparação com a propagação quântica exata mostra que não só a evolução quântica de um sistema classicamente caótico pode ser reproduzida sem menção a caos, como seu abandono provê uma aproximação de qualidade superior.

Sabbe sattā bhavantu sukhitattā

Dukkham eva hi, na koci dukkhito,
kārako na, kiriyā va vijjati,
atthi nibbuti, na nibbuto pumā,
maggam atthi, gamako na vijjati.

For suffering is, but no sufferer,
not the doer, but certainly the deed is found,
peace is, but not the appeased one,
the way is, but the walker is not found.

Visuddhimagga XVI 90, Bhadantācariya Buddhaghosa

Acknowledgements

As my scientific career begins, I start to understand the role played by the advisor in a student's life. Most people I know did not have the opportunity to learn from the true exponents of a field, especially the ones like Alfredo: They are very rare, and I was very lucky. In the last couple of years, due to Alfredo's introduction, I was yet again incredibly lucky to have met and worked with Gert, who was responsible for reshaping my very immature view regarding theoretical physics throughout my PhD. I just could never have hoped to have such good advisors, who I thank dearly for all the patience and availability during these years.

I would also like to thank my mother for being my safe place in each and every way. As my world shook, she was the pillar that reminded me that all bad weather eventually gives in to clear skies. I also thank my dad, who did the best he could.

It is unclear if I'll die a physicist, but I'm absolutely sure I'll die a climber. It was through climbing that I met my best friends, that I've known the trust and love that form through the fear and the pain; that I've felt the cold, the heat, the tears that form when you're about to die – and in the end, past those deaths, the rebirths into blessed realms. I am forever grateful to my in- and outdoor climbing partners, who made life bearable:

> Adrimara Radin, Alexandre Luchesi, Alexandre Magalhães, Alexis Hernández, Amanda Danielle (mamãe), Ana Araujo, André Ilha, Antônio Paulo Faria, Arthur Estevez, Bruno Camerano, Caio Vermelho, Camron Guthrie, Carol Antonucci, Cassius Palauro, Cláudio França, Cristina Almeida, Eduardo "RC", Fernando Araujo, Fernando Mello, Guilherme Faoro, Guilherme Silva, Gustavo Sampaio, Joaquim Lyrio, Jorge Alexandre "Prussik", Julio Campanella, Paulo Mascarin, Renata "Kikinha" Bradford, Rodrigo Guizzardi, Rodrigo Leo, Sérgio Ricardo, Seblen Mantovani (papai), Suzana Hinds, Tadeu Cardoso, Wayler Muñoz, and probably others,

and to the friends and acquaintances who died in the mountains during the writing of this dissertation, especially Leandro "Mr. Bean" Iannotta... somehow, I feel as if they had died in my place.

Within the physics community, I thank Alexis Hernández (again), Breno Giacchinni, Bruno Ximenez, Daniella Leite, Felipe Monteiro, Filipe Batista, Nei Lopes, Ranieri Nery, Raúl Vallejos, Roberto Sarthour, Sebastião Dias, Tobias Micklitz, and lastly Fernando Melllo (also again, but who deserves a triple-thank-you as he is the one who introduced me to climbing).

I have somehow conserved some friendships outside the realms of climbing and physics. Thus, I also thank Iam Palatnik, Amanda Nicotina and Vinicius Harres, who remain close despite the distances. I'm also immensely thankful to Adriana Benítez and Carolina Bouchardet, who have played fundamental roles in my life.

It's also important to keep in mind that CBPF depends on a large number of undervalued and underpaid workers to keep its doors open (while it can). I would like to thank all security guards and, especially, Gil, Maria José and Sheila for keeping my office clean. Regarding Bete and Ricardo, I think it's safe to assume CBPF would simply implode if not for their lifesaving bureaucratic problem-solving. I would *not* like to thank the carpentry chief Eurídes, whom I have unsuccessfully been asking to fix my door for the past 3 years.

Contents

Chapter 0

Introduction

> It takes a lifetime to learn the shakuhachi flute: The earlier you start, the longer it takes.
>
> Zen saying

Non-relativistic classical mechanics, the first theory to emerge in full form within physics, is responsible for the description of our everyday life: "large" objects, "small" speeds, "low" energies. Evidently, for a long time no one knew these limitations existed, and classical mechanics was believed to be omnipotent until a series of experiments performed in the beginning of the XX century evinced that, in the end, nature was larger than everyday life. As a consequence, theories that deal with large speeds, small objects, and high energies had to be developed in order to explain a rapidly increasing set of mysterious experimental data.

Every physical theory directly depends on experimental parameters upon which it is tuned in order to agree with measurements. In this dissertation, the only parameter we care about is Planck's constant h, which allows us to define what we mean by microscopic and macroscopic. We do not consider relativistic effects, curved space-times, quantum field theories or dark matter. Worse yet, we deal only with the specific set of hamiltonian systems, which is well-behaved when compared to the general case. In a way, it can be said that we deal with the simplest possible systems nature has to offer, especially because we specialize even more and treat exclusively the case of a single degree of freedom. Why so much simplification? Well, it turns out nature is complicated. These simple systems are already astonishingly rich in intricate phenomena that, to this day, have not fallen prey to rigorous mathematical descriptions and remain elusive to intuition.

0.1 A brief historical account

Planck's constant h, the experimental parameter that defines the limit between classical and quantum, has dimensions of angular momentum, energy×time, or action: Large actions are classical, while small actions are quantum. Evidently, "small" and "large" must be defined with respect to h or, more often, its reduced form $\hbar = h/2\pi$. This reduced Planck's constant was shown by Bohr to quantize the angular momentum of the electron in the hydrogen atom, giving us an idea of how tiny it is: The electron orbiting the simplest atom in nature has an angular momentum of $\hbar$ in its ground state. Even slightly larger atoms than hydrogen can have electrons with angular momenta of several $\hbar$s [Mil01].

Due to the smallness[1] of $\hbar$, it didn't take long for methods relying on large actions to be developed: Not even 3 years after Schrödinger's equation was introduced, van Vleck published his famous paper introducing asymptotic solutions, later called *semiclassical approximations*, in quantum mechanics

[1] This is an often misinterpreted point: There is no "small" $\hbar$ limit – $\hbar$ is a constant! Semiclassical mechanics is not the result of a limit taken over $\hbar$, but on the actions (even though the net effect is the same). The connection between classical and quantum mechanics should be exact not when $\hbar = 0$, but when the classical action is infinite – therefore, it should never be exact. It is *not* possible to recover classical mechanics from quantum mechanics exactly, because $\hbar$ is not zero, inasmuch as the classical action is not infinite. What happens, of course, is that quantum effects become muffled as the classical action increases until the system can be considered *effectively* classical.

[Vle28]. One of the main theoretical values of these approximations is that they provide a direct link between the theory of matter waves (quantum mechanics) and the theory of phase-space waves (Hamilton-Jacobi theory). The superposition of states in quantum mechanics could then be mapped into the superposition of branches of classical generating functions, a subject most physicists in the 1920s mastered, as classical mechanics was basically the whole of physics at that time.

Since $\hbar$ is a very small quantity, semiclassical mechanics appears very promising. The simplest semiclassical rendering of quantum phenomena, namely the mapping between quantum numbers and the invariant tori in integrable systems, was considered by Einstein *before* Schrödinger's equation was even discovered, where as usual Einstein went several decades ahead of his time by identifying the problem of quantizing chaos [AD05]. Time-dependent phenomena, on the other hand, were not really explored until the second half of the XXth century, since obtaining the classical trajectories employed in semiclassical propagation can only be done by hand for very simple systems. With the advent of computers, however, what was earlier of only theoretical value started to be effectively applied for practical calculations, shedding light on two problems: First, Einstein's insight was rediscovered and the problem of the semiclassical quantization of chaotic systems could no longer be ignored; And second, that van Vleck's method is simply too cumbersome to be applied to most non-trivial systems.

Regarding the first problem above, we note that Planck's constant does not only define a size-scale, but is also responsible for filtering dynamical complexity. Since Schödinger's equation is linear, but Hamilton's equations are generally non-linear, classical dynamics happens to be much more complicated than its quantum correspondent due to the presence of chaos – Somehow, nature demands chaos to be washed out when transitioning from large to small systems. As semiclassical methods use classical trajectories to reproduce quantum behavior, it was unlikely that they could work for the case of classically chaotic evolution, since the quantum end result would somehow have to turn classical chaos into quantum integrability. The second problem has to do with looking for classical trajectories: The short-time propagator devised by van Vleck, later generalized for longer times by Gutzwiller [Lit91], is expressed as a sum over classical trajectories that fulfill specific boundary conditions. Linear systems have only a single trajectory obeying these conditions, but non-linearities introduce the need to numerically look for and select the trajectories entering the semiclassical sum – the more trajectories included, the better. As if this numerical root-search were not enough, the final propagator constantly diverges when traversing over trajectories that are near their classical turning points, requiring algorithms specifically aimed at avoiding these infinities. Despite these difficulties, the semiclassical propagator was successfully applied to the stadium billiard in the early 1990s, and it was shown that not only the semiclassical calculations were astonishingly accurate, but that the intrinsic chaotic nature of the underlying classical trajectories was no impeditive in applying the method [TH91]. Adding to that, the semiclassical solution remained accurate for at least 4 times the previously theorized threshold, employing classical trajectories densily packed in phase-space regions with areas smaller than h.

A significant revival of the field followed[2] , with chemists using semiclassical propagation to model classically chaotic reactions (*e.g.* [CB92, SH94, Gro96, SJ99, CB97]) and upper-bounds for accuracy being casually broken [STH92, TGU95, Mai00]. Many applications of semiclassical propagation were only possible due to the problems with implementing the van Vleck-Gutzwiller propagator being bypassed by employing the Integral Representations proposed in the 1970s, in which the sum over trajectories was transformed into an integral over positions and momenta [Mil70]. Adding to their implementation ease, the integral representations did not diverge at classical turning points – A huge advantage. The Herman-Kluk (HK) propagator, a particular integral representation linked to coherent-state representations [HK84], quickly became the tool of choice of most chemists. Despite the [apparent] lack of a rigorous exposition, the HK propagator has endured the test of time: More than 30 years after its introduction, it is still the dominant integral representation in both chemistry and physics. However, it is rather unfortunate that there are almost no studies comparing it with exactly solvable quantum systems, its success being based on error estimates and autocorrelations that provide little intuition due to the processes modeled being too complicated. As the HK propagator is not exactly solvable

[2]For a very good review of what was happening in the field of semiclassical methods in the 1990s, see the presentation by Voros in [Vor96]. It does not look like any of the problems enumerated by him was really solved by now.

even for the simple harmonic oscillator (while each and every other semiclassical propagator is), it does not really make comparisons easier.

Both the van Vleck-Gutzwiller and Herman-Kluk propagators result in a kernel used to evolve wavefunctions, which have no classical interpretation. Since there is genuine interest in transitioning between classical and quantum regimes, it would be nice to have a description in terms of something classical and quantum mechanics have in common: phase space. The Wigner function has become an important tool in several areas of physics (*e.g.* quantum optics and resonant-cavity quantum electrodynamics [LD97, LGWR12, DEW$^+$13, Git07]), and has the nice property of possessing a well-defined classical limit: Here, the fundamental characteristics of quantum mechanics are completely erased and we recover purely classical propagation (still as a function of $\hbar$, of course).

Although semiclassical propagators for the Wigner function have been around for decades, only recently were Integral Representations for Wigner evolution developed [dAI14]. Without any mentioning to wavefunctions, the semiclassical phase-space propagators depend only on density operators and are supposedly rigged for application to both closed and open quantum systems – at least in theory, because the latter have not yet been tested.

0.2 The problems considered

In this dissertation, we used the propagation of coherent states as a tool to understand the connections and contrasts between time-dependent phenomena in the quantum and classical worlds. By employing both integrable and chaotic systems, we performed direct tests of Integral Representations and established a previously unknown role played by regular orbits in semiclassical evolution. The work performed here can be divided into three stages:

1. Implementing the Final Value Representation (FVR) of Ozorio de Almeida *et al* [dAVZ13] for the semiclassical propagation of the Wigner function of coherent states in the homogeneous Kerr system, which is an integrable 4th order system having the remarkable property of being exactly solvable both classical and quantum mechanically;

2. Testing the Herman-Kluk propagator for the same problem as above, then expanding the tests to the coserf map, which is an exactly quantizable chaotic map that we devised in order to have a planar toy model for which trajectories did not diverge;

3. Creating and implementing an algorithm to erase the coserf system's chaotic orbits and replace them by regular ones, and then use the Herman-Kluk propagator to semiclassically evolve coherent states employing either the chaotic or regular trajectories, comparing the approximations to the exact quantum result.

The objective of item 1. is quite clear: We wanted to test a new propagator and see if it worked. The Kerr system, which we used for tests, is an especially interesting testbed due to its quantum evolution presenting an intricate structure of fractional revival patterns that should be hard to reproduce semiclassically. For 2., what we aimed for was at the same time a comparison between the HK propagator and the FVR and, later, the semiclassical description of a new softly chaotic system on the plane. For 3., it can be said that we had our eyes on a larger prey, namely that we wanted to see how fundamental was classical chaos for quantum propagation: If quantum mechanics is already linear, why not filter chaos since the beginning by substituting it by regularity?

0.3 Outline of results

A brief appetizer of what we concluded from our investigations follows.

1. The FVR was capable of semiclassically reproducing the Kerr system's quantum evolution for essentially all time values, achieving a striking accuracy even for fractional revival patterns such as the Schödinger's cat. The classical evolution for these patterns does not resemble in any way what is seen in the quantum system, and an explanation is provided in terms of interferences

of classical trajectories. Despite the FVR's success, classical vestiges can still be spotted in the semiclassical Wigner function, but these do not spoil measurable objects obtained from it.

2. The Herman-Kluk propagator was remarkably accurate and reproduced the quantum Kerr system flawlessly. Besides, since the Kerr system is closed, there is no specific need to use a phase-space method to analyze it and the HK propagator was much faster to calculate than the FVR. Due to these reasons, we applied it to the coserf system, where it proved to be incredibly accurate even when the initial coherent state was placed in a large chaotic sea.

3. The erasing of classical chaos *improved* the quality of semiclassical approximations and showed that, apparently, quantum propagation is not only blind to classical chaos, but fares better without it.

These results can be found in the following papers[3]:

1. G. M. Lando, R. O. Vallejos, G.-L. Ingold and A. M. Ozorio de Almeida, Quantum revival patterns from classical phase-space trajectories, arXiv:1809.04139, 2018;

2. G. M. Lando and A. M. Ozorio de Almeida, Semiclassical evolution in phase space for a softly chaotic system, arXiv:1907.06298, 2019;

3. G. M. Lando and A. M. Ozorio de Almeida, Quantum-chaotic evolution reproduced from effective integrable trajectories, arXiv:1909.02600, 2019.

The results from item 1. compose the whole of Chapter 6, while Chapter 7 is devoted to items 2. and 3..

0.4 How this dissertation is organized[4]

Classical mechanics is used extensively in this dissertation, and it is rather unfortunate that there are very few references on lagrangian submanifolds, generating functions and product manifolds outside mathematical literature. I then chose to dedicate Chapter 1, which is a little more mathematical than the others, to a self-contained presentation of the classical machinery needed in the following chapters. I also rely heavily on numerical methods in classical mechanics, especially on the subject of splitting symplectic integrators, to which I dedicate most of Chapter 2, where these integrators are also shown to be equivalent to the discrete mappings obtained from periodically kicked hamiltonians and associated to continuous systems build from effective hamiltonian functions.

Since "the formalism of quantum mechanics has become more familiar to physicists than the more elementary structure of classical mechanics" [dA98], standard quantum theory is enumerated very briefly in Chapter 3, as our objective is to arrive quickly at semiclassical methods and the Weyl-Wigner representations. A much more detailed discussion on quantum mechanics is provided in an appendix, such that the flow of ideas in the main body is [hopefully] not disturbed. The rest of Chapter 3 deals mostly with a topic not used anywhere to obtain our results, which is Wentzel-Kramers-Brillouin theory. I chose to write a rather comprehensive exposition on this subject because, in the end, all semiclassical propagators are obtained by the same methods employed in WKB theory. Also, since this dissertation deals with strategies that were developed to compensate the shortcomings of van Vleck-Gutzwiller's propagator, I consider it fundamental to have a clear understanding of what these shortcomings are. The Herman-Kluk propagator, which is very important for us, is introduced in this chapter using a similar strategy by which is was "derived", but my exposition is nowhere as rigorous as the one used to obtain the van Vleck-Gutzwiller propagator. The interested reader should consult [MFL06], which provides, in my opinion, the most credible derivation of the HK propagator.

I then move to phase space in Chapter 4. As the Weyl-Wigner representations are not as well-known as the position and momenum ones, a self-contained presentation on the subject is included

[3]The last two papers contain some inconsistencies with what is presented in this thesis, mostly in the definition of Ehrenfest times, and shall be amended in later versions.

[4]As it reflects my personal opinions, this section is written in first person.

here. In Chapter 5 the semiclassical ideas of Chapter 3 are expanded to deal with the Weyl-Wigner representations, and we deduce the main tool for the results provided in Chapter 6: the Final Value Representation for Wigner evolution. Chapter 6 also includes a test of the Herman-Kluk propagator for the Kerr system and the adaptation of our numerical methods to deal with general systems.

Chapter 7 contains all of the results regarding the propagation of coherent states employing chaotic trajectories, implemented to the coserf system. After attesting for the accuracy of the Herman-Kluk propagator, we move on to describe the process of chaos-erasure using the effective hamiltonians introduced in Chapter 2.

In order not to obscure the presentation, I relegated several important aspects to appendices – many of which were originally in the main text, but were judged too technical to be there. Appendix A enumerates a bit of differential geometry, used extensively in Chapter 1, and also proves some minor lemmas. Appendix B presents the proofs of several lemmas in the theory of linear symplectomorphisms that are used in later chapters, all very simple. In Appendix C I include a "personal" take on quantum mechanics, a little bit of the theory of Gel'fand triples and rigged Hilbert spaces, and the Segal-Bargmann representation – all used indirectly in the main text. Appendix D is a brief informal description of stationary-phase approximations, and Appendix E presents a detailed calculation of the pure Weyl-Wigner propagators for linear flows, using the van Vleck-Gutzwiller propagator as input. Lastly, Appendix F includes several snipets of Python code used to obtain our results, a comparison between our main programming languages (Python and Julia) and the computational times, grid sizes and details for the numerical work done in Chapters 6 and 7.

Bibliography

[AD05] Stone A. D. Einstein's unknown insight and the problem of quantizing chaos. *Physics Today*, (58):37, 2005.

[CB92] G. Campolieti and P. Brumer. Semiclassical collision theory in the initial value representation: Efficient numerics and reactive formalism. *J. Chem. Phys.*, 96:5969, 1992.

[CB97] G. Campolieti and P. Brumer. Semiclassical initial value theory for dissociation dynamics. *J. Chem. Phys.*, 107:791, 1997.

[dA98] A. M. Ozorio de Almeida. The Weyl representation in classical and quantum mechanics. *Phys. Rep.*, 295:265, 1998.

[dAI14] A. M. Ozorio de Almeida and G.-L. Ingold. Metaplectic sheets and caustic traversals in the Weyl representation. *J. Phys. A: Math. Theor.*, 47:105303, 2014.

[dAVZ13] A. M. Ozorio de Almeida, R. O. Vallejos, and E. Zambrano. Initial or final values for semiclassical evolutions in the Weyl-Wigner representation. *J. Phys. A: Math. Theor*, 46:135304, 2013.

[DEW+13] T. Douce, A. Eckstein, S. P. Walborn, A. Z. Khoury, S. Ducci, A. Keller, T. Coudreau, and P. Milman. Direct measurement of the biphoton Wigner function through two-photon interference. *Sci. Rep*, 3:3530, 2013.

[Git07] A. V. Gitin. Optical systems for measuring the Wigner function of a laser beam by the method of phase-spatial tomography. *Quantum. Electron.*, 37:85, 2007.

[Gro96] F. Grossman. Time-dependent semiclassical calculation of resonance lifetimes. *Chem. Phys. Lett.*, 262:470, 1996.

[HK84] M. F. Herman and E. Kluk. A semiclassical justification for the use of non-spreading wavepackets in dynamics calculations. *Chem. Phys.*, 91:27, 1984.

[LD97] L. G. Lutterbach and L. Davidovich. Method for direct measurement of the Wigner function in cavity QED and ion traps. *Phys. Rev. Lett.*, 78:2547, 1997.

[LGWR12] G. B. Lemos, R. M. Gomes, S. P. Walborn, and P. H. S. Ribeiro. Experimental observation of quantum chaos in a beam of light. *Nat. Commun.*, 3:1211, 2012.

[Lit91] R. G. Littlejohn. The van Vleck formula, Maslov theory, and phase space geometry. *J. Stat. Phys.*, 68:7, 1991.

[Mai00] N. T. Maitra. Semiclassical maps: A study of classically forbidden transitions, sub-h structure, and dynamical localization. *J. Chem. Phys.*, 112:531, 2000.

[MFL06] E. Martín-Fierro and J. M. G. Llorente. Derivation of semiclassical asymptotic initial value representations of the quantum propagator. *Chem. Phys.*, (322):13, 2006.

[Mil70] W. H. Miller. Semiclassical theory of atom-diatom collisions: Path integrals and the classical s matrix. *J. Chem. Phys.*, 1970:1949, 1970.

[Mil01] W. H. Miller. The semiclassical initial value representation: A potentially practical way for adding quantum effects to classical molecular dynamics simulations. *J. Phys. Chem. A*, (105):2942, 2001.

[SH94] M. A. Sepúlveda and E. J. Heller. Semiclassical analysis of hierarchical spectra. *J. Chem. Phys.*, 101:8016, 1994.

[SJ99] D. V. Shalashilin and B. Jackson. Initial value representation for the classical propagator and S-matrix with the help of coherent states. *Chem. Phys. Lett.*, 291:143, 1999.

[STH92] M. A. Sepúlveda, S. Tomsovic, and E. J. Heller. Semiclassical propagation: How long can it last? *Phys. Rev. Lett.*, 69:402, 1992.

[TGU95] S. Tomsovic, M. Grinberg, and D. Ullmo. Semiclassical trace formulas of near-integrable systems: Resonances. *Phys. Rev. Lett.*, 75:4346, 1995.

[TH91] S. Tomsovic and E. J. Heller. Semiclassical dynamics of chaotic motion: Unexpected long-time accuracy. *Phys. Rev. Lett*, 67:664, 1991.

[Vle28] J. H. Van Vleck. The correspondence principle in the statistical interpretation of quantum mechanics. *Proc. Natl. Acad. Sci. USA*, 14:178, 1928.

[Vor96] A. Voros. Aspects of semiclassical theory in the presence of classical chaos. *Prog. Theo. Phys. Supp.*, 116:116, 1996.

Chapter 1

Symplectic ingredients of classical mechanics

> For me, understanding is not so much a demand for mathematical rigor; rather, it is an anxiety to grasp intuitive plausibility. Then again, the very effort to achieve rigor has been for me a terrific boost to intuition. Rigor cleans the window through which intuition shines.
>
> Ellis D. Cooper in *Mathematical Mechanics*

Analytical mechanics employs generalized coordinates to model physical systems. The term *generalized* refers to the fact that the equations of motion are no longer obtained from vector sums, as in Newton's second law, and variables can be endowed with a more general structure. For example: One cannot sum two points on a circle to obtain another point on the circle, because the circle is not a vector space. We can, however, use points on a circle as generalized positions and associate them with velocities/momenta. The equations of motion are then obtained exclusively from differentiation, so the only requirement placed on generalized positions is that they must be represented by differentiable functions. Since each generalized position represents a degree of freedom and is matched with a momentum or velocity, n degrees of freedom require the use of $2n$-dimensional spaces. These spaces must be composed of a base space, its elements being the positions themselves, and at every point we must have a vector space on which momenta/velocities can be defined. This structure naturally emerges if we consider the space of positions to be a differentiable manifold. Then, velocities and momenta are elements of the tangent and cotangent spaces at a point, respectively, with corresponding bundles. The study of even-dimensional spaces obtained in this way is encompassed in the field of *symplectic geometry*, and it is impossible to attain a clear geometrical picture of classical mechanics without it. We here give a brief and self-contained presentation of the concepts required for further chapters, largely based on [dS11, AMRC80, Spi10], with particular emphasis in generating functions and lagrangian submanifolds.

1.1 The symplectic category

An isomorphism is the morphism of the category of vector spaces; a diffeomorphism is the morphism of the category of differential manifolds; a homomorphism is the morphism of the category of groups. Morphisms are important because they define what *equivalence* means within a set of objects, *e.g* all vector spaces of the same dimension are linearly equivalent because they are isomorphic, meaning that there is no test capable of discriminating them – as far as linear algebra goes, they are the same. We now define the category of symplectic manifolds and its morphisms.

1.1.1 Manifolds and bundles

Let X be a smooth, n-dimensional manifold[1]. Let us first make sense of its associate tangent and cotangent spaces. Start with the coordinate chart $(U, \{q_1, \ldots, q_n\})$ of $U \subset X$, with homeomorphisms $q_i : U \longrightarrow \mathbb{R}^n$. Then, at any $a \in U$, the manifold structure of X allows us to identify the following canonical homeomorphisms for U and its tangent and cotangent charts:

$$\begin{aligned}(U, \{q_1, \ldots, q_n\}) &\sim (\mathbb{R}^n, \{e_1, \ldots, e_n\}) \\ \left(T_aU, \left\{ \frac{\partial}{\partial q_1}\Big|_a, \ldots, \frac{\partial}{\partial q_n}\Big|_a \right\}\right) &\sim (\mathbb{R}^n, \{e_1, \ldots, e_n\}) \\ (T^*_aU, \{(dq_1)_a, \ldots, (dq_n)_a\}) &\sim (\mathbb{R}^n, \{e_1, \ldots, e_n\}) \,,\end{aligned}$$

such that any point $x \in U$ is mapped to $\{q_1, \ldots, q_n\}(x) \stackrel{\text{def}}{=} \{x_1, \ldots, x_n\}$, and any vector $v \in T_aU$ and 1-form $\alpha \in T^*_aU$ have coordinates $v = \{v_1, \ldots, v_n\}$ and $\alpha = \{\alpha_1, \ldots \alpha_n\}$ in their respective canonical bases, *i.e.*

$$v = \sum_{i=1}^{n} v_i \frac{\partial}{\partial q_i}\Big|_a \,, \qquad \alpha = \sum_{i=1}^{n} \alpha_i (dq_i)_a \,.$$

This is all we need about X, *i.e.* a smooth manifold is by definition locally homeomorhic to $\mathbb{R}^n$, and so are its tangent and cotangent spaces. Now, since $a = \{a_1, \ldots, a_n\}$ in the chart $\{q_1, \ldots q_n\}$, we have the following disjoint union of tangent and cotangent spaces:

$$\begin{aligned}TU &= \bigsqcup_{a \in U} T_aU = \{a, v\} = \{a_1, \ldots, a_n, v_1 \ldots, v_n\} \sim (\mathbb{R}^{2n}, e_1, \ldots, e_{2n}) \\ T^*U &= \bigsqcup_{a \in U} T^*_aU = \{a, \alpha\} = \{a_1, \ldots, a_n, \alpha_1 \ldots, \alpha_n\} \sim (\mathbb{R}^{2n}, e_1, \ldots, e_{2n}) \,,\end{aligned}$$

which are the tangent and cotangent *bundles* of X in the neighbourhood U, respectively. In the above we have also defined the map $\{q_1, \ldots, q_n, p_1, \ldots, p_n\} \longmapsto \{q, p\}$ which condenses coordinates in a chart.

1.1.2 Canonical and tautological forms

Let $\omega \in \Omega^2(X)$ be a de Rham 2-form on X, *i.e* for each $a \in X$ the map $\omega_a : T_aX \times T_aX \to \mathbb{R}$ is skew-symmetric bilinear and varies smoothly with a. The 2-form ω is said to be *symplectic* if it is non-degenerate and closed, *i.e.* if $d\omega = 0$ and for all $a \in X$ we have $\omega_a(u, v) = 0$, $\forall v \in T_aX \Longrightarrow u = 0$. As we saw earlier, T^*U is itself a $2n$-dimensional manifold. For $T^*U = \mathbb{R}^{2n}$, it is easy to show that the 2-form $\omega = dq \wedge dp = dq_1 \wedge dp_1 + \cdots + dq_n \wedge dp_n$ is a symplectic form over $\mathbb{R}^{2n}$ [dS11], and that $\omega = -d\alpha$, where $\alpha = p \cdot dq = p_1\, dq_1 + \ldots p_n\, dq_n$.

Definition 1.1.1. We call ω and α the **canonical** and **tautological forms**, respectively.

1.1.3 Symplectic manifolds and morphisms

We begin tying in cotangent bundles and canonical forms through

Definition 1.1.2. The pair (M, ω) of a cotangent bundle and a canonical form is a **symplectic manifold**.

Symplectic manifolds exist that are not cotangent bundles, but here will be mentioned only in passing. Unless one is interested in the *global* structure of a particular manifold it is not necessary to delve into pathological cases since, as in the study of vector spaces, it is often easier to work with a simpler space that is equivalent to the one we are interested in. For this, we must define what *equivalence* in the category of symplectic manifolds means. From linear algebra it is obvious that all symplectic vector spaces of the same dimension are locally isomorphic, *i.e.* indistinguishable as vector spaces, but are they also indistinguishable in some symplectic sense? Just as in riemannian geometry, which uses the metric, symplectic equivalence is defined *via* the canonical form.

[1]Differential manifolds will model our space of generalized positions. We include our conventions regarding this category in Appendix A.

Definition 1.1.3. We say $(M_1, \omega_1) \sim (M_2, \omega_2)$ iff there exists a diffeomorphism $f : M_1 \longrightarrow M_2$ that pullsback canonical forms, namely $f^*\omega_2 = \omega_1$. We then say M_1 and M_2 are **symplectomorphic** and f is a **symplectomorphism**[2].

We expect symplectic equivalence to be stronger than linear equivalence, since it involves the canonical form. Amazingly, symplectic equivalence is locally just as strong as linear equivalence, such that all symplectic manifolds of the same dimension are locally symplectomorphic. This is an important statement in the field and is given by

Theorem 1.1.4. (Darboux) Let (M, ω) be a $2n$-dimensional symplectic manifold and $U \subset M$. Let $\omega = dQ \wedge dP$ in a cotangent chart $(T^*U, \{Q, P\})$, where we use the condensed coordinates $\{Q, P\} = \{Q_1, \ldots, Q_n, P_1, \ldots, P_n\}$. Then there exists a symplectomorphism $f : M \longrightarrow \mathbb{R}^{2n}$ such that $f^*(dq \wedge dp) = dQ \wedge dP$, where $dq \wedge dp$ is the canonical form on $\mathbb{R}^{2n}$.

Proof. Can be found in [dS11] or [AMRC80] (we recommend the former). The proof is too technical to be included here. □

The importance of the above theorem cannot be overstated – It shows that any conclusion obtained from the simplest possible symplectic manifold, namely $(\mathbb{R}^{2n}, dq \wedge dp)$, is locally valid for all symplectic manifolds with the same dimension: Conclusions using these manifolds are, therefore, quite general. There are no fundamental symplectic invariants as in *e.g.* riemannian geometry: The symplectic form is much more malleable than the riemannian metric, all due to its skew-symmetry instead of the metric's positive-definiteness [Spi10].

1.2 Vector fields and flows

We now start to endow symplectic manifolds with additional structure. Of fundamental importance is the action of tangent bundle elements, *i.e.* vector fields, on the base manifold. Due to the non-degeneracy of the canonical form, there is a single primitive for each vector field contraction with ω – we will see this is precisely the statement of Hamilton's equations[3].

1.2.1 Hamiltonian fields and Hamilton's equations

Let (M, ω) be a $2n$-dimensional symplectic manifold. As seen in the previous section, $\omega = -d\alpha$ and ω is non-degenerate, so the following contraction is unique:

$$\omega = -d\alpha \quad \Longrightarrow \quad \imath_X\omega = \imath_X(-d\alpha) \quad \Longrightarrow \quad \imath_X\omega = d[-\alpha(X)]\,,$$

where the contraction is defined by $\imath_X\omega \stackrel{\text{def}}{=} \omega(X, \cdot)$. By representing the evaluation $d[-\alpha(X)]$ by dH and writing $X = X_H$, we have shown that there is a unique vector field on M such that

$$\imath_{X_H}\omega = dH\,, \tag{1.1}$$

the equation above being a coordinate-free version of the usual hamiltonian equations of motion.

Definition 1.2.1. The vector field X_H associated to H by (1.1) is the [hamiltonian] **vector field** generated by H. Its unique integral curves $\rho_t : \mathbb{R} \times M \longrightarrow M$ are its [hamiltonian] **flow**. The set $\{y : y = \rho_t(x)\,, \forall t \in \mathbb{R}\}$ is the **orbit** of x.

We shall make extended use of Hamilton's equations, but almost never in such coordinate-free form as (1.1). To show that the fields defined by (1.1) are equivalent to the ones obtained from Hamilton's

[2]These are known in physics as *canonical transformations*, and sometimes the use of the word "symplectomorphism" is restricted to canonical transformations that are linear. We here follow the conventions in mathematics and use the "symplectomorphism" term generally, prepending "linear" when this is the case. Regarding f^*, it is the pullback induced by f, acting on k-forms as $f^*d\alpha = d(\alpha \circ f)$ (see Appendix A).

[3]We assume all hamiltonian functions and vector fields to be autonomous, *i.e* time-independent, unless stated.

equations, we express (1.1) using a cotangent chart on T^*_aM and its tangent counterpart, centered at $a \in M$, with which we locally write $X_H = (X_H)_q\partial_q + (X_H)_p\partial_p$ (a is omitted in the basis). Then[4],

$$\begin{aligned}
&\iota_{X_H}\omega = dH \\
\iff &(dq \wedge dp)\left[(X_H)_q \cdot \frac{\partial}{\partial q} + (X_H)_p \cdot \frac{\partial}{\partial p}\right] = \left(\frac{\partial H(q,p)}{\partial q}\right)\cdot dq + \left(\frac{\partial H(q,p)}{\partial p}\right)\cdot dp \\
\iff &(X_H)_q \cdot dp - (X_H)_p \cdot dq = \left(\frac{\partial H(q,p)}{\partial q}\right)\cdot dq + \left(\frac{\partial H(q,p)}{\partial p}\right)\cdot dp \\
\implies &X_H = \frac{\partial H}{\partial p}\cdot\frac{\partial}{\partial q} - \frac{\partial H}{\partial q}\cdot\frac{\partial}{\partial p}\,.
\end{aligned} \tag{1.2}$$

It might not be that obvious that (1.1), just by fixing the form of the vector field X_H as above, establishes that X_H satisfies the usual form of Hamilton's equations found in physics. The identification is, however, rather trivial: Let ρ_t be the flow of X_H, satisfying

$$\begin{cases} \dfrac{d\rho_t}{dt} = X_H \circ \rho_t \\ \rho_0 = I \end{cases} \qquad \implies \qquad \rho_t(q,p) = \exp\left[tX_H(q,p)\right](q,p)\,,$$

Notation is often abused and flow $\rho_t(q,p)$ written as (q_t, p_t), which is rather harmless and we shall frequently do. Using the fixed form for X_H in (1.2), we have

$$\begin{aligned}
\frac{d\rho_t(q,p)}{dt} = X_H\left[\rho_t(q,p)\right] \quad &\iff \quad \frac{\partial\rho_t}{\partial q}\cdot\frac{dq}{dt} + \frac{\partial\rho_t}{\partial p}\cdot\frac{dp}{dt} = \frac{\partial H}{\partial p}\cdot\frac{\partial\rho_t}{\partial q} - \frac{\partial H}{\partial q}\cdot\frac{\partial\rho_t}{\partial p} \\
&\iff \quad \frac{\partial\rho_t}{\partial q}\cdot\left(\frac{dq}{dt} - \frac{\partial H}{\partial p}\right) + \frac{\partial\rho_t}{\partial p}\cdot\left(\frac{dp}{dt} + \frac{\partial H}{\partial q}\right) = 0
\end{aligned}$$

implying Hamilton's equations

$$\frac{dq}{dt} = \frac{\partial H}{\partial p}\,, \qquad \frac{dp}{dt} = -\frac{\partial H}{\partial q} \quad \iff \quad \frac{dx}{dt} = \mathcal{J}\left(\frac{dH}{dx}\right)\,, \tag{1.3}$$

where in the equivalence we have further compacted the equations of motion writing an arbitrary point in M as $x = (q,p) = (q_1,\ldots,q_n,p_1,\ldots,p_n)$, the derivative being shorthand for the gradient with respect to each of its coordinates,

$$\frac{d}{dx} = \left(\frac{\partial}{\partial q}, \frac{\partial}{\partial p}\right) = \left(\frac{\partial}{\partial q_1},\ldots,\frac{\partial}{\partial q_n},\frac{\partial}{\partial p_1},\ldots,\frac{\partial}{\partial p_n}\right)$$

and

$$\mathcal{J} = \begin{pmatrix} \mathbf{0}_{n\times n} & \mathbf{1}_{n\times n} \\ -\mathbf{1}_{n\times n} & \mathbf{0}_{n\times n} \end{pmatrix}\,, \quad \text{or, in components,} \quad \mathcal{J}_{ij} = \begin{cases} 0\ , i \neq j \pm n \\ 1\ , i = j - n \\ -1\,, i = j + n \end{cases}\,. \tag{1.4}$$

Definition 1.2.2. The matrix $\mathcal{J}$ above is the **canonical matrix**.

The canonical matrix emerges when $dq \wedge dp$ acts on arbitrary elements of $T_aM \sim \mathbb{R}^{2n}$:

$$\begin{aligned}
\omega_a(u,v) &= (dq\wedge dp)(u,v) \\
&= (dq\wedge dp)\left(u_q\partial_q + u_p\partial_p, v_q\partial_q + v_p\partial_p\right) \\
&= dq\left(u_q\partial_q + u_p\partial_p\right)\, dp\left(v_q\partial_q + v_p\partial_p\right) - dq\left(v_q\partial_q + v_p\partial_p\right)\, dp\left(u_q\partial_q + u_p\partial_p\right) \\
&= u_qv_p - u_pv_q \\
\implies \quad \omega_a(u,v) &= u\cdot\mathcal{J}v\,.
\end{aligned}$$

[4]We endow manifolds with a local metric "$\cdot$" that, being isomorphic to an euclean space, all charts can be associated with. For its construction, see Corollary 1.2.3.

Corollary 1.2.3. Every symplectic manifold admits a locally euclidean metric: For any x, $y \in \mathbb{R}^{2n}$ define $\omega(\mathcal{J}x, y) = (\mathcal{J}x) \cdot \mathcal{J}y = x \cdot (\mathcal{J}^T \mathcal{J} y) \stackrel{\text{def}}{=} x \cdot y$. This is the implicit metric every time we write a dot product.

Using the canonical matrix, we can characterize the very important subgroup of linear symplectomorphisms, for which the transformation is given by a linear operator (we extend this discussion in Appendix B).

Proposition 1.2.4. Let $\mathcal{M} : \mathbb{R}^{2n} \longmapsto \mathbb{R}^{2n}$ be a linear transformation. It is a symplectomorphism iff $\mathcal{M}^T \mathcal{J} \mathcal{M} = \mathcal{J}$.

Proof. Since $f^*\omega = \omega$, we have

$$\mathcal{M}^*\omega(x,y) = \omega(\mathcal{M}x, \mathcal{M}y) = \omega(x,y) \quad \Longleftrightarrow \quad x \cdot \left(\mathcal{M}^T \mathcal{J} \mathcal{M}\right) y = x\mathcal{J}y \quad \Longrightarrow \quad \mathcal{M}^T \mathcal{J} \mathcal{M} = \mathcal{J}\,.$$

□

Corollary 1.2.5. If $\mathcal{M}$ is a linear symplectomorphism, $\det \mathcal{M} = \pm 1$.

Definition 1.2.6. If a linear symplectomorphism has determinant $+1$, we say its matrix is **symplectic**. The set of all symplectic matrices is the **symplectic group** $\mathrm{Sp}(n)$.

1.2.2 Brackets

The evaluation of the canonical form on the hamiltonian fields generated by two functions, say f and g, is

$$\omega_a(X_f, X_g) = (dq \wedge dp)\left(\frac{\partial f}{\partial p}\cdot\frac{\partial}{\partial q} - \frac{\partial f}{\partial q}\cdot\frac{\partial}{\partial p}, \frac{\partial g}{\partial p}\cdot\frac{\partial}{\partial q} - \frac{\partial g}{\partial q}\cdot\frac{\partial}{\partial p}\right) = \frac{\partial f}{\partial q}\cdot\frac{\partial g}{\partial p} - \frac{\partial f}{\partial p}\cdot\frac{\partial g}{\partial q} = \frac{df}{dx}\cdot\mathcal{J}\left(\frac{dg}{dx}\right)$$

$$\Longrightarrow \quad \omega_a(X_f, X_g) = \{f, g\} = [X_f, X_g]\,, \tag{1.5}$$

where (1.5) defines two intrinsically connected backets that explore the Lie-algebraic structure of the set of vector fields over a manifold using either their hamiltonians or the fields themselves.

Definition 1.2.7. The brackets of functions $\{f, g\}$ and vector fields $[X_f, X_g]$ are the **Poisson bracket** and **commutator**, respectively.

The classical evolution in (1.3) can then be written in terms of the Poisson bracket by identifying $f \equiv x$,

$$\{x, H\} = \mathcal{J}\left(\frac{dH}{dx}\right) = \dot{x}\,,$$

while for an arbitrary function $f_t(q,p)$ we have

$$\begin{aligned}\frac{df_t(q,p)}{dt} &= \frac{\partial f_t(q,p)}{\partial t} + \left(\frac{\partial f_t(q,p)}{\partial q}\right)\cdot\frac{dq}{dt} + \left(\frac{\partial f_t(q,p)}{\partial p}\right)\cdot\frac{dp}{dt} \\ &= \frac{\partial f_t(q,p)}{\partial t} + \left(\frac{\partial f_t(q,p)}{\partial q}\right)\cdot\frac{\partial H(q,p)}{\partial p} - \left(\frac{\partial f_t(q,p)}{\partial p}\right)\cdot\frac{\partial H(q,p)}{\partial q} \\ &= \frac{\partial f_t(q,p)}{\partial t} + \{f, H\}\,;\end{aligned}$$

if f is autonomous, we get

$$\frac{\partial f}{\partial t} = -\{f, H\}\,. \tag{1.6}$$

Definition 1.2.8. The equation above is the **Liouville equation**.

We can also express the action of X_H on a function f in terms of Poisson brackets:

$$X_H(f) = \left(\frac{\partial H}{\partial p}\frac{\partial}{\partial q} - \frac{\partial H}{\partial q}\frac{\partial}{\partial p}\right)(f) = \{f, H\}\,, \tag{1.7}$$

and using X_H the flow can be generally expressed as the Taylor series:

$$\rho_t(x) = \exp\left(tX_H\right)(x) = \left(I + tX_H + \frac{t^2}{2}X_H^2 + \dots\right)(x) = x + t\{x, H\} + \frac{t^2}{2}\{\{x, H\}, H\} + \dots \tag{1.8}$$

Notice the equation above is non-linear in x.

Example 1.2.9. (The free particle) For the hamiltonian and vector field

$$H(p) = \frac{p^2}{2} \quad \Longrightarrow \quad X_H = \frac{\partial H}{\partial p}\frac{\partial}{\partial q} = p\frac{\partial}{\partial q}\,,$$

we happen to have idempotency:

$$\left(I + tX_H + \frac{t^2}{2}X_H^2 + \dots\right) = I + p\frac{\partial}{\partial q} + \frac{t^2}{2}\overbrace{\left[p\frac{\partial}{\partial q}\left(p\frac{\partial}{\partial q}\right)\right]}^{=0} + 0 + 0 + \dots = I + p\frac{\partial}{\partial q}\,,$$

so that

$$\rho_t(x)\big|_{x_0} = \left(I + tp\frac{\partial}{\partial q}\right)(q, p)\big|_{x_0} = (q_0, p_0) + t\,(p_0, 0)\ . \qquad \divideontimes$$

Example 1.2.10. (The SHO) We now have

$$H(q, p) = \frac{p^2}{2} + \frac{q^2}{2} \quad \Longrightarrow \quad X_H = \frac{\partial H}{\partial p}\frac{\partial}{\partial q} - \frac{\partial H}{\partial q}\frac{\partial}{\partial p} = p\frac{\partial}{\partial q} - q\frac{\partial}{\partial p}\,.$$

Therefore,

$$\begin{aligned}
\rho_t(x) &= \exp\left(tX_H\right)x = \exp\left[t\left(p\frac{\partial}{\partial q} - q\frac{\partial}{\partial p}\right)\right](q, p) \\
&= \left(q + tp - \frac{t^2 q}{2!} - \frac{t^3 p}{3!} + \frac{t^4 q}{4!} + \dots,\ p - tq - \frac{t^2 p}{2!} + \frac{t^3 q}{3!} + \frac{t^4 p}{4!}\dots\right) \\
&= \left(\left(1 - \frac{t^2}{2!} + \frac{t^4}{4!} - \dots\right)q + \left(t - \frac{t^3}{3!} + \dots\right)p, \left(1 - \frac{t^2}{2!} + \frac{t^4}{4!} - \dots\right)p - \left(t - \frac{t^3}{3!} + \dots\right)q\right)
\end{aligned}$$

$$\Longrightarrow\ \rho_t(x)\big|_{x_0} = (q_0\cos t + p_0\sin t, p_0\cos t - q_0\sin t)\ . \qquad \divideontimes$$

Example 1.2.11. (The inverted SHO) Here we have a change of sign:

$$H(q, p) = \frac{p^2}{2} - \frac{q^2}{2} \quad \Longrightarrow \quad X_H = \frac{\partial H}{\partial p}\frac{\partial}{\partial q} - \frac{\partial H}{\partial q}\frac{\partial}{\partial p} = p\frac{\partial}{\partial q} + q\frac{\partial}{\partial p}\,,$$

So

$$\begin{aligned}
\rho_t(x) &= \exp\left(tX_H\right)x = \exp\left[t\left(p\frac{\partial}{\partial q} + q\frac{\partial}{\partial p}\right)\right](q, p) \\
&= \left(q + tp + \frac{t^2 q}{2!} + \frac{t^3 p}{3!} + \frac{t^4 q}{4!} + \dots,\ p + tq + \frac{t^2 p}{2!} + \frac{t^3 q}{3!} + \frac{t^4 p}{4!}\dots\right) \\
&= \left(\left(1 + \frac{t^2}{2!} + \frac{t^4}{4!} + \dots\right)q + \left(t + \frac{t^3}{3!} + \dots\right)p, \left(1 + \frac{t^2}{2!} + \frac{t^4}{4!} + \dots\right)p + \left(t + \frac{t^3}{3!} + \dots\right)q\right)
\end{aligned}$$

$$\Longrightarrow\ \rho_t(x)\big|_{x_0} = (q_0\cosh t + p_0\sinh t, p_0\cosh t + q_0\sinh t)\ . \qquad \divideontimes$$

1.3 Submanifolds and product manifolds

In this section we show how classical mechanics naturally asks for a description in terms of product manifolds in order to accommodate the time-dependence in the flow and characterize symplectomorphisms *via* generating functions. A consequence is the emergence of lagrangian submanifolds.

1.3.1 Movement as a symplectomorphism

A very important symplectomorphism is recognized in movement itself.

Proposition 1.3.1. Any hamiltonian flow ρ_t is a 1-parameter family of symplectomorphisms.

Proof. From the Lemmas in Section A.2 and the fact that $\rho_0 = I$,

$$\frac{d}{dt}\rho_t^*\omega = \rho_t^*\mathcal{L}_{X_H}\omega = \rho_t^*\left(d\imath_{X_H}\omega + \imath_{X_H}d\omega\right) = \rho_t^*\left(ddH - \imath_{X_H}dd\alpha\right) = 0 \quad \Longrightarrow \quad \rho_t^*\omega = \omega\,, \quad \forall t\,,$$

where in the first equality we used Lemma A.2.2 and, in the second, Lemma A.2.1. □

Corollary 1.3.2. The Taylor expansion of the flow given in (1.8), *i.e.*

$$\rho_t(x) \approx x + t\{x,H\} + \frac{t^2}{2}\{\{x,H\},H\} + \frac{t^3}{3!}\{\{\{x,H\},H\},H\} + \dots \quad ,$$

is not a symplectomorphism.

Proof. It is enough to show this in first order:

$$(\rho_t^*\omega)(x) = (\omega\circ\rho_t)(x) = \omega(x + t\{x,H\} + \mathcal{O}(t^2)) = \omega\left(x + t\frac{dx}{dt} + \mathcal{O}(t^2)\right) \neq \omega(x)\,.$$

□

We then see that the vector field associated to the approximation in (1.8) is time dependent and, therefore, does not conserve energy. This establishes that approximating the hamiltonian flow by a simple Taylor series in time is only useful for short times. If there is inherent interest in periodic flows, for instance, this approximation is useless, since it does not respect flow topology. We return to this point in Chapter 2.

1.3.2 Lagrangian submanifolds and twisted forms

We have proven that every diffeomorphism emerging as a hamiltonian flow is a symplectomorphism, but we expect the set of symplectomorphisms to be smaller than that of diffeomorphisms, since conservation of the canonical form is not generally guaranteed. We have discussed how the existence of a symplectomorphism is guaranteed for neighborhoods of symplectic manifolds of the same dimension, but we haven't said anything about finding them. Let (M_1,ω_1) and (M_2,ω_2) be $2n$-dimensional symplectic manifolds and $\psi : M_1 \longrightarrow M_2$ a general diffeomorphism. When is ψ a symplectomorphism, *i.e.* $\psi^*\omega_2 = \omega_1$? To answer this question we will need the concept of submanifolds that are everythere orthogonal with respect to the canonical form and, besides, have maximum dimension:

Definition 1.3.3. Given the $2n$-dimensional symplectic manifold (M,ω), an n-dimensional submanifold $Y \subset M$ is **lagrangian** if $\omega|_Y = 0$.

Notice that we always have $\omega = -d\alpha$, but only on a lagrangian manifold $\omega = 0$, so $d\alpha = 0 \Longrightarrow \alpha = dS$, valid locally by Poincaré's lemma[5]. This simple consequence will soon make lagrangian submanifolds the most important objects in the theory of semiclassical approximations and quantization. They are especially prominent when dealing with product manifolds, since all [relevant] symplectomorphisms can be characterized in terms of generating functions for lagrangian submanifolds. To see this, start by defining the product manifold $M_1 \times M_2$ and the canonical projections π_1 and π_2 by means of the diagram below:

[5]Poincaré's lemma states that in a smooth manifold any closed form is locally exact, *i.e.* we can decrease the form's domain until we find a primitive [AMRC80].

$$\begin{array}{ccccc} (x_1,x_2) & & M_1\times M_2 & & (x_1,x_2) \\ \big\downarrow & & \pi_1\big\downarrow \quad \big\downarrow\pi_2 & & \big\downarrow \\ x_1 & & M_1 \quad M_2 & & x_2 \end{array}$$

Proposition 1.3.4. The 2-form $\omega = \lambda_1(\pi_1)^*\omega_1 + \lambda_2(\pi_2)^*\omega_2$ is canonical on $M_1 \times M_2$.

Proof.

$$\begin{cases} d\omega & = \lambda_1\pi_1^* d\omega_1 + \lambda_2\pi_2^* d\omega_2 = 0 \\ \omega((x_1,x_2),(y_1,y_2)) & = \lambda_1\omega_1(x_1,x_2) + \lambda_2\omega_2(y_1,y_2) \neq 0 \end{cases} .$$

□

We are then inclined to take ω with $\lambda_1 = \lambda_2 = 1$, forming the symplectic product manifold $(M_1 \times M_2, \omega)$. This 2-form, however, is not appropriate to describe the symplectic structure of its separate components.

Definition 1.3.5. A 2-form ω is said to be **twisted** if we adopt $\lambda_1 = 1$ and $\lambda_2 = -1$. This new 2-form is written as $\omega^\sigma \stackrel{\text{def}}{=} \pi_1^*\omega_1 - \pi_2^*\omega_2$. Naturally, it has a twisted primitive $\alpha^\sigma \stackrel{\text{def}}{=} -\pi_1^*\alpha_1 + \pi_2^*\alpha_2$

We then obtain a classification of all symplectomorphisms by means of their graphs acting on the twisted form:

Proposition 1.3.6. A diffeomorphism $\psi : M_1 \longrightarrow M_2$ is a symplectomorphism iff its graph Γ_ψ is a lagrangian submanifold of $(M_1 \times M_2, \omega^\sigma)$.

Proof. A submanifold of $(M_1 \times M_2, \omega^\sigma)$ is lagrangian iff $\omega^\sigma = 0 \Longleftrightarrow \Gamma_\psi^*\omega^\sigma = 0$. In terms of the graph of ψ, namely

$$\begin{aligned} \Gamma_\psi : M_1 &\longrightarrow M_1 \times M_2 \\ x_1 &\longmapsto (x_1, \psi(x_1)) \quad , \end{aligned}$$

we must have

$$\begin{aligned} \Gamma_\psi^*\,\omega^\sigma &= 0 \\ \Gamma_\psi^*\,\pi_1^*\,\omega_1 - \Gamma_\psi^*\,\pi_2^*\,\omega_2 &= 0 \\ (\pi_1\circ\Gamma_\psi)^*\omega_1 - (\pi_2\circ\Gamma_\psi)^*\omega_2 &= 0 \\ I^*\omega_1 - \psi^*\omega_2 &= 0 \\ \Longleftrightarrow \quad \omega_1 &= \psi^*\omega_2 \quad , \end{aligned}$$

where we have used the graph's definition to write $(\pi_1 \circ \Gamma_\psi)(x) = x$ and $(\pi_2 \circ \Gamma_\psi)(x) = \psi(x)$. □

The proposition above shows the twisted product manifold is an extremely important object. In fact, when it comes to symplectomorphisms, it is more important than the base manifolds M_1 and M_2 due to the proved exactness of its tautological form when restricted to the graph of a symplectomorphism.

1.3.3 Extended manifolds

An important example of product manifold emerges when considering the hamiltonian flow ρ_t acting on M. It is sometimes desirable to immerse M into the $(1+2n)$-dimensional space that constitutes the domain of ρ_t, namely $\mathbb{R} \times M$, paired with a new canonical form ω_t. To fix an expression for ω_t, we

start by requiring the equations of motion to be the same when projected on M: Using the projection on the second component, $\pi_2(\mathbb{R}\times M)=M$, we express this as

$$(\pi_2^*\circ\imath_{X_H})\,\omega_t = dH \quad\Longrightarrow\quad \pi_2^*\,\omega_t=\omega=-d\alpha\,.$$

Writing $\pi_1(\mathbb{R}\times M)=\mathbb{R}$, an immediate solution is

$$\pi_1^*\omega_t = dH\wedge dt \quad\Longrightarrow\quad \omega_t=\omega+dH\wedge dt=-d\alpha_t\,,\quad \alpha_t=\alpha-Hdt\,.$$

Definition 1.3.7. The product manifold $(\mathbb{R}\times M,\omega_t)$ is the **extended manifold** associated to (M,ω). The forms ω_t and α_t are the **extended canonical** and **tautological forms**, respectively, but the latter is usually referred to as the **Poincaré-Cartan integral invariant**.

Notice the Poincaré-Cartan integral invariant can be written as

$$\alpha_t=\alpha-Hdt=p\cdot dq-Hdt \quad\Longrightarrow\quad \alpha_t=[p\cdot\dot q-H(p,q)]\,dt=L_t(q,\dot q)\,dt\,,\quad p=\frac{\partial L_t(q,\dot q)}{\partial\dot q}\,.$$

Definition 1.3.8. The function $L_t(q,\dot q)$, which exchanges a cotangent description by a tangent one, is called the **lagrangian**.

We suspect this is where lagrangian manifolds inherit their name from: We need them to define lagrangian functions (or at least to integrate them).

1.4 Generating functions and Hamilton-Jacobi theory

We now describe the structure of general symplectomorphisms, which are intrinsically connected with usual and extended product manifolds, generating functions and, thus, lagrangian submanifolds. We are then naturally led to the notion of invariant tori associated to action-angle coordinates.

1.4.1 The Hamilton-Jacobi equation

Proposition 1.3.6 says that there are as many lagrangian submanifolds in $M_1\times M_2$ as there are symplectomorphisms from $M_1\longrightarrow M_2$. However, notice that, for the twisted tautological form α^σ,

$$\omega^\sigma=-d\alpha^\sigma\Longrightarrow\Gamma_\psi^*\omega^\sigma=0\Longleftrightarrow\alpha^\sigma=dS \tag{1.9}$$

so that there are also as many closed[6] 1-forms on $M_1\times M_2$ as there are symplectomorphisms and lagrangian submanifolds.

Definition 1.4.1. The function $S\in C^\infty(M_1\times M_2)$, primitive to the twisted tautological form α^σ, is called a **generating function** for the lagrangian submanifold $(x,\psi(x))$.

The simplest product manifold is the extended $(\mathbb{R}\times M,\omega_t)$ associated to an initial symplectic manifold (M,ω). Here, the condition (1.9) written in terms of the Poincaré-Cartan invariant,

$$\begin{aligned}\alpha_t=dS_t \quad\Longleftrightarrow\quad dS_t(q)=p\cdot dq-H_t(q,p)\,dt \quad&\Longrightarrow\quad S_t(q)=\int_{q_0}^{q_t}p\cdot dq-\int_0^t d\tau\,H_\tau(q,p)\\ &\Longleftrightarrow\quad S_t(q)=\int_0^t d\tau\,L_\tau(q,(\dot q))\,,\end{aligned} \tag{1.10}$$

where we are now assuming the hamiltonian to be non-autonomous for generality. Notice we could only integrate $\alpha_t=L_tdt$ so easily because we are on a lagrangian manifold. We then immediately have

$$p=\frac{\partial S_t(q)}{\partial q}\,,\qquad \frac{\partial S_t(q)}{\partial t}+H_t\left(q,\frac{\partial S_t(q)}{\partial q}\right)=0\,. \tag{1.11}$$

[6] In fact, there are as many *equivalence classes* of 1-forms, *i.e.* $[\alpha]=\alpha+c$, $c\in\mathbb{R}$, but this is just a technicality.

Definition 1.4.2. The equation above is the **Hamilton-Jacobi equation**, and the generating function S_t that satisfies it is said to be **admissible**.

For the autonomous hamiltonians which we have been considering up to now the Hamilton-Jacobi equation assumes the form

$$H(q, \partial_q S) = E\,, \quad E \in \mathbb{R}\,,$$

which is just a re-statement of the principle of energy conservation, now in terms of the generating function. The graph of S, namely $\Gamma_S = (t, q, S(q))$, defines the relevant extended lagrangian manifold in $\mathbb{R} \times M$. Since we are mostly interested in the autonomous case, we will often consider the restriction $M \supset \pi_2(\Gamma_S) = (q, S(q))$, which is a true lagrangian submanifold.

1.4.2 Product manifolds and the Legendre transform

Consider now the submanifold $M \times \phi(M) \subset M \times M$, where ϕ is a symplectomorphism. The points in $M \times \phi(M)$ have the form $(q, p, \phi(q, p))$. Writing $\phi(q, p) = (Q, P)$ we have

$$\begin{aligned} \Gamma_\phi^* \omega^\sigma = 0 \quad &\iff \quad dQ \wedge dP - dq \wedge dp = 0 \\ &\implies \quad dQ \wedge dP + dK_t(Q, P) \wedge dt - dq \wedge dp - dH_t(q, p) \wedge dt = 0\,, \end{aligned}$$

where in the second line we have extended the twisted canonical form to $\mathbb{R} \times M \times M$, defining K as the transformed hamiltonian. Four obvious types of generating function immediately arise as primitives to the above equation, depending on what variables we choose them to be functions of:

$$\begin{aligned} &(dQ \wedge dP - dq \wedge dp) + d\left[K_t(Q, P) - H_t(q, p)\right] \wedge dt = 0 \\ \iff \quad &\begin{cases} dS_t^1(Q, q) = -P \cdot dQ + p \cdot dq + \left[K_t(Q, P) - H_t(q, p)\right] dt \\ dS_t^2(P, q) = Q \cdot dP + p \cdot dq + \left[K_t(Q, P) - H_t(q, p)\right] dt \\ dS_t^3(Q, p) = -P \cdot dQ - q \cdot dp + \left[K_t(Q, P) - H_t(q, p)\right] dt \\ dS_t^4(P, p) = Q \cdot dP - q \cdot dp + \left[K_t(Q, P) - H_t(q, p)\right] dt \end{cases}, \end{aligned} \tag{1.12}$$

where the primitives correspond to the infamous "generating function types" of Goldstein [GJS01]. Notice that even thought they are all different, they are all primitives for the canonical form, sharing the same exterior differential – just as there are infinite possible primitives for the same derivative in calculus. In exterior calculus, however, there is a way to travel between primitives by using exact differentials, which can be immediately understood from a single calculation: Take the generating function $dS_t^1(Q, q)$ as an example and, ignoring its time-component (which is the same for all generating functions), notice that

$$\begin{aligned} dS_t^1(Q, q) = -P \cdot dQ + p \cdot dq &= (Q \cdot dP - Q \cdot dP) - P \cdot dQ + p \cdot dq \\ &= -\left(Q \cdot dP + P \cdot dQ\right) + Q \cdot dP + p \cdot dq \\ &= -d(Q \cdot P) + Q \cdot dP + p \cdot dq \\ &= d\left[-Q \cdot P + S_t^2(P, q)\right] \\ \implies \quad S_t^1(Q, q) &= -Q \cdot P + S_t^2(P, q)\,. \end{aligned}$$

The reasoning above shows that even though we do not have a closed expression for $S_t^1(Q, q)$, we are able to express it in terms of $S_t^2(P, q)$. What we have done can also be interpreted as exchanging a description in terms of (Q, q) for one in terms of (P, q). Evidently, the time-component is unaltered by such transformation.

Definition 1.4.3. The transformation described above is known as a **Legendre transform**.

Notice that all generating functions satisfy the same differential equation with respect to time,

$$\frac{\partial S_t}{\partial t} = K_t(Q,P) - H_t(q,p)\,, \tag{1.13}$$

with the expressions for Q and P always fixed as $P = -\partial_Q S_t$, $Q = \partial_P S_t$. The expression above is sometimes referred to as the *Hamilton-Jacobi equation for generating functions* [Arn89]. It's easy to see that, taking $K_t(Q,P) = 0$, we recover the original Hamilton-Jacobi equation (1.11) – which makes sense, since in this case we are just projecting back to $\mathbb{R}\times M$. Another option is to fix the transformed hamiltonian as a quadractic form, linearizing the final hamiltonian vector field:

$$K_t(Q,P) = K_t(X) = \frac{1}{2} X\cdot \mathcal{A}_t X \quad\Longrightarrow\quad \dot{X} = \mathcal{A}_t X\,.$$

Due to the presence of natural *resonances* in hamiltonian vector fields [Arn89, dA90, AMRC80], it is generally impossible to find such linearizing transformation. The process of "linearizing as much as possible" is performed using especial symplectic algorithms, resulting in a transformed hamiltonian expressed as a *Birkhoff normal form*. This elimination process is the key to prove the famous Komolgorov-Arnol'd-Moser (KAM) theorem [HI03].

1.4.3 Action-angle variables and invariant tori

The most interesting realization of (1.13) is obtained when we consider $K_t(Q,P) = K_t(Q)$, *i.e.* we look for a generating function S_t whose symplectomorphism is not as powerful to linearize the final vector field, but ends up eliminating the momentum-dependence of the transformed hamiltonian[7]. In this case the equations of motion are trivially found to be:

$$\dot{Q} = 0\,,\quad \dot{P} = -\frac{\partial K_t(Q)}{\partial Q} \quad\Longrightarrow\quad Q_t = Q_0\,,\quad P_t = P_0 - \int dt\left(\frac{\partial K_t(Q)}{\partial Q}\right), \tag{1.14}$$

which represent a type of rectification, since in (q,p) coordinates we can have a very complicated flow but in (Q,P) it is always parallel to the P axis. Notice that finding such S_t is tantamount to integrating the hamiltonian vector field X_H, since if it exists the flow is integrated by the quadratures in (1.14).

A simple, explicit transformation $(q,p)\longmapsto(\nu,I)$ fulfilling (1.14) can be found for autonomous hamiltonians. For this, we employ the "type 2" time-independent generating function $S^2(I,q)$, for which, by (1.12),

$$p = \frac{\partial S^2(I,q)}{\partial q}\,,\quad \nu = \frac{\partial S^2(I,q)}{\partial I}\,,\quad K(I) = H(q,p) = H\left(q, \frac{\partial S^2(I,q)}{\partial I}\right), \tag{1.15}$$

where we *force* the dependence of K in ν to vanish. We then have

$$\dot{I} = 0,\quad \dot{\nu} = \frac{\partial K(I)}{\partial I} \quad\Longrightarrow\quad I_t = I_0\,,\quad \nu_t = \nu_0 - t\left(\frac{\partial K(I)}{\partial I}\right)_{I=I_0}. \tag{1.16}$$

The equations above, which are just (1.14) expressed in terms of (I,ν), define a free particle for each I_0, since the speed of ν_t is then a constant. If the flow of H was already formed by compact submanifolds, no information is lost in compactifying[8] the variable ν_t and interpreting each of its components as an angular coordinate in $\mathbb{R}^2$, so $0\le\nu_t\le 2\pi$ for each component of $\nu_t = (\nu_{1,t},\ldots,\nu_{n,t})$. This is depicted in Fig. 1.1. We then have

$$dS(q,I) = p\cdot dq - \nu\cdot dI \quad\Longrightarrow\quad S(q,I)|_{I=I_0} = \int_{q_0}^{q_t} p\cdot dq \quad\Longrightarrow\quad S(I) = \oint_{\gamma(I)} p\cdot dq\,,$$

where we have integrated over a full circuit $\gamma(I)$. For this closed circuit, (1.15) fixes

$$\frac{dS(I)}{dI} = 2\pi - 0 \quad\Longrightarrow\quad S(I) = 2\pi I \quad\Longrightarrow\quad I = \frac{1}{2\pi}\oint_{\gamma(I)} p\cdot dq\,. \tag{1.17}$$

[7] Or position, it doesn't matter: We can exchange them using the linear symplectomorphism $(q,p)\longmapsto(-p,q)$.

[8] Any closed, non-self-intersecting curve on the plane is diffeomorphic to $\mathbb{S}^1$ [Spi99].

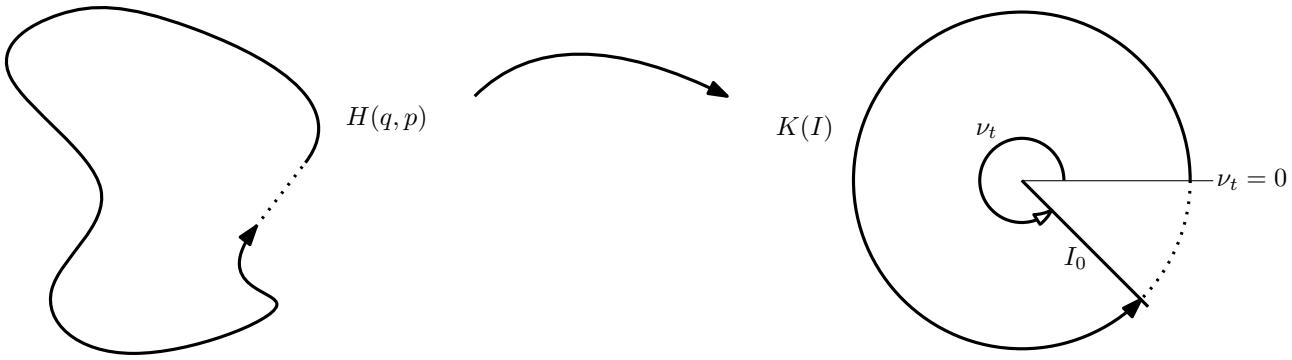

Figure 1.1: Parametrizing a curve on $\mathbb{R}^2$ in terms of (I, ν). The original compact flow $\rho_t(q,p)$, whose value at each point lies in a level curve of $H(q,p)$, is mapped to a circle in the (I,ν) coordinates. This circle is a level curve of $K(I)$, which does not depend on ν.

Definition 1.4.4. The variables (I, ν) are called **action and angle variables**, respectively.

If a problem admits a solution (1.17) so that (1.16) is fulfilled, a bounded orbit can be described using a set of n action-angle variables, each of then representing a circle in phase space. Since the product of n circles is a torus, the orbit is then constrained to the surface of an n-dimensional *lagrangian torus*. Due to the constraining, this torus is also said to be *invariant*, since a general lagrangian submanifold will evolve when acted upon by the flow, but the tori remain static.

1.5 Centers and Chords

The generating functions described in the previous section do not exhaust the possibilities, after all there is an infinite number of them. The generating functions that mix position and momentum in (1.12) have the characteristic that they deal either with new momenta and old positions, or vice-versa. In this section, following [Wei72], we define generating functions that mix new and old variables symmetrically.

1.5.1 The symmetrized canonical form

Coming back to index notation, notice that we can symmetrize the canonical form on a chart in $\mathbb{R}^{2n}$ as

$$\omega = \sum_{i=1}^{n} dq_i \wedge dp_i = \sum_{i=1}^{n} \left(\frac{dq_i \wedge dp_i - dp_i \wedge dq_i}{2} \right) = \frac{1}{2} \sum_{i,\,j=1}^{2n} \mathcal{J}_{ij}\, dx_i \wedge dx_j \quad ,$$

where $x = (q,p) = (q_1, \ldots, q_n, p_1, \ldots, p_n)$ and $\mathcal{J}$ is the canonical matrix (1.4). The symplectic condition of Definition 1.1.3 now reads

$$\Gamma_f^* \omega^\sigma = 0 \quad \Longleftrightarrow \quad f^*\omega - \omega = 0 \quad \Longleftrightarrow \quad \sum_{i,\,j=1}^{2n} \mathcal{J}_{ij}\, d(x_i \circ f) \wedge d(x_j \circ f) - dx_i \wedge dx_j = 0 \quad . \tag{1.18}$$

Define $x \circ f \stackrel{\text{def}}{=} X$ such that $X(a) = x(f(a))$, which for the prototype product manifold is just $f(a)$ in the trivial chart $x = I$. Just as in the earlier sections, where the fact that $\Gamma_f^* \omega^\sigma = 0$ allowed us to define a generating function in the product manifold, we will now do the same for the symmetrized twisted form.

Proposition 1.5.1. The 1-forms

$$\phi(f) = \sum_{i,j}^{2n} \mathcal{J}_{ij}\, (X_i - x_i)\; d\left(\frac{X_j + x_j}{2} \right) , \quad \psi(f) = -\sum_{i,j}^{2n} \mathcal{J}_{ij} \left(\frac{X_j + x_j}{2} \right) d\,(X_i - x_i) \;,$$

are primitives for the left hand side of (1.18), *i.e.* $d\phi(f) = d\psi(f) = \Gamma_f^* \omega^\sigma$.

Proof. We specialize in $\phi(f)$, since the procedure is exactly the same for $\psi(f)$. Taking the exterior derivative of $\phi(f)$ we have

$$d\phi(f) = \frac{1}{2}\sum_{i,j}^{2n} \mathcal{J}_{ij} d\left(X_i - x_i\right) \wedge d\left(X_j + x_j\right) = \frac{1}{2}\sum_{i,j}^{2n} \mathcal{J}_{ij}\left[dX_i \wedge dX_j + dX_i \wedge dx_j - dx_i \wedge dX_j - dx_i \wedge dx_j\right]$$

$$= \frac{1}{2}\sum_{i,j}^{2n} \mathcal{J}_{ij}\left[dX_i \wedge dX_j - dx_i \wedge dx_j\right] - \frac{1}{2}\sum_{i,j}^{2n} \mathcal{J}_{ij}\left[\left(\frac{\partial X_i}{\partial x_i}\right) dx_i \wedge dx_j + \left(\frac{\partial X_j}{\partial x_j}\right) dx_j \wedge dx_i\right].$$

Since the indexes are dull, we can exchange i by j in the second sum in the equation above:

$$\sum_{i,j}^{2n} \mathcal{J}_{ij}\left(\frac{\partial X_i}{\partial x_i}\right) dx_i \wedge dx_j + \sum_{i,j}^{2n} \mathcal{J}_{ij}\left(\frac{\partial X_j}{\partial x_j}\right) dx_j \wedge dx_i = \sum_{i,j}^{2n} \mathcal{J}_{ij}\left(\frac{\partial X_i}{\partial x_i}\right) dx_i \wedge dx_j$$

$$+ \sum_{i,j}^{2n} \mathcal{J}_{ji}\left(\frac{\partial X_i}{\partial x_i}\right) dx_i \wedge dx_j$$

$$= \sum_{i,j}^{2n} \mathcal{J}_{ij}\left[\frac{\partial X_i}{\partial x_i}\right]\left(dx_i \wedge dx_j - dx_i \wedge dx_j\right) = 0\,,$$

where we have used the fact that $\mathcal{J}^T = -\mathcal{J}$. □

1.5.2 Center and chord generating functions

The 1-forms of the previous section are much easier to understand by defining the variables

$$\eta_j = (X_j + x_j)/2\,, \quad \text{and} \quad \xi_i = X_i - x_i\,,$$

with which the primitives in Proposition 1.5.1 can be written concisely as

$$\phi(f) = \sum_{i,j}^{2n} \mathcal{J}_{ij}\xi_i\, d\eta_j\,, \qquad \psi(f) = -\sum_{i,j}^{2n} \mathcal{J}_{ij}\eta_j\, d\xi_i\,,$$

and since both $\phi(f)$ and $\psi(f)$ are closed on the same lagrangian submanifold, there is a neighborhood where there are generating functions $S(\eta)$ and $\widetilde{S}(\xi)$ such that $dS(\eta) = \phi(f)$ and $d\widetilde{S}(\xi) = \psi(f)$. Therefore,

$$dS(\eta) = \sum_{i,j}^{2n} \mathcal{J}_{ij}\xi_i\, d\eta_j = \mathcal{J}\xi \cdot d\eta\,, \qquad d\widetilde{S}(\xi) = -\sum_{i,j}^{2n} \mathcal{J}_{ij}\eta_j\, d\xi_i = -\mathcal{J}\eta \cdot d\xi\,,$$

where we have preferred to write S and $\widetilde{S}$ as functions of η and ξ and leave the dependence on the symplectomorphism f implicit. We will also represent quantities associated to ξ with a $\tilde{}$ to differentiate them[9] from functions of η, and the forms above give rise to the separate equations

$$\xi = -\mathcal{J}\left[\frac{dS(\eta)}{d\eta}\right], \qquad \eta = \mathcal{J}\left[\frac{d\widetilde{S}(\xi)}{d\xi}\right]. \tag{1.19}$$

Definition 1.5.2. The variables ξ and η are the **center** and the **chord** associated to the evolution $x_0 \longmapsto \rho_t(x_0)$. The functions $S(\eta)$ and $\widetilde{S}(\xi)$ are the **center** and **chord generating functions**.

The reason for naming these variables as we did is shown in Fig. 1.2.

[9] We will use the same notation to represent quantities related to each other *via* Fourier transforms in quantum mechanics – which, as we will see in Chapter 3, will be semiclassically connected to Legendre transforms.

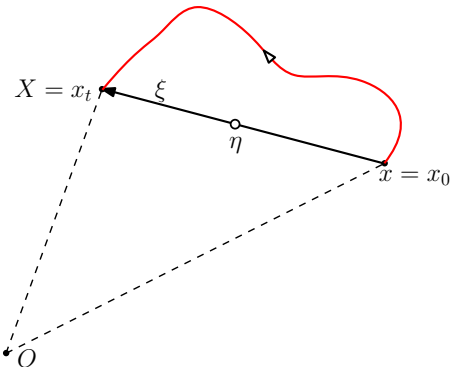

(a) Centers and chords for $x \longmapsto X$.

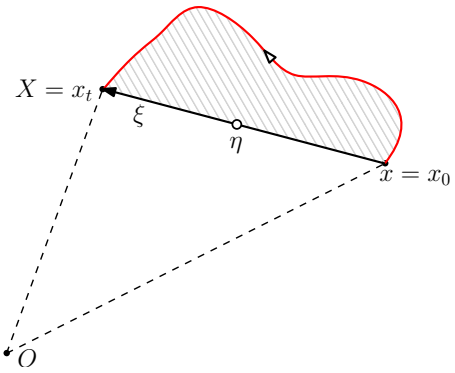

(b) Geometry of generating functions.

Figure 1.2: (a) The evolution $x_0 = x \longmapsto X = \rho_t(x)$ can be naturally interpreted in terms of the chord ξ and the center η for the orbit traced by x, shown in red. The equation for $S(\eta)$ in (1.19) means that by using the center generating function we can determine the corresponding chord through its derivatives, interpreting classical evolution as a translation by ξ. On the other hand, the equation for $\widetilde{S}(\xi)$ in (1.19) represents the evolution as a reflection around the chord η. (b) The generating functions are just different ways of interpreting the dashed-gray area enclosed by the chord ξ.

Example 1.5.3. The generating functions $\widetilde{S}(\xi) = \xi \cdot \mathcal{J} v$ and $S(\eta) = v \cdot \mathcal{J}\eta$ implicitly define classical reflections and translations by v, since by (1.19)

$$\xi = -\mathcal{J}\left(\frac{\partial S(\eta)}{\partial \eta}\right) = -\mathcal{J}^2 v = v\,, \qquad \eta = \mathcal{J}\left(\frac{\partial \widetilde{S}(\xi)}{\partial \xi}\right) = -\mathcal{J}^2 v = v\,,$$

so in the first case v defines the center, and in the second, the chord. ⁕

The center and chord generating functions interpret evolution as either a *translation* by ξ or a *reflection* around η [dA98]. Defining the classical translation and reflection operators as

$$\mathcal{R}_\eta(x) = 2\eta - x\,, \qquad \mathcal{T}_\xi(x) = x + \xi\,, \tag{1.20}$$

we can describe the mapping $x_0 \longmapsto x_t = \rho_t(x_0)$ as $x_t = \mathcal{R}_\eta(x_0) = 2\eta - x_0$ or $x_t = \mathcal{T}_\xi(x_0) = x_0 + \xi$. These operators follow a very simple algebra, as can be seen in

Lemma 1.5.4. The classical translation and reflection operators of (1.20) form a group, obeying

$$\begin{aligned} &\text{i)} \quad \mathcal{R}_\eta \circ \mathcal{T}_\xi = \mathcal{R}_{\eta - \frac{\xi}{2}} \qquad ; \qquad \text{ii)} \quad \mathcal{T}_\xi \circ \mathcal{R}_\eta = \mathcal{R}_{\eta + \frac{\xi}{2}} \\ &\text{iii)} \quad \mathcal{T}_\xi \circ \mathcal{T}_{\xi'} = \mathcal{T}_{\xi+\xi'} \qquad ; \qquad \text{iv)} \quad \mathcal{R}_\eta \circ \mathcal{R}_{\eta'} = T_{\xi+\xi'}\,. \end{aligned}$$

Proof. The proof is trivial:

$$\begin{aligned} &\text{i)} \quad (\mathcal{R}_\eta \circ \mathcal{T}_\xi)(x) = \mathcal{R}_\eta(x+\xi) = 2(\eta - \xi/2) - x = \mathcal{R}_{\eta - \frac{\xi}{2}}(x)\,; \\ &\text{ii)} \quad (\mathcal{T}_\xi \circ \mathcal{R}_\eta)(x) = \mathcal{T}_\xi(2\eta - x) = 2(\eta + \xi/2) - x = \mathcal{R}_{\eta + \frac{\xi}{2}}(x)\,; \\ &\text{iii)} \quad (\mathcal{T}_\xi \circ \mathcal{T}_{\xi'})(x) = \mathcal{T}_\xi(x+\xi') = x + \xi + \xi' = \mathcal{T}_{\xi+\xi'}(x)\,; \\ &\text{iiv)} \quad (\mathcal{R}_\eta \circ \mathcal{R}_{\eta'})(x) = \mathcal{R}_\eta(2\eta' - x) = 2(\eta - \eta') - x + x = \mathcal{T}_{2(\eta-\eta')}(x)\,. \end{aligned}$$

□

1.5.3 Extended center and chord generating functions

The relationship between the center and chord generating functions is similar to the one followed by their position and momentum equivalents described in the earlier section. For instance,

$$\begin{aligned} d\widetilde{S}(\xi) &= -\mathcal{J}\eta \cdot d\xi = -\mathcal{J}\eta \cdot d\xi + (\mathcal{J}\xi \cdot d\eta - \mathcal{J}\xi \cdot d\eta) \\ &= -\mathcal{J}\eta \cdot d\xi - \mathcal{J}\xi \cdot d\eta + dS(\eta) = d[-\mathcal{J}\xi \cdot \eta + S(\eta)] \\ \Longrightarrow \quad \widetilde{S}(\xi) &= S(\eta) + \xi \cdot \mathcal{J}\eta\,. \end{aligned}$$

This was predictable since, on the level of 1-forms, both $dS(\eta)$ and $d\widetilde{S}(\xi)$ were primitives to the same 2-form $\Gamma_f^*\omega^\sigma$, forcing $S(\eta)$ and $\widetilde{S}(\xi)$ to be related via Legendre transforms on the level of functions as described in Section 1.4.2. We can also naturally extend the generating functions as

$$\widetilde{S}_t(\xi) = -\int_{\xi_0}^{\xi_t} \mathcal{J}\eta \cdot d\xi - \int_0^t dt\, H(\xi_t)\,, \qquad S_t(\eta) = \int_{\eta_0}^{\eta_t} \mathcal{J}\xi \cdot d\eta - \int_0^t dt\, H(\eta_t)\,, \tag{1.21}$$

which are condensed expressions for the Poincaré-Cartan integral invariant on $\mathbb{R} \times M \times M$. The geometrical meaning of generating functions above will be important in later chapters. Let us describe this for the case of centers, which we depict in Fig. 1.2(b). Here, the evolution from $x_0 \longmapsto x_t$ is described by the center $\eta = (x_t + x_0)/2$, from which the generating function defines the chord ξ through (1.19). The meaning of $S_t(\eta)$ in (1.21) is, therefore, the area of the region enclosed by the orbit $\rho_t(x_0)$ and the chord ξ – which is the segment linking the initial and final points.

Notice that, if we had used the chord generating function, the geometrical meaning described above would be exactly the same, but variables would be obtained from the chord instead.

Bibliography

[AMRC80] R. Abraham, J. E. Marsden, T. Ratiu, and R. Cushman. *Foundations of Mechanics*. Benjamin/Cummings, 2nd edition, 1980.

[Arn89] V. I. Arnold. *Mathematical Methods of Classical Mechanics*. Springer, 2nd edition, 1989.

[dA90] A. M. Ozorio de Almeida. *Hamiltonian Systems: Chaos and Quantization*. Cambridge University Press, 2nd edition, 1990.

[dA98] A. M. Ozorio de Almeida. The Weyl representation in classical and quantum mechanics. *Phys. Rep.*, 295:265, 1998.

[dS11] A. Cannas da Silva. *Introduction to Symplectic and Hamiltonian Geometry*. Editora IMPA, 2011.

[GJS01] H. Goldstein, C. P. Poole Jr, and J. L. Safko. *Classical Mechanics*. Addison-Wesley, 3rd edition, 2001.

[HI03] J. Hubbard and Y. Ilyashenko. A proof of Komolgorov's theorem. *Disc. Cont. Dyn. Sys.*, 4:1, 2003.

[Spi99] M. Spivak. *A Comprehensive Introduction to Differential Geometry, Vol. 1.* Publish or Perish, 3rd edition, 1999.

[Spi10] M. Spivak. *Physics for Mathematicians: Mechanics I.* Publish or Perish, 1st edition, 2010.

[Wei72] A. Weinstein. The invariance of Poincaré's generating function for canonical transformations. *Invent. Math.*, (16):202, 1972.

Chapter 2

Numerical methods and discretization

> From my experience, it is when we least want to work with something that we end up making a living out of it.
>
> Jair Koiller

We start this chapter by presenting the standard theory of splitting symplectic integrators, used to solve Hamilton's equations while preserving the flow's symplecticity. Although our discussion is quite general, we emphasize 2-step integrators and the troublesome case of non-separable hamiltonian functions. The 2-step symplectic integrators are then promoted to discrete hamiltonian maps and shown to be equivalent to the flows obtained from periodically kicked hamiltonians, which are generally chaotic. As we have not yet spoken about chaos and integrability, we also briefly enumerate some aspects of chaos theory that are needed to understand our results.

2.1 Going with the flow

In this section we describe how to solve Hamilton's equations, *i.e.* integrate hamiltonian vector fields. As is usually the case with numerical methods, the theoretical background is quite beautiful on its own, employing concepts of Lie group theory and differential geometry.

2.1.1 Splitting symplectic integrators: First order theory

We have already shown that movement, *i.e.* the flow that integrates Hamilton's equations, is a 1-parameter family of symplectomorphisms with respect to time. We can express this flow both as an exponential of a time-independent vector field or as a Poisson-bracket series using (1.7):

$$\rho_t = \exp\left(tX_H\right) = \exp\left(-t\{H,\cdot\}\right) .$$

Now, the Baker-Hausdorff-Campbell (BHC) formula (actually the Zessenhaus formula [Yos90, Sch88]) allows us to split the exponential as

$$\exp\left(tX_H\right) = \exp\left[t\left(\frac{\partial H}{\partial p}\frac{\partial}{\partial q} - \frac{\partial H}{\partial q}\frac{\partial}{\partial p}\right)\right] = \exp\left[t\left(\frac{\partial H}{\partial p}\frac{\partial}{\partial q}\right)\right]\exp\left[t\left(\frac{\partial H}{\partial q}\frac{\partial}{\partial p}\right)\right] + \mathcal{O}(t^2)\,,$$

which is not particularly useful at this stage. However, if our Hamiltonian has the form

$$H(q,p) = F(p) + V(q) \quad \Longleftrightarrow \quad X_H = X_F + X_V\,,$$

the splitting of vector fields implies

$$\exp\left(tX_H\right) = \exp\left[t\left(X_F + X_V\right)\right] = \exp\left(tX_F\right)\exp\left(tX_V\right) + \mathcal{O}(t^2) \quad \Longleftrightarrow \quad \rho_t^H = \rho_t^F \circ \rho_t^V + \mathcal{O}(t^2)\,, \tag{2.1}$$

that is, if our Hamiltonian can be written as a sum of "kinetic" and "potential" terms that are separate functions of position or momentum, we can approximate movement as the successive action of two

Hamiltonian flows: The first generated by $V(q)$, and the second by $F(p)$. Since, generally, $\{F, V\} \neq 0$, the ordering of flows is not commutative, although the error has the same order in t:

$$\begin{cases} \rho_t^H = \rho_t^F \circ \rho_t^V + \mathcal{O}(t^2) \\ \rho_t^H = \rho_t^V \circ \rho_t^F + \mathcal{O}(t^2) \end{cases} \quad , \qquad \text{but} \qquad \rho_t^F \circ \rho_t^V \neq \rho_t^V \circ \rho_t^F \, !$$

Definition 2.1.1. Hamiltonians of the form $H(q,p) = F(p) + V(q)$ are called **separable**.

The splitting given by (2.1) gets better as t is decreased, and the group property of Hamiltonian flows can be used to our advantage by discretizing time as a function of a small parameter ϵ:

$$\rho_{t+s} = \rho_t \circ \rho_s \quad \Longrightarrow \quad \rho_{\epsilon N} = \overbrace{\rho_\epsilon \circ \rho_\epsilon \ldots \rho_\epsilon}^{N \text{ times}} = (\rho_\epsilon)^N, \quad t = \epsilon N \, .$$

Any hamiltonian flow can then be split as a sequence of infinitesimal flows. For the particular case of separable Hamiltonians we have the possibilities

$$\begin{cases} \rho_t^H \approx (\rho_\epsilon^F \circ \rho_\epsilon^V)^N \stackrel{\text{def}}{=} (\rho_\epsilon^{FV})^N \\ \rho_t^H \approx (\rho_\epsilon^V \circ \rho_\epsilon^F)^N \stackrel{\text{def}}{=} (\rho_\epsilon^{VF})^N \end{cases} \quad , \quad t = \epsilon N \, , \tag{2.2}$$

where we have defined ρ_ϵ^{FV} and ρ_ϵ^{VF} based on the chosen ordering. We can, therefore, approximate the total flow by N iterations of the composite infinitesimal flows generated by the Hamiltonians V and F, which are just shears and can be solved exactly:

$$H = V(q) \quad \Longrightarrow \quad \begin{cases} \dot{q} = 0 \\ \dot{p} = -\partial_q V \end{cases} \quad \Longrightarrow \quad \rho_\epsilon^V : \begin{pmatrix} q_0 \\ p_0 \end{pmatrix} \longmapsto \begin{pmatrix} q_0 \\ p_0 - \epsilon \, \partial_q V(q_0) \end{pmatrix} = \begin{pmatrix} q_\epsilon \\ p_\epsilon \end{pmatrix}$$

$$H = F(p) \quad \Longrightarrow \quad \begin{cases} \dot{q} = +\partial_p F \\ \dot{p} = 0 \end{cases} \quad \Longrightarrow \quad \rho_\epsilon^F : \begin{pmatrix} q_0 \\ p_0 \end{pmatrix} \longmapsto \begin{pmatrix} q_0 + \epsilon \, \partial_p F(p_0) \\ p_0 \end{pmatrix} = \begin{pmatrix} q_\epsilon \\ p_\epsilon \end{pmatrix}$$

Notice that each shear above is expressed as a triangular matrix, being thus symplectic by Lemma B.1.3. Starting with an initial (q_0, p_0), for *e.g.* ρ_ϵ^{FV} the continuous flow is then decomposed as the discrete sequence

$$(q_0,p_0) \stackrel{\rho_\epsilon^V}{\longmapsto} (q_0,p_\epsilon) \stackrel{\rho_\epsilon^F}{\longmapsto} (q_\epsilon,p_\epsilon) \stackrel{\rho_\epsilon^V}{\longmapsto} (q_\epsilon,p_{2\epsilon}) \stackrel{\rho_\epsilon^F}{\longmapsto} (q_{2\epsilon},p_{2\epsilon}) \stackrel{\rho_\epsilon^V}{\longmapsto} \cdots \stackrel{\rho_\epsilon^F}{\longmapsto} (q_{N\epsilon},p_{N\epsilon}) \quad ,$$

with $t = N\epsilon$. Since the parameter ϵ is fixed and indexing by a natural number is much simpler, we now take the successive applications of ρ_t^{FV} to map the system from $(q_0, p_0) \longmapsto (q_N, p_N)$ indexing by iteration step, *e.g.* the sequence above becomes

$$(q_0,p_0) \xrightarrow{\rho_\epsilon^F \circ \rho_\epsilon^V} (q_1,p_1) \xrightarrow{\rho_\epsilon^F \circ \rho_\epsilon^V} (q_2,p_2) \xrightarrow{\rho_\epsilon^F \circ \rho_\epsilon^V} \cdots \xrightarrow{\rho_\epsilon^F \circ \rho_\epsilon^V} (q_N,p_N) \, .$$

The map from (q_{i-1}, p_{i-1}) to (q_i, p_i) can then be expressed using either half-steps or a concatenated single form:

$$\begin{cases} \text{first} & \begin{cases} q_{i-\frac{1}{2}} = q_{i-1} \\ p_{i-\frac{1}{2}} = p_{i-1} - \epsilon \, \partial_q V(q_{i-1}) \end{cases} \\ \text{second} & \begin{cases} q_i = q_{i-\frac{1}{2}} + \epsilon \, \partial_p F(p_{i-\frac{1}{2}}) \\ p_i = p_{i-\frac{1}{2}} \end{cases} \end{cases} \quad \Longleftrightarrow \quad \rho_t^{FV} : \begin{pmatrix} p_{i-1} \\ q_{i-1} \end{pmatrix} \longmapsto \begin{pmatrix} p_{i-1} - \epsilon \, \partial_q V(q_{i-1}) \\ q_{i-1} + \epsilon \, \partial_p F(p_i) \end{pmatrix} = \begin{pmatrix} p_i \\ q_i \end{pmatrix} \tag{2.3}$$

the equivalence being verifiable by direct substitution. The alternative ordering presented in (2.2) reverses shears:

$$\begin{cases} \text{first} & \begin{cases} q_{i-\frac{1}{2}} = q_{i-1} + \epsilon \, \partial_p F(p_{i-1}) \\ p_{i-\frac{1}{2}} = p_{i-1} \end{cases} \\ \text{second} & \begin{cases} q_i = q_{i-\frac{1}{2}} \\ p_i = p_{i-\frac{1}{2}} - \epsilon \, \partial_q V(q_{i-\frac{1}{2}}) \end{cases} \end{cases} \quad \Longleftrightarrow \quad \rho_t^{VF} : \begin{pmatrix} q_{i-1} \\ p_{i-1} \end{pmatrix} \longmapsto \begin{pmatrix} q_{i-1} + \epsilon \, \partial_p F(p_{i-1}) \\ p_{i-1} - \epsilon \, \partial_q V(q_i) \end{pmatrix} = \begin{pmatrix} q_i \\ p_i \end{pmatrix} . \tag{2.4}$$

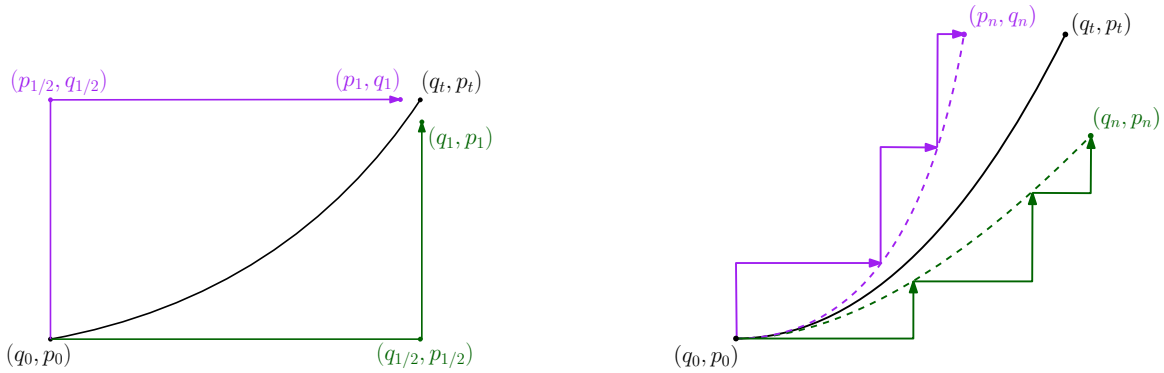

(a) Approximating a continous flux by two discrete steps.

(b) The maps (2.3) and (2.4) are not equivalent.

Figure 2.1: (a) The black curve is the exact evolution $(q_0, p_0) \longmapsto (q_t, p_t) = \rho_t^H(q_0, p_0)$, which we approximate by a single iteration of maps (2.3) (purple) and (2.4) (green). The half-steps for both algorithms are shown in fractional coordinates. The distance between the final approximated points and the exact one is of $\mathcal{O}(t^2)$, so it is best to choose a higher number of steps, each with a smaller step-size ϵ, leading us to the panel on the right. (b) Here, we use several iterations of the maps to approximate the exact flow. The associated hamiltonian, however, is not that of the original system, but of the effective approximations in (2.5), displayed here as dashed lines. The errors are grossly exaggerated for ease of visualization, since panel (b) should be more precise than panel (a).

A visual depiction of both algorithms is provided in Fig. 2.1. Note that, since the composition of symplectic mappings is obviously symplectic[1], the combined mappings in (2.3) and (2.4) are also symplectic.

Definition 2.1.2. Numerical strategies that split the Hamiltonian flow into small symplectic pieces, such as (2.3) and (2.4), are called **splitting symplectic integrators (SSIs)[2].**

As mentioned earlier, since the potential and kinetic terms do not commute, the approximations (2.3) and (2.4) are of $\mathcal{O}(\epsilon^2)$, which renders these SSIs *first-order* approximations – the order is defined by the error in *energy*, not in the trajectories. To show why this makes sense notice that, again by the BHC formula,

$$\begin{cases} \rho_\epsilon^{FV} = \exp\left(\epsilon X_F\right) \exp\left(\epsilon X_V\right) = \exp\left[\epsilon\left(X_F + X_V\right) + \left(\frac{\epsilon^2}{2}\right)\omega(X_V, X_F) + \mathcal{O}(\epsilon^3)\right] \stackrel{\text{def}}{=} \exp\left[\epsilon X_{\mathcal{H}^{FV}}\right] \\ \rho_\epsilon^{VF} = \exp\left(\epsilon X_V\right) \exp\left(\epsilon X_F\right) = \exp\left[\epsilon\left(X_V + X_F\right) + \left(\frac{\epsilon^2}{2}\right)\omega(X_F, X_V) + \mathcal{O}(\epsilon^3)\right] \stackrel{\text{def}}{=} \exp\left[\epsilon X_{\mathcal{H}^{VF}}\right] \end{cases}.$$

Thus, the hamiltonians associated to each composite flow are not the original H, but the perturbative series

$$\begin{cases} \mathcal{H}^{FV}(q,p) = F + V + \left(\frac{\epsilon}{2}\right)\{V, F\} + \mathcal{O}(\epsilon^2) = H(q,p) + \mathcal{O}(\epsilon) \\ \mathcal{H}^{VF}(q,p) = F + V - \left(\frac{\epsilon}{2}\right)\{V, F\} + \mathcal{O}(\epsilon^2) = H(q,p) + \mathcal{O}(\epsilon)\,, \end{cases}, \tag{2.5}$$

which differ from H by a term of at least $\mathcal{O}(\epsilon)$. This is why we refer to the splitting schemes in (2.2) as first-order SSIs. We will also call them *2-step* SSIs, since we will briefly deal with integrators employing more steps.

Definition 2.1.3. The perturbed hamiltonians in (2.5) are called **effective hamiltonians** for H.

Notice one of the effective hamiltonians misses the original H from above, and the other from below. Since ϵ is a free parameter, it is evident that the Poisson-bracket series in (2.5) do not always converge. We can nevertheless choose a small enough step-size such that they converge in a neighborhood of

[1] Let $\mathcal{M}$ and $\mathcal{N}$ be symplectic. Then $(\mathcal{M}\mathcal{N})^T\mathcal{J}(\mathcal{M}\mathcal{N}) = \mathcal{N}^T(\mathcal{M}^T\mathcal{J}\mathcal{M})\mathcal{N} = \mathcal{N}^T\mathcal{J}\mathcal{N} = \mathcal{J}$. □

[2] Technically, these would be called *explicit* integrators, since they depend exclusively on the system's current state to iterate it. The more expensive implicit methods require knowledge of the future for iteration and shall not be used anywhere in this thesis, so we omit the "explicit".

some phase-space point. A consequence of choosing small values for ϵ, however, is that the number of map iterations N that we need to perform in order to approximate long propagation times can be very large, since $N = t/\epsilon$. It would be nice to eliminate terms in the effective hamiltonians in order to get smaller errors for the same ϵ, a procedure that will turn up to be very similar to the normalization of a hamiltonian function mentioned in Subsection 1.4.2. We then need to move on to the theory of higher-order symplectic integrators.

2.1.2 Splitting symplectic integrators: General theory

The reason that rendered the 2-step SSIs developed earlier first-order approximations was that the commutator of potential and kinetic terms did not vanish. There are more clever ways, however, to split the action of ρ_t^H in order to eliminate further orders in the BHC expansion defining the effective hamiltonian. For instance, the BHC series for the split used earlier is

$$\exp(\epsilon X)\exp(\epsilon Y) = \exp(\epsilon Z) \quad \Longrightarrow \quad Z = X + Y + \frac{\epsilon}{2}[X,Y] + \frac{\epsilon^2}{12}\left([X,[X,Y]] + [Y,[Y,X]]\right) + \mathcal{O}(\epsilon^3);$$

But a different splitting can indeed cancel the $[X,Y]$ term due to the commutator's antisymmetry, *e.g.*

$$\begin{aligned}\exp\left(\frac{\epsilon X}{2}\right)\exp(\epsilon Y)\exp\left(\frac{\epsilon X}{2}\right) = \exp(\epsilon Z) \implies Z &= \frac{X}{2} + \frac{X}{2} + Y + \frac{\epsilon}{4}\overbrace{\left([X,Y]+[Y,X]\right)}^{=0} + \mathcal{O}(\epsilon^2) \\ &= X + Y + \frac{\epsilon^2}{6}\left(\frac{[Y,[Y,X]]}{2} + \frac{[X,[Y,X]]}{4}\right) + \mathcal{O}(\epsilon^4)\,,\end{aligned}$$

so that, by simply splitting the flow in three instead of two steps, we obtain a second order SSI. Notice that canceling the $[X,Y]+[Y,X]$ term results in the vanishing of all terms proportional to it, so *all* odd powers of ϵ disappear – this is why the next term is of $\mathcal{O}(\epsilon^4)$. The shear ordering corresponding to this particular splitting, in analogy with (2.3), is

$$\left\{\begin{array}{ll} \text{first} & \begin{cases} q_{i-\frac{2}{3}} = q_{i-1} \\ p_{i-\frac{2}{3}} = p_{i-1} - \left(\frac{\epsilon}{2}\right)\partial_q V(q_{i-1}) \end{cases} \\ \text{second} & \begin{cases} q_{i-\frac{1}{3}} = q_{i-\frac{2}{3}} + \epsilon\,\partial_p F(p_{i-\frac{2}{3}}) \\ p_{i-\frac{1}{3}} = p_{i-\frac{2}{3}} \end{cases} \\ \text{third} & \begin{cases} q_i = q_{i-\frac{1}{3}} \\ p_i = p_{i-\frac{1}{3}} - \left(\frac{\epsilon}{2}\right)\partial_q V(q_{i-\frac{1}{3}}) \end{cases} \end{array}\right. \quad \Longrightarrow \quad \rho_t^H = (\rho^V_{\epsilon/2}\circ\rho^F_\epsilon\circ\rho^V_{\epsilon/2})^N + \mathcal{O}(\epsilon^3) \overset{\text{def}}{\approx} (\rho^{VFV}_\epsilon)^N\,,$$

for $X = X_V$ and $Y = X_F$. The effective hamiltonian for the above splitting algorithm is then

$$\mathcal{H}^{VFV}(q,p) = F + V + \frac{\epsilon^2}{24}\{2F+V,\{F,V\}\} + \mathcal{O}(\epsilon^3) = H(q,p) + \mathcal{O}(\epsilon^2)\,,$$

which corresponds to a second order SSI because the error in energy is of $\mathcal{O}(\epsilon^2)$. Since the effective hamiltonian above only contains even powers of ϵ, it is also symmetric with respect to time-reversal (compare with the hamiltonians in (2.5), which are not). Evidently, we could also have started with a shear in position, ending with $\mathcal{H}^{FVF}$ – in fact, there are clearly infinite ways to split the flow. Given that flows form a group, we can choose any possible splitting by shears

$$\rho_t^H = \rho_{s_1}\circ\rho_{s_2}\circ\cdots\circ\rho_{s_n}\,,$$

as long as the final times match. Since any splitting strategy is valid, we are also left wondering what sort of criterium to use. Yoshida [Yos90] uses the simplest possible prescription that added splittings should cancel further orders in the effective Hamiltonian expansion and showed that 2 and 3-step SSIs can be combined to form integrators of any desired order. These early algorithms, however,

turn out to be inefficient for many degrees of freedom. More recent papers use different splitting prescriptions [MA92] to devise SSIs that are efficient and machine-precise even for many degrees of freedom [BCF$^+$13, TS13]. Interestingly, the number of splittings used is usually very large, since it was shown that a large number of steps can actually render computations surprisingly more efficient due to the path traced by iterated points being smoother [RCV19].

2.1.3 The flow of non-separable hamiltonians

While it may look like the theory devised up to now solves the problem of numerical integration of hamiltonian vector fields, it only works if our hamiltonian function is separable. This is a somewhat significant limitation, since the effective hamiltonians themselves are necessarily non-separable due to the commutators mixing functions of position and momentum. A very clever algorithm recently proposed in [Tao16] deals with non-separable hamiltonians by injecting them in a higher dimensional space in which, surprisingly, they become separable. We proceed to a brief exposition of this method but leave all hard-analysis and error estimates aside (for these, see [Tao16]).

Let our symplectic manifold be the prototype $(\mathbb{R}^{2n}, dQ\wedge dP)$ and $H : \mathbb{R}^{2n} \to \mathbb{R}$ a completely general, smooth hamiltonian function, for which we have Hamilton's equations and initial value problem

$$\imath_{X_H}(dQ \wedge dP) = dH(Q,P) \quad \Longrightarrow \quad \begin{cases} \dot{Q} = \dfrac{\partial H(Q,P)}{\partial P} \\ \dot{P} = -\dfrac{\partial H(Q,P)}{\partial Q} \end{cases} \quad , \qquad (Q,P)\big|_{t=0} = (Q_0, P_0)\,,$$

and as always our variables represent condensed coordinates, *e.g.* $Q = (Q_1, Q_2, \ldots, Q_n)$. The *augmented Hamiltonian* $\mathbb{H}$ is defined as

$$\begin{aligned} \mathbb{H} : \mathbb{R}^{4n} \times \mathbb{R} &\longrightarrow \mathbb{R} \\ \{(q,p,x,y),\omega\} &\longmapsto \mathbb{H}(q,p,x,y;\omega) = H(q,y) + H(x,p) + \omega\left[\frac{(q-x)^2}{2} + \frac{(p-y)^2}{2}\right] \\ &\qquad \stackrel{\text{def}}{=} H_A + H_B + \omega H_C\,. \end{aligned}$$

The parameter ω is a coupling constant whose significance will be postponed. The augmented space is then taken as $(\mathbb{R}^{4n}, dq\wedge dp + dx\wedge dy)$, and we have the augmented initial value problem

$$\imath_{X_{\mathbb{H}}}(dq\wedge dp + dx\wedge dy) = dH_A + dH_B + \omega\, dH_C$$

$$\iff \quad \begin{cases} \dot{q} = \dfrac{\partial \mathbb{H}(q,p,x,y)}{\partial p} = \dfrac{\partial H_A}{\partial p} + \omega(p-y) \\ \dot{p} = -\dfrac{\partial \mathbb{H}(q,p,x,y)}{\partial q} = \dfrac{\partial H_B}{\partial q} - \omega(q-x) \\ \dot{x} = \dfrac{\partial \mathbb{H}(q,p,x,y)}{\partial y} = \dfrac{\partial H_B}{\partial y} - \omega(p-y) \\ \dot{y} = -\dfrac{\partial \mathbb{H}(q,p,x,y)}{\partial x} = \dfrac{\partial H_A}{\partial x} + \omega(q-x) \end{cases} \quad , \quad (q,p,x,y)\big|_{t=0} = (Q_0, P_0, Q_0, P_0)\,.$$

The initial value problem in the augmented space above is simply a *cloning* of the problem in the original space, except for the terms proportional to ω. Since we indeed want the system to be a clone, we must fix $x_t = q_t$ and $y_t = p_t$, so that the terms proportional to ω vanish for the solutions, allowing us to ignore them when dealing with the projections $(q,p,x,y) \longmapsto (q,y)$ and $(q,p,x,y) \longmapsto (x,p)$. The former projections are separable and can be immediately seen as mixed shears in the augmented space, being easily solvable. Take, for instance, the former projection described, for which we have an

initial value problem involving solely $H_A = H(q, y)$:

$$H_A : \begin{cases} \dot{q} = 0 \\ \dot{p} = -\partial_q H(q,y) \\ \dot{x} = +\partial_y H(q,y) \\ \dot{y} = 0 \end{cases} \implies \rho_t^A : \begin{pmatrix} q_t \\ p_t \\ x_t \\ y_t \end{pmatrix} \longmapsto \begin{pmatrix} q_0 \\ p_0 - t\,\partial_q H(q_0, y_0) \\ x_0 + t\,\partial_y H(q_0, y_0) \\ y_0 \end{pmatrix}$$

with $(q, p, x, y) = (q_0, p_0, x_0, y_0) = (Q_0, P_0, Q_0, P_0)$. The flow associated to H_B is, analogously,

$$H_B \implies \begin{cases} \dot{q} = +\partial_p H(x,p) \\ \dot{p} = 0 \\ \dot{x} = 0 \\ \dot{y} = -\partial_x H(x,p) \end{cases} \implies \rho_t^B : \begin{pmatrix} q_t \\ p_t \\ x_t \\ y_t \end{pmatrix} \longmapsto \begin{pmatrix} q_0 + t\,\partial_p H(x_0, p_0) \\ p_0 \\ x_0 \\ y_0 - t\,\partial_x H(x_0, p_0) \end{pmatrix}$$

with the same initial conditions. The initial value problem for H_C can be considered separately and is easily solved analytically:

$$\omega H_C \implies \begin{cases} \dot{q} = \omega(p - y) \\ \dot{p} = -\omega(q - x) \\ \dot{x} = -\omega(p - y) \\ \dot{y} = \omega(q - x) \end{cases} \implies \rho_{t,\omega}^C : \begin{pmatrix} q_t \\ p_t \\ x_t \\ y_t \end{pmatrix} \longmapsto \begin{bmatrix} \begin{pmatrix} q_0 + x_0 \\ p_0 + y_0 \end{pmatrix} + R(\delta) \begin{pmatrix} q_0 - x_0 \\ p_0 - y_0 \end{pmatrix} \\ \begin{pmatrix} q_0 + x_0 \\ p_0 + y_0 \end{pmatrix} + R(\delta) \begin{pmatrix} q_0 - x_0 \\ p_0 - y_0 \end{pmatrix} \end{bmatrix}$$

with

$$R(\delta) = \begin{pmatrix} \cos(\delta) & \sin(\delta) \\ -\sin(\delta) & \cos(\delta) \end{pmatrix}, \qquad \delta = 2\omega t\,.$$

Of course, in the augmented space we must still include the flux generated by H_C, even though we can neglect it when considering the projections. Fixing $t = \epsilon N$, as in the previous subsections, the final flow can be expressed as the 5-step splitting [Str68]

$$\bar{\rho}_\epsilon = \left(\rho_{\epsilon/2}^A \circ \rho_{\epsilon/2}^B \circ \rho_{\epsilon,\omega}^C \circ \rho_{\epsilon/2}^B \circ \rho_{\epsilon/2}^A\right)^N + \mathcal{O}(\epsilon^3)\,, \quad t = \epsilon N\,, \tag{2.6}$$

which as an error of $\mathcal{O}(\epsilon^3)$ in the trajectories, rendering is a second order SSI (higher-order algorithms are presented in [Tao16]). Since the coordinates (x, y) are clones of (q, p), the solution can be projected back to $(\mathbb{R}^{2n}, dQ \wedge dP)$ by either $(q, p, x, y) \longmapsto (q, p)$ or $(q, p, x, y) \longmapsto (x, y)$.

We now stop to describe the role played by ω. Note how ω is the factor that deviates $\mathbb{H}$ from being simply the sum $H_A + H_B$, which in principle should work as well. This type of solution was investigated by Pihajoki in [Pih14], where it was discovered that the solutions obtained by this method diverge for times of $\mathcal{O}(1)$. Pihajoki himself suggests a fix that mixes augmented variables similarly to our term ωH_C, but the gain in convergence had the collateral effect of violating symplecticity. The form of H_C devised by Tao solves all these problems and produces a true symplectic integrator that mixes augmented variables in such a way that divergences are indeed avoided. Unfortunately, the hard analysis regarding error estimates due to varying ω is too intricate to be included here[3]. What is important to us is that we can simply increase ω until convergence in the solutions is attained. Computational cost appears to be independent of ω, as argued by Tao.

2.2 Hamiltonian dynamical systems

Now that we know how to solve the equations of motion, let us bind together flows and geometry, as up to now we have been dealing with flows without paying much attention to the manifold on which

[3] Tao's article [Tao16] is comprised of a single page describing the method and all the rest is dedicated to ω.

they are defined. However, it is clearly necessary to say something about this domain, since it is expected that the same evolution rule will produce very different results depending on whether it is defined *e.g.* on a compact manifold (such as the torus or sphere) or on the plane. This gives rise to the concept of a *system*, which is effectively what we use to model the real world.

Definition 2.2.1. A **hamiltonian system** is the triple (M, ω, ρ_t^H) of a symplectic manifold and a hamiltonian flow. For the prototype $(\mathbb{R}^{2n}, dq \wedge dp)$, we will refer to M as the **phase space**.

Hamiltonian systems are usually defined in terms of the hamiltonian function, not its flow, since each hamiltonian has unique vector field and flow. Here, however, we will deal a lot with SSIs that cannot be rigorously derived from any hamiltonian function, although they are usually linked to δ-perturbed hamiltonians (see Subsection 2.2.2). Defining systems using the evolution law is standard in the theory of dynamical systems, and will make our life much simpler – we already have too many different kinds of continuous and discrete evolution laws in this dissertation. Several other definitions of dynamical systems are possible depending on whether one is focusing on measure-theoretical properties, topology, etc, but we will stick to the one above and usually just state where the flow acts on instead of writing the whole triple.

2.2.1 Continuous flows and discretization

All the theory of Chapter 1 assumed the flow to be continuous, since we always considered time as a real number. In this case there is not much to say except to contextualize what was presented up to now: Starting with a hamiltonian function H defined on M, we define our system of interest. Its flow ρ_t^H can be obtained by integrating its vector field numerically using the theory presented in Section 2.1, where we showed that the approximating numerical algorithms are in fact connected to effective hamiltonians. For 2-step SSIs, for instance, a single continuous hamiltonian gives rise to two discrete hamiltonian systems, depending on the chosen ordering: For the same time-discretization $t = \epsilon N$,

$$(M, \omega, \rho_t^H) \xrightarrow{H \longmapsto \mathcal{H}^{FV}} (M, \omega, (\rho_\epsilon^{FV})^N)$$
$$(M, \omega, \rho_t^H) \xrightarrow{H \longmapsto \mathcal{H}^{VF}} (M, \omega, (\rho_\epsilon^{VF})^N)$$

For small ϵ we evidently have $(M, \omega, (\rho_\epsilon^{FV})^N) \approx (M, \omega, (\rho_\epsilon^{VF})^N) \approx (M, \omega, \rho_t^H)$, but we will soon let ϵ assume arbitrary values. We remind the reader that the discretized flows *cannot* be extracted from the effective hamiltonians, they just "conserve" them (if they converge).

2.2.2 Symplectic integrators as hamiltonian maps

The discretized flows ρ_ϵ^{VF} and ρ_ϵ^{FV} emerged as discrete numerical algorithms used to approximate a continuous hamiltonian flow for small ϵ. However, since they are symplectic for all ϵ, we can consider what happens for arbitrary ϵ. The parameter ϵ, however, does not define a time *per se*, but rather the distance between map iterations. In this context it is then intuitive to interpret ϵ as a *kicking strength*, and since it does not need to be small we will substitute it for the letter T. Since the convergence of the effective hamiltonians depends on us choosing small enough kicking strengths, large T values mean that the discretized flows are no longer obtained from a conserved hamiltonian: They form completely different systems when compared to the one they approximate when T is small.

Example 2.2.2. (The standard map) The 1-parameter family of discrete symplectomorphisms

$$\begin{cases} p_i = p_{i-1} + T \sin(q_{i-1}) \\ q_i = q_{i-1} + T p_i \end{cases}$$

is immediately seen to be a 2-step SSI by considering $F(p) = p^2/2$ and $V(q) = \cos(q)$. It is usually presented in the renormalized form obtained by the substitution $p \longmapsto p/T$, namely

$$\begin{cases} \dfrac{p_i}{T} = \dfrac{p_{i-1}}{T} + T\sin(q_{i-1}) \\ q_i = q_{i-1} + \dfrac{T\,p_i}{T} \end{cases} \quad \Longrightarrow \quad \begin{cases} p_i = p_{i-1} + K\sin(q_{i-1}) \\ q_i = q_{i-1} + p_i \end{cases} \quad , \quad K = T^2\,,$$

such that changes in the kicking strength K only affect the momentum coordinate. The map above was devised by B. Chirikov [Chi79] and forms the standard system, which is usually defined acting on $[0, 2\pi] \times [0, 2\pi]$ or $\mathbb{R} \times [0, 2\pi]$.

Discrete systems like the one above are usually obtained from periodically kicked hamiltonians of the form

$$H_t(q,p) = F(p) + TV(q)\sum_k \delta(t - Tk)\,, \quad k \in \mathbb{N}\,,$$

where the δ function plays the role of creating infinitely strong kinetic kicks at $t = Tk$, and otherwise evolution is free and given by $F(p)$ (usually taken as $p^2/2$). Using the hamiltonian above and manipulating the δ in a formal way, we do arrive at the same expressions as the 2-step SSIs we have been using, but suppress a significant amount of intuition. Besides, the 2-step integrators naturally led us to effective hamiltonians, which play a fundamental role in this dissertation – we then stick to the SSIs and set the kicked hamiltonians aside.

Definition 2.2.3. Discrete flows obtained by considering SSIs for arbitrary kicking strengths are **hamiltonian maps**. In this context we will represent them by the symbol U instead of ρ.

Evidently, these maps are called hamiltonian because they are derived as discretizations of a hamiltonian flow – they are symplectic and present all the characteristics of the flows described in Chapter 1, although adaptations might be necessary. We must, for instance, discretize things that were continuous earlier. As an example, we now show that it is possible to define a lagrangian for each iteration of a hamiltonian map. For this, let's get briefly back to small kicking strengths and choose the time-discretization $t = \epsilon N$ of (1.10), so

$$S_t(q) = \int_0^t d\tau\, L_\tau(q,\dot{q}) = \lim_{\epsilon\to 0}\left\{\sum_{i=0}^{N} L_\tau\left(q_i, \frac{q_i - q_{i-1}}{\epsilon}\right)\epsilon\right\} \approx \sum_{i=0}^{N} L_\tau\left(q_i, \frac{q_i - q_{i-1}}{\epsilon}\right)\epsilon\,,$$

where the approximation gets better as ϵ is decreased and, consequently, N is increased. The discretization above, however, is entirely valid for arbitrary kicking strengths T, although it is no longer an approximation to a continuous integral: It is an *exact* lagrangian for the corresponding hamiltonian map iteration. Therefore, there is a generating function $S_i(q_i, q_{i-1})$ such that, analogously to the continuous case,

$$S_i(q_i, q_{i-1}) = TL_i\left(q_i, \frac{q_{i-1} - q_i}{\epsilon}\right), \quad S(q_0, q_N) = \sum_{i=0}^{N} S_i(q_i, q_{i-1})T$$
$$p_i = \frac{\partial S_i(q_i, q_{i-1})}{\partial q_i}\,, \quad p_{i-1} = -\frac{\partial S_i(q_i, q_{i-1})}{\partial q_{i-1}}\,.$$

It's important to keep in mind that for different shear-orderings we get different lagrangians and actions. For U_T^{FV} and U_T^{VF}, for example, the corresponding actions are not the same, since derivatives are evaluated at different points: For U_T^{VF} we have

$$q_i = q_{i-1} + T\left(\frac{\partial F(p)}{\partial p}\right)_{p=p_i} \quad \Longrightarrow \quad \frac{q_i - q_{i-1}}{T} = \left.\frac{\partial F(p)}{\partial p}\right|_{p=p_i} \tag{2.7}$$

but for U_T^{FV}

$$q_i = q_{i-1} + T\left(\frac{\partial F(p)}{\partial p}\right)_{p=p_{i-1}} \quad \Longrightarrow \quad \frac{q_i - q_{i-1}}{T} = \left.\frac{\partial F(p)}{\partial p}\right|_{p=p_{i-1}}\,. \tag{2.8}$$

N. B.: From now on, every time we talk about hamiltonian maps as dynamical systems we will employ the letter U instead of ρ, *i.e.* every time the parameter ϵ represents more than just an iteration step, but a real kicking strength, it will be written as T and the map will be *e.g.* U_T^{FV} instead of ρ_T^{FV}. This is because we will use several different mappings and flows and we do not want to confuse the reader with the same symbol representing both a physically meaningless numerical discretization algorithm and a real dynamical system. Thus, remember: If we write ρ_ϵ^{FV}, it should be taken as a theoretically void SSI, but U_T^{FV} is a real discrete evolution law with physical significance.

2.2.3 Integrability and chaos

As shown earlier, the hamiltonian maps are associated to effective hamiltonians that may not be conserved for large kicking strengths, opening the door to chaotic behavior. In this section we enumerate some facts of chaotic motion that will be used in the future, without the pretension of covering any *real* chaos theory, *i.e.* we do not talk about symbolic dynamics, topology, ergodicity and mixing, or even really define chaos in a mathematically satisfactory way. The little we need is complicated enough.

In Subsection 1.4.3 we have shown that it is sometimes possible to find a symplectomorphism that allows us to express the flow in terms of action and angle coordinates, defining n-dimensional lagrangian tori in a $2n$-dimensional symplectic manifold. Since tori are compact sets and there is no continuous function that maps open sets to closed sets, the action-angle symplectomorphism will only exist if the flow is restricted to a compact domain. As the flow is stationary when the vector field is null, bounded flows are forced to orbit a point in the manifold.

Definition 2.2.4. A point where the vector field vanishes is a **fixed point**. If the flow in its vicinity is bounded, the fixed point **elliptic** – otherwise it is **hyperbolic** or a **saddle point**.

Saddle points are combinations of hyperbolic and elliptic points and will not be mentioned again, since they do not occur on the plane. Action-angle coordinates can then only exist in the neighbourhood of an elliptic fixed point, a situation already mentioned in Subsection 1.4.3.

Definition 2.2.5. If the action-angle coordinates can be defined *globally*, then the system at hand is said to be **integrable**. Otherwise, it is **chaotic**.

Let us now develop some intuition regarding the definitions given above. Let us start with a 4-dimensional phase space, which although might look like an unintuitive start, is not that bad since we can treat the neighbourhood of an elliptic fixed point as a 2-dimensional torus $\mathbb{T}^2$ – a doughnut. The orbits trace curves on the surface of this torus, having constant actions and angles that are generally very complicated functions of these actions. Take now a specific orbit with its 2 action-angle variables $I = (I_1, I_2)$ and $\nu = (\nu_1, \nu_2)$, respectively. Each pair (I_k, ν_k) defines a circle, and if $\nu_1/\nu_2 \in \mathbb{Q}^n$ the flow eventually closes on itself and the orbit ends up being periodic. If ratio ν_1/ν_2 is irrational, however, the orbit never closes on itself – we call it *quasi-periodic*. Notice that, since the requisite for being periodic is to have rational frequencies, periodic orbits are dense on the torus but have zero measure. Quasi-periodic orbits, however, are clearly a set of full measure.

We now come to the orbits for which action-angle coordinates cannot be found. There are many subtleties regarding concepts like ergodicity, strong and weak mixing, etc, that one is bound to stumble upon while pursuing a precise definition of chaos [dA90]. We will deal with these orbits by exclusion: Chaotic orbits are the ones that, well... are bounded but do not form tori. In numerical simulations they will be impossible to miss – its much easier to see chaos than to properly define it.

Definition 2.2.6. Periodic and quasi-periodic orbits are called **regular**, as opposed to **chaotic**.

We can then contextualize what it means for a system to be integrable: For each and every region of the manifold a flow acts on, action-angle variables can be defined – choose a point, and it will lie on a torus. Since these tori are lagrangian manifolds, we can then state this precisely as: A system is integrable when its invariant tori provide a *lagrangian foliation* of phase space (this term will be important in Chapter 3). Thus, the $2n$-dimensional phase space of a hamiltonian system can be decomposed as a dense, disjoint union of n-dimensional tori. Therefore, a system can only be

integrable if it posseses n conserved actions and, therefore, n quantities invariant with respect to its hamiltonian flow.

Corollary 2.2.7. There is no chaos in 1-dimensional autonomous hamiltonian systems, since their phase space is foliated by inverse images of the hamiltonian function: $M = \sqcup_i H^{-1}(E_i)$.

The corollary above is of extreme importance for us: It states that the SSIs presented earlier, which we promoted to hamiltonian maps, might not be integrable due to the effective hamiltonian failing to be conserved. In fact, this is basically an affirmative: All SSIs obtained from a non-quadratic[4] hamiltonian will have a T-threshold above which they are chaotic, even though the original hamiltonian that generated these SSIs is integrable on the plane[5].

We now include a very brief description of the most important result in the field of classical chaos, the Komolgorov-Arnol'd-Moser (KAM) theorem, which will be mentioned several times in this dissertation and is sure to be addressed in basically any text about chaos. We have already met with invariant tori several times, for which there are action and angle variables describing orbits that might be periodic or quasi-periodic. The question attacked by the KAM theorem is: If I have an integrable system with hamiltonian H_0 and perturb it to create $H_0 + \epsilon H_1$, what happens to my invariant tori? If the perturbation is integrable the answer is trivial: Nothing, since the final system will also be integrable. We are then led to consider non-linear perturbations, for which the KAM theorem states: If the angle variables of your unperturbed orbits, bound to walk over invariant tori, are *irrational enough*, they will stretch and deform but will not be destroyed. Periodic and quasi-periodic orbits that do not fulfill the "irrational enough" condition [HI03], namely the *Diophantine condition* $|r_1\nu_1 + ... + r_n\nu_n| \geq C|k|^{-1-n}$, with $r_i \in \mathbb{Z}$ and C is a constant, will eventually collapse into multi-dimensional Cantor sets (the "cantori" [Per79]). As KAM theory assumes some differentiability of the flow to transform it to a normal form, but neither the Cantor sets nor the tori fulfill them for sufficiently high perturbation strengths ϵ, it is eventually necessary to move to the realm of Aubry-Mather theory, which weakens the assumptions necessary in the KAM domain [Per79]. In the end, the only thing the reader must remember about KAM theory to understand this dissertation is that it is impossible to destroy all invariant tori by perturbing an initially integrable system: Many will be destroyed, but some will always remain or re-form.

Bibliography

[BCF+13] S. Blanes, F. Casas, A. Farrés, J. Laskar, J. Makazaga, and A. Muruad. New families of symplectic splitting methods for numerical integration in dynamical astronomy. *App. Num. Math.*, 68:58, 2013.

[Chi79] B. V. Chirikov. A universal instability of many-dimensional oscillator systems. *Phys. Rep.*, 52:263, 1979.

[dA90] A. M. Ozorio de Almeida. *Hamiltonian Systems: Chaos and Quantization*. Cambridge University Press, 2nd edition, 1990.

[Gut90] M. Gutzwiller. *Chaos in Classical and Quantum Mechanics*. Springer-Verlag, 1990.

[HI03] J. Hubbard and Y. Ilyashenko. A proof of Komolgorov's theorem. *Disc. Cont. Dyn. Sys.*, 4:1, 2003.

[MA92] R. I. McLachlan and P. Atela. The accuracy of symplectic integrators. *Nonlinearity*, 5:541, 1992.

[Per79] I. C. Percival. Variational principles for invariant tori and cantori. *Nonlin. Dyn.*, (57):302, 1979.

[Pih14] P. Pihajoki. Explicit methods in extended phase space for inseparable hamiltonian problems. *Celest. Mech. Dyn. Astron.*, 3:211, 2014.

[RCV19] J. Roulet, S. Choi, and J. Vaníček. Efficient geometric integrators for nonadiabatic quantum dynamics. II. The diabatic representation. *J. Chem. Phys*, 150:204113, 2019.

[Sch88] R. Scharf. The Campbell-Baker-Hausdorff expansion for classical and quantum kicked dynamics. *J. Phys. A: Math. Gen.*, 21:2007, 1988.

[Str68] G. Strang. On the construction and comparison of difference schemes. *SIAM J. Num. An.*, 5:506, 1968.

[Tao16] M. Tao. Explicit symplectic approximation of nonseparable hamiltonians: Algorithm and long time performance. *Phys. Rev. E*, 95:043303, 2016.

[TS13] K. Tselios and T. E. Simos. Optimized fifth order symplectic integrators for orbital problems. *Revista Mexicana de Astronomía y Astrofísica*, 49:11, 2013.

[Yos90] H. Yoshida. Construction of higher order symplectic integrators. *Phys. Lett. A*, 150:162, 1990.

[4] If the hamiltonian is quadratic the SSI is a linear transformation, which cannot be chaotic *and* hamiltonian at the same time. There are non-hamiltonian linear maps that generate chaotic systems, though, like the baker's map or Arnold's cat map [Gut90]. This shows the importance of the system's *domain*: The most boring transformation possible on the plane can be chaotic on the torus.

[5] On the plane, the effective hamiltonians themselves are also integrable – this will be fundamental in Chapter 7.

Chapter 3

Wentzel-Kramers-Brillouin theory

All theory, my dear friend, is gray,
But the golden tree of life springs ever green.

J. W. von Goethe in *Faust, Vol. I*

The quantum mechanical wavefunction is a complex object: at each $q \in \mathbb{R}^n$ and $t \in \mathbb{R}$, we have $\psi_t(q) \in \mathbb{C}^n$. Thus, for every q and t we can write it in polar form

$$\psi_t(q) = A_t(q, \hbar) \exp\left[\frac{iS_t(q,\hbar)}{\hbar}\right], \tag{3.1}$$

where we divide by $\hbar$ in order for the exponential to be dimensionless – this is an early sign that S must be somehow related to a generating function, since $\hbar$ has units of action. Although the ansatz above is valid for every *point*, it might be impossible to find A and S so that it is valid for the whole evolution. Adding to that, we have no idea about how the amplitude and the phase depend on $\hbar$. The Wentzel–Kramers–Brillouin (WKB) approximation assumes quantum mechanics depends smoothly on $\hbar$, allowing one to expand both the amplitude Vand the phase in the ansatz (3.1) in Taylor series. We begin with a quick discussion on quantum mechanics, which is followed by the WKB approximation of stationary states. We then include time-dependence and obtain an expression for the semiclassical propagator in terms of WKB approximations, resulting in the well-known van Vleck formula. Lastly, we introduce the concept of *integral representation*, the fundamental technique in this dissertation, and briefly expose the problem of the semiclassical quantization of chaos.

3.1 Position and momentum in quantum theory

Quantum mechanics, just as its classical equivalent, is concerned with the description of stationary and dynamical processes. In strong contrast to the classical world, however, the equations governing quantum evolution are always linear, implying that chaos is not allowed in the microscopic world. These equations can be written in two equivalent forms associated with the pictures of Schrödinger and Heisenberg: The former places time-dependence on evolving quantum states, while the latter evolves the theory's self-adjoint operators instead. The equations of movement for each picture are

$$\text{Schrödinger equation:} \quad i\hbar\frac{\partial|\psi_t\rangle}{\partial t} = \hat{H}|\psi_t\rangle\,, \quad \hat{H} = \hat{H}^\dagger\,, \quad |\psi_{t\in\mathbb{R}}\rangle \in \mathbb{P}\left(\mathfrak{L}_2\right)$$

$$\text{Heisenberg equation:} \quad i\hbar\left(\frac{d\hat{A}_t}{dt}\right) = -[\hat{H}, \hat{A}_t]\,, \quad \hat{H} = \hat{H}^\dagger\,, \quad \hat{A}_t = \hat{A}_t^\dagger\,.$$

The set $\mathbb{P}(\mathfrak{L}_2)$ is the projectivization of the space of square-integrable functions acting on $\mathbb{R}^n$, representing our space of quantum states – the *kets* (see Appendix C for details). Notice how similar Heisenberg's equation is to Liouville's in (1.6), such that the simple substitution $\{\,,\,\} \longmapsto [\,,\,]/i\hbar$ and the erasing of "hats" formally maps one into the other: This prescription is known as *Dirac* or *canonical*

quantization. It is an incomplete quantization procedure and does not generally provide the correct quantum correspondent of a classical system.

In the Schrödinger picture it is necessary to choose a basis in which to express the kets, which are vectors. Since $\mathfrak{L}_2$ is infinite-dimensional, but also a Hilbert space, it is reflexive and we can define a set of *bras* acting as linear functionals on kets through the inner product of $\mathfrak{L}_2$ [Bar95, BPT15]. The existence of a countable orthonormal basis in $\mathfrak{L}_2$ is also guaranteed due to its separability [BPT15], so there exists a Hamel basis in which any ket can be expanded. In physics, however, it is costumary to deal with position and momentum operators that follow the formal equations

$$\hat{q}|q\rangle = q|q\rangle\,, \qquad \hat{p}|p\rangle = p|p\rangle\,,$$

which do not make any sense in $\mathfrak{L}_2$, since the position and momentum kets are not normalizable. Besides, such kets could never form bases in any Hilbert space, since q is real and a basis in $\mathfrak{L}_2$ must be countable [BPT15].

It is impossible to make sense of position and momentum eigenstates within Hilbert space theory only, and for a rigorous exposition there are two immediate choices: Either formulate quantum mechanics using the spectral theory of self-adjoint operators [Hel08, Mor16], or make sense of position/momentum eigenvectors by leaving (or extending) the safe realm of Hilbert spaces. The latter stategy is more mathematically accessible and involves the use of *rigged Hilbert spaces*, which employ a stronger norm and allow for the incorporation of Schwartz distributions into quantum mechanics [dlM01]. We discuss some fundamentals of a distributional formulation of quantum mechanics in Appendix C, but here we just affirm that the bra-ket formalism *can* be made mathematically rigorous.

We shall employ the usual conventions in physics, which include expressing an arbitraty ket $|\psi\rangle$ in either position or momentum representations as $\langle q|\psi\rangle = \psi(q)$ and $\langle p|\psi\rangle = \widetilde{\psi}(p)$, respectively. These representations are defined as: The position (resp. momentum) representation is the one where each component of the position (momentum) operator acts as a multiplication by a real number, and each component of the momentum (position) operator acts as differentiation with respect to position (momentum). Then, the operators

$$\hat{T}(a,\hat{p}) = \exp\left[\frac{i}{\hbar}\,(a\cdot\hat{p})\right]\,, \qquad \hat{T}(a,\hat{q}) = \exp\left[-\frac{i}{\hbar}\,(a\cdot\hat{q})\right] \tag{3.2}$$

act as the generators of translations by a in the position and momentum representations [Bal08, dA98], respectively:

$$\hat{T}(a,\hat{p})|q\rangle = |q+a\rangle\,, \qquad \hat{T}(a,\hat{q})|p\rangle = |p+a\rangle\,.$$

The inner product used is just a notational convention and means, for instance, $a\cdot\hat{q} \stackrel{\text{def}}{=} a_1\hat{q}_1+...+a_n\hat{q}_n$. The Schrödinger equation itself can be also cast into *e.g.* the position representation, resulting in

$$i\hbar\frac{\partial\langle q|\psi_t\rangle}{\partial t} = \langle q|\hat{H}|\psi_t\rangle \quad\Longleftrightarrow\quad i\hbar\frac{\partial\psi_t(q)}{\partial t} = \hat{H}\left(q, -i\hbar\frac{\partial}{\partial q}\right)\psi_t(q)\,,$$

and [a reformulation of] the Riesz duality implies that $\widetilde{\psi}_t(p)$ can be uniquely obtained as the Fourier transform of $\psi_t(q)$ for all values of t [Bar95].

Another basis commonly used in physics is formed by the eigenvectors of the anihilation operator $\hat{a} \stackrel{\text{def}}{=} (\hat{p}-i\hat{q})/\sqrt{2}$, known as *coherent states*. In the position representation, they are given by

$$\langle q|\alpha\rangle = \left(\frac{1}{\pi\hbar}\right)^{\frac{1}{4}}\exp\left\{-\left(\frac{1}{2}\right)\left[q-\Re(\alpha)\right]^2 + \left(\frac{i\Im(\alpha)}{\hbar}\right)\left[q-\Re(\alpha)\right]\right\}\,, \tag{3.3}$$

and will be used extensively in this dissertation. Just as position and momentum, coherent states can also be interpreted as a distributional basis in the rigged-space formalism, except that they are said to be *over-complete* due to $\langle\alpha|\beta\rangle \neq \delta(\beta-\alpha)$, while for position and momentum the equality holds. The description in terms of the coherent-state basis is known in the mathematical literature as the *Segal-Bargmann representation* [Fol89]. This whole discussion is extended in Appendix C.

3.2 Stationary WKB states

We now proceed to semiclassical mechanics. Time-independent problems in quantum mechanics are rather straightforward, since they depend only on the hamiltonian operator – its just linear algebra (or Sturm-Liouville theory). Time-propagation, however, depends also on the initial state, being generally much more intricate. Looking for eigenvectors, *i.e.* stationary states with respect to time evolution, is therefore a good place to start our semiclassical treatment.

3.2.1 The WKB ansatz

The WKB ansatz for a one-dimensional stationary wavefunction $\psi(q)$ is a modification of (3.1) and takes the form

$$\psi(q) = A(q) \exp\left[\frac{iS(q)}{\hbar}\right],$$

where $A(q)$ and $S(q)$ depend analytically on $\hbar$, but we omit this dependence to simplify notation. The ansatz, therefore, consists of associating each eigenstate to an amplitude and a phase. To characterize them, we introduce this ansatz in the time-independent Schrödinger equation, where we assume a hamiltonian of the form $\hat{H} = \hat{p}^2/2 + \hat{V}(\hat{q})$:

$$\begin{aligned} & \left[\hat{H}(q, -i\hbar\,\partial_q) - E\right]\psi(q) = 0 \\ \iff \quad & \frac{\partial^2\psi(q)}{\partial q^2} - \left[\frac{V(\hat{q}) - E}{\hbar^2}\right]\psi(q) = 0 \\ \iff \quad & -\frac{\hbar}{2}\left[AS'' + 2A'S' + \hbar A''\right] + \left\{\frac{1}{2}\left(S'\right)^2 + (V - E)\right\} = 0\,. \end{aligned}$$

Through the identification $p = \partial S/\partial q = S'$, the term within curly brackets is immediately recognized as the time-independent Hamilton-Jacobi equation of Subsection 1.4.1, placing a strong requirement on the function $S(q)$: it must be an admissible[1] generating function for the lowest order $\mathcal{O}(\hbar^0)$. We assume this is the case and get rid of the curly brackets, proceeding to the square bracket term. For a solution valid up to $\mathcal{O}(\hbar^2)$, we ignore the last term and obtain

$$AS'' + 2A'S' = 0\,,$$

known as the *homogeneous transport equation* [BW12]. It is trivially solved in the one-dimensional case:

$$AS'' + 2A'S' = 0 \quad \iff \quad \left(A^2S'\right)' = 0 \quad \implies \quad A = C\left(S'\right)^{-\frac{1}{2}}, \quad C \in \mathbb{C}\,, \tag{3.4}$$

from which we see that the quantity A^2S' is conserved. In higher dimensions this derivative is a divergence, and the homogeneous transport equation ends up being the time-independent continuity equation $\nabla(\rho\,\zeta) = 0$, with $p = S'$ and $\zeta = A^2$ representing the velocity field and the density, respectively. Since the density A^2 is conserved, we must have the Radon-Nikodym [Bar95] derivative

$$\frac{\sqrt{dq}}{\sqrt{dp}} = \frac{\widetilde{A}(p)}{A(q)}\,,$$

a strong indicative that WKB theory should actually be formulated in terms of half-densities instead of densities [BW12, GS12], especially because of difficulties that occur due to lagrangian manifolds changing orientation. In physics, however, the square-roots are usually taken care of by using a change of coordinates in an integral form of the condition for amplitude conservation:

$$\begin{aligned} \int_{\mathbb{R}^n} dq\, A^2(q) = \int_{\mathbb{R}^n} dp\, \widetilde{A}^2(p) \quad & \iff \quad \int_{\mathbb{R}^n} dq\, A^2(q) = \int_{\mathbb{R}^n} dq\, \left|\det\left(\frac{\partial p}{\partial q}\right)\right| \widetilde{A}^2(p) \\ & \iff \quad A^2(q) = \left|\det\left(\frac{\partial p}{\partial q}\right)\right| \widetilde{A}^2(p) \\ & \iff \quad A(q) = \left|\det\left(\frac{\partial^2 S(q)}{\partial q^2}\right)\right|^{\frac{1}{2}} \widetilde{A}(p) \end{aligned}$$

[1] For the meaning of *admissible*, see Definition 1.4.2.

We can easily see a source of trouble in (3.4): If $S' = p = 0$, the approximation diverges, forming the well-known *classical turning points*, where the potential energy becomes equal to the total energy:

$$\begin{aligned} H(q,p) = \frac{p^2}{2} + V(q) \quad &\implies \quad p = \pm\sqrt{2\left[H(q,p) - V(q)\right]} \\ p = 0 \quad &\iff \quad V(q) = H(q,p)\,, \end{aligned}$$

This divergence is not limited to the expansions's truncation at $\mathcal{O}(\hbar)$. To see this, assume $A = A_0$ as in (3.4) is the $\mathcal{O}(\hbar^0)$ term in the A series and proceed to the next order in $\hbar$, namely A_1. The result follows from an equivalent computation to that of A_0 and reads

$$\begin{aligned} \left[\hat{H}(q, -i\hbar\,\partial_q) - E\right]\left[(A_0 + \hbar A_1)\exp\left(\frac{iS}{\hbar}\right)\right] = 0 \\ \iff \quad A_1 S'' + 2A'S' = iA_0''\,, \end{aligned}$$

where we have ignored an $\mathcal{O}(\hbar^3)$ term (and assumed S to be admissible and to satisfy the homogeneous transport equation). It is clear that each term A_k in the $\hbar$-series of A can be obtained recursively as

$$A_k S'' + 2A_k' S' = iA_{k-1}''\,,$$

with A_0 as A in (3.4). The equation above is known as the *inhomogeneous transport equation*. Notice that a blow up in A_0 is reflected in all orders of A.

3.2.2 Polarizations and classical turning points

The classical return points, where $\partial_q S(q) = 0$, clearly depend on the chart we use to describe $S(q)$ – we could have simply chosen the use a momentum chart instead. There is nothing wrong with the generating function itself nor with its lagrangian manifold: It is the *projection* to the position axis that was problematic. As a generating function, S can be expressed in a completely coordinate-independent form as $S = \int \alpha$, so that

$$\omega = dq \wedge dp = -d\alpha \quad \implies \quad \begin{cases} \alpha &= p\,dq \\ \alpha &= -q\,dp \\ \alpha &= \frac{1}{2}(p\,dq - q\,dp) \\ \vdots &= \quad \vdots \end{cases}, \tag{3.5}$$

where we can run from one chart to the other through the Legendre transforms of Section 1.4. A general solution for α is easily found, since

$$\omega = -d\alpha \quad \iff \quad \alpha = f(q,p)\,dq + g(q,p)\,dp \quad \implies \quad -d\alpha = \left(\frac{\partial g}{\partial p} - \frac{\partial f}{\partial q}\right) dq \wedge dp\,,$$

such that if we have a general $\alpha = f(q,p)\,dq + g(q,p)\,dp$ it will be a primitive for ω iff $\partial_p g - \partial_q f = 1$. Notice this places no restriction on the derivatives of $\partial_q g$ and $\partial_p f$, such that there is indeed an infinite number of non-trivial local expressions for α. We will, however, focus on the first two possibilities in (3.5), for which we have the generating functions[2]

$$dS(q) = p \cdot dq \quad \implies \quad p = \frac{\partial S(q)}{\partial q}\,, \qquad \text{and} \qquad d\widetilde{S}(p) = -q \cdot dp \quad \implies \quad q = -\frac{\partial \widetilde{S}(p)}{\partial p}\,, \tag{3.6}$$

corresponding to the lagrangian submanifolds $(q, \partial_q S(q))$ and $(-\partial_p \widetilde{S}(p), p)$, which are embedded in a chart symplectomorphic to $(\mathbb{R}^{2n}, dq \wedge dp)$. Since both $S(q)$ and $\widetilde{S}(p)$ are homeomorphisms, we have then obtained two ways of potentially decomposing a symplectic manifold as graphs of generating functions described in terms of either position or momentum charts.

Definition 3.2.1. A decomposition of a symplectic manifold M as the disjoint union of lagrangian submanifolds is a **lagrangian foliation**. Each element in the foliation is a **lagrangian leaf**. The different possible parametrizations of leaves are called **polarizations**[3].

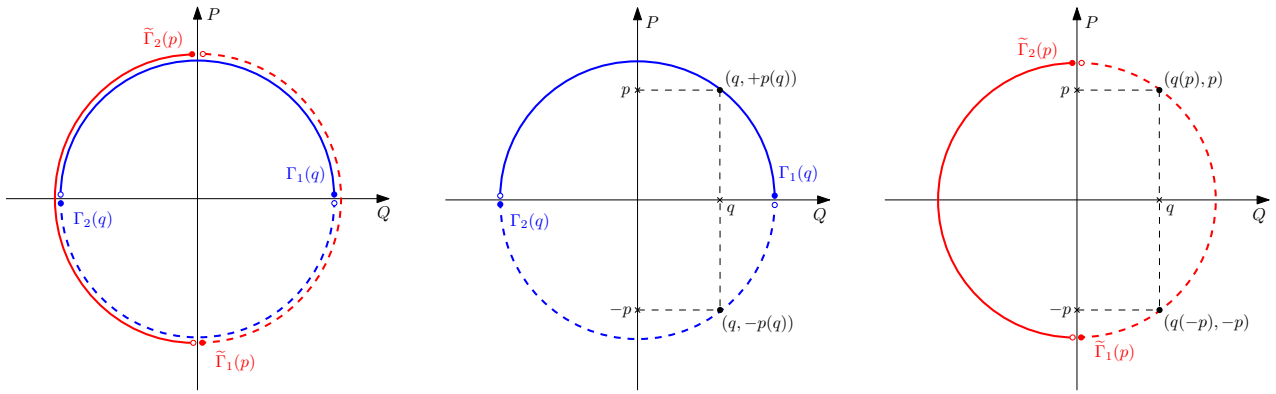

(a) Branches of $S(q)$ and $\widetilde{S}(p)$

(b) A point is described in two charts using $S(q)$.

(c) The same point is in a single chart of $\widetilde{S}(p)$.

Figure 3.1: The geometry of lagrangian graphs for the SHO. (a) Here, we see that the branches of $S(q)$ and $\widetilde{S}(p)$ are glued at different points in phase space, which are exactly where the classical turning points are defined. (b,c) A point that requires two charts in the graph of a generating function is always parametrized by a single chart for a description in terms of its Legendre transform.

Example 3.2.2. (The SHO): The one-dimensional simple harmonic oscillator was defined in Example 3.3.1 by the hamiltonian $H(q,p) = p^2/2 + q^2/2$, with $(q,p) \in \mathbb{R}^2$. The pre-image $H^{-1}(E)$ of any $E \in \mathbb{R}$, *i.e.* each lagrangian leaf, is a circle and is parametrized by at least two charts. A position polarization can be chosen by noticing that we can solve for momentum as $p = \pm\sqrt{2H(q,p) - q^2}$, expressing the branches of $S(q)$ as the charts $\Gamma_1(q) = (q, +p(q))$ and $\Gamma_2(q) = (q, -p(q))$. The position can be isolated as well, giving $q = \pm\sqrt{2H(q,p) - p^2}$, and forming the momentum polarization with branches $\widetilde{\Gamma}_1(p) = (+q(p), p)$ and $\widetilde{\Gamma}_2(p) = (-q(p), p)$, this time of $S(p)$. Fig. 3.1(a) depicts a leaf in which it is obvious that we change charts in position and momentum polarizations at different points, *i.e.* they failure at different regions, allowing for the interchange of descriptions near a classical turning point. In Fig. 3.1(b) we show a point that needs two position charts might need only one for its momentum equivalent, shown in Fig. 3.1(c). ⁂

The choice of a polarization corresponds to expressing the WKB ansatz as either

$$\psi(q) = A(q) \exp\left[\frac{iS(q)}{\hbar}\right] \qquad \text{or} \qquad \widetilde{\psi}(p) = \widetilde{A}(p) \exp\left[\frac{i\widetilde{S}(p)}{\hbar}\right], \tag{3.7}$$

which correspond to the position and momentum representations of $|\psi\rangle$. As we saw earlier, we have

$$S(q) = \int p \cdot dq \qquad \text{and} \qquad \widetilde{S}(p) = -\int q \cdot dp\,,$$

and using (3.6), we have the concomitant equalities for the arbitrary vector field X:

$$\begin{cases} d\alpha = 0 \implies dS = p \cdot dq \implies dS(X) = 0 \iff dq(X) = 0 \\ d\alpha = 0 \implies d\widetilde{S} = -q \cdot dp \implies d\widetilde{S}(X) = 0 \iff dp(X) = 0 \end{cases},$$

which are mutually valid iff we have the null vector field $X = 0$ or $\alpha = 0$, the latter being generally impossible, since it would imply $\omega = 0$ everywhere. This means that whenever we have a caustic in $S(q)$, we necessarily *do not* have a caustic in $\widetilde{S}(p)$. The position and momentum polarizations are, therefore, "semiclassically conjugate", in the sense that each point in a symplectic manifold can be described in a divergence-less manner by employing either polarizations: We just need to change from one to the other near a classical turning point.

[2]The notation $dS(q)$ used here does *not* mean that we evaluate the differential on a field q. It's just notation to distinguish choices of generating functions, representing the coordinates with respect to which we can differentiate.

[3]This is not the usual meaning of "polarization" found in geometric quantization. Here, the term is used as the semiclassical equivalent of "representation" in quantum mechanics (see (3.7)).

3.2.3 Stationary phase approximations and semiclassical superposition

We can then use the Fourier transform to express the WKB ansatz in momentum polarization as

$$\widetilde{\psi}(p) = \int dq\, \psi(q) \exp\left(-\frac{ip\cdot q}{\hbar}\right) = \int dq\, A(q) \exp\left(\frac{i}{\hbar}[-p\cdot q + S(q)]\right), \tag{3.8}$$

where, as discussed in Chapter 1, the phase is just the momentum generating function due to the Legendre duality $dS(p) = d[-p\cdot q + S(q)]$. The integral above is exact, but our WKB approximations are not. Just as we have done for the Schödinger equation, we are interested in an expansion in $\hbar$. The integrals above display highly oscillatory behavior for large actions due to the sine and cosine in the complex exponential, so that most contributions to the complete integral end up being canceled when the numerator and denominator in the phase are not numerically close. An approximation to the full integral as a sum around the regions $p\cdot q - S(q) \approx \hbar$ is, therefore, believed to be a good one – in fact, it has errors of the same order as the WKB ansatz itself with respect to $\hbar$ (see Appendix D).

Definition 3.2.3. The approximation of (3.8) based on the smallness of $\hbar$ when compared to $S(q)$, *i.e.* based on considering the non-oscillatory contributions arising from $p\cdot q - S(q) \approx \hbar \approx 0$, is a **stationary phase approximation** (SPA).

We sketch a bit of the theory concerning these integrals in Appendix D. Here, we just present the result of performing a SPA in (3.8) away from a turning point in momentum space,

$$\widetilde{\phi}(p) = \sum_j A(q^{(j)}) \left|\det\left[\frac{\partial^2 S(q)}{\partial q^2}\right]_{q=q^{(j)}}\right|^{\frac{1}{2}} \exp\left(\frac{i}{\hbar}[-p\cdot q^{(j)} + \widetilde{S}(q^{(j)})]\right) \exp\left(\frac{\pi\hbar\,\widetilde{\alpha}_j}{4}\right), \tag{3.9}$$

where the index j runs over all the critical points of $-p\cdot q + \widetilde{S}(q)$ and

$$\widetilde{\alpha} = \text{sign}\left\{\det\left[\frac{\partial^2 S(q)}{\partial q^2}\right]_{q=q^{(j)}}\right\}$$

is the signature of $\partial_q^2 \widetilde{S}$, *i.e.* its number of positive minus negative eigenvalues. The critical points $q^{(j)}$ over which we are summing satisfy, for each p in the domain of $\widetilde{\phi}$,

$$\frac{\partial}{\partial q}\left[p\cdot q - S(q)\right]\Big|_{q=q^{(j)}} = 0 \quad\Longrightarrow\quad \frac{\partial S(q)}{\partial q}\Big|_{q=q^{(j)}} = p \quad\Longrightarrow\quad \mathfrak{p}(q^{(1)}) = \mathfrak{p}(q^{(2)}) = \cdots = p\,, \tag{3.10}$$

where $\mathfrak{p} \overset{\text{def}}{=} \partial_q S(q)$. As shown earlier, there are as many such positions *per leaf* as there are charts needed to parametrize the leaf itself. Formula (3.9) is then telling us that to move from the position to the momentum polarization we must sum over all branches of $\widetilde{S}(p)$, since each branch defines a different critical point $q^{(j)}$. For hamiltonians expressed in the form $F(p) + q^2/2$, each lagrangian leaf in the momentum polarization has only two branches, but if we allow for more complicated dependence on q it might be impossible to isolate the positions, *i.e.* to find analytically which branches need to be included in (3.9).

Definition 3.2.4. The process of looking for the branches to be included in the WKB wavefunction is called **root-searching**.

In physics literature it is standard to skip this ruminative step, where we interpret what effectively comes out of the SPA, and just write it as a sum over the branches of $\widetilde{S}(p)$,

$$\widetilde{\phi}(p) = \sum_j A^{(j)}(p) \exp\left(\frac{i}{\hbar}\left[\widetilde{S}^{(j)}(p) + \frac{\pi\hbar\,\widetilde{\alpha}_j}{4}\right]\right)$$

which we now know to be equivalent to (3.9) due to each fixed momentum p being associated to several critical positions $q^{(j)}$ through (3.10), and each position defining a corresponding branch of

$\widetilde{S}(p)$. Mathematically, this is just a sum over branches, but if we interpret this from a physical point of view, we see that the SPA allowed us to write a momentum wavefunction as a *sum* of several WKB ansätze. In the semiclassical wavefunctions associated to a lagrangian submanifold, the embedded generating function's multiple branches *superpose*, meaning that WKB wavefunctions should be able to reproduce quantum interference patterns – even though they are completely based on classical quantities.

In our reasoning, we have started from the position polarization. However, there is no preference with respect to which polarization to use, so we could just as well have started with momentum. The SPA would then be performed in an inverse-Fourier transform with phase $p\cdot q+\widetilde{S}(p)$, so the end result includes a sum over all momenta that fulfill the boundary condition $q=-\partial_p\widetilde{S}(p)$, resulting this time in a sum over the branches of $S(q)$. Thus, the general form of the WKB wavefunction in the position polarization is also a sum over branches:

$$\phi(q)=\sum_j A^{(j)}(q)\exp\left(\frac{i}{\hbar}\left[S^{(j)}(q)+\frac{\pi\hbar\,\alpha^{(j)}}{4}\right]\right),$$

with boundary conditions necessary for each q in the domain of ϕ:

$$\frac{\partial}{\partial p}\left[p\cdot q+\widetilde{S}(p)\right]\Big|_{q=q^{(j)}}=0 \quad\Longrightarrow\quad \frac{\partial\widetilde{S}(p)}{\partial p}\Big|_{p=p^{(j)}}=-q \quad\Longrightarrow\quad \mathfrak{q}(p^{(1)})=\mathfrak{q}(p^{(2)})=\cdots=q\,,$$

where $\mathfrak{q}\overset{\text{def}}{=}-\partial_p\widetilde{S}(p)$. Analogously to the momentum case, hamiltonians of the form $p^2/2+V(q)$ generate lagrangian leafs that have only two branches in the position polarization. The SHO of Example 3.2.2 is therefore *very* special, since its leafs in both the momentum and position polarizations have the same number of branches.

3.3 Time-dependent WKB theory

Extending the previous section's results to time-dependent WKB wavefunctions happens to be rather intuitive, but with the added complication that the root-searching of the earlier section now takes place in a product manifold.

3.3.1 WKB wavefunctions in extended phase space

Classically, allowing the WKB ansätze in (3.7) to acquire time-dependence is tantamount to formulating a semiclassical theory in the extended product manifold: Since our phases and amplitudes will be functions of initial and final positions and momenta, with generating functions that can depend on them in all sorts of ways, the background manifold should be $\rho_t(M)\times M$ – which is lagrangian, as have seen in Chapter 1. This manifold, when extended, was shown in Sec. 1.4 to be naturally associated with Poincaré-Cartan integral invariants. If we ignore how the wavefunctions depend on positions and momenta and just allow phases and amplitudes to be time-dependent, *i.e.*

$$\phi_t(q)=A_t(q)\exp\left[\frac{iS_t(q)}{\hbar}\right] \qquad\text{and}\qquad \widetilde{\phi}_t(p)=A_t(p)\exp\left[\frac{iS_t(p)}{\hbar}\right], \tag{3.11}$$

Schödinger's equation with $\hat{H}=\hat{p}^2/2+\hat{V}(\hat{q})$ gives, for $\phi_t(q)$,

$$\begin{aligned}
&\left[\hat{H}(q,-i\hbar\,\partial_q)-\partial_t\right]\psi_t(q)=0\\
\iff\quad &\frac{\partial^2\psi_t(q)}{\partial q^2}-\frac{1}{\hbar^2}\left[V(\hat{q})-\frac{\partial}{\partial t}\right]\psi(q)=0\\
\iff\quad &-\frac{\hbar}{2}\left\{\frac{\partial(A_t^2)}{\partial t}+\frac{\partial}{\partial q}\left[A_t^2\left(\frac{\partial S}{\partial q}\right)\right]+\hbar\left(\frac{\partial^2 A_t}{\partial q}\right)\right\}+\left\{\frac{1}{2}\left(\frac{\partial S}{\partial q}\right)^2+\left(V-\frac{\partial S_t}{\partial t}\right)\right\}=0\,.
\end{aligned}$$

Ignoring the $\mathcal{O}(\hbar^2)$ term we obtain the continuity equation for $\rho = A_t^2$ in its full form for $\mathcal{O}(\hbar)$ as a requisite,

$$\frac{\partial(A_t^2)}{\partial t} + \frac{\partial}{\partial q}\left[A_t^2\left(\frac{\partial S}{\partial q}\right)\right] = 0\,, \tag{3.12}$$

together with the time-dependent Hamilton-Jacobi equation

$$H\left(\hat{q}, -i\hbar\frac{\partial S_t}{\partial q}\right) + \frac{\partial S_t}{\partial t} = 0\,,$$

which selects admissible generating functions only – now time-dependent. As time-evolution is a result of classical evolution of positions and momenta from (q,p) to $(q',p') = \rho_t(q,p)$, the generating functions are precisely the Poincaré-Cartan forms for position and momentum:

$$S_t(q',q) = -\int_q^{q'} p\cdot dq - \int_0^t dt\, H(q,p)\,, \qquad \widetilde{S}_t(p',p) = \int_p^{p'} q\cdot dp - \int_0^t dt\, H(q,p)\,, \tag{3.13}$$

$$\frac{\partial S_t(q',q)}{\partial q'} = p'\,, \quad \frac{\partial \widetilde{S}_t(q',q)}{\partial q} = -p\,, \qquad \frac{\partial \widetilde{S}_t(p',p)}{\partial p'} = q'\,, \quad \frac{\partial \widetilde{S}_t(p',p)}{\partial p} = -q\,, \tag{3.14}$$

which can be interpreted as *pure* position/momentum polarizations. This is due to the fact that in the present product manifold we can also employ the *mixed* polarizations formed by the graphs of $S_t(q',p)$ and $S_t(p',q)$, obtained via Legendre transformations of the above[4]. We can then rewrite (3.11) using explicit dependencies in the initial and final positions/momenta in the pure polarizations as

$$\phi_t(q',q) = A_t(q',q)\exp\left(\frac{i}{\hbar}S_t(q',q)\right)\,, \qquad \widetilde{\phi}_t(p',p) = \widetilde{A}_t(p',p)\exp\left(\frac{i}{\hbar}\widetilde{S}_t(p',p)\right)\,,$$

where (q,p) and (q',p') are the position and momentum at $t=0$ and $t=t$, namely $(q',p') = \rho_t(q,p)$. To relate the two polarizations in (3.13) we can use Fourier transforms[5] with respect to p and p':

$$\begin{aligned}\widetilde{\phi}_t(p',p) &= \int dq'dq\,\phi_t(q',q)\exp\left[\frac{i}{\hbar}\left(-p'\cdot q' + p\cdot q\right)\right] \\ &= \int dq'dq\,A_t(q',q)\exp\left[\frac{i}{\hbar}\left(S_t(q',q) - p'\cdot q' + p\cdot q\right)\right]\,,\end{aligned}$$

which, evaluating using an SPA with respect to q, gives

$$\widetilde{\phi}_t(p',p) \approx \int dq' \sum_{\text{roots}} A_t(q',q)\left|\det\left(\frac{\partial^2 S_t(q',q)}{\partial q^2}\right)\right|^{-\frac{1}{2}}\exp\left[\frac{i}{\hbar}\left(S_t(q',q) - p'\cdot q' + p\cdot q\right) - \frac{i\pi\alpha}{4}\right]\,, \tag{3.15}$$

where α is the signature of $\partial_q^2 S$. The stationary condition on the phase implies, as expected, that we must sum over all initial positions $q^{(j)}$ such that

$$\begin{aligned}\frac{\partial}{\partial q}\left\{S_t(q',q) - p'\cdot q' + p\cdot q\right\} = 0 \quad &\Longrightarrow \quad \left.\frac{\partial S_t(q',q)}{\partial q}\right|_{q=q^{(j)}} = -p \\ &\Longleftrightarrow \quad \mathfrak{p}(q',q^{(1)}) = \mathfrak{p}(q',q^{(2)}) = ... = p\,,\end{aligned} \tag{3.16}$$

with $\mathfrak{p} \stackrel{\text{def}}{=} -\partial_q S_t(q',q)$, so that we must sum over all initial positions with initial momentum p. Now, since the integral in (3.15) is convergent with respect to q', we can perform a second SPA with respect to the final positions:

$$\begin{aligned}\widetilde{\phi}_t(p',p) \approx \sum_{\text{more roots}} A_t(q',q)\left|\det\left(\frac{\partial^2 S_t(q',q)}{\partial q^2}\right)\right|^{-\frac{1}{2}}\left|\det\left(\frac{\partial^2 S_t(q',q)}{\partial q'^2}\right)\right|^{-\frac{1}{2}} \\ \exp\left[\frac{i}{\hbar}\left(S_t(q',q) - p'\cdot q' + p\cdot q\right) + \frac{i\pi(\widetilde{\alpha}' - \widetilde{\alpha})}{4}\right]\,,\end{aligned} \tag{3.17}$$

[4]These are associated to the so called *Kirkwood representations* [Kir33, BJ84].

[5]These enter with different signs due to initial and final coordinates having opposing signs in (3.14), which have to be recovered in the SPA (see (3.16)).

where the stationary phase condition gives the more substantial root-search

$$\begin{aligned}\frac{\partial}{\partial q'}\left\{S_t(q',q)-p'\cdot q'-p\cdot q\right\}=0 \quad &\Longrightarrow \quad \left.\frac{\partial S_t(q',q)}{\partial q'}\right|_{q'=q'^{(j)}}=p' \\ &\Longleftrightarrow \quad \mathfrak{p}'(q'^{(1)},q)=\mathfrak{p}(q'^{(2)},q)=...=p'\,,\end{aligned}$$

with $\mathfrak{p}' \stackrel{\text{def}}{=} -\partial_{q'}S_t(q',q)$, which filters (3.16) and states that it is not enough to just sum over all initial positions: We must sum over initial positions that connect p and p' *at the same time*. Notice that, since $\mathfrak{p}'(q,p)=p$, this can be parametrized in terms of initial variables: Coming briefly back to explicit time-dependencies, the roots $\mathfrak{p}'=\mathfrak{p}_t$ fulfill

$$\mathfrak{p}_t(q_0,p_0)=p_t\,, \qquad \mathfrak{p}_0(q_0,p_0)=p_0\,. \tag{3.18}$$

Due to the "nice" properties of WKB wavefunctions, there are several identities that can be employed in order to simplify the expression (3.17). First, notice that amplitude conservation (3.12) implies

$$\begin{aligned}A_t^2(q',q)\left|\det\left(\frac{\partial^2 S_t(q',q)}{\partial q^2}\right)\right|^{-1}\left|\det\left(\frac{\partial^2 S_t(q',q)}{\partial q'^2}\right)\right|^{-1} &= A_t^2(q',q)\left|\det\left(\frac{\partial p(q)}{\partial q}\right)\right|^{-1}\left|\det\left(\frac{\partial p'(q')}{\partial q'}\right)\right|^{-1} \\ &= \widetilde{A}_t^2(p',p)\,.\end{aligned}$$

Secondly, the combined sets of roots imply that we must sum over all initial and final momenta that fulfill (3.18), but just as in the time-independent case, there are as many such momenta as there are branches in $\widetilde{S}_t(p',p)$, so the sum over roots is really only a sum over the branches $\widetilde{S}_t^{(j)}(p',p)$. Thirdly, since we can transition between generating functions using Legendre transforms, we quickly identify the phase in (3.17) as

$$S_t(q',q)-p'\cdot q'+p\cdot q=\widetilde{S}_t(p',p)\,. \tag{3.19}$$

Lastly, we shall write the signature difference as

$$\frac{\widetilde{\alpha}}{4}-\frac{\widetilde{\alpha}'}{4}=\frac{\widetilde{\kappa}}{2}\,, \tag{3.20}$$

which we justify in Section 3.3.3. The final expression for $\widetilde{\phi}_t(p',p)$ is, therefore [Lit91, Gut90, dA90],

$$\widetilde{\phi}_t(p',p)=\sum_j \widetilde{A}_t^{(j)}(p',p)\exp\left(\frac{i}{\hbar}\left[\widetilde{S}_t^{(j)}(p',p)-\frac{\hbar\pi\widetilde{\kappa}^{(j)}}{2}\right]\right)\,,$$

running over the j branches of $\widetilde{S}_t(p',p)$ or, equivalently, all the trajectories fulfilling the boundary conditions (3.18). The accuracy of this wavefunction is completely dependent on how many such trajectories are included in the sum.

Just as in the time-independent case, we have started with the position polarization without any particular reason. The exact same procedure applied to $\widetilde{\phi}(p',p)$ results in the WKB wavefunction in position polarization:

$$\phi_t(q',q)=\sum_j A_t^{(j)}(q',q)\exp\left(\frac{i}{\hbar}\left[S_t^{(j)}(q',q)-\frac{\hbar\pi\kappa^{(j)}}{2}\right]\right)\,, \tag{3.21}$$

where the sum over branches of $S_t(q',q)$ is equivalent to the boundary conditions

$$\left.\frac{\partial\widetilde{S}_t(p',p)}{\partial p'}\right|_{p'=p'^{(j)}}=-q'\,, \quad \left.\frac{\partial\widetilde{S}_t(p',p)}{\partial p}\right|_{p=p^{(j)}}=q \quad \Longleftrightarrow \quad \mathfrak{q}_t(q_0,p_0)=q_t\,, \quad \mathfrak{q}_0(q_0,p_0)=q_0\,,$$

where in the last equation we parametrized the root-search in terms of initial variables, obtaining the equivalent to (3.18). Naturally, $\mathfrak{q}_0=\mathfrak{q}\stackrel{\text{def}}{=}\partial_p\widetilde{S}_t(p',p)$ and $\mathfrak{q}_t=\mathfrak{q}'\stackrel{\text{def}}{=}-\partial_{p'}\widetilde{S}_t(p',p)$.

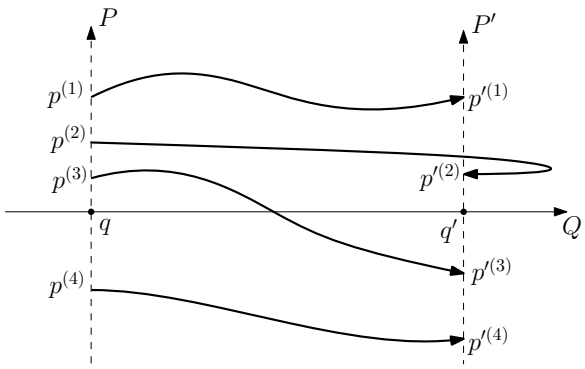

Figure 3.2: Several different trajectories start at q and end at q' for the same time-interval t. This is only possible because they all have different initial momenta and the underlying dynamics is non-linear.

Example 3.3.1. (The SHO) As seen in Example , for the SHO we have

$$\begin{pmatrix} q' \\ p' \end{pmatrix} = \begin{pmatrix} \cos t & \sin t \\ -\sin t & \cos t \end{pmatrix} \begin{pmatrix} q \\ p \end{pmatrix} .$$

Imagine two solutions, $\mathfrak{q}_t^1(q,p)$ and $\mathfrak{q}_t^2(q,p)$, which fulfill $\mathfrak{q}_t^1(q,p^1) = \mathfrak{q}_t^2(q,p^2) = q'$. This amounts to

$$q' = q\cos t + p_1 \sin t = q\cos t + p_2 \sin t \quad \Longleftrightarrow \quad p_2 - p_1 = 0\,.$$

Thus, for the SHO there is only a single solution that connects q to q' (this is true for any linear flow – see Proposition B.1.1).

3.3.2 The van Vleck–Gutzwiller propagator

The quantum propagator provides a general algorithm for obtaining solutions to the Schrödinger equation: Instead of solving for a specific initial state, it allows us to represent the evolution of any initial wavefunction as an integral. Evidently, we need to choose a particular representation, *e.g.*

$$\begin{aligned}
\langle q|\psi_t\rangle = \langle q|\hat{U}_t|\psi_0\rangle &= \int_{\mathbb{R}^n} dQ\, \langle q|\hat{U}_t|Q\rangle\langle Q|\psi_0\rangle = \int_{\mathbb{R}^n} dQ\, \mathcal{K}_t(q,Q)\psi_0(Q) \\
&= \int_{\mathbb{R}^n} dP\, \langle q|\hat{U}_t|P\rangle\langle P|\psi_0\rangle = \int_{\mathbb{R}^n} dQ\, \mathcal{K}_t(q,P)\psi_0(P)\,; \\
\langle p|\psi_t\rangle = \langle p|\hat{U}_t|\psi_0\rangle &= \int_{\mathbb{R}^n} dP\, \langle p|\hat{U}_t|P\rangle\langle P|\psi_0\rangle = \int_{\mathbb{R}^n} dP\, \mathcal{K}_t(p,P)\psi_0(P) \\
&= \int_{\mathbb{R}^n} dQ\, \langle p|\hat{U}_t|Q\rangle\langle Q|\psi_0\rangle = \int_{\mathbb{R}^n} dQ\, \mathcal{K}_t(p,Q)\psi_0(Q)\,,
\end{aligned}$$

and, of course, many more types of representations are also possible, corresponding to different polarizations when considered semiclassically. Since the propagator in the position representation is the kernel

$$\mathcal{K}_t(q,q') = \langle q|\hat{U}_t|q'\rangle\,,$$

if we consider q' to be just q, then $\hat{U}_t|q\rangle$ corresponds semiclassically to the final position at time t. Then, an interesting interpretation for the propagator follows [Lit91]: Let q and q' be the position at $t = 0$ and $t = t$, respectively. Then for a short time $t = \epsilon$, we have

$$\lim_{\epsilon\to 0^+} \mathcal{K}_\epsilon(q,q') = \delta(q'-q)\,,$$

such that we obtain a simple way of thinking about the propagator: For $t > 0$, $\mathcal{K}_t(q,q')$ is the solution $\psi_t(q')$ of the time-dependent Schrödinger equation subject to the initial condition $\psi_0 = \delta(q'-q)$. If we can find a semiclassical expression for the evolved Dirac's delta $\delta(q'-q)$, we can obtain the final semiclassical wavefunction from the simple integral

$$\psi_t(q') = \int dq\, \mathcal{K}_t(q,q')\psi_0(q) = \int dq\, \delta(q'-q)\psi_0(q)\,.$$

One can immediately see a problem with looking for a representation of a Dirac's delta in the position polarization: It is singular and doesn't exist. However, as we have already seen that divergences in one polarization do not spoil the others, we can employ mixed or the momentum polarizations[6] in order to represent $\delta(q'-q)$.

We start by writing some distributional properties of $A_t(q',q)$ under coordinate changes leading to mixed polarizations. First, notice we can define the mixed amplitude and phase $A_t(q,p')$ and $S_t(q,p')$ using the conservation of amplitudes and Legendre transforms:

$$A_t(q,p') = A_t(q,q')\left|\det\left(\frac{\partial q'}{\partial p'}\right)\right|^{\frac{1}{2}}, \qquad S(q,p') = S(q,q') - p'\cdot q'\,. \tag{3.22}$$

Since the amplitude is also invariant with respect to time-evolution,

$$A_t^2(q,p')\,dp' = A_0^2(q,p)\,dp \quad\Longrightarrow\quad A_0(q,p) = A_t(q,p')\left|\det\left(\frac{\partial p'}{\partial p}\right)\right|^{\frac{1}{2}}, \tag{3.23}$$

and $S_t(q,p)$ is just $S_0(q,p')$. Combining (3.22) and (3.23) we have an expression for $A_t(q',q)$ in terms of the mixed polarization (q,p):

$$A_t(q,q') = A_0(q,p)\left|\det\left(\frac{\partial p}{\partial q'}\right)\right|^{\frac{1}{2}}.$$

To understand why this polarization is appropriate, we notice that the final position q' is a function of q and p:

$$q' = q'(q,p)\,, \quad q'(q,p)\big|_{t=0} = q\,,$$

so $\delta(q'-q) = \delta(q'(q,p)-q)$, with $\delta(q'(q,p)-q)_{t=0} = \delta(0)$. Since $p'(q,p)_{t=0} = p$, we can use the Fourier expression

$$\begin{aligned}\lim_{t\to 0}\left[\delta(q'(q,p)-q)\right] &= \lim_{t\to 0}\left[\left(\frac{1}{2\pi\hbar}\right)^{\frac{n}{2}}\int_{\mathbb{R}^n} dp'\,\exp\left\{\frac{i}{\hbar}\left[p'\cdot(q'(q,p)-q)\right]\right\}\right]\\ &\equiv \lim_{t\to 0}\left\{A_t(q,p')\exp\left[\frac{i}{\hbar}S_t(q,p')\right]\right\}\\ &= A_0(q,p)\,.\end{aligned}$$

That is, in order to identify the first and second lines in the equations above, all we have to do is to fix $A_0(q,p) = 1/(2\pi\hbar)^{n/2}$, since the phase vanishes. Substituting these results into (3.21):

$$\begin{aligned}\delta(q'-q) &= \sum_j A_t^{(j)}(q,q')\exp\left(\frac{i}{\hbar}\left[S_t^{(j)}(q',q) - \frac{\hbar\pi\kappa^{(j)}}{2}\right]\right)\\ &= \exp\left(\frac{i\pi\alpha_0}{4}\right)\sum_j A_0^{(j)}(q,p)\left|\det\left(\frac{\partial p}{\partial q'}\right)\right|_j^{\frac{1}{2}}\exp\left(\frac{i}{\hbar}\left[S_t^{(j)}(q,q') - \frac{\hbar\pi\kappa^{(j)}}{2}\right]\right)\\ &= \exp\left(\frac{i\pi\alpha_0}{4}\right)\left(\frac{1}{2\pi\hbar}\right)^{\frac{n}{2}}\sum_j\left|\det\left(\frac{\partial^2 S^{(j)}(q,q')}{\partial q'\partial q}\right)\right|^{\frac{1}{2}}\exp\left(\frac{i}{\hbar}\left[S_t^{(j)}(q,q') - \frac{\hbar\pi\kappa^{(j)}}{2}\right]\right),\end{aligned}$$

although we do not yet know the initial signature α_0, which stands for the number of positive minus negative eigenvalues of the mixed hessian of $S_t(q,p')$ at $t=0$. Since

$$\lim_{t\to 0}\left\{\frac{\partial^2 S_t(q,p')}{\partial q\,\partial p'}\right\} = -\lim_{t\to 0}\left\{\frac{\partial q'}{\partial q}\right\},$$

[6]The classic paper dealing with this subject, namely [Lit91], employs the pure momentum polarization, while here we use the shorter path provided by mixed polarizations.

the initial eigenvalues are all negative and equal to -1, and since the dimension of the hessian above is n, there are n negative eigenvalues. Substituting $\exp(i\pi\alpha_0/4) = \exp(-i\pi n/4)$, we arrive at our final result:

$$\mathcal{K}_t^{\mathrm{vV}}(q,q') = \left(\frac{1}{2\pi i\hbar}\right)^{\frac{n}{2}} \sum_j \left|\det\left(\frac{\partial^2 S^{(j)}(q,q')}{\partial q'\partial q}\right)\right|^{\frac{1}{2}} \exp\left(\frac{i}{\hbar}\left[S_t^{(j)}(q,q') - \frac{\hbar\pi\kappa^{(j)}}{2}\right]\right), \tag{3.24}$$

where we have defined the propagator $\mathcal{K}_t^{\mathrm{vV}}(q,q')$ as the WKB expression for the Dirac's delta distribution $\delta(q'-q)$, q' being interpreted as a final position: $q' = q_t$, $q = q_0$.

Definition 3.3.2. The semiclassical propagator in (3.24) is known as the **van Vleck[-Gutzwiller] propagator**, the **primitive propagator** or sometimes simply as **"the" semiclassical propagator**.

Even though the van Vleck propagator beautifully intertwines classical and quantum mechanics, it suffers from the taxing root-search problem that we have described in the previous sections. Even when an efficient algorithm to select trajectories is devised, one is still faced with the task of dealing with the several divergences that are bound to happen when

$$\frac{\partial q'}{\partial p} \longrightarrow 0 \quad\Longleftrightarrow\quad \frac{\partial p'}{\partial q} \longrightarrow \pm\infty \quad\Longleftrightarrow\quad \frac{\partial^2 S_t(q',q)}{\partial q'\partial q} \longrightarrow \pm\infty\,. \tag{3.25}$$

Definition 3.3.3. The points where the second derivatives of the action fulfill (3.25) are **caustics**.

As can be seen, caustics are a generalization of the classical turning points of Section 3.2, and are completely dependent on which polarization we chose: Classical turning points in momentum are not the same as in position (see Fig. 3.1), allowing us to interchange polarizations when nearing a caustic occurring for a particular one – a technique we employed several times before. Using Airy functions, it is possible to express the propagator as a *uniform approximation*, rendering it convergent over a caustic [BM72], but as soon as the second caustic is reached it breaks down and needs to be modified – it is a local method. Since we would like a solution that not only globally avoids infinities, but is also independent of the root-search procedure, more elaborate methods need to be devised. Before developing these new methods, however, we stop for a moment to understand what are these divergences plaguing the van Vleck propagator.

3.3.3 Monodromy matrices, caustics and the Maslov index

Double derivatives of generating functions have persistently appeared in semiclassical amplitudes – for now, they appear one at a time, but will emerge simultaneously for propagators more intricate than van Vleck's. As we have done earlier, we can rewrite these double derivatives as a single derivative of final coordinates with respect to initial ones, *e.g.*

$$\frac{\partial^2 S(q,q')}{\partial q'\,\partial q} = \left(\frac{\partial q'}{\partial p}\right)^{-1}, \qquad \frac{\partial^2 \widetilde{S}(p,p')}{\partial p'\,\partial p} = \left(\frac{\partial p'}{\partial q}\right)^{-1},$$

etc. We employ again the notation $q' \equiv q_t$ and $q \equiv q_0$ in order to explicitly include time dependence, so a propagated phase-space point x_0 is brought to $x_t = \rho_t(x_0)$, where ρ_t is the hamiltonian flow. The derivatives of the action can be condensed in the matrix

$$\mathcal{M}_t(x_0) = \left.\frac{d\rho_t(x)}{dx}\right|_{x=x_0} = \left.\frac{dx_t}{dx}\right|_{x=x_0} = \left(\begin{array}{cc} \dfrac{\partial q_t(q,p)}{\partial q} & \dfrac{\partial q_t(q,p)}{\partial p} \\ \dfrac{\partial p_t(q,p)}{\partial q} & \dfrac{\partial p_t(q,p)}{\partial p} \end{array}\right)_{(q,p)=(q_0,p_0)}. \tag{3.26}$$

Definition 3.3.4. The matrix $\mathcal{M}_t$ above is the **monodromy matrix**.

Since the flow obeys $\dot\rho_t(x) = X_H[\rho_t(x)] = \mathcal{J}H'[\rho_t(x)]$ and ρ_t is of class C^∞, by the chain rule we have

$$\frac{d\mathcal{M}_t(x)}{dt} = \frac{d}{dt}\left\{\frac{d\rho_t(x)}{dx}\right\} = \frac{d}{dx}\left[\dot\rho_t(x)\right] = \mathcal{J}H''\left[\rho_t(x)\right]\left(\frac{d\rho_t(x)}{dx}\right),$$

where H' and H'' are the jacobian and the hessian of H, respectively. Thus, the monodromy matrix satisfies the linear differential equation

$$\dot{\mathcal{M}}(x_t) = \mathcal{J}H''(x_t)\mathcal{M}(x_t)\,.$$

Since the monodromy matrix can be identified as the first order term in an expansion of the flow around x_0 and the flow is a symplectomorphism, the monodromy is clearly a symplectic matrix.

The monodromy terms appeared due to performing integrals *via* the SPA, together with their signatures in the phase. In (3.20) we expressed the signature difference after crossing a caustic as a multiple of 2, which we now justify and expand. We first state the basic result from linear algebra that if a $2n$-dimensional matrix A is invertible, then the number of its positive and negative eigenvalues is equal to the dimension of the space: Denoting the number of positive and negative eigenvalues by ν_+ and ν_-, respectively, we have $2n = \nu_+ + \nu_- \implies \mathrm{sign}(A) = 2(n - \nu_-)$. The difference in signatures after crossing a caustic, where A becomes singular, is then given by $\kappa = \mathrm{sign}(A) - \mathrm{sign}(A') = 2(\nu'_- - \nu_-)$, which is why we took κ to be an even number. Consider now the evaluation of eigenvalues along a curve: Every time ν'_- increased by 1 we must have ν_- decreasing by 1, since the dimension is an invariant. This reflects in κ as $2(\nu'_- - \nu_-) = 2[(\nu'_- + 1) - (\nu_- - 1)] = 2(\nu'_- - \nu_-) + 4$, meaning that $\kappa = 2(\nu'_- - \nu_-)$ is actually an equivalence class with 4 elements [dG06], *i.e.* $[\kappa] \in \{0, 1, 2, 3\}$. Since the value of κ increases by one at each caustic and we begin at $\kappa = 0$, what this index is effectively doing is counting how many caustics we have passed along a particular curve on a lagrangian manifold *modulo* 4 – but the exponential is also an equivalence class with 4 elements:

$$\exp\left(\frac{i\pi\kappa}{2}\right) \in \{1, i, -1, -i\}\,, \forall \kappa \in \mathbb{Z}\,,$$

so we can interpret κ as the exact caustic count along a curve, since when it crosses 4 caustics both the equivalent class $[\kappa]$ and the exponential reset to their initial values.

Definition 3.3.5. The index κ, measuring the number of caustics crossed in a particular direction along a lagrangian submanifold, is the **Maslov index**.

The arguments presented above are focused on a particular direction, but are general due to van Vleck's propagator being a sum over trajectores, which are curves. The disjoint union of these curves reconstructs the full evolving lagrangian manifold – they are 1-dimensional lagrangian leaves , after all.

3.3.4 Integral representation for the van Vleck propagator

The semiclassical propagator in (3.24) is seldom considered on its own, being usually employed in calculations as a kernel:

$$\langle\psi|\hat{U}_t|\phi\rangle = \int_{\mathbb{R}^{2n}} dq\, dq'\, \langle\psi|q\rangle\langle q|\hat{U}_t|q'\rangle\langle q'|\psi\rangle \approx \int_{\mathbb{R}^{2n}} dq\, dq'\, \mathcal{K}_t^{\mathrm{vV}}(q, q')\psi^*(q)\phi(q')\,,$$

where the q and q' variables are classically connected in the sense that at $t = 0$ the system is at q, while at $t = t$ it is at q'. The semiclassical propagator includes a sum over all trajectories connecting $q \longleftrightarrow q'$ for the fixed time t, indexed by initial momenta. Substituting the van Vleck propagator (3.24) in the equation above,

$$\langle\psi|\hat{U}_t|\phi\rangle \approx \left(\frac{1}{2\pi i\hbar}\right)^{\frac{n}{2}} \int_{\mathbb{R}^{2n}} dq\, dq' \sum_j \left|\det\left(\frac{\partial^2 S_t^{(j)}(q', q)}{\partial q \partial q'}\right)\right|^{\frac{1}{2}} \exp\left(\frac{i}{\hbar}\left[S_t^{(j)}(q', q) - \frac{\hbar\pi\kappa^{(j)}}{2}\right]\right)\psi^*(q)\phi(q')\,, \tag{3.27}$$

As q' is a function of initial positions and momenta, we can write (3.27) with explicit dependencies as

$$\langle\psi|\hat{U}_t|\phi\rangle \approx \left(\frac{1}{2\pi i\hbar}\right)^{\frac{n}{2}} \int_{\mathbb{R}^{2n}} dq\, dq'(q, p) \sum_j \left|\det\left(\frac{\partial q'(q, p)}{\partial p}\right)\right|^{-\frac{1}{2}}_{p=p^{(j)}} \times \exp\left(\frac{i}{\hbar}\left[S_t(q'(q, p^{(j)}), q) - \frac{\hbar\pi\kappa^{(j)}}{2}\right]\right)\psi^*(q)\phi(q')\,. \tag{3.28}$$

At this point we invoke an observation made by Heller [TH91], although in a slightly different context: The sum over roots takes place on a set of initial momenta $p^{(j)}$, which is a subset of all momenta defined in $\mathbb{R}^n$. The condition for a root p to be selected, namely $\mathfrak{q}'(q,p) - q' = 0$, can be written in terms of Dirac's delta distribution as

$$\delta(\mathfrak{q}'(q,p) - q')\,,$$

with q fixed, so that every time the variable p runs over $p = p^{(j)}$, the corresponding trajectory is selected. This appears very clearly when integrating the equation above:

$$\int dp\,[\delta(\mathfrak{q}'(q,p) - q')] = \int d\mathfrak{q}' \left|\det\left(\frac{\partial \mathfrak{q}'(q,p)}{\partial p}\right)\right|^{-1} \delta(\mathfrak{q}'(q,p) - q') = \sum_j \left|\det\left(\frac{\partial q'}{\partial p}\right)\right|^{-1}_{p=p^{(j)}}\,.$$

Even more importantly, notice that the calculations above immediately imply

$$\int dp \left|\det\left(\frac{\partial \mathfrak{q}'(q,p)}{\partial p}\right)\right|^{\frac{1}{2}} \delta(\mathfrak{q}'(q,p) - q') = \sum_j \left|\det\left(\frac{\partial q'}{\partial p}\right)\right|^{-\frac{1}{2}}_{p=p^{(j)}}\,, \tag{3.29}$$

which is a well-behaved integral since the amplitude is never singular. This nice expression for the root-search can be substituted in (3.28) to give

$$\begin{aligned}\langle\psi|\hat{U}_t|\phi\rangle \approx \left(\frac{1}{2\pi i\hbar}\right)^{\frac{n}{2}} \int_{\mathbb{R}^{2n}} dq\,dp\,dq'(q,p) \left|\det\left(\frac{\partial \mathfrak{q}'(q,p)}{\partial p}\right)\right|^{\frac{1}{2}} \delta(\mathfrak{q}'(q,p) - q') \\ \times \exp\left(\frac{i}{\hbar}\left[S_t(\mathfrak{q}'(q,p),q) - \frac{\hbar\pi\kappa}{2}\right]\right)\psi^*(q)\phi(\mathfrak{q}'(q,p))\,,\end{aligned}$$

which, integrating with respect to q' but writing the final variable as $q' = q'(q,p)$, results in [Mil01]

$$\langle\psi|\hat{U}_t|\phi\rangle \approx \left(\frac{1}{2\pi i\hbar}\right)^{\frac{n}{2}} \int_{\mathbb{R}^{2n}} dq\,dp \left|\det\left(\frac{\partial q'}{\partial p}\right)\right|^{\frac{1}{2}} \exp\left(\frac{i}{\hbar}\left[S_t(q',q) - \frac{\hbar\pi\kappa}{2}\right]\right)\psi^*(q)\phi(q')\,. \tag{3.30}$$

What is accomplished in the expression above is one of the benchmark achievements in the history of semiclassical mechanics: Besides substituting the root search by an integral, the diverging amplitude in the van Vleck propagator is inverted and now, instead of blowing up, converges to zero at a caustic.

Definition 3.3.6. A semiclassical algorithm that represents propagation as an integral is an **integral representation**, and if the integral is a function of initial variables such as (3.30), it is called an **Initial Value Representation (IVR)**. If it had used final variables, we would call it a **Final Value Representation (FVR)**.

3.3.5 The Herman-Kluk propagator

Naturally, there are multiple representations from which we can extract expressions such as (3.30), and we can transition between them through Fourier and Legendre transforms as usual. Consider, for instance, expressing the wavefunctions in the momentum representation:

$$\psi^*(q) = \left(\frac{1}{2\pi\hbar}\right)^{\frac{n}{2}} \int_{\mathbb{R}^n} d\mathfrak{p}\,\exp\left[\left(\frac{i}{\hbar}\right)\mathfrak{p}\cdot q\right]\widetilde{\psi}^*(\mathfrak{p})\,,\quad \phi(q') = \left(\frac{1}{2\pi\hbar}\right)^{\frac{n}{2}} \int_{\mathbb{R}^n} dq'\exp\left[-\left(\frac{i}{\hbar}\right)\mathfrak{p}'\cdot q'\right]\widetilde{\phi}(\mathfrak{p}')\,,$$

and substitute them in (3.30) to get

$$\langle\psi|\hat{U}_t|\phi\rangle \approx \left(\frac{i^{-\frac{1}{3}}}{2\pi\hbar}\right)^{\frac{3n}{2}} \int_{\mathbb{R}^{4n}} dq\,dp\,d\mathfrak{p}\,d\mathfrak{p}' \left|\det\left(\frac{\partial q'}{\partial p}\right)\right|^{\frac{1}{2}} \exp\left(\frac{i}{\hbar}\left[S_t(q',q) - \mathfrak{p}'\cdot q' + \mathfrak{p}\cdot q\right]\right)\widetilde{\psi}^*(\mathfrak{p})\,\widetilde{\phi}(\mathfrak{p}')\,,$$

where we have neglected the Maslov index κ, which will soon reemerge in a new form. As in (3.19), we recognize the generating function in the phase as $\widetilde{S}_t(\mathfrak{p}',\mathfrak{p})$, and performing the change of coordinates

$p \longmapsto q'(q,p)$ we have

$$\begin{aligned}\langle\psi|\hat{U}_t|\phi\rangle &\approx \left(\frac{i^{-\frac{1}{3}}}{2\pi\hbar}\right)^{\frac{3n}{2}} \int_{\mathbb{R}^{4n}} dq\, dq'\, d\mathfrak{p}\, d\mathfrak{p}' \left|\det\left(\frac{\partial p}{\partial q'}\right)\right| \left|\det\left(\frac{\partial q'}{\partial p}\right)\right|^{\frac{1}{2}} \exp\left(\frac{i}{\hbar}\left[\widetilde{S}_t(\mathfrak{p}',\mathfrak{p})\right]\right) \widetilde{\psi}^*(\mathfrak{p})\, \widetilde{\phi}(\mathfrak{p}') \\ &= \left(\frac{i^{-\frac{1}{3}}}{2\pi\hbar}\right)^{\frac{3n}{2}} \int_{\mathbb{R}^{4n}} dq\, dq'\, d\mathfrak{p}\, d\mathfrak{p}' \left|\det\left(\frac{\partial q'}{\partial p}\right)\right|^{-\frac{1}{2}} \exp\left(\frac{i}{\hbar}\left[\widetilde{S}_t(\mathfrak{p}',\mathfrak{p})\right]\right) \widetilde{\psi}^*(\mathfrak{p})\, \widetilde{\phi}(\mathfrak{p}')\,.\end{aligned}$$

We can now perform SPAs with respect to q and q' to obtain

$$\langle\psi|\hat{U}_t|\phi\rangle \approx \left(\frac{1}{2\pi i\hbar}\right)^{\frac{n}{2}} \int_{\mathbb{R}^{2n}} d\mathfrak{p}\, d\mathfrak{p}' \sum_j \left|\det\left(\frac{\partial \mathfrak{p}'}{\partial q}\right)\right|_j^{-\frac{1}{2}} \exp\left(\frac{i}{\hbar}\left[\widetilde{S}_t^{(j)}(\mathfrak{p}',\mathfrak{p}) - \frac{\hbar\pi\widetilde{\kappa}^{(j)}}{2}\right]\right) \widetilde{\psi}^*(\mathfrak{p})\, \widetilde{\phi}(\mathfrak{p}')\,, \tag{3.31}$$

which is just the propagator expressed in terms of the momentum polarization for van Vleck's propagator and we have reintroduced the Maslov index in momentum polarization, $\widetilde{\kappa}$, and performed the sum over roots as in (3.18). Using the same trick as in (3.29), we finally get the momentum IVR

$$\langle\psi|\hat{U}_t|\phi\rangle \approx \left(\frac{1}{2\pi i\hbar}\right)^{\frac{n}{2}} \int_{\mathbb{R}^{2n}} dq\, dp \left|\det\left(\frac{\partial q'}{\partial p}\right)\right|^{\frac{1}{2}} \exp\left(\frac{i}{\hbar}\left[\widetilde{S}_t(p',p) - \frac{\hbar\pi\widetilde{\kappa}}{2}\right]\right) \widetilde{\psi}^*(p)\, \widetilde{\phi}(p')\,.$$

Evidently, we could have also derived the result above starting from the momentum expression for (3.24), which appeared naturally in (3.31). What if we had not chosen the momentum representation? We could, in principle, use the Segal-Bargmann transforms of $\psi(q)$ and $\phi(q)$ (see Appendix C), namely

$$\psi(q) = \langle q|\psi\rangle \propto \int_{\mathbb{C}^n} d\alpha\, \alpha(q)\psi(\alpha)\,, \qquad \phi(q') = \langle q'|\psi\rangle \propto \int_{\mathbb{C}^n} d\alpha'\, \alpha'(q')\phi(\alpha')\,,$$

with static and dynamic coherent states

$$\begin{aligned}\alpha(q) &\propto \exp\left\{-\frac{|q-\Re(\alpha)|^2}{2} + \frac{i\Im(\alpha)}{\hbar}\cdot[q-\Re(\alpha)]\right\} \\ \alpha'(q') &\propto \exp\left\{-\frac{|q'-\Re(\alpha')|^2}{2} + \frac{i\Im(\alpha')}{\hbar}\cdot[q'-\Re(\alpha')]\right\}.\end{aligned}$$

This is equivalent to looking for an expression for the semiclassical propagator in a coherent-state basis. The final expression would look like

$$\langle\psi|\hat{U}_t|\phi\rangle \approx\!\!\!\!\!\propto \int_{\mathbb{R}^{4n}} dq\, dq'\, d\alpha\, d\alpha' \left|\det\left(\frac{\partial q'}{\partial p}\right)\right|^{-\frac{1}{2}} \exp\left(\frac{i}{\hbar}\left[\Phi\right]\right) \psi^*(\alpha)\, \phi(\alpha')\,,$$

where

$$\Phi = S_t(q',q) + \left(\frac{i\hbar}{2}\right)|q-\Re(\alpha)|^2 + \left(\frac{i\hbar}{2}\right)|q'-\Re(\alpha')|^2 + \Im(\alpha)\cdot[q-\Re(\alpha)] - \Im(\alpha')\cdot[q'-\Re(\alpha')]\,.$$

This integral appears in a different context in [HK], and is evaluated by performing stationary phase approximations with respect to q and q'. The stationary phase conditions on the phase are then

$$\begin{aligned}\frac{S_t(q',q)}{\partial q} + i\hbar[q-\Re(\alpha)] + \Im(\alpha) = 0 \quad &\Longleftrightarrow \quad \Im(\alpha) - p + i\hbar[q-\Re(\alpha)] = 0 \\ \frac{S_t(q',q)}{\partial q'} + i\hbar[q'-\Re(\alpha')] - \Im(\alpha') = 0 \quad &\Longleftrightarrow \quad -\Im(\alpha') + p' + i\hbar[q'-\Re(\alpha')] = 0\,,\end{aligned}$$

which fix the form of the coherent states in a way that integrating with respect to *e.g.* $d\alpha$ is equivalent to $dq\, dp$: The difficulty of moving to a higher dimensional complex space is only apparent, since even though we are integrating over complex trajectories, they have their form fixed based on real boundary

conditions. The determinants arising from the SPAs, further jacobians and coordinate changes are analysed in [HK] and the final integral is expressed as

$$\langle\psi|\hat{U}_t|\phi\rangle \approx \left(\frac{1}{2\pi\hbar}\right)^{\frac{n}{2}} \int_{\mathbb{R}^{2n}} dq\, dp \left|\det\left(\frac{\partial\alpha'}{\partial\alpha}\right)\right|^{\frac{1}{2}} \exp\left(\frac{i}{\hbar}\left[S_t(q,p)\right]\right) \alpha(q)\,\alpha'(q')\,\psi^*(q)\,\phi(q')\,, \quad (3.32)$$

with the determinant in the pre-factor easily calculated as

$$\det\left(\frac{\partial\alpha'}{\partial\alpha}\right) \equiv \det\left(\frac{\partial\alpha_t}{\partial\alpha_0}\right) = \det\left\{\frac{1}{2}\left[\left(\frac{\partial p_t}{\partial p_0}+\frac{\partial q_t}{\partial q_0}\right)+i\left(\frac{1}{\hbar}\frac{\partial p_t}{\partial q_0}-\hbar\frac{\partial q_t}{\partial p_0}\right)\right]\right\}.$$

Notice the primed variables are all functions of the unprimed ones, *e.g.* $q' = q'(q,p) \equiv q_t(q_0,p_0)$. Also, since the linear complexification does not change the value of the classical action[7], the phase is still the integral of the lagrangian with respect to time.

Definition 3.3.7. The propagator in (3.32) is the **Herman-Kluk propagator**.

Notice that the Herman-Kluk propagator has a complex amplitude, which cannot be zero due to the symplecticity of the monodromy matrix (see Appendix B). This amplitude, however, changes branch in the complex plane as time evolves, and it was shown by Kay that tracking the branch that renders the amplitude continuous with respect to time evolution is equivalent to obtaining the correct Maslov phase across a caustic [Swe11, Kay94, dLC16].

The Herman-Kluk propagator has received a considerable amount of criticism, *e.g.* it was argued that it cannot be obtained as a semiclassical approximation to a coherent state propagator due to a missing factor [BdAK$^+$01]; [DE06], however, establishes a connection between this factor and a linearization. In [Kay94] a derivation from first principles is attempted based on the non-bijective nature of the Bargmann transform, *i.e.* on the over-completeness of the coherent state basis, but then a multitude of equivalent propagators is possible and it is not clear why this particular expression would be anything special – which it is, because other options supposed to be equivalent to it are not as accurate. By formulating WKB theory in the Segal-Bargmann representation, the final word on the subject of whether or not the HK propagator is derivable as an asymptotic approximation appears to have been written [MFL06], but why it is so much accurate than other semiclassical propagators is still a mystery [Kay93].

3.4 Integrability and chaos in WKB theory

The WKB method exposes a deep connection between quantum mechanics and classical generating functions and, therefore, the lagrangian submanifolds they define. In Chapter 2 we have shown that for integrable systems the generating functions give rise to tori, from which we extract the lagrangian foliations required by WKB to mimic quantum representations. It is important to remember that these tori are *invariant*, *i.e.* they remain still under the action of the flow, and can be quantized directly using time-independent WKB theory – although in this context it is usually called Einstein-Brillouin-Keller (EBK) theory. When we do not have a complete foliation by tori, the leaves associated to chaotic orbits will not form invariant sets: These leaves evolve in time, such that summing over their branches becomes generally impossible. If we have graphs composed *exclusively* of such leaves (dubbed as *hard chaos*), we can use the connection between ergodicity and Random Matrix Theory (RMT) to obtain some information about our system. However, if time-evolving leaves are intertwinned with invariant tori (the so called *soft chaos* scenario), neither EBK nor RMT theories are applicable.

The time-dependent scenario, however, is considerably simpler: We do not need to sum over branches, so we can simply ignore the fact that our lagrangian submanifolds can have extremely complicated evolutions. As we only need to sum over *trajectories*, the only clear impeditive for the application of semiclassical methods to quantum propagation is the tangling of classical orbits in regions smaller than h. As is well known in the field [TH91], this turns out to be a weak impeditive, and chaotic orbits are frequently successfully employed in semiclassical propagation – although for how long they should work remains an open problem [STH92].

[7] The mapping taking the position and momentum basis to the coherent-state basis is a linear complexification and conserves the canonical form – see Appendix B.

Bibliography

[Bal08] L. E. Ballentine. *Quantum Mechanics: A Modern Development*. World Scientific, 2008.

[Bar95] R. G. Bartle. *The Elements of Integration and Lebesgue Measure*. Wiley-Interscience, 1st edition, 1995.

[BdAK+01] M. Baranger, M. A. M. de Aguiar, F. Keck, H. J. Korsch, and B. Schellhaaß. Semiclassical approximations in phase space with coherent states. *J. Phys. A: Math. Theor.*, 34:7227, 2001.

[BJ84] N. L. Balazs and B. K. Jennings. Wigner's function and other distribution functions in mock phase spaces. *Phys. Rep.*, 104:347, 1984.

[BM72] M. V. Berry and K. E. Mount. Semiclassical approximations in wave mechanics. *Rep. Prog. Phys.*, 35:315, 1972.

[BPT15] G. Botelho, D. Pellegrino, and E. Teixeira. *Fundamentos de Análise Funcional*. SBM, 2nd edition, 2015.

[BW12] S. Bates and A. Weinstein. *Lectures on the Geometry of Quantization*. draft, 2012.

[dA90] A. M. Ozorio de Almeida. *Hamiltonian Systems: Chaos and Quantization*. Cambridge University Press, 2nd edition, 1990.

[dA98] A. M. Ozorio de Almeida. The Weyl representation in classical and quantum mechanics. *Phys. Rep.*, 295:265, 1998.

[DE06] S. A. Deshpande and G. Ezra. On the derivation of the Herman-Kluk propagator. *J. Phys. A: Math. Theor.*, 39:5067, 2006.

[dG06] M. de Gosson. *Symplectic Geometry and Quantum Mechanics*. Birkhauser, 2006.

[dLC16] G. di Liberto and M. Ceotto. The importance of the pre-exponential factor in semiclassical molecular dynamics. *J. Chem. Phys.*, 145:144107, 2016.

[dlM01] R. de la Madrid. *The role of the rigged Hilbert space in Quantum Mechanics*. draft, 2001.

[Fol89] G. B. Folland. *Harmonic Analysis in Phase Space*. Princeton University Press, 1989.

[GS12] V. Guillemin and S. Sternberg. *Semi-classical analysis*. draft, 2012.

[Gut90] M. Gutzwiller. *Chaos in Classical and Quantum Mechanics*. Springer-Verlag, 1990.

[Hel08] G. Helmberg. *Introduction to Spectral Theory in Hilbert Space*. Dover, 2008.

[Kay93] K. G. Kay. Numerical study of semiclassical initial value methods for dynamics. *J. Chem. Phys.*, 100:4432, 1993.

[Kay94] K. G. Kay. Integral expressions for the semiclassical time-dependent propagator. *J. Chem. Phys.*, 100:4377, 1994.

[Kir33] J. G. Kirkwood. Quantum statistics of almost classical assemblies. *Phys. Rev.*, (44):31, 1933.

[Lit91] R. G. Littlejohn. The van Vleck formula, Maslov theory, and phase space geometry. *J. Stat. Phys.*, 68:7, 1991.

[MFL06] E. Martín-Fierro and J. M. G. Llorente. Derivation of semiclassical asymptotic initial value representations of the quantum propagator. *Chem. Phys.*, (322):13, 2006.

[Mil01] W. H. Miller. The semiclassical initial value representation: A potentially practical way for adding quantum effects to classical molecular dynamics simulations. *J. Phys. Chem. A*, (105):2942, 2001.

[Mor16] V. Moretti. *Mathematical Foundations of Quantum Mechanics: An Advanced Short Course*. draft, 2016.

[STH92] M. A. Sepúlveda, S. Tomsovic, and E. J. Heller. Semiclassical propagation: How long can it last? *Phys. Rev. Lett.*, 69:402, 1992.

[Swe11] D. W. H. Swenson. *Quantum Effects from Classical Trajectories: New Methodologies and Applications for Semiclassical Dynamics*. PhD dissertation, 2011.

[TH91] S. Tomsovic and E. J. Heller. Semiclassical dynamics of chaotic motion: Unexpected long-time accuracy. *Phys. Rev. Lett*, 67:664, 1991.

Chapter 4

The Weyl-Wigner representations

> In my opinion, quantum mechanics is revolutionary because it shows that an idea does not have to be amenable to human understanding in order to be correct.
>
> Alfredo M. Ozorio de Almeida

The position representation in quantum mechanics was defined as the one where the position operator acts as a multiplication, and the momentum operator as differentiation with respect to position. The duality between position and momentum allows us to define the momentum representation as the one where these roles are reversed, namely position acts as differentiation and momentum as multiplication. Representing a quantum system as a function of position and momentum *simultaneously* requires us to find a way to mix representations – a non-trivial task required to develop a phase-space formulation of quantum theory. By constructing operators that are generators of translations in momentum and position spaces at once, we obtain the Weyl representation of quantum mechanics – with the unfortunate drawback that these simultaneous-translation operators are not self-adjoint. The reflection operators obtained from them, however, are self-adjoint and provide us with the Wigner function, which has a well-defined classical limit. It is then interesting to establish limits for which classical propagation is enough to approximate quantum evolution, which we pursue in terms of autocorrelation functions.

4.1 Translation and reflection operators

In order to move to phase space, we must find a way to mix position and momentum together in quantum mechanics. Instead of looking for a ket that is a function of position and momentum simultaneously, we can look for operators whose *domain* is phase space. Since it is perfectly possible to write an operator that acts as a translation in both position and momentum representations simultaneously, *i.e.* $\langle p|\hat{\mathfrak{T}}|q\rangle \propto \langle p+\xi_p|q+\xi_q\rangle$, this is the starting point to obtain the Weyl-Wigner representation of quantum mechanics.

4.1.1 Weyl-Wigner symbols

A mixed translation in both position and momentum spaces can be formed by mixing the simple translations in (3.2):

$$\hat{\mathfrak{T}}(\xi) \stackrel{\text{def}}{=} \exp\left\{\frac{i}{\hbar}\left(\xi_p\cdot\hat{q}-\xi_q\cdot\hat{p}\right)\right\} = \exp\left\{\frac{i}{\hbar}\left(\xi\cdot\mathcal{J}\hat{\eta}\right)\right\}, \tag{4.1}$$

where $\xi = (\xi_q,\xi_p) = (\xi_{q_1},\ldots,\xi_{q_n},\xi_{p_1},\ldots,\xi_{p_n})$ and $\hat{\eta} = (\hat{q}_1,\ldots,\hat{q}_n,\hat{p}_1,\ldots,\hat{p}_n)$ are the position and momentum components of the phase space vector ξ and the operator $\hat{\eta}$, respectively, and $\mathcal{J}$ is given in (1.4).

Definition 4.1.1. The operators $\hat{\mathfrak{T}}$ in (4.1) are the **Heisenberg** or **translation operators**.

Since $[\hat{q},\hat{p}] = i\hbar\hat{I}$, the operator $\hat{\mathfrak{T}}$ can be split using the Baker-Hausdorff-Campbell (BHC) formula as

$$\hat{\mathfrak{T}}(\xi) = \exp\left\{\frac{i}{\hbar}\left(\xi_p\cdot\hat{q} - \xi_q\cdot\hat{p}\right)\right\} = \exp\left[\frac{i}{\hbar}\left(\xi_p\cdot\hat{q}\right)\right]\exp\left[-\frac{i}{\hbar}\left(\xi_q\cdot\hat{p}\right)\right]\exp\left\{-\left(\frac{1}{2\hbar^2}\right)\left[\xi_p\cdot\hat{q},\xi_q\cdot\hat{p}\right]\right\}$$
$$= \hat{T}(\xi_p,\hat{q})\hat{T}(\xi_q,\hat{p})\exp\left[-\left(\frac{i}{2\hbar}\right)\xi_q\cdot\xi_p\right],$$

where the translations in the last line are the ones in (3.2). Using again the BHC formula, it is easy to see that

$$\hat{\mathfrak{T}}(\xi_2)\hat{\mathfrak{T}}(\xi_1) = \exp\left\{\frac{i}{\hbar}\left(\xi_2\cdot\mathcal{J}\hat{\eta}\right)\right\}\exp\left\{\frac{i}{\hbar}\left(\xi_1\cdot J\hat{\eta}\right)\right\} = \exp\left\{\frac{i}{\hbar}\left(\xi_1+\xi_2\right)\cdot\mathcal{J}\hat{\eta}\right\}\exp\left[-\left(\frac{i}{2\hbar}\right)\xi_1\cdot\mathcal{J}\xi_2\right]$$
$$= \hat{\mathfrak{T}}(\xi_1+\xi_2)\exp\left[-\left(\frac{i}{2\hbar}\right)\xi_1\cdot\mathcal{J}\xi_2\right] \tag{4.2}$$

and, obviously, $\hat{\mathfrak{T}}(0) = \hat{I}$ and $\hat{\mathfrak{T}}^\dagger(\xi) = \hat{\mathfrak{T}}(-\xi)$, so that these operators are not self-adjoint. Tracing with respect to position, however, we obtain

$$\mathrm{tr}\left[\hat{\mathfrak{T}}(\xi)\right] = \int_{\mathbb{R}^n} dq\,\langle q|\hat{T}(\xi)|q\rangle = \int dq\,\exp\left[\left(\frac{i}{2\hbar}\right)\xi_p\cdot\xi_q\right]\langle q|\hat{T}(\xi_q,\hat{p})\hat{T}(\xi_p,\hat{q})|q\rangle$$
$$= \exp\left[\left(\frac{i}{2\hbar}\right)\xi_p\cdot\xi_q\right]\int dq\,\exp\left[\left(\frac{i}{\hbar}\right)\xi_p\cdot q\right]\langle q|q+\xi_q\rangle$$
$$= (2\pi\hbar)^n\exp\left[\left(\frac{i}{2\hbar}\right)\xi_p\cdot\xi_q\right]\delta(\xi)$$
$$\equiv (2\pi\hbar)^n\delta(\xi),$$

where the last equivalence is due to that fact that, as an integral kernel,

$$\exp\left[\left(\frac{i}{2\hbar}\right)\xi_p\cdot\xi_q\right]\delta(\xi) = \exp\left[\left(\frac{i}{2\hbar}\right)\xi_p\cdot\xi_q\right]\Big|_{\xi}\delta(\xi) = \delta(\xi).$$

We then have the Hilbert-Schmidt norm

$$\mathrm{tr}\left[\hat{\mathfrak{T}}(\xi_2)\hat{\mathfrak{T}}^\dagger(\xi_1)\right] = \mathrm{tr}\left[\hat{\mathfrak{T}}(\xi_2)\hat{\mathfrak{T}}(-\xi_1)\right] \equiv (2\pi\hbar)^n\delta(\xi_2-\xi_1). \tag{4.3}$$

The space of operators that act over a Hilbert space $\mathfrak{H}$ is a vector space, so what we have just found out is that the translation operators form a basis in this space: Any of its elements can be expanded as

$$\hat{U} = \left(\frac{1}{2\pi\hbar}\right)^n\int d\xi\,\widetilde{U}(\xi)\hat{\mathfrak{T}}(\xi),\quad \hat{U}:\mathfrak{H}\longrightarrow\mathfrak{H},\quad \hat{U}\hat{U}^\dagger = \hat{I}.$$

Definition 4.1.2. The coefficient $\widetilde{U}(\xi)$ in (4.3) is the **Weyl symbol** of $\hat{U}$.

The Weyl symbol can be easily obtained using the orthogonality in (4.3):

$$\hat{U} = \left(\frac{1}{2\pi\hbar}\right)^n\int d\xi'\,\widetilde{U}(\xi')\hat{\mathfrak{T}}(\xi') \quad\Longleftrightarrow\quad \mathrm{tr}\left[\hat{U}\hat{\mathfrak{T}}^\dagger(\xi)\right] = \left(\frac{1}{2\pi\hbar}\right)^n\int d\xi'\,\widetilde{U}(\xi')\,\mathrm{tr}\left[\hat{\mathfrak{T}}(\xi')\hat{\mathfrak{T}}^\dagger(\xi)\right]$$
$$= \frac{(2\pi\hbar)^n}{(2\pi\hbar)^n}\int d\xi'\,\widetilde{U}(\xi')\exp\left[\left(\frac{i}{2\hbar}\right)\xi\cdot\mathcal{J}\xi'\right]\delta(\xi'-\xi)$$
$$\Longrightarrow\quad \mathrm{tr}\left[\hat{U}\hat{\mathfrak{T}}^\dagger(\xi)\right] = \widetilde{U}(\xi). \tag{4.4}$$

As we saw earlier, the translation operators can be decomposed as a product of separate translations in momentum and position plus a phase. Each of these translations is restricted to the momentum or

position representation, and can therefore be associated with a Pontryagin dual. To this end, notice that we can compose a Fourier transform and a translation, the final action being:

$$\begin{aligned}\int d\alpha \exp\left(-\frac{i\alpha p}{\hbar}\right)\hat{T}(\alpha,\hat{p}) \quad : \quad \psi(q) &\longmapsto \int d\alpha \exp\left(-\frac{i\alpha p}{\hbar}\right)\psi(q+\alpha) \\ &= \int dQ \exp\left(-\frac{i(Q-q)p}{\hbar}\right)\psi(Q) \\ &= \exp\left(\frac{iqp}{\hbar}\right)\widetilde{\psi}(p)\,,\end{aligned}$$

and equivalently for the position translation acting in momentum space. We can then define the family

$$\hat{\mathfrak{R}}(\eta) = \frac{1}{(4\pi\hbar)^n}\int d\xi \exp\left[\frac{i}{\hbar}\left(\xi\cdot\mathcal{J}\eta\right)\right]\hat{\mathfrak{T}}(\xi)\,. \tag{4.5}$$

Definition 4.1.3. The Pontryagin dual obtained by integration with respect to the kernel $\exp\left[\frac{i}{\hbar}\left(\xi\cdot\mathcal{J}\eta\right)\right]$ is the **symplectic Fourier transform**.

Definition 4.1.4. The operators $\hat{\mathfrak{R}}$ in (4.5) are the **Großmann-Royer** or **reflection operators**.

Our interest in $\hat{\mathfrak{R}}$ lies in the fact that, as $\hat{\mathfrak{T}}(\xi)$ forms basis, so does $\hat{\mathfrak{R}}(\eta)$:

$$\hat{U} = \left(\frac{1}{2\pi\hbar}\right)^n \int d\eta\, U(\eta)\hat{\mathfrak{R}}(\eta)\,, \quad \hat{U}:\mathfrak{H}\longrightarrow\mathfrak{H}\,, \quad \hat{U}\hat{U}^\dagger = \hat{I}\,, \tag{4.6}$$

which is obvious by the Fourier transform properties. Unlike $\mathfrak{T}$, however, the reflection operators are self-adjoint. This is proved in the following lemma, which also shows where $\mathfrak{R}$ receives its name from.

Lemma 4.1.5. The translation and reflection operators follow the algebra

$$\begin{aligned}&\text{i)} \quad \hat{\mathfrak{R}}(\eta)\hat{\mathfrak{T}}(\xi) = \exp\left[-\frac{i}{\hbar}\left(\xi\cdot\mathcal{J}\eta\right)\right]\hat{\mathfrak{R}}\left(\eta-\frac{\xi}{2}\right) \\ &\text{ii)} \quad \hat{\mathfrak{T}}(\xi)\hat{\mathfrak{R}}(\eta) = \exp\left[-\frac{i}{\hbar}\left(\xi\cdot\mathcal{J}\eta\right)\right]\hat{\mathfrak{R}}\left(\eta+\frac{\xi}{2}\right) \\ &\text{iii)} \quad \hat{\mathfrak{T}}(\xi_2)\hat{\mathfrak{T}}(\xi_1) = \exp\left[-\frac{i}{2\hbar}\left(\xi_1\cdot\mathcal{J}\xi_2\right)\right]\hat{\mathfrak{T}}(\xi_1+\xi_2) \\ &\text{iv)} \quad \hat{\mathfrak{R}}(\eta_2)\hat{\mathfrak{R}}(\eta_1) = \exp\left[-\frac{i}{\hbar}\left(\eta_2\cdot\mathcal{J}\eta_1\right)\right]\hat{\mathfrak{T}}[2(\eta_2-\eta_1)]\,,\end{aligned}$$

which is just a projective operator version of the algebra followed by classical reflections and translations in Lemma 1.5.4.

Proof. iii) was already proved in (4.2) and we can use it to prove i):

$$\begin{aligned}\hat{\mathfrak{R}}(\eta)\hat{\mathfrak{T}}(\xi) &= \frac{1}{(4\pi\hbar)^n}\int d\xi' \exp\left[-\frac{i}{\hbar}\left(\xi'\cdot\mathcal{J}\eta\right)\right]\hat{\mathfrak{T}}(\xi')\hat{\mathfrak{T}}(\xi) \\ &= \frac{1}{(4\pi\hbar)^n}\int d\xi' \exp\left\{-\frac{i}{\hbar}\left[\xi'\cdot\mathcal{J}\left(\eta-\frac{\xi}{2}\right)\right]\right\}\hat{\mathfrak{T}}(\xi'+\xi) \\ &= \frac{1}{(4\pi\hbar)^n}\int d\Xi \exp\left\{-\frac{i}{\hbar}\left[(\Xi-\xi)\cdot\mathcal{J}\left(\eta-\frac{\xi}{2}\right)\right]\right\}\hat{\mathfrak{T}}(\Xi) \\ &= \exp\left[-\frac{i}{\hbar}\left(\xi\cdot\mathcal{J}\eta\right)\right]\hat{\mathfrak{R}}\left(\eta-\frac{\xi}{2}\right)\,.\end{aligned}$$

Since ii) follows from a computation identical to the one performed above, we now proceed to iv).

Using ii),

$$\begin{aligned}\hat{\mathfrak{R}}(\eta_2)\hat{\mathfrak{R}}(\eta_1) &= \frac{1}{(4\pi\hbar)^n}\int d\xi \exp\left[-\frac{i}{\hbar}(\xi\cdot\mathcal{J}\eta_2)\right]\hat{\mathfrak{T}}(\xi)\hat{\mathfrak{R}}(\eta_1)\\ &= \frac{1}{(4\pi\hbar)^n}\int d\xi \exp\left\{-\frac{i}{\hbar}\left[\xi\cdot\mathcal{J}\left(\eta_1-\eta_2\right)\right]\right\}\hat{\mathfrak{R}}\left(\eta_1+\frac{\xi}{2}\right)\\ &= \frac{1}{(4\pi\hbar)^n}\int d\Pi \exp\left\{-\frac{i}{\hbar}\left[2\left(\Pi-\eta_1\right)\cdot\mathcal{J}\left(\eta_2-\eta_1\right)\right]\right\}\hat{\mathfrak{R}}\left(\Pi\right)\\ &= \exp\left[-\frac{i}{\hbar}\left(\eta_2\cdot\mathcal{J}\eta_1\right)\right]\hat{\mathfrak{T}}[2(\eta_2-\eta_1)]\,.\end{aligned}$$

□

Notice that, by iv), we have $\hat{\mathfrak{R}}(0)=\hat{\mathfrak{R}}^2(\eta)=\hat{I}$. Of course, we also have $\hat{\mathfrak{R}}(\eta)=\hat{\mathfrak{R}}^\dagger(\eta)$ and, again from iv), the reflection basis can be shown to be orthonormal:

$$\begin{aligned}&\hat{\mathfrak{R}}(\eta_2)\hat{\mathfrak{R}}(\eta_1) = \exp\left[-\frac{i}{\hbar}\left(\eta_2\cdot\mathcal{J}\eta_1\right)\right]\hat{\mathfrak{T}}[2(\eta_2-\eta_1)]\\ \implies\quad &\mathrm{tr}\left[\hat{\mathfrak{R}}(\eta_2)\hat{\mathfrak{R}}(\eta_1)\right] = (2\pi\hbar)^n\exp\left[-\frac{i}{\hbar}\left(\eta_2\cdot\mathcal{J}\eta_1\right)\right]\delta(\eta_2-\eta_1)\equiv(2\pi\hbar)^n\delta(\eta_2-\eta_1)\,,\end{aligned}\tag{4.7}$$

such that the decomposition in (4.6) is indeed valid.

Corollary 4.1.6. The operators $\hat{\mathfrak{T}}(\xi)$ and $\hat{\mathfrak{R}}(\eta)$ form a projective unitary representation of the translation and reflection group of Lemma 1.5.4. Hence the name given to $\hat{\mathfrak{R}}(\eta)$.

We can now use (4.7) to invert the decomposition (4.6), obtaining the expansion coefficient $U(\eta)$:

$$\begin{aligned}&\hat{U} = \left(\frac{1}{2\pi\hbar}\right)^n\int d\eta'\,U(\eta')\hat{\mathfrak{R}}(\eta')\\ \implies\quad &\mathrm{tr}\left[\hat{U}\hat{\mathfrak{R}}(\eta)\right] = \left(\frac{1}{2\pi\hbar}\right)^n\int d\eta'\,U(\eta')\mathrm{tr}\left[\hat{\mathfrak{R}}(\eta')\hat{\mathfrak{R}}(\eta)\right]\\ &\qquad\qquad = \int d\eta'\,U(\eta')\exp\left[-\frac{i}{\hbar}\left(\eta'\cdot\mathcal{J}\eta\right)\right]\delta(\eta'-\eta)\\ \implies\quad &\mathrm{tr}\left[\hat{U}\hat{\mathfrak{R}}(\eta)\right] = U(\eta)\,.\end{aligned}\tag{4.8}$$

Definition 4.1.7. The coefficient $U(\eta)$ above is the **Wigner symbol** of $\hat{U}$.

By mixing position and momentum operators and retaining duality with respect to the symplectic Fourier transform, *i.e.*

$$U(\eta) = \left(\frac{1}{2\pi\hbar}\right)^{\frac{n}{2}}\int d\xi\exp\left[\frac{i}{\hbar}\left(\xi\cdot\mathcal{J}\eta\right)\right]\widetilde{U}(\xi)\,,\tag{4.9}$$

a description in terms of Wigner and Weyl symbols is the phase-space analogue of the Heisenberg picture of quantum mechanics, where the emphasis is placed on operators instead of state vectors.

Definition 4.1.8. The descriptions in terms of Weyl or Wigner symbols are the **Weyl-Wigner representations**.

The Weyl-Wigner representations provide a phase-space rendering of the *density operator* $\hat{\varrho}$ [Bal08]. The fact that all quantum systems can be described by density operators implies that these representations are very general and can be adapted to describe open quantum systems, whereas a representation based on the wavefunction is applicable only to systems describing *pure states* – that is, states for which a wavefunction can be defined.

4.1.2 The Wigner function

The normalized chord and center symbols to the density operator $\hat{\varrho}$, given by

$$\chi(\xi) = \left(\frac{1}{2\pi\hbar}\right)^n \mathrm{tr}\left[\hat{\varrho}\,\hat{\mathfrak{T}}(\xi)\right] \qquad \text{and} \qquad W(\eta) = \left(\frac{1}{2\pi\hbar}\right)^n \mathrm{tr}\left[\hat{\varrho}\,\hat{\mathfrak{R}}(\eta)\right], \tag{4.10}$$

deserve special treatment.

Definition 4.1.9. The Weyl and Wigner symbols $\chi(\xi)$ and $W(\eta)$ are the **characteristic** and **Wigner functions** of the system described by $\hat{\varrho}$, respectively.

We can trace with respect to position to obtain expressions for the characteristic and Wigner functions in terms of the density operator in position representation. Using the decomposition of translation operators in terms of position and momentum,

$$\begin{aligned}
\chi(\xi) &= \left(\frac{1}{2\pi\hbar}\right)^n \mathrm{tr}\left[\hat{\varrho}\,\hat{\mathfrak{T}}(\xi)\right] \\
&= \left(\frac{1}{2\pi\hbar}\right)^n \int dq \left\langle q \middle| \hat{\varrho}\left\{\hat{T}(\xi_p,\hat{q})\hat{T}(\xi_q,\hat{p})\exp\left[-\left(\frac{i}{2\hbar}\right)\xi_q\cdot\xi_p\right]\right\}\middle| q\right\rangle \\
&= \left(\frac{1}{2\pi\hbar}\right)^n \exp\left[-\frac{i}{2\hbar}\left(\xi_q\cdot\xi_p\right)\right]\int dq\,\langle q\,|\hat{\varrho}|\,q+\xi_q\rangle \exp\left\{\frac{i}{\hbar}\left[\xi_p\cdot(q+\xi_q)\right]\right\} \\
\implies \quad \chi(\xi) &= \left(\frac{1}{2\pi\hbar}\right)^n \int d\gamma \left\langle \gamma - \frac{\xi_q}{2}\middle|\hat{\varrho}\middle|\gamma+\frac{\xi_q}{2}\right\rangle \exp\left[\frac{i}{\hbar}\left(\xi_p\cdot\gamma\right)\right],
\end{aligned} \tag{4.11}$$

where γ was defined by the change of variables $q \longmapsto \gamma - \xi_q/2$. Taking the symplectic Fourier transform we obtain the position representation for the Wigner function:

$$\begin{aligned}
W(\eta) &= \frac{1}{(2\pi\hbar)^n}\int d\xi \exp\left[\frac{i}{\hbar}\left(\xi\cdot\mathcal{J}\eta\right)\right]\chi(\xi) \\
&= \left(\frac{1}{2\pi\hbar}\right)^n \int d\gamma\, d\xi_q\, d\xi_p \left\langle \gamma - \frac{\xi_q}{2}\middle|\hat{\varrho}\middle|\gamma+\frac{\xi_q}{2}\right\rangle \exp\left[\frac{i}{\hbar}\left(\xi_p\cdot\gamma\right)\right]\exp\left[\frac{i}{\hbar}\left(\xi_q\cdot\eta_p - \xi_p\cdot\eta_q\right)\right] \\
&= \left(\frac{1}{2\pi\hbar}\right)^n \int d\gamma\, d\xi_q\, d\xi_p \left\langle \gamma - \frac{\xi_q}{2}\middle|\hat{\varrho}\middle|\gamma+\frac{\xi_q}{2}\right\rangle \exp\left\{\frac{i}{\hbar}\left[\xi_p\cdot(\gamma-\eta_q)\right]\right\}\exp\left[\frac{i}{\hbar}\left(\xi_q\cdot\eta_p\right)\right] \\
&= \left(\frac{1}{2\pi\hbar}\right)^n \int d\gamma\, d\xi_q \left\langle \gamma - \frac{\xi_q}{2}\middle|\hat{\varrho}\middle|\gamma+\frac{\xi_q}{2}\right\rangle \delta(\gamma-\eta_q)\exp\left[\frac{i}{\hbar}\left(\xi_q\cdot\eta_p\right)\right] \\
\implies \quad W(\eta) &= \left(\frac{1}{2\pi\hbar}\right)^n \int d\gamma \left\langle \eta_q - \frac{\gamma}{2}\middle|\hat{\varrho}\middle|\eta_q+\frac{\gamma}{2}\right\rangle \exp\left[\frac{i}{\hbar}\left(\gamma\cdot\eta_p\right)\right].
\end{aligned} \tag{4.12}$$

Notice that the position element of the density operator in both (4.11) and (4.12) is a type of spatial correlation, for which we cannot guarantee positivity. Since the Wigner function is obtained as a coefficient in an expansion in a basis of self-adjoint operators, its reality is guaranteed – but it can still be negative. For the characteristic function the basis is not even self-adjoint and it is generally complex. Nevertheless, we can employ (4.12) to deduce properties that make the Wigner function interesting despite the fact that it is not a true probability distribution[1]. First, we notice that

$$\begin{aligned}
\int d\eta_p\, W(\eta) &= \left(\frac{1}{2\pi\hbar}\right)^n \int d\gamma\, d\eta_p \left\langle \eta_q - \frac{\gamma}{2}\middle|\hat{\varrho}\middle|\eta_q+\frac{\gamma}{2}\right\rangle \exp\left[\frac{i}{\hbar}\left(\gamma\cdot\eta_p\right)\right] \\
&= \left(\frac{1}{2\pi\hbar}\right)^n \int d\Gamma\, d\eta_p\, \langle\eta_q|\hat{\varrho}|\eta_q+\Gamma\rangle \exp\left[\frac{2i}{\hbar}\left[\eta_p\cdot(\eta_q-\Gamma)\right]\right] \\
&= \int d\Gamma\, \langle\Gamma|\hat{\varrho}|2\eta_q+\Gamma\rangle\,\delta\left(\Gamma-\eta_q\right) \\
\implies \quad \int d\eta_p\, W(\eta) &= \langle\eta_q|\hat{\varrho}|\eta_q\rangle\ ;
\end{aligned} \tag{4.13}$$

[1] The characteristic function's properties can be accessed with equivalent calculations using (4.11)).

and, analogously,

$$\int d\eta_p\, W(\eta) = \langle \eta_q|\hat{\varrho}|\eta_q\rangle$$

$$\iff \quad \left(\frac{1}{2\pi\hbar}\right)^n \int d\eta_q \left\{\int d\eta_p \exp\left[\frac{i}{\hbar}\,(\eta_p\cdot\mathcal{J}\eta_q)\right] W(\eta)\right\} = \left(\frac{1}{2\pi\hbar}\right)^n \int d\eta_q\, \langle \eta_q|\hat{\varrho}|\eta_q\rangle \exp\left[\frac{i}{\hbar}\,(\eta_p\cdot\mathcal{J}\eta_q)\right]$$

$$\implies \quad \int d\eta_q\, W(\eta) = \langle \eta_p|\hat{\varrho}|\eta_p\rangle\ . \tag{4.14}$$

Therefore, the Wigner function provides a complete description of a quantum system. Of course, both (4.13) and (4.14) imply

$$\int d\eta_p d\eta_q\, W(\eta) = \int d\eta_q d\eta_p\, W(\eta) = 1\,,$$

so everything up to now is consistent and the Wigner function is normalized. Many more identities concerning Wigner and characteristic functions are discussed in [dA98].

4.2 Weyl-Wigner dynamics

As the density operator is expanded in either translation or reflection bases, the time-evolution of the Weyl-Wigner symbols can be expressed as both the evolved density operator expanded in static bases or the static operator expanded in evolving bases. This constitutes the core of the semiclassical approximations to be derived in Chapter 5, and shall be developed in this section.

4.2.1 Quantum evolution

Although the expressions (4.11) and (4.12) are useful for explicit calculations and are the ones usually found in literature, the condensed expressions (4.10) are invaluable when dealing with theoretical considerations. The time-evolution of the characteristic and Wigner functions, for example, can be succinctly written using the evolution for the density operator $\varrho_t = \hat{U}_t\hat{\varrho}\,\hat{U}_t^\dagger$, whose details are provided in Appendix C. Together with the invariance of the trace with respect to permutations, we have

$$\chi_t(\xi) \propto \mathrm{tr}\left[\hat{\varrho}_t\,\hat{\mathfrak{T}}(\xi)\right] = \mathrm{tr}\left[\hat{U}_t\hat{\varrho}\,\hat{U}_t^\dagger\,\hat{\mathfrak{T}}(\xi)\right], \quad W_t(\eta) \propto \mathrm{tr}\left[\hat{\varrho}_t\,\hat{\mathfrak{R}}(\eta)\right] = \mathrm{tr}\left[\hat{U}_t\hat{\varrho}\,\hat{U}_t^\dagger\,\hat{\mathfrak{R}}(\eta)\right]$$

$$\implies \quad \chi_t(\xi) = \left(\frac{1}{2\pi\hbar}\right)^n \mathrm{tr}\left[\hat{\varrho}\,\hat{\mathfrak{T}}_t(\xi)\right], \quad W_t(\eta) = \left(\frac{1}{2\pi\hbar}\right)^n \mathrm{tr}\left[\hat{\varrho}\,\hat{\mathfrak{R}}_t(\eta)\right]\,, \tag{4.15}$$

so that, just as in the Heisenberg picture, the evolved characteristic and Wigner functions can be obtained from keeping the density operator still, while evolving either translation or reflection operators. Using the symplectic Fourier transform we can also evidently write

$$W_t(\eta) = \left(\frac{1}{2\pi\hbar}\right)^n \int d\xi \exp\left[-\frac{i}{\hbar}\,(\eta\cdot\mathcal{J}\xi)\right]\chi_t(\xi)\,, \quad \chi_t(\xi) = \left(\frac{1}{2\pi\hbar}\right)^n \int d\eta \exp\left[\frac{i}{\hbar}\,(\eta\cdot\mathcal{J}\xi)\right] W_t(\eta)\,. \tag{4.16}$$

A simple lemma sheds light on the formulas above.

Lemma 4.2.1. The translation and reflection operators have the following Wigner-Weyl symbols:

$$\text{i)}\ \left[\hat{\mathfrak{R}}(\eta)\right](\eta') \equiv (2\pi\hbar)^n\delta(\eta'-\eta)\,, \qquad \text{ii)}\ \left[\hat{\mathfrak{R}}(\eta)\right](\xi') = 2^{-n}\exp\left[-\frac{i}{\hbar}\,(\xi'\cdot\mathcal{J}\eta)\right]\,,$$

$$\text{iii)}\ \left[\hat{\mathfrak{T}}(\xi)\right](\xi') \equiv (2\pi\hbar)^n\delta(\xi'-\xi)\,, \qquad \text{iv)}\ \left[\hat{\mathfrak{T}}(\xi)\right](\eta') = \exp\left[\frac{i}{\hbar}\,(\xi\cdot\mathcal{J}\eta')\right]$$

Proof. Take the trace of 4.1.5. i) and iii) were already indirectly proved in (4.3) and (4.7). □

Thus, we can interpret the symplectic Fourier transform as a decomposition of $\hat{\mathfrak{R}}$ and $\hat{\mathfrak{T}}$ themselves in translation and reflection bases:

$$\hat{\mathfrak{R}}(\eta) = \frac{1}{(4\pi\hbar)^n}\int d\xi \exp\left[-\frac{i}{\hbar}\,(\xi\cdot\mathcal{J}\eta)\right]\hat{\mathfrak{T}}(\xi) = \frac{1}{(2\pi\hbar)^n}\int d\xi\left\{\left[\hat{\mathfrak{R}}(\eta)\right](\xi)\right\}\hat{\mathfrak{T}}(\xi)$$

$$\hat{\mathfrak{T}}(\eta) = \frac{1}{(2\pi\hbar)^n}\int d\eta \exp\left[\frac{i}{\hbar}\,(\xi\cdot\mathcal{J}\eta)\right]\hat{\mathfrak{R}}(\eta) = \frac{1}{(2\pi\hbar)^n}\int d\eta\left\{\left[\hat{\mathfrak{T}}(\xi)\right](\eta)\right\}\hat{\mathfrak{R}}(\eta)\,,$$

Using (4.15) with time dependence either in the density operator or the translation/reflection operators, Lemma 4.2.1 allows us to write the Wigner function of (4.16) as

$$W_t(\eta) = \left(\frac{1}{\pi\hbar}\right)^n \int d\xi \left\{ \left[\hat{\mathfrak{R}}(\eta)\right](\xi) \right\} \chi_t(\xi) \tag{4.17}$$

$$= \left(\frac{1}{\pi\hbar}\right)^n \int d\xi \left\{ \left[\hat{\mathfrak{R}}_t(\eta)\right](\xi) \right\} \chi_0(\xi)\,. \tag{4.18}$$

Equation (4.17) interprets Wigner evolution as a static reflection in the Weyl representation, integrated against an evolving characteristic function. However, as seen in (4.18), we can also interpret Wigner dynamics as a static characteristic function integrated against a time-evolving reflection as the kernel. The same reasoning can be obviously applied to the characteristic function, for which

$$\chi_t(\xi) = \left(\frac{1}{2\pi\hbar}\right)^n \int d\eta \left\{ \left[\hat{\mathfrak{T}}(\xi)\right](\eta) \right\} W_t(\eta) \tag{4.19}$$

$$= \left(\frac{1}{2\pi\hbar}\right)^n \int d\eta \left\{ \left[\hat{\mathfrak{T}}_t(\xi)\right](\eta) \right\} W_0(\eta)\,. \tag{4.20}$$

Notice the cross-behavior: We use the characteristic function to evolve the Wigner function, and vice-versa. This is due to Lemma 4.2.1: The Wigner symbol for a reflection, just as the Weyl symbol for a translation, are Dirac's delta functions. Since the characteristic function is expressed as a symplectic Fourier transform of the Wigner function, it makes sense that the evolved case follows the same rule, which resumes to the static case when $t = 0$ by Lemma 4.2.1.

4.2.2 The classical limit

As seen in Example 1.5.3, the generating functions in the exponentials of (4.17) and (4.19) can be classically interpreted as generators of translations and reflections. By exponentiating them, what we are building are the Wigner and Weyl symbols for the quantum generators of translations and reflections. Now, we can use (4.18) and (4.20) to establish a further classical analogy: If *e.g.* $\widetilde{S}(\xi) = \xi \cdot \mathcal{J}\eta$ generates a classical reflection by η, then $\widetilde{S}_t(\xi) = \xi \cdot \mathcal{J}\eta_t$ describes dynamics in terms of reflections by a time-evolving center, since

$$\widetilde{S}_t(\xi) = \xi \cdot \mathcal{J}\eta_t \quad \Longrightarrow \quad \frac{\partial \widetilde{S}_t(\xi)}{\partial \xi} = \mathcal{J}\eta_t\,, \qquad S_t(\eta) = \xi_t \cdot \mathcal{J}\eta \quad \Longrightarrow \quad \frac{\partial S_t(\eta)}{\partial \eta} = -\mathcal{J}\xi_t\,,$$

where in the second equation we have expanded this to the center generating function.

Theorem 4.2.2. The evolution of the Wigner function has a well-defined classical limit, given by

$$W(\eta_t) = \left(\frac{1}{\pi\hbar}\right)^n \int d\xi \exp\left[-\frac{i}{\hbar}\left(\xi \cdot \mathcal{J}\eta_t\right)\right] \chi_0(\xi)\,,$$

where the coordinate η_t obeys Hamilton's equations $\dot{\eta}_t = \{\eta_t, H\}$.

Proof. The proof is very simple: Using the ideas developed earlier, we just identify the time-evolving Weyl symbol in (4.18) with *minus* the exponential of its classical version, *i.e.* $-\widetilde{S}_t(\xi)$:

$$W_t(\eta) = \left(\frac{1}{\pi\hbar}\right)^n \int d\xi \left\{ \left[\hat{\mathfrak{R}}_t(\eta)\right](\xi) \right\} \chi_0(\xi) \approx \left(\frac{1}{\pi\hbar}\right)^n \int d\xi \exp\left[-\frac{i}{\hbar}\left(\xi \cdot \mathcal{J}\eta_t\right)\right] \chi_0(\xi) = W(\eta_t)\,.$$

To show this makes sense, suppose we calculate the Wigner evolution at a point $\eta_t = (q_t, p_t)$ which,

by definition, evolves according to Hamilton's equations:

$$\begin{aligned}
\frac{dW(q_t,p_t)}{dt} &= \left(\frac{1}{\pi\hbar}\right)^n \frac{\partial}{\partial t}\left\{\int d\xi_q\, d\xi_p\, \exp\left[-\frac{i}{\hbar}\left(\xi_q\cdot p_t - \xi_p\cdot q_t\right)\right]\chi_0(\xi)\right\} \\
&= \left(\frac{1}{\pi\hbar}\right)^n \left\{-\frac{i\dot{p}_t}{\hbar}\left(\int d\xi_q\, d\xi_p\,(\xi_q)\, \exp\left[-\frac{i}{\hbar}\left(\xi_q\cdot p_t - \xi_p\cdot q_t\right)\right]\chi_0(\xi)\right)\right. \\
&\qquad \left. +\frac{i\dot{q}_t}{\hbar}\left(\int d\xi_q\, d\xi_p\,(\xi_p)\, \exp\left[-\frac{i}{\hbar}\left(\xi_q\cdot p_t - \xi_p\cdot q_t\right)\right]\chi_0(\xi)\right)\right\} \\
&= \left(\frac{\partial H(q_t,p_t)}{\partial q_t}\right)\frac{\partial}{\partial p_t}\left\{\left(\frac{1}{\pi\hbar}\right)^n \int d\xi_q\, d\xi_p\ \exp\left[-\frac{i}{\hbar}\left(\xi_q\cdot p_t - \xi_p\cdot q_t\right)\right]\chi_0(\xi)\right\} \\
&\qquad -\left(\frac{\partial H(q_t,p_t)}{\partial p_t}\right)\frac{\partial}{\partial q_t}\left\{\left(\frac{1}{\pi\hbar}\right)^n \int d\xi_q\, d\xi_p\ \exp\left[-\frac{i}{\hbar}\left(\xi_q\cdot p_t - \xi_p\cdot q_t\right)\right]\chi_0(\xi)\right\} \\
&= \left(\frac{\partial H(q_t,p_t)}{\partial q_t}\right)\left(\frac{\partial W(q_t,p_t)}{\partial p_t}\right) - \left(\frac{\partial H(q_t,p_t)}{\partial p_t}\right)\left(\frac{\partial W(q_t,p_t)}{\partial q_t}\right) \\
\iff \quad \frac{dW(\eta_t)}{dt} &= -\left\{W(\eta_t), H(\eta_t)\right\}\,, \qquad (4.21)
\end{aligned}$$

which is just the Liouville equation[2] (1.6). □

The Wigner representation allows us to define a classical limit [Gro46, Moy49], which is something that does not exist in the Schrödinger picture of quantum mechanics: There are no "classical wavefunctions" or even "classical operators", since Dirac's quantization condition, when applied to the Heisenberg picture, does not really tell us how to obtain classical operators corresponding to quantum ones (*i.e.* to dequantize operators). The *Moyal formulation* [Moy49] of quantum mechanics is completely based on (4.21), using it to define an *algebraic deformation* in terms of a poissonian structure $\{\{,\}\}$, the *Moyal bracket*, for which

$$\dot{W}_t = -\{\{W_t, H_t\}\} = -\{W_t, H_t\} + \mathcal{O}(\hbar)\,.$$

Just as there are rigorous formulations of quantum mechanics using spectral theory and C*-algebras, which employ deformation theory, the Moyal formulation is the phase-space way to deform the Poisson bracket and develop a rigorous classical limit in quantum theory. However, it is rather hopeless from the numerical point of view: The Moyal equation above is not really "meant" to be solved, being of a more "contemplative" nature. The geometrical theory which we have been using so far when interpreting things in terms of centers and chords does not lead to a much simpler algorithm to solve for the *exact* Wigner evolution, but has a somewhat natural semiclassical limit that we shall develop in the following chapter. This theory can be found in the review [dA98], our main reference for this chapter, being first developed in [Gro76, Roy77, BJ84].

Coherent state dynamics

As mentioned in Chapter 3, coherent states are the quantum equivalent of classical phase-space points and this dissertation will be mostly focused on their propagation. Using the wavefunction (3.3) and (4.12), the Wigner function for a coherent state centered at $\alpha = (\Re(\alpha), \Im(\alpha))$ on the phase plane is given by

$$\begin{aligned}
W(q,p) &= \left(\frac{1}{2\pi\hbar}\right)\int d\gamma \left\langle q-\frac{\gamma}{2}\middle|\hat{\varrho}\middle|q+\frac{\gamma}{2}\right\rangle \exp\left(\frac{i\gamma\cdot p}{\hbar}\right) \\
&= \left(\frac{1}{4\pi\hbar}\right)^{\frac{1}{2}}\int d\gamma\, \exp\left\{-\frac{1}{2\hbar}\left|q+\frac{\gamma}{2}-\Re(\alpha)\right|^2 + \frac{1}{2\hbar}\left|q-\frac{\gamma}{2}-\Re(\alpha)\right|^2 + \frac{i\gamma}{\hbar}\cdot\left[\Im(\alpha)-p\right]\right\} \\
\Longrightarrow W(q,p) &= \left(\frac{1}{\pi\hbar}\right)\exp\left\{-\frac{1}{\hbar}\left|q-\Re(\alpha)\right|^2 - \frac{1}{\hbar}\left|p-\Im(\alpha)\right|^2\right\}\,,
\end{aligned}$$

[2]Notice that, due to the characteristic function employing the kernel $\exp[i...]$ instead of $\exp[-i...]$, there is a sign difference and we do not recover the Liouville equation – The characteristic function does not provide us with a meaningful classical limit (quite obvious, since it's a complex object).

or, more compactly,

$$W(\eta) = \left(\frac{1}{\pi\hbar}\right) \exp\left(-\frac{|\eta-\alpha|^2}{\hbar}\right), \qquad \eta = (q,p)\,.$$

The expression above shows that coherent states conserve their gaussian form when represented in phase space. The characteristic function, easily obtained by a symplectic Fourier transform of the equation above, is given by

$$\chi(\xi) = \exp\left[-\frac{1}{\hbar}\left(\frac{|\xi|^2}{4} - i\alpha\cdot\mathcal{J}\xi\right)\right], \qquad \xi = (q,p)\,,$$

which we can employ to derive the classical evolution of the Wigner function using Theorem 4.2.2:

$$\begin{aligned} W(\eta_{-t}) &= \left(\frac{1}{\pi\hbar}\right)\int d\xi \exp\left[-\frac{i}{\hbar}\left(\xi\cdot\mathcal{J}\eta_t\right)\right]\chi_0(\xi) \\ &= \left(\frac{1}{\pi\hbar}\right)\int d\xi \exp\left[-\frac{i}{\hbar}\left(\xi_q p_t - \xi_p q_t\right)\right]\exp\left\{-\frac{1}{\hbar}\left[\frac{(\xi_q^2+\xi_p^2)}{4} - i(\Re(\alpha)\xi_p - \Im(\alpha)\xi_q)\right]\right\}. \end{aligned}$$

Completing the square, performing the gaussian integral above and substituting $t \longmapsto -t$ to describe forward propagation,

$$W(q_t,p_t) = \left(\frac{1}{\pi\hbar}\right)\exp\left\{-\frac{1}{\hbar}\left[q_{-t}-\Re(\alpha)\right]^2 - \frac{1}{\hbar}\left[p_{-t}-\Im(\alpha)\right]^2\right\},$$

which we can write compactly as

$$W(\eta_t) = \left(\frac{1}{\pi\hbar}\right)\exp\left(-\frac{|\eta_{-t}-\alpha|^2}{\hbar}\right), \qquad \eta_t = (q_t,p_t)\,. \tag{4.22}$$

Again, the coherent states present us with a remarkable property: The classical evolution of a coherent state in the Wigner representation is just the Wigner function for the coherent state evaluated along the classical trajectory (but notice the negative sign in (4.22)).

4.2.3 Characteristic times and the autocorrelation function

Interpreting the classical approximations as zeroth-order terms in an $\hbar$-series, just as in Moyal's formulation, we see that the phenomenon of quantum superposition can be interpreted as a correction to classical propagation, *i.e.* the zeroth-order term is classical, and the following terms are associated to the classical one interfering with itself. Of course, if the initial Wigner function is highly non-classical and oscillatory, the $\mathcal{O}(\hbar)$ term is the most significant, since $\hbar^2$ is already tiny with respect to the classical action. It is expected, therefore, that a $\mathcal{O}(\hbar)$ truncation of quantum propagation is already enough to recover most of quantum mechanics – which constituted the basis of Chapter 3.

As quantum dynamics is singular with respect to the limit $\hbar \longrightarrow 0$, the use of asymptotic analysis becomes unavoidable and will be the focus of later chapters. For very short times, however, we expect the zeroth-order term[3]

$$\left[\hat{\mathfrak{R}}_t(\eta)\right](\xi) \approx \exp\left[-\frac{i}{\hbar}\left(\xi\cdot\mathcal{J}\eta_t\right)\right]$$

to provide meaningful results, since for these tiny times the initial distribution, implicitly assumed to be localized, has not yet deformed under quantum evolution to start interfering with itself. In fact, the classical approximation in the Wigner-Weyl representations has been used in chemistry to model large molecules and provides very good results in many cases (see [Liu15] for a recent review). This is because the classical action for these systems is large when compared to $\hbar$, so that they lie closer to the classical than to the quantum world: $S \gg \hbar$, so $S/\hbar$ is only slow varying in a small region, outside

[3]Note that, even though we talk about *classical evolution*, $\hbar$ is ubiquitous. Everything still breaks down in the limit $\hbar \longrightarrow 0$, mostly because this limit is meaningless (as discussed in the Introduction).

of which it is rapidly oscillating and the Riemann-Lebesgue lemma applies[4] – this allows for the use of stationary phase approximations, which are the bread and butter of asymptotic analysis.

A nice way to find out the time-limit over which the classical approximations of Theorem 4.2.2 are enough to model quantum systems is through the interferences of the Wigner function with its starting value:

$$A_t^2 = 2\pi \int d\eta \, W_t(\eta) W_0(\eta) \,, \tag{4.23}$$

since this object should present very different behaviors under classical and quantum propagations for long enough times.

Definition 4.2.3. The function A_t in (4.23) is the **autocorrelation function**.

Indeed, the autocorrelation function in (4.23) is just the Wigner-function way of writing the usual squared autocorrelation $|\langle\psi_t|\psi_0\rangle|^2$. The following subsections should be read while comparing with Fig. 4.1.

Autocorrelation for the classical evolution of coherent states

A_t represents the normalized area of intersection between the initial Wigner function and its evolution, so if the evolution is purely classical all interference is positive (classical evolution cannot make a positive initial distribution become negative). If the dynamics takes place in a bounded phase-space region, we expect A_t to begin at $A_0 = 1$ and to gradually lose intensity to reach $A_t \approx 0$, representing the moment at which it has evolved away from the initial region and the intersection has a minimum. Shortly after nearing 0, however, we have two possibilities:

- The classical dynamics is integrable, so the initial distribution is propagated along regular orbits that end up bringing back some pieces of the Wigner function back to the initial region, increasing A_t;
- The classical dynamics is chaotic, therefore ergodic, and after a while scattered portions of the propagated Wigner function end up reaching the initial region, increasing A_t.

In a word: $A_0 = 1$, then it moves to $A_t \approx 0$, and then it increases. Due to dynamics being symplectic and, thus, conserving areas, we expect it to stabilize for long enough times, representing an intersection area that approaches a constant due to Poincaré recurrence – which is completely general and does not depend on the dynamical nature of the system. For discrete evolution, however, the autocorrelation might never reach a constant value and develop some small oscillatory behavior.

Autocorrelation for the quantum evolution of coherent states

There is no quantum chaos, so we only need to worry about regular dynamics in the quantum case. We expect A_t to behave exactly as its classical equivalent in the sense that it starts at 1 and drops close to 0, so the classical and quantum autocorrelation functions should match in this time regime. However, whereas the classically evolved Wigner function remained positive for all times and the intersection area was always positive, the quantum Wigner function will interfere with itself and generate negative-valued fringes. These fringes will end up caught in the region occupied by the initial Wigner function and will provide negative contributions to A_t, which will alternate with the positive contributions: In the quantum case, A_t oscillates.

Oscillations in the autocorrelation function should be dominant for quantum propagation after a certain time, which we proceed and define as τ_E. It represents the instant at which the quantum and the classical autocorrelation functions no longer match – that is, the classical propagation is no longer a good approximation to the quantum one.

Definition 4.2.4. The time τ_E is the **Ehrenfest time**.

(a) Classical evolution before τ_E.

(b) Quantum evolution before τ_E.

(c) Classical evolution after τ_E.

(d) Quantum evolution after τ_E.

Figure 4.1: In all panels, the dashed-gray region represents the initial Wigner function. (a) The classical Wigner function, in black, is evolved for a short time and has a single tip inside the gray region – A_t is small. (b) The same, but for the quantum evolution, with its positive and negative interferences represented in blue and red, respectively. Notice A_t is the same as in (a). (c) The classical Wigner function is now evolved for a time long enough for it to come back to the initial gray region, so A_t should start to rise. (d) The same, but for the quantum Wigner function, for which we now have interferences falling *inside* the initial gray area. These interferences create negative contributions in A_t, forbid it to remain constant and cause it to oscillate as time evolves – classical and quantum A_ts are no longer identical.

The Ehrenfest time establishes an interesting time-scale, especially for quantum systems whose classical counterparts are chaotic, since it is both connected with the start of quantum oscillations *and* with the speed at which initially close phase-space points diverge when propagated under chaotic dynamics (thus, they are connected to Lyapunov exponents [SVT12]). When analyzing chaotic systems in this dissertation, we will often choose to represent propagation times in terms of Ehrenfest-time multiples.

For high-dimensional systems that occupy vast phase-space regions, it takes a long time for the propagated distribution to return and interfere with its initial self. This is exactly the case for the systems successfully modeled by the classical approximation by the chemists, which from a physicist's point of view are monstrously large. Within the chemical community, the classical Wigner function is usually referred to as the *Linearized Semiclassical Initial Value Representation* (LSC-IVR), and is obtained using a very different [and somewhat cumbersome] line of reasoning (see [Liu15] for a review). It is also referred to in physics as the *Truncated Wigner Approximation* (TWA), and a nice review in this context can be found in [Pol10].

Bibliography

[Bal08] L. E. Ballentine. *Quantum Mechanics: A Modern Development*. World Scientific, 2008.

[BJ84] N. L. Balazs and B. K. Jennings. Wigner's function and other distribution functions in mock phase spaces. *Phys. Rep.*, 104:347, 1984.

[dA98] A. M. Ozorio de Almeida. The Weyl representation in classical and quantum mechanics. *Phys. Rep.*, 295:265, 1998.

[Gro46] H. J. Groenewold. On the principles of elementary quantum mechanics. *Physica*, 12:405, 1946.

[Gro76] A. Grossmann. Parity operator and quantization of delta-functions. *Commun. Math. Phys.*, 48:191, 1976.

[Liu15] J. Liu. Recent advances in the linearized semiclassical initial value representation/classical wigner model for the thermal correlation function. *Int. J. Quantum Chem.*, 115:657, 2015.

[Moy49] J. E. Moyal. Quantum mechanics as a statistical theory. *Proc. Camb. Phil. Soc.*, 45:99, 1949.

[Pol10] A. Polkovnikov. Phase space representation of quantum dynamics. *Ann. Phys.*, 325:1790, 2010.

[Roy77] A. Royer. Wigner function as the expectation value of a parity operator. *Phys. Rev. A*, 15:449, 1977.

[SVT12] R. Schubert, R. O. Vallejos, and F. Toscano. How do wave packets spread? Time evolution on Ehrenfest time scales. *J. Phys. A: Math. Theor.*, 45:215307, 2012.

[4]The Riemann-Lebesgue lemma establishes the conditions on which we expect the integral $\int dx f(x) \exp(ig(x)/\hbar)$ to vanish due to the measure of positive and negative oscillation regions canceling each other.

Chapter 5

Semiclassical approximations in phase space

> (...) o que merece especulada atenção do observador, da vida de cada um, não é o seguimento encadeado de seu fio e fluxo, em que apenas muito de raro se entremostra algum aparente nexo lógico ou qualquer desperfeita coerência; mas sim as bruscas alterações ou mutações – estas, pelo menos, ao que têm de parecer, amarradinhas sempre ao invisível, ao mistério.
>
> J. Guimarães Rosa in *A estória do homem pinguelo (Estas Estórias)*

In Chapter 3 we used SPAs to obtain a semiclassical formulation of standard position-momentum quantum mechanics, and we now do the same for the the Weyl-Wigner representations. As we have seen in Chapter 4, the description in terms of the Wigner function is entirely analogous to using the more standard position-momentum wavefunctions, but with the bonus of a well-defined classical limit. It is then possible to analyze evolution in three different regimes: Classical, quantum and semiclassical. We start by obtaining the Weyl-Wigner symbols for the propagator restricted to linear systems, which are rather easy to generalize using the same reasoning as in 3. Later, we consider the propagation of arbitrary operators, where it becomes clear that the problem of general propagation is entirely characterized by the semiclassical evolution of translations and reflections, which we manage to solve. We then devise IVRs and, especially, a FVR for Wigner evolution, providing in detail the means for its calculation. This chapter is entirely based on [dAVZ13], although we employ different notational conventions.

5.1 The semiclassical propagator in the Weyl-Wigner representation

For sufficiently short times there is only one trajectory connecting two distinct points in phase space and caustics were still not reached (see Appendix B), so the van Vleck propagator of Section 3.3.2 is represented by a single term:

$$\mathcal{K}_t^{\mathrm{vV}}(q,q') = \left(\frac{1}{2\pi i\hbar}\right)^{\frac{n}{2}} \left|\det\left(\frac{\partial^2 S(q,q')}{\partial q \partial q'}\right)\right|^{\frac{1}{2}} \exp\left[\frac{i}{\hbar}S(q,q')\right] . \tag{5.1}$$

The case of linear systems is very particular because the formula above is not an approximation, but general and exact – the only thing missing is the allowance for a change of branch in S (*i.e.* the inclusion of the Maslov index). In this section we employ a strategy devised by Berry [Ber89] in which we calculate the semiclassical propagator in phase space through the Weyl-Wigner symbols of the van Vleck propagator above, gradually generalizing it from the linear case to arbitrary systems and long times.

5.1.1 Weyl-Wigner symbols for linear flows

We shall use the van Vleck propagator (5.1) as starting point to obtain expressions for the Weyl and Wigner symbols (4.4) and (4.8) for the evolution operator corresponding to linear flows – that is, flows that have the form

$$x' = \mathcal{M}_t x \quad \iff \quad \begin{pmatrix} q' \\ p' \end{pmatrix} = \begin{pmatrix} A_t & B_t \\ C_t & D_t \end{pmatrix} \begin{pmatrix} q \\ p \end{pmatrix} ,$$

where each block is a function of time exclusively. These flows substantially simplify the expressions for the center and chord generating functions, which become (see Appendix B)

$$\widetilde{S}_t(\xi) = \xi \cdot \widetilde{\mathcal{B}}_t \xi/4 \,, \qquad \widetilde{\mathcal{B}_t} = J\,(\mathcal{M}_t - I)^{-1}(\mathcal{M}_t + I) \tag{5.2}$$

$$S_t(\eta) = \eta \cdot \mathcal{B}_t \eta \,, \qquad \mathcal{B}_t = J\,(I + \mathcal{M}_t)^{-1}(I - \mathcal{M}_t) \,, \tag{5.3}$$

where $\widetilde{\mathcal{B}}$ and $\mathcal{B}$ are known as the *Cayley parametrizations* of $\mathcal{M}_t$.

Now, the Weyl symbol for short times can be generally expressed in terms of the van Vleck propagator in (5.1) by inserting it in (4.4):

$$\begin{aligned} \widetilde{U}_t(\xi) = \operatorname{tr}\left[\hat{U}_t \hat{\mathfrak{T}}(\xi)\right] = \operatorname{tr}\left[\hat{\mathfrak{T}}(-\xi)\hat{U}_t\right] &= \int dq\, dq'\, \langle q|\hat{U}_t|q'\rangle\langle q'|\hat{\mathfrak{T}}(-\xi)|q\rangle \\ &= \exp\left(\frac{i\xi_q \cdot \xi_p}{2\hbar}\right) \int dq\, dq'\, \exp\left(\frac{iq \cdot \xi_p}{\hbar}\right) \mathcal{K}_t^{\mathrm{vV}}(q,q')\langle q'|q - \xi_q\rangle \\ &= \exp\left(\frac{i\xi_q \cdot \xi_p}{2\hbar}\right) \int dq\, \exp\left(\frac{iq \cdot \xi_p}{\hbar}\right) \mathcal{K}_t^{\mathrm{vV}}(q, q - \xi_q) \,. \end{aligned} \tag{5.4}$$

However, evaluating the integral above is much simpler for linear flows, since in this case the SPA is exact and results in

$$\widetilde{U}_t(\xi) = |\det(\mathcal{M}_t - I)|^{-\frac{1}{2}} \exp\left\{\frac{i}{\hbar}\left[\widetilde{S}_t(\xi) + \frac{\hbar\pi\widetilde{\alpha}}{4}\right]\right\} , \quad \widetilde{\alpha} = \operatorname{sign}\left\{\left(\frac{\partial^2 \widetilde{S}_t(\xi)}{\partial \xi^2}\right)\right\} , \tag{5.5}$$

with $\widetilde{S}_t(\xi)$ as in (5.2). The complete calculations are provided in Appendix E, together with the passage to the center symbol using the symplectic Fourier transform of the above, namely

$$U_t(\eta) = 2^n |\det(I + \mathcal{M}_t)|^{-\frac{1}{2}} \exp\left\{\frac{i}{\hbar}\left[S_t(\eta) + \frac{i\pi\alpha}{4}\right]\right\} , \quad \alpha = \operatorname{sign}\left\{\left(\frac{\partial^2 S_t(\eta)}{\partial \eta^2}\right)\right\} , \tag{5.6}$$

with $S_t(\eta)$ as in (5.3). The short-time propagations in (5.5) and (5.6) can be easily extended for long times: As the flow is linear, Lemma B.1.1 ascertains root-searching will never be required, so the only correction that needs to be included is a change of signature in $\partial_\eta^2 S_t(\eta)$ or $\partial_\xi^2 \widetilde{S}_t(\xi)$. By the same argument of Subsection 3.3.3, the signature entering the phase will be the number of negative eigenvalues of the hessians before the caustic minus after the caustic – these are even-numbers which we define as σ and $\widetilde{\sigma}$ [dA98, dAI14]. Thus, we have the long-time propagators for linear dynamics:

$$\widetilde{U}_t(\xi) = |\det(\mathcal{M}_t - I)|^{-\frac{1}{2}} \exp\left\{\frac{i}{\hbar}\left[\widetilde{S}_t(\xi) + \frac{\hbar\pi\widetilde{\sigma}}{2}\right]\right\} , \qquad \widetilde{S}_t(\xi) = \xi \cdot \widetilde{\mathcal{B}}_t \xi/4 \,,$$

$$U_t(\eta) = 2^n |\det(I + \mathcal{M}_t)|^{-\frac{1}{2}} \exp\left\{\frac{i}{\hbar}\left[S_t(\eta) + \frac{i\pi\sigma}{2}\right]\right\} , \qquad S_t(\eta) = \eta \cdot \mathcal{B}_t \eta \,,$$

with $\tilde{\mathcal{B}}_t$ and $\mathcal{B}_t$ as in (5.2) and (5.3). Notice the Weyl representation is singular for $t = 0$, since $\mathcal{M}_0 = I$.

Example 5.1.1. (Weyl-Wigner caustics for the SHO) Let us examine the caustic structure of the SHO, for which

$$\mathcal{M}_t = \begin{pmatrix} \cos t & \sin t \\ -\sin t & \cos t \end{pmatrix} \quad \Longrightarrow \quad \mathcal{M}_0 = \begin{pmatrix} 1 & 0 \\ 0 & 1 \end{pmatrix} , \quad \mathcal{M}_\pi = \begin{pmatrix} -1 & 0 \\ 0 & -1 \end{pmatrix} .$$

The case $t = 0$ depicts a caustic in $\widetilde{U}_t(\xi)$: Since $\xi = 0$, all centers have the same chord. For $t = \pi$, we have a caustic in $U_t(\eta)$: Since η is at the origin, all chords joining diametrically opposing points on a same orbit have the same center. This latter case is depicted in Fig. 5.1. Notice that, since the $\widetilde{U}_t(\xi)$ has no caustic at $t = \pi$, we can exchange polarizations when approaching this time value. ⋇

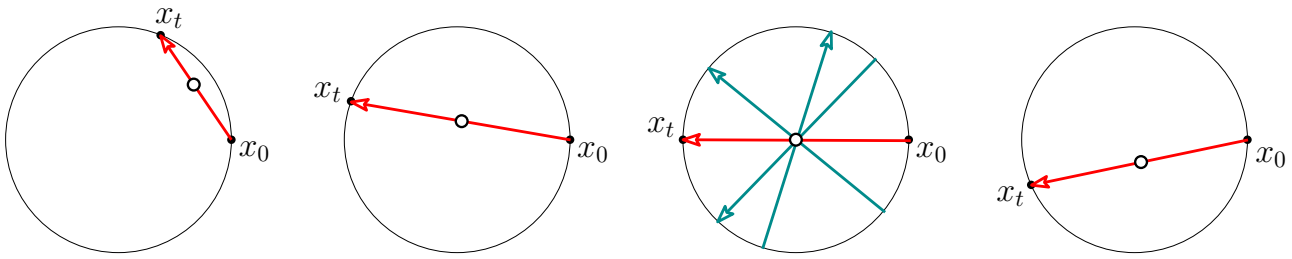

Figure 5.1: Center caustics for the SHO: The evolution leading $x_0 \longmapsto x_t$ is well-described in the Wigner formalism for times up to $t = \pi$, each center corresponding to a single chord. However, when passing through $t = \pi$, there are infinite chords with the same center (shown in cyan) and the Wigner symbol diverges. After the caustic is passed, however, the Wigner symbol is again well defined. By exchanging between Wigner and Weyl symbols we can avoid any caustic, since their associate center and chord polarizations are never singular at the same time.

5.1.2 Semiclassical symbols for the evolution operator

The generalization from the linearized case to general flows can be obtained by inserting the general van Vleck propagator in (5.4) and approximating it using SPAs. Here, however, we choose a simpler path that follows from a trivial identification: The semiclassical amplitudes appearing in the Weyl and Wigner symbols, namely

$$\widetilde{A}^2(\xi) = \left|\det\left(\mathcal{M} - I\right)\right|^{-1} \qquad \text{and} \qquad \widetilde{A}^2(\eta) = \left|\det\left(\frac{I+\mathcal{M}}{2}\right)\right|^{-1},$$

can have their arguments identified with

$$\mathcal{M} - I = \frac{d}{dx}\left(\mathcal{M}x - x\right) = \frac{d\xi(x)}{dx}, \qquad \frac{\mathcal{M}+I}{2} = \frac{d}{dx}\left(\frac{\mathcal{M}x+x}{2}\right) = \frac{d\eta(x)}{dx}, \tag{5.7}$$

So that the linear propagators of the earlier section can be written as

$$\widetilde{U}_t(\xi(x)) = \left|\det\left(\frac{d\xi(x)}{dx}\right)\right|^{-\frac{1}{2}} \exp\left\{\frac{i}{\hbar}\left[\widetilde{S}_t(\xi(x)) + \frac{i\pi\widetilde{\sigma}}{2}\right]\right\} \tag{5.8}$$

$$U_t(\eta(x)) = \left|\det\left(\frac{d\eta(x)}{dx}\right)\right|^{-\frac{1}{2}} \exp\left\{\frac{i}{\hbar}\left[S_t(\eta(x)) + \frac{i\pi\sigma}{2}\right]\right\}. \tag{5.9}$$

After performing so many SPAs in all sorts of representations, we can leave calculations on the side and use our semiclassical intuition to generalize the propagators above to non-linear systems. The first thing we must have in mind is that, for short-enough times, the propagators for general systems must look exactly as above, since short times can be well approximated by quadratic propagation. The changes that will take place have to do with the non-linearity of the flow, which was represented earlier by $\mathcal{M}_t x$, but is now given by $\rho_t(x)$. The amplitudes in (5.7) must be generalized to

$$\begin{cases} \dfrac{d}{dx}\left(\rho_t(x) - x\right) & = \dfrac{d\rho_t(x)}{dx} - I = \mathfrak{M}_t(x) - I \\ \dfrac{d}{dx}\left(\dfrac{\rho_t(x)+x}{2}\right) & = \dfrac{1}{2}\left(\dfrac{d\rho_t(x)}{dx} + I\right) = \dfrac{\mathfrak{M}_t(x)+I}{2} \end{cases}, \tag{5.10}$$

where $\mathfrak{M}(x)$ is the monodromy matrix of Section 3.3.3 calculated at the point x. In the same way, the generating functions are no longer quadratic functions of chords and centers, being generally not even analytical. We then have, for short times, the same propagators as in (5.8) and (5.9), except that the proper amplitudes are now given in (5.10) and the generating functions are general. Extending them for long times is immediate and follows the same steps as in Chapter 3: Trajectories will have to be added to the sum and selected through root-searching, just as in (E.2), but now the solution is not unique:

$$\frac{\partial}{\partial\xi}\left(\widetilde{S}(\xi) + \xi\cdot\mathcal{J}\eta\right) \iff \left.\frac{\partial\widetilde{S}(\xi)}{\partial\xi}\right|_{\xi=\xi^{(j)}} = -\mathcal{J}\eta \iff \mathfrak{n}(\xi^{(1)}) = \mathfrak{n}(\xi^{(2)}) = \ldots = \eta, \tag{5.11}$$

with $\mathfrak{n} \stackrel{\text{def}}{=} \mathcal{J}\partial_\xi \widetilde{S}$. The instruction given above is, in words: The semiclassical contribution at the fixed center η is given by the sum over all chords centered on it. The SPA for centers provides the analogous search

$$\frac{\partial}{\partial \eta}\left(S(\eta) - \xi \cdot \mathcal{J}\eta\right) \quad \Longleftrightarrow \quad \left.\frac{\partial S(\eta)}{\partial \eta}\right|_{\eta=\eta^{(j)}} = \mathcal{J}\xi \quad \Longleftrightarrow \quad \mathfrak{z}(\eta^{(1)}) = \mathfrak{z}(\eta^{(2)}) = ... = \xi\,, \tag{5.12}$$

with $\mathfrak{z} \stackrel{\text{def}}{=} -\mathcal{J}\partial_\eta S$. Again, root-searching for these chords/centers is equivalent to summing over the branches of S and $\widetilde{S}$. Combining everything up to now, we finally write the completely general expressions for the Weyl and Wigner symbols[1]:

$$\widetilde{U}_t(\xi(x)) = \sum_j \left|\det\left(\frac{d\xi(x)}{dx}\right)\right|^{-\frac{1}{2}}_{x=x^{(j)}} \exp\left\{\frac{i}{\hbar}\left[\widetilde{S}_t(\xi(x^{(j)})) + \frac{i\pi\widetilde{\sigma}^{(j)}}{2}\right]\right\} \tag{5.13}$$

$$U_t(\eta(x)) = \sum_j \left|\det\left(\frac{d\eta(x)}{dx}\right)\right|^{-\frac{1}{2}}_{x=x^{(j)}} \exp\left\{\frac{i}{\hbar}\left[S_t(\eta(x^{(j)})) + \frac{i\pi\sigma^{(j)}}{2}\right]\right\}, \tag{5.14}$$

where the root-search for each propagator is a parametrization of (5.11) and (5.12) in terms of x: The correct $x^{(j)}$ is defined, for each propagator above, as

$$\mathfrak{n}(\xi^{(1)}(x)) = \mathfrak{n}(\xi^{(2)}(x)) = ... = \eta \quad \Longleftrightarrow \quad \mathfrak{n}(\xi(x^{(1)})) = \mathfrak{n}(\xi(x^{(2)})) = ... = \eta\,;$$
$$\mathfrak{z}(\eta^{(1)}(x)) = \mathfrak{z}(\eta^{(2)}(x)) = ... = \xi \quad \Longleftrightarrow \quad \mathfrak{z}(\eta(x^{(1)})) = \mathfrak{z}(\eta(x^{(2)})) = ... = \xi\,,$$

respectively.

The semiclassical propagators, just as almost everything in this dissertation, were obtained from stationary phase approximations. We have already met with the several shortcomings of "raw" propagators in Chapter 3, which are also manifest in the expressions above: They diverge at caustics and require root-searching. Notice, however, that the divergences in the propagators above are different from what was described in WKB theory.

5.1.3 Phase-space caustics and Conley-Zehnder indexes

Unlike the caustic singularities of Chapter 3, the zeros appearing in the Weyl-Wigner representations are a function of the whole monodromy matrix instead of its individual components. They are also different among themselves, reflecting that, just as position and momentum, we can exchange between the Weyl and the Wigner polarizations when a caustic is approached in either one – a fact we have already used earlier. Thus, just as in Chapter 3, these indexes are modified every time we are forced to change polarization in order to avoid caustics.

Definition 5.1.2. The indexes σ and $\widetilde{\sigma}$ are the **Conley-Zehnder indexes**.

These indexes count the zeros of $\det\left[\mathfrak{M}_t(x) - I\right]$ and $\det\left[\mathfrak{M}_t(x) + I\right]$, while in WKB theory we only counted the zeros of a single monodromy matrix component. This renders the semiclassical Wigner functions considerably more computationally expensive then semiclassical wavefunctions, but it's a price one is required to pay to formulate semiclassical theory in phase space. The extra complexities associated to the semiclassical propagation of Wigner functions are unavoidable when dealing with non-unitary evolution, although they might be overkill for the case of closed quantum systems.

In the end, all indexes arising due to exchanging between parametrizations of a lagrangian foliation (*i.e.* polarizations) are related [dG06, AG]. When choosing parametrizations employing position and momentum, we were expressing the same lagrangian manifold using two different descriptions that were singular at different regions. Using chords and centers, we have the exactly same situation, except we choose a more intricate parametrization employing Cayley transforms (see Appendix B). Caustics, therefore, occur at different regions, but the Conley-Zehnder indexes can still be understood as a caustic count – not the same caustics, however: For position and momentum they happened when the derivatives of the position-position generating function exploded, but now they happen when $\mathfrak{M}_t$ has eigenvalues equal to $+1$ or -1.

[1] Notice that, in the terminology of Chapter 3, employing either the center and chord generating functions is tantamount to choosing between the *center* or *chord polarizations* in the product manifold.

5.1.4 Initial value representations

Following Chapter 3, we now attempt to get rid of root-searches and infinities in the raw propagators (5.13) and (5.14). For this, we use the exactly same reasoning as in Section 3.3.4: Start by expressing the root-search equations (5.11) and (5.12) as a function of the initial point:

$$\delta(\mathfrak{z}(x)-\xi) \qquad \text{and} \qquad \delta(\mathfrak{n}(x)-\eta)\,,$$

so that if $\mathfrak{z}(x)=\xi$ this particular root is selected. Then,

$$\begin{aligned}\int dx\,\left|\det\left(\frac{d\mathfrak{z}(x)}{dx}\right)\right|^{\frac{1}{2}}\delta(\mathfrak{z}(x)-\xi) &= \sum_j \left|\det\left(\frac{d\xi(x)}{dx}\right)\right|^{-\frac{1}{2}}_{x=x^{(j)}} \\ \int dx\,\left|\det\left(\frac{d\mathfrak{n}(x)}{dx}\right)\right|^{\frac{1}{2}}\delta(\mathfrak{n}(x)-\eta) &= \sum_j \left|\det\left(\frac{d\eta(x)}{dx}\right)\right|^{-\frac{1}{2}}_{x=x^{(j)}}\,.\end{aligned} \tag{5.15}$$

We shall perform the subsequent calculations exclusively for the Wigner symbol, but the generalization to the Weyl symbol is immediate. To use the equalities obtained above, the key is to use the symplectic Fourier transform (4.9) and write

$$\begin{aligned} & U(\eta)=\left(\frac{1}{2\pi\hbar}\right)^n\int d\xi\exp\left[\frac{i}{\hbar}\,(\xi\cdot\mathcal{J}\eta)\right]\widetilde{U}(\xi) \\ \Longrightarrow\quad & U(\eta)\approx\left(\frac{1}{2\pi\hbar}\right)^n\int d\xi(x)\sum_j\left|\det\left(\frac{d\xi(x)}{dx}\right)\right|^{-\frac{1}{2}}_{x=x^{(j)}}\exp\left\{\frac{i}{\hbar}\left[\xi(x)\cdot\mathcal{J}\eta+\widetilde{S}_t^{(j)}(\xi(x))+\frac{i\pi\widetilde{\sigma}^{(j)}}{2}\right]\right\}. \end{aligned}$$

Now, substitute the sum by (5.15),

$$\begin{aligned} U(\eta)=\left(\frac{1}{2\pi\hbar}\right)^n\int dx\,d\xi(x)\left|\det\left(\frac{d\mathfrak{z}(x)}{dx}\right)\right|^{\frac{1}{2}}\delta(\mathfrak{z}(x)-\xi(x)) \\ \times\exp\left\{\frac{i}{\hbar}\left[\xi(x)\cdot\mathcal{J}\eta+\widetilde{S}_t(\xi^{(j)}(x))+\frac{i\pi\widetilde{\sigma}^{(j)}}{2}\right]\right\}. \end{aligned}$$

and integrate with respect to ξ to get

$$U(\eta)\approx\left(\frac{1}{2\pi\hbar}\right)^n\int dx\,\left|\det\left(\frac{d\xi(x)}{dx}\right)\right|^{\frac{1}{2}}\exp\left\{\frac{i}{\hbar}\left[\xi(x)\cdot\mathcal{J}\eta+\widetilde{S}_t(\xi(x))+\frac{i\pi\widetilde{\sigma}}{2}\right]\right\}.$$

The same procedure applied to the Weyl symbol gives

$$\widetilde{U}_t(\xi)\approx\left(\frac{1}{\pi\hbar}\right)^n\int dx\,\left|\det\left(\frac{d\eta(x)}{dx}\right)\right|^{\frac{1}{2}}\exp\left\{\frac{i}{\hbar}\left[\xi\cdot\mathcal{J}\eta(x)+S_t(\eta(x))+\frac{i\pi\sigma}{2}\right]\right\}.$$

The integral representations above, which are integrals with respect to the initial phase-space point x (thus belonging to the class of IVRs), are the direct equivalents of what was developed in Section 3.3.4: They get rid of infinities and require no root-searching.

5.2 Semiclassical evolution of general operators

Up to now we have focused on the evolution operator $\hat{U}_t$. However, this is not enough to be able to propagate arbitrary operators in phase space. For this, we need to understand how translations and reflections evolve semiclassically.

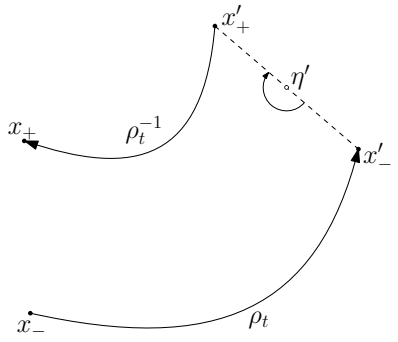

(a) The $x_- \longmapsto x_+$ circuit as viewed in the center picture.

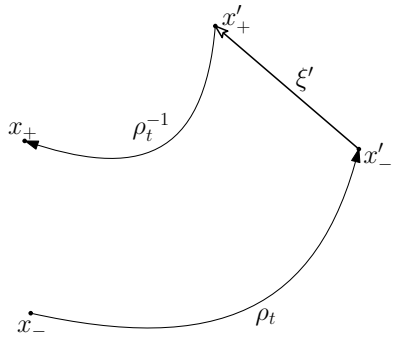

(b) The $x_- \longmapsto x_+$ circuit as viewed in the chord picture.

Figure 5.2: (a) The semiclassical Wigner representation calls for the interpretation of the circuit $x_- \longmapsto x_+$ as being constructed by the composition of the flow ρ_t, followed by a reflection around η', and finally by the inverse flow ρ_t^{-1}. (b) In the semiclassical Weyl representation, the only difference is that the intermediate step is given by a translation by the chord ξ'.

5.2.1 The geometry of phase-space propagation

From Chapter 4 we know that we can use the cyclic property of the trace to move time-dependence to reflection and translation operators, resulting in the evolved symbols

$$A_t(\eta) = \mathrm{tr}\left[\hat{A}\,\hat{\mathfrak{R}}_t(\eta)\right], \quad \hat{\mathfrak{R}}_t(\eta) = \hat{U}_t^\dagger\,\hat{\mathfrak{R}}(\eta)\,\hat{U}_t$$
$$\widetilde{A}_t(\xi) = \mathrm{tr}\left[\hat{A}\,\hat{\mathfrak{T}}_t(\xi)\right], \quad \hat{\mathfrak{T}}_t(\eta) = \hat{U}_t^\dagger\,\hat{\mathfrak{T}}(\xi)\,\hat{U}_t\,.$$

Introducing four resolutions of the identity in the position basis, we have

$$A_t(\eta) = \int_{\mathbb{R}^{4n}} dq_0\,dq_1\,dq_2\,dq_3\,\left\{\langle q_0|\hat{U}_t|q_1\rangle\langle q_1|\hat{\mathfrak{R}}_t(\eta)|q_2\rangle\langle q_2|\hat{U}_t^\dagger|q_3\rangle\right\}\langle q_3|\hat{A}|q_0\rangle$$
$$\widetilde{A}_t(\xi) = \int_{\mathbb{R}^{4n}} dq_0\,dq_1\,dq_2\,dq_3\,\left\{\langle q_0|\hat{U}_t|q_1\rangle\langle q_1|\hat{\mathfrak{T}}(\xi)|q_2\rangle\langle q_2|\hat{U}_t^\dagger|q_3\rangle\right\}\langle q_3|\hat{A}|q_0\rangle\,.$$

where the terms in curly brackets can be semiclassically interpreted using the van Vleck propagator, which we do in the following. Notice that understanding how translations and reflections evolve will allow us to describe the semiclassical evolution of any $\hat{A}$.

The center view

The semiclassical Wigner symbol can be written as

$$A_t(\eta') \approx \int_{\mathbb{R}^{4n}} dq_0\,dq_1\,dq_2\,dq_3\,\left\{\mathcal{K}_t^{\mathrm{vV}}(q_0,q_1)\langle q_1|\hat{\mathfrak{R}}(\eta')|q_2\rangle\mathcal{K}_t^{\mathrm{vV}}(q_3,q_0)\right\}\langle q_3|\hat{A}|q_0\rangle\,, \tag{5.16}$$

where the van Vleck propagators allows us to associate a momentum p_i with the position q_i, $i = 0, 1, 2, 3$ through the generating functions entering their phases. What the equation above is telling us is that the evolution inside the curly brackets allows for the classical phase-space interpretation

$$(q_0,p_0) \xrightarrow{\rho_t} (q_1,p_1) \xrightarrow{\mathfrak{R}_{\eta'}} (q_2,p_2) \xrightarrow{\rho_t^{-1}} (q_3,p_3)\,,$$

where $\mathfrak{R}$ represents a classical reflection around η'. The evolution entering the semiclassical reflection can then be described in three steps:

1. Start with $x_- = (q_0,p_0)$ and evolve it using the flow to build $(q_1,p_1) = x'_- = \rho_t(x_-)$;
2. Reflect the point x'_- around η' and define $(q_2,p_2) = x'_+ = \mathfrak{R}_{\eta'}(x'_-) = 2\eta' - x'_-$;
3. Evolve the point x'_+ *backwards* using the inverse flow to get $(q_3,p_3) = x_+ = \rho_t^{-1}(x'_+)$.

The value of $\hat{A}$ depends, as can be seen, both on the center η' and on the initial point x_-, which parametrizes the whole circuit. This circuit is depicted in Fig. 5.2(a).

The chord view

Now, the version equivalent to (5.16) takes the form

$$A_t(\xi') \approx \int_{\mathbb{R}^{4n}} dq_0\, dq_1\, dq_2\, dq_3 \left\{ \mathcal{K}_t^{\mathrm{vV}}(q_0,q_1)\langle q_1|\hat{\mathfrak{T}}(\xi')|q_2\rangle \mathcal{K}_t^{\mathrm{vV}}(q_3,q_0)\right\} \langle q_3|\hat{A}|q_0\rangle\,,$$

allowing for the classical interpretation

$$(q_0,p_0) \xrightarrow{\rho_t} (q_1,p_1) \xrightarrow{\mathfrak{T}_{\xi'}} (q_2,p_2) \xrightarrow{\rho_t^{-1}} (q_3,p_3)\,,$$

where $\mathfrak{T}_{\xi'}$ represents a classical translation by ξ'. The evolution is then given in three steps:

1. Start with $x_- = (q_0,p_0)$ and evolve it using the flow to build $(q_1,p_1) = x'_- = \rho_t(x_-)$;
2. Translate the point x'_- by the chord ξ' and define $(q_2,p_2) = x'_+ = \mathfrak{T}_{\xi'}(x'_-) = \xi' + x'_-$;
3. Evolve the point x'_+ *backwards* using the inverse flow to get $(q_3,p_3) = x_+ = \rho_t^{-1}(x'_+)$.

The value of $\hat{A}$ now depends on both the chord ξ' and on the initial point x_-. This circuit is depicted in Fig. 5.2(b).

5.2.2 IVRs for the Weyl-Wigner symbols

We now proceed to approximate the expressions

$$\begin{cases} A_t(\eta) = \left(\dfrac{1}{\pi\hbar}\right)^n \displaystyle\int d\xi \left\{\left[\hat{\mathfrak{R}}_t(\eta)\right](\xi)\right\} \widetilde{A}(\xi) \approx \left(\dfrac{1}{\pi\hbar}\right)^n \int d\xi \left\{\left[\hat{\mathfrak{R}}_t(\eta)\right](\xi)\right\}^{\mathrm{SC}} \widetilde{A}(\xi) \\ \widetilde{A}_t(\xi) = \left(\dfrac{1}{2\pi\hbar}\right)^n \displaystyle\int d\eta \left\{\left[\hat{\mathfrak{T}}_t(\xi)\right](\eta)\right\} A(\eta) \approx \left(\dfrac{1}{2\pi\hbar}\right)^n \int d\eta \left\{\left[\hat{\mathfrak{T}}_t(\xi)\right](\eta)\right\}^{\mathrm{SC}} A(\eta) \end{cases}$$

using the geometry presented in the earlier section and the IVRs of Section 5.1.4. First, notice that the classical flow that brings $x_- \longmapsto x_+$ in Fig. 5.2(a) is given by

$$x_+(\eta',x_-) = (\rho_{-t}\circ\mathcal{R}_{\eta'}\circ\rho_t)(x_-)\,,$$

while in Fig. 5.2(b) it is

$$x_+(\xi',x_-) = (\rho_{-t}\circ\mathcal{T}_{\xi'}\circ\rho_t)(x_-)\,.$$

Since the classical flow depends on both η'/ξ' and the initial point x_-, the generating functions that will give rise to these centers and chords will also have dependencies in the form $S_t(\eta(\eta',x_-))$ and $\widetilde{S}_t(\xi(\xi',x_-))$. The semiclassical propagators corresponding to this compound evolution have the form

$$\begin{aligned} \left\{\left[\hat{\mathfrak{R}}_t(\eta')\right](\xi)\right\}^{\mathrm{SC}} &= \sum_j \left|\det\left(\frac{d\xi(\eta',x_-)}{dx_-}\right)\right|_j^{\frac{1}{2}} \exp\left\{\frac{i}{\hbar}\left[\widetilde{S}_t^{(j)}(\xi(\eta',x_-)) + \frac{i\pi\widetilde{\sigma}^{(j)}}{2}\right]\right\} \\ \left\{\left[\hat{\mathfrak{T}}_t(\xi')\right](\eta)\right\}^{\mathrm{SC}} &= \sum_j \left|\det\left(\frac{d\eta(\xi',x_-)}{dx_-}\right)\right|_j^{\frac{1}{2}} \exp\left\{\frac{i}{\hbar}\left[S_t^{(j)}(\eta(\xi',x_-)) + \frac{i\pi\sigma^{(j)}}{2}\right]\right\}, \end{aligned}$$

where the sum runs over the branches of $\widetilde{S}$ and S. Using the logic of the earlier section, we arrive at the IVRs

$$A_t(\eta') \approx \left(\frac{1}{2\pi\hbar}\right)^n \int dx_- \left|\det\left(\frac{d\xi(\eta',x_-)}{dx_-}\right)\right|^{\frac{1}{2}} \exp\left\{\frac{i}{\hbar}\left[\widetilde{S}_t(\xi(\eta',x_-)) + \frac{i\pi\widetilde{\sigma}}{2}\right]\right\} \widetilde{A}(\xi(\eta',x_-)) \quad (5.17)$$

$$\widetilde{A}_t(\xi') \approx \left(\frac{1}{\pi\hbar}\right)^n \int dx_- \left|\det\left(\frac{d\eta(\xi',x_-)}{dx_-}\right)\right|^{\frac{1}{2}} \exp\left\{\frac{i}{\hbar}\left[S_t(\eta(\xi',x_-)) + \frac{i\pi\sigma}{2}\right]\right\} A(\eta(\xi',x_-))\,. \quad (5.18)$$

What do the propagators above mean? Well, in both cases x_- runs over the same circuit, presented in a slightly different way in Fig. 5.3(a), the difference is that in the Wigner representation the intermediate

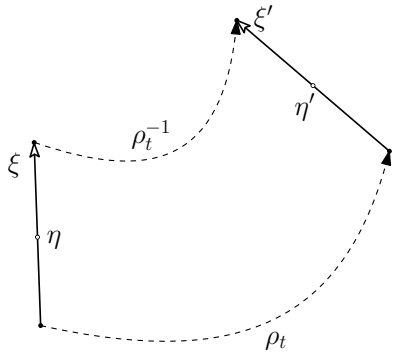

(a) Reinterpretation of Figs. 5.2(a) and 5.2(b) as an evolving chord ξ.

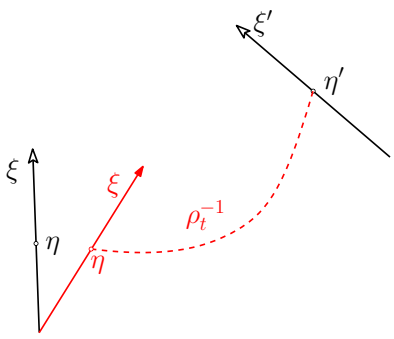

(b) Evolving η' backwards to η doesn't work: we end up with a different initial chord ξ.

Figure 5.3: (a) We re-interpret the circuit performed by x_- as a final chord/center evolving backwards to an initial chord/center. The variables we take as starting point are now $x'_\pm$, from which we form either ξ' or η' depending on whether we are in the Wigner or Weyl representations, respectively. This is just a way of simplifying dependencies in the IVRs (5.17) and (5.18). (b) The area of the circuit $x_- \longmapsto x_+$ is given by the area of the dashed-green quadrilateral, *plus* the area in gray, *minus* the area in pink. These latter areas are given by the center generating functions evaluated at the midpoints between $x_\pm$ and $x'_\pm$, defined as $\eta_\pm$.

step is a reflection, while in the Weyl representation it is a translation – The Wigner symbol tells us how to calculate evolution using a center, and the Weyl symbol does the same, but using a chord. Now, both propagations are functions of variables we still haven't defined, namely initial chords and centers ξ and η, which are very easy to infer: $\xi = x_+ - x_-$ is the chord joining our starting point x_- and its final arrival, x_+; and η is just the midpoint $(x_+ + x_-)/2$ (see Fig. 5.3(a)). We now use the Wigner symbol as a probe to understand this scenario.

Since the Wigner symbol is expressed as a function of chords, we can then reinterpret the circuit in Fig. 5.2(b) as evolving and initial *chord* from $\xi \longmapsto \xi'$, parametrizing the whole evolution as a function of x_- as in Fig. 5.3(a). A subtle observation renders this interpretation cumbersome: The only available data for us are the *initial* point x_- and the *final* center η', which is where we want to calculate our symbol. If the initial center η were available, we could simply reflect x_- around it to create x_+, defining the initial chord to be propagated to ξ'. Can we define this center without using the whole circuit? Isn't η just the inverse $\rho_{-t}(\eta')$? Unfortunately, no: There's only one situation in which the midpoint between two arbitrary phase-space points remains being the midpoint when evolved – linear evolution. This can be simply put as: The only case in which lines evolve into lines is when evolution is linear. The backwards-evolved center η obtained by $\rho_{-t}(\eta')$, therefore, does not coincide with the true center η. This is depicted in Fig. 5.3(b).

By interpreting $\xi(x_-) \longmapsto \xi'(x_-)$ in the Wigner representation, we are therefore required to perform the complete circuit $x_- \longmapsto x_+$ in order to obtain the required variables[2]. It is a cumbersome method because it uses input that is defined at unmatched times, but taking a look at Fig. 5.3(a) we then wonder if it's not easier to just *backwards-evolve* ξ', since in this case it is absolutely true that x'_+ is obtained by reflecting x'_- around η'. This would provide an integral representation using *final* centers η' and *final* points x'_- as input, eliminating the problems of initial variables defined at unmatched times.

5.2.3 FVRs for the Weyl-Wigner symbols

Following the reasoning proposed by the end of the last section, let us interpret evolution not as $\xi(x_-) \longmapsto \xi'(x_-)$, but as $\xi(x'_-) \longleftarrow \xi'(x'_-)$. Our initial variable is now x'_-, which we reflect around η' to obtain $x'_+ = 2\eta' - x'_-$. These form the final chord ξ' which we can backwards-evolve to $\xi = \rho_{-t}(x'_+) - \rho_{-t}(x'_-) = x_+ - x_-$. Alternatively, we can also start from η' and ξ' to obtain $x'_\pm = \eta' \pm \xi'/2$.

[2]The flow ρ_t is generally numerical and introduces an error ϵ, meaning that we miss the exact spot x'_- by ϵ and later backwards evolve it again, missing x'_+ again by ϵ (the intermediate reflection is exact). It can then be argued that the double error propagation is also a disadvantage of this method [dAVZ13].

This latter approach is the one we follow now. Since x_- is now a function of final chords, we have

$$\frac{d\xi(\eta',\xi')}{dx_-(\eta',\xi')} = \left(\frac{d\xi(\eta',\xi')}{d\xi'}\right)\left(\frac{dx_-(\eta',\xi')}{d\xi'}\right)^{-1}$$
$$\implies \quad \left|\det\left(\frac{d\xi(\eta',\xi')}{dx_-(\eta',\xi')}\right)\right|^{\frac{1}{2}} dx_- = \left|\det\left(\frac{d\xi(\eta',\xi')}{d\xi'}\right)\right|^{\frac{1}{2}} d\xi' \,,$$

and analogously for centers,

$$\left|\det\left(\frac{d\eta(\xi',\eta')}{dx_-(\xi',\eta')}\right)\right|^{\frac{1}{2}} dx_- = \left|\det\left(\frac{d\eta(\xi',\eta')}{d\eta'}\right)\right|^{\frac{1}{2}} d\eta' \,.$$

Using which we finally arrive at final value representations corresponding to the IVRs (5.17) and (5.18):

$$A_t(\eta') \approx \left(\frac{1}{2\pi\hbar}\right)^n \int d\xi' \left|\det\left(\frac{d\xi(\xi',\eta')}{d\xi'}\right)\right|^{\frac{1}{2}} \exp\left\{\frac{i}{\hbar}\left[\widetilde{S}_t(\xi(\xi',\eta')) + \frac{i\pi\widetilde{\sigma}}{2}\right]\right\} \widetilde{A}(\xi(\xi',\eta')) \quad (5.19)$$
$$\widetilde{A}_t(\xi') \approx \left(\frac{1}{\pi\hbar}\right)^n \int d\eta' \left|\det\left(\frac{d\eta(\eta',\xi')}{d\eta'}\right)\right|^{\frac{1}{2}} \exp\left\{\frac{i}{\hbar}\left[S_t(\eta(\eta',\xi')) + \frac{i\pi\sigma}{2}\right]\right\} A(\eta(\eta',\xi')) \,.$$

Now, the procedure to obtain the variables used in the equation above is much simpler than for the IVRs, and can be enumerated for both representations as:

1. Begin with independent variables given by final chords and centers ξ' and η', from which we extract the final phase-space points as $x'_\pm = \eta' \pm \xi'/2$;
2. Propagate the $x'_\pm$ above backwards to build $x_\pm = \rho_{-t}(x_\pm)$, which we use to write the initial chords and centers as $\eta = (x_+ + x_-)/2$ and $\xi = x_+ - x_-$;
3. Perform calculations and, for the Wigner or Weyl symbols, integrate over ξ' or η', respectively.

The formula (5.19) is the most important one for the first part of the results obtained in this dissertation. However, in the present state it is not computationally applicable, since we have explained how to obtain the employed variables but not how to calculate its terms.

5.3 FVR for Wigner functions

In this section we obtain closed expressions for all the terms included in the FVR (5.19).

The amplitude

We now obtain a closed expression for the amplitude in (5.19). Since

$$\xi' = \mathcal{R}_{\eta'}(x'_-) - x'_- = 2(\eta' - x'_-) \quad \implies \quad d\xi' = 2dx'_- \,,$$

the amplitude can be written as

$$\frac{d\xi}{d\xi'} = \frac{1}{2}\frac{d\xi}{dx'_-} \,. \quad (5.20)$$

Lemma 5.3.1. The complete circuit performed by $x_- \longmapsto x_+ = (\rho_{-t} \circ \mathcal{R}_{\eta'} \circ \rho_t)(x_-)$ has a monodromy matrix $\mathfrak{M}$ expressible as

$$\mathfrak{M}_t = -\mathcal{M}_t^{-1}(x_+)\mathcal{M}_t(x_-) \,, \qquad \mathcal{M}_t(x_\pm) = \left.\frac{d\rho_t(x)}{dx}\right|_{x=x_\pm} \,,$$

where $\mathcal{M}_t(x_\pm)$ represent the monodromies for each segment $x_\pm \longrightarrow x'_\pm$.

Proof. The monodromy for the complete circuit is given by $\mathfrak{M}_t = dx_+/dx_-$, for which

$$\begin{aligned}
\left.\frac{dx_+}{dx_-}\right|_{\eta',x_-} &= \left.\frac{d}{dx_-}\left[(\rho_{-t}\circ\mathcal{R}_{\eta'}\circ\rho_t)(x_-)\right]\right|_{x_-} \\
&= \left\{\frac{d\rho_{-t}\left[(R_{\eta'}\circ\rho_t)(x_-)\right]}{d\left[(R_{\eta'}\circ\rho_t)(x_-)\right]}\right\}\Bigg|_{(R_{\eta'}\circ\rho_t)(x_-)}\left\{\frac{dR_{\eta'}\left[\rho_t(x_-)\right]}{d\left[\rho_t(x_-)\right]}\right\}\Bigg|_{\rho_t(x_-)}\left.\frac{d\rho_t(x_-)}{dx_-}\right|_{x_-} \\
&= \left\{\frac{d\rho_{-t}(x'_+)}{dx'_+}\right\}\Bigg|_{x'_+}\left\{\frac{d(2\eta'-x'_-)}{dx'_-}\right\}\Bigg|_{x'_-}\left.\frac{d\rho_t(x_-)}{dx_-}\right|_{x_-}.
\end{aligned}$$

Notice, however, that

$$\begin{cases}
\left.\dfrac{d\rho_{-t}(x'_+)}{dx'_+}\right|_{x'_+} = \left.\dfrac{dx_+}{dx'_+}\right|_{x'_+} = \left[\dfrac{dx'_+}{dx_+}\right]^{-1}\Bigg|_{x_+} = \mathcal{M}_t^{-1}(x_+) \\
\left.\dfrac{d\rho_t(x_-)}{dx_-}\right|_{x_-} = \left.\dfrac{dx'_-}{dx_-}\right|_{x_-} = \mathcal{M}_t(x_-) \\
\dfrac{d(2\eta'-x'_-)}{dx'_-} = -I
\end{cases}.$$

Therefore, the monodromy matrix for the complete cycle is given as a function of the monodromies for each segment as

$$\mathfrak{M}_t = \mathcal{M}_t^{-1}(x_+)[-I]\mathfrak{M}_t(x_-) = -\mathcal{M}_t^{-1}(x_+)\mathcal{M}_t(x_-)\,.$$

□

Substituting the lemma above in (5.20) we have

$$\begin{aligned}
\frac{d\xi}{d\xi'} = \left(\frac{1}{2}\right)\frac{d\xi}{dx'_-} = \left(\frac{1}{2}\right)\left(\frac{d(x_+-x_-)}{dx_-}\right)\left(\frac{dx_-}{dx'_-}\right) &= \left(\frac{1}{2}\right)\left[-\mathcal{M}_t^{-1}(x_+)\mathcal{M}_t(x_-)-I\right]\mathcal{M}_t^{-1}(x_-) \\
&= -\left(\frac{1}{2}\right)\left[\mathcal{M}_t^{-1}(x_+)+\mathcal{M}_t^{-1}(x_-)\right]
\end{aligned}$$

and, finally,

$$\begin{aligned}
\left|\det\left(\frac{d\xi}{d\xi'}\right)\right| &= \left|\det\left(\frac{\mathcal{M}_t^{-1}(x_+)+\mathcal{M}_t^{-1}(x_-)}{2}\right)\right| \\
&= \left(\frac{1}{2^{2n}}\right)\det(\mathcal{M}_t(x_-))\left|\det\left(\mathcal{M}_t^{-1}(x_+)+\mathcal{M}_t^{-1}(x_-)\right)\right|\det(\mathcal{M}_t(x_+)) \\
&= \left(\frac{1}{2^{2n}}\right)\left|\det\left(\mathcal{M}_t(x_+)+\mathcal{M}_t(x_-)\right)\right|\,,
\end{aligned}$$

where we used the fact that $\det\mathcal{M}_t(x_-)=1$. We obtain the final expression for the amplitude as

$$\left|\det\left(\frac{d\xi}{d\xi'}\right)\right|^{\frac{1}{2}} = \left|\det\left(\frac{\mathcal{M}_t(x_+)+\mathcal{M}_t(x_-)}{2}\right)\right|^{\frac{1}{2}}, \qquad \mathcal{M}_t(x_\pm) = \left.\frac{d\rho_t(x)}{dx}\right|_{x=x_\pm}, \tag{5.21}$$

where we recover a factor of $1/2^n$ missing from (4.15) of [dAVZ13] (as already noted in [Buc15]).

The action

The action $\widetilde{S}_t(\xi(\xi',\eta'))$ employs chords and centers simultaneously, since the initial ξ is a function of η'. We can un-mix polarizations by using the Legendre transforms presented in Chapter 1, *i.e.*

$$\widetilde{S}_t(\xi(\xi',\eta')) = \xi\cdot\mathcal{J}\eta - S_t(\eta'(\eta))\,,$$

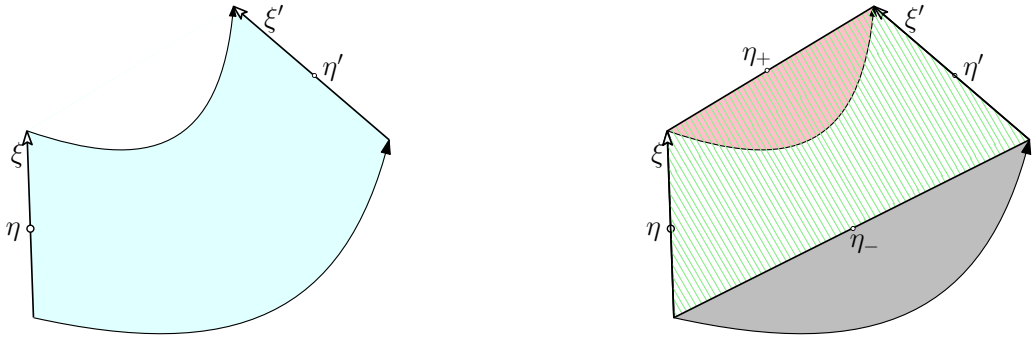

(a) The area traveled by $\xi \longmapsto \xi'$.

(b) Decomposition of the area.

Figure 5.4: (a) The symplectic area of the circuit $x_- \longmapsto x_+$ is now interpreted as the area traveled by the initial chord ξ while evolving to ξ' – of course, it makes more sense to picture this area as being covered by ξ' while evolving backwards to ξ. (b) This area can be decomposed as the symplectic area of the dashed-green quadrilateral, *plus* the area in gray, *minus* the area in pink. These latter areas are given by the center generating functions evaluated at the midpoints between $x_\pm$ and $x'_\pm$, defined as $\eta_\pm$. The symplectic area of the quadrilateral is just $(x'_- - x_+)\cdot\mathcal{J}(x'_+ - x_+)/2$, expressed in terms of centers and chords as $(\eta-\eta')\cdot J(\xi+\xi')/4$.

where $S_t(\eta'(\eta))$ is the center generating function in the extended product manifold:

$$S_t(\eta'(\eta)) = \int_\eta^{\eta'} \mathcal{J}\xi\cdot d\eta - \int_0^t dt\, H(\eta) = \int_\eta^{\eta'} \mathcal{J}\xi\cdot d\eta - [(H(x_+) - H(x_-)]t\,,$$

where the first term represents the area of traveled by ξ while evolving to ξ', *i.e.* the area of the circuits considered in the earlier sections. As we can see in Fig. 5.4, this area can be decomposed into three terms: the two symplectic areas that join $x_\pm \longmapsto x'_\pm$ and the symplectic area of the quadrilateral joining the points in the circuit by straight lines. From Section 1.5.3, we identify the gray and pink areas in Fig. 5.4(b) as the extended center generating functions $S_t(\eta_\pm)$ calculated at the midpoints $\eta_\pm = (x'_\pm + x_\pm)/2$, while the symplectic area of the quadrilateral is trivially given by $(\eta-\eta')\cdot J(\xi+\xi')/4$. Thus, we have

$$\widetilde{S}_t(\xi(\xi',\eta')) = \xi\cdot\mathcal{J}\eta - \frac{1}{4}\left[(\eta-\eta')\cdot J(\xi+\xi')\right] - S_t(\eta_+) + S_t(\eta_-) + [H(x_+) - H(x_-)]\,t\,. \quad (5.22)$$

with $S_t(\eta_\pm)$ as in (1.21).

The indexes

The Conley-Zehnder indexes are the caustic count of $x_- \longmapsto x_+$, except that when the caustics are hit during the forward step $x_- \longmapsto x'_-$, the indexes are positive; while for the backward step $x'_+ \longmapsto x_+$ they are negative. We provide more details on their calculation in Appendix F.

The final formula

Gathering the results obtained in the earlier subsections, we can express the Wigner function using the FVR by setting $\widetilde{A} = \chi$, the characteristic function at $t = 0$, resulting in

$$W_t(\eta') = \left(\frac{1}{2\pi\hbar}\right)^n \int d\xi' \left|\det\left(\frac{d\xi(\xi',\eta')}{d\xi'}\right)\right|^{\frac{1}{2}} \exp\left[\frac{i}{\hbar}\left(\widetilde{S}_t(\xi(\xi',\eta')) + \frac{\hbar\pi\tilde{\sigma}}{2}\right)\right]\chi(\xi(\eta',\xi'))\,, \quad (5.23)$$

with amplitude and action as in (5.21) and (5.22), respectively. The only thing left is to choose an initial state to propagate through its characteristic function $\chi(\xi)$.

Bibliography

[AG] V. I. Arnol'd and A. B. Givental'. *Symplectic Geometry.*

[Ber89] M. V. Berry. Quantum scars of classical closed orbits in phase space. *Proc. R. Soc. Lond. A*, (423):219, 1989.

[Buc15] J. V. Bucher. *Semiklassik fur den Kerr-Hamiltonian*. Bachelorarbeit, 2015.

[dA98] A. M. Ozorio de Almeida. The Weyl representation in classical and quantum mechanics. *Phys. Rep.*, 295:265, 1998.

[dAI14] A. M. Ozorio de Almeida and G.-L. Ingold. Metaplectic sheets and caustic traversals in the Weyl representation. *J. Phys. A: Math. Theor.*, 47:105303, 2014.

[dAVZ13] A. M. Ozorio de Almeida, R. O. Vallejos, and E. Zambrano. Initial or final values for semiclassical evolutions in the Weyl-Wigner representation. *J. Phys. A: Math. Theor*, 46:135304, 2013.

[dG06] M. de Gosson. *Symplectic Geometry and Quantum Mechanics*. Birkhauser, 2006.

Chapter 6

Numerical simulations: The Kerr system

> The truth will set you free. But not until it is finished with you.
>
> D. Foster Wallace in *Infinite Jest*

As seen in Chapter 2, non-separable hamiltonians present significant difficulties for numerical algorithms. The most important continuous system in this dissertation, the *[homogeneous] Kerr system*, is obtained from the flow of the non-separable hamiltonian

$$H(q,p) = \left(p^2+q^2\right)^2 . \tag{6.1}$$

This system is an invaluable toy model due to its flow being analytical despite it being obtained from a 4th order hamiltonian. Remarkably, it is also exactly solvable for the quantum propagation of a coherent state and presents an intriguing and kaleidoscopic evolution, which we reproduce semiclassically in this chapter. Computational details are provided in Appendix F.

6.1 Classical dynamics

In this brief section we apply the classical theory developed in the main body of this dissertation: First, we obtain the classical flow associated to (6.1) by using the concepts presented in Chapter 1; Then, we use this flow to classically propagate Wigner functions in phase space, following Section 4.2.2.

We begin by calculating the flow generated by the hamiltonian (6.1). For the vector field, we have

$$X_H = \frac{\partial H}{\partial p}\frac{\partial}{\partial q} - \frac{\partial H}{\partial q}\frac{\partial}{\partial p} = 4\left(p^2+q^2\right)\left(p\frac{\partial}{\partial q} - q\frac{\partial}{\partial p}\right) = \omega(q,p)\left(p\frac{\partial}{\partial q} - q\frac{\partial}{\partial p}\right) ,$$

which is just the SHO vector field presented in Example 1.2.10 multiplied by $\omega(q,p) = 4|x|^2$. Its integration follows the exact same steps of Example 1.2.10:

$$\rho_t(x) = \exp\left(tX_H\right)(x) = \exp\left[\omega(q,p)t\left(p\frac{\partial}{\partial q} - q\frac{\partial}{\partial p}\right)\right](q,p)$$

$$\implies \quad \rho_t(x_0) = \begin{pmatrix} \cos\left[\omega(x_0)t\right] & \sin\left[\omega(x_0)t\right]] \\ -\sin\left[\omega(x_0)t\right] & \cos\left[\omega(x_0)t\right] \end{pmatrix}\begin{pmatrix} q_0 \\ p_0 \end{pmatrix} , \quad \omega(x_0) = 4(q_0^2+p_0^2) . \tag{6.2}$$

The orbits for the Kerr system, just as the SHO's, are circles. The fundamental distinction between them is that the latter has a constant angular speed per orbit, while for the Kerr system each orbit has its own angular frequency $\omega(q_0,p_0)$. Since $\omega(q_0,p_0)$ represents the squared-radius of the circular orbit, we see that the angular speed is monotonically increasing with the distance from the origin: Outer orbits move faster than inner orbits. The net-effect of differing angular speeds is the disfiguring of an initial phase-space distribution into a filament that gets thinner as time evolves. This can be seen in phase space by employing (4.22) for the propagation of the Wigner function of a coherent state initially centered at $(q_0,p_0) = (5,0)$, using the Kerr flow (6.2). This is displayed in Fig. 6.1.

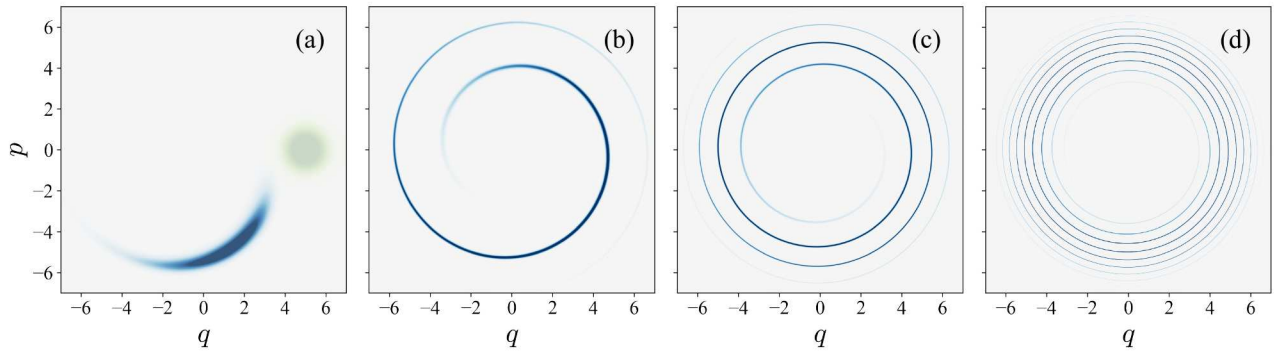

Figure 6.1: The Wigner function of a coherent state, initially centered at $(q = 5, p = 0)$, shown in green in panel (a), is evolved using (4.22) by the flow (6.2) for (a) $t = 0.013$; (b) $t = 0.071$; (c) $t = \pi/20$ and (d) $t = \pi/8$. Since the outer angular speeds are larger, the right extremity moves faster and starts deforming the initial state in (a). For the longer time in (b), the center of the initial coherent state has performed a little more than a complete revolution around the origin, and in (c) and (d), the initial state has already deformed into a thin spiraling filament.

6.2 Quantum dynamics

The quantum propagation of a coherent state by the Kerr system is more intricate that its classical counterpart. In fact, when we said that this propagation was exact, we were not accurate: It is not exact for *all* times, but for a dense subset of all times. In this section we apply standard quantum theory to solve for the propagation of a coherent state under Kerr dynamics, describing in detail its complex structure of revival patterns. We then use the theory of Chapter 4 to move the wavefunction to phase space and visualize the undeniably beautiful geometry of its Wigner function. We conclude the quantum-classical analogies with an analysis of autocorrelation functions.

From now on we shall assume $\hbar = 1$. What does this mean, if $\hbar$ is a constant? In a way, what we are doing is measuring our actions in units of $\hbar$, *i.e.* $S \longmapsto \hbar S \Longrightarrow S/\hbar \longmapsto S/1$. We do this because $\hbar$ is so small that, in order to see quantum interference, we would have to perform calculations on a "quantum grid". The assumption $\hbar = 1$ is therefore equivalent to a rescaling our classical actions to an $\hbar$-scale.

6.2.1 Coherent-state evolution and revival patterns

The classical Kerr system (6.1) is valuable due to being simultaneously non-trivial and exact. In terms of action-angle coordinates for the SHO, its hamiltonian can be written as

$$H_{\text{Kerr}}(I) = 4I^2\,, \quad I = \frac{p^2+q^2}{2}\,,$$

so that the Kerr system is arguably the simplest non-quadratic system that retains analyticity and mixes position and momentum [YS86, AP89]. Note that also we have the immediate quantization of the action in terms of the number operator $\hat{n}$ as $\hat{I} = \hat{n} + \hat{1}/2$, so the canonical quantization can be immediately employed without any ordering problems:

$$H_{\text{Kerr}} = (p^2+q^2)^2 = 4I^2 \quad \longmapsto \quad \hat{H}_{\text{Kerr}} = (\hat{p}^2+\hat{q}^2)^2 = 4\left(\hat{n}+\frac{\hat{1}}{2}\right)^2 = (2\hat{n}+\hat{1})^2\,,$$

where we have used the SHO's number operator, defined in terms of the annihilation operator as $\hat{n} = \hat{a}^\dagger\hat{a}$ (see Appendix C). As we are interested in the time-evolution of coherent states, we have

$$\begin{aligned}|\alpha_t\rangle = \exp\left[-it\hat{H}_{\text{Kerr}}\right]|\alpha\rangle &= \exp\left\{-it\left(2\hat{n}+\hat{1}\right)^2\right\}\left[e^{-\frac{|\alpha|^2}{2}}\sum_{m=0}^{\infty}\frac{\alpha^m}{\sqrt{m!}}|m\rangle\right] \\ &= e^{-\frac{|\alpha|^2}{2}-it}\sum_{m=0}^{\infty}\frac{1}{\sqrt{m!}}\left[\alpha\exp\left(-4it\right)\right]^m\left\{\exp\left[-4im^2t\right]\right\}|m\rangle\,, \qquad (6.3)\end{aligned}$$

where we have used the decomposition of a coherent state in terms of SHO eigenvectors [Bal08], represented by $|m\rangle$. Notice that, for $k \in \mathbb{Z}$, the substitution $t \longmapsto k\pi/4$ in the expression above implies $|\alpha_{k\pi/4}\rangle = |\alpha_0\rangle$, so that the propagation of a coherent state under the Kerr system's dynamics reconstructs the initial state for integer multiples of $\pi/4$ [YS86].

Definition 6.2.1. The reproduction of the initial state is called a **full revival**, and the time $T_{\text{rev}} = \pi/4$ is called the **revival time** for the Kerr system.

Thus, the Kerr system is periodic with period equal to the revival time. The exponential term inside curly brackets in (6.3) is also periodic and its period can be found from

$$4m^2t - 4(m+n)^2t = 2\pi k\,, \quad k \in \mathbb{Z} \quad \Longrightarrow \quad (2nm+n^2)t = 2\pi k\,.$$

If we choose rational multiples of the revival time, namely $t = (a/b)T_{\text{rev}}$, this simplifies to

$$(2mn+n^2)T_{\text{rev}} = 2\pi k \quad \Longrightarrow \quad (2mn+n^2)\frac{a}{b} = k \quad \overset{m\longmapsto b/2}{\Longrightarrow} \quad (m+2b)a \in \mathbb{Z}\,, \quad \forall m\,,$$

so we guarantee a period of $b/2$ whenever $q \neq 4$ – therefore, from now on we assume b to be odd. The exponential in the curly brackets of (6.3) can then be expanded in a Fourier series for $t = (2a/b)T_{\text{rev}}$:

$$\exp\left[-4im^2t\right] = \exp\left[-\frac{4\pi im^2a}{2b}\right] = \sum_{s=0}^{b-1} c_s \exp\left[-\frac{2\pi ism}{b}\right]\,, \quad c_s = \frac{1}{b}\sum_{r=0}^{b-1}\exp\left[\frac{2\pi im}{b}\,(s-am)\right]\,,$$

so the coherent state's time-evolution is significantly simplified to

$$\begin{aligned}
|\alpha_{\pi a/2b}\rangle &= e^{-\frac{|\alpha|^2}{2}-\frac{i\pi a}{2b}}\sum_{s=0}^{b-1}\sum_{m=0}^{\infty}\frac{c_s}{\sqrt{m!}}\left[\alpha\exp\left(-\frac{2\pi ia}{b}\right)\right]^m\exp\left[-\frac{2\pi ism}{b}\right]|m\rangle \\
&= e^{-\frac{|\alpha|^2}{2}-\frac{i\pi a}{2b}}\sum_{s=0}^{b-1}\sum_{m=0}^{\infty}\frac{c_s}{\sqrt{m!}}\left\{\alpha\exp\left[-\frac{2\pi i}{b}\,(a+s)\right]\right\}^m|m\rangle \\
\Longrightarrow \quad |\alpha_{\pi a/2b}\rangle &= e^{-\frac{i\pi a}{2b}}\sum_{k=0}^{b-1}c_k\left|\alpha\exp\left[-\frac{2\pi i}{b}\,(a+k)\right]\right\rangle\,, \qquad (6.4)
\end{aligned}$$

where the big ket in the equation above is just a coherent state with the α-value multiplied by the exponential. The coefficients c_k, for odd values of b, can be obtained recursively:

$$\begin{aligned}
c_{k'} = \frac{1}{q}\sum_{n=0}^{q-1}\exp\left[2\pi i\left(\frac{k'}{b}n - \frac{a}{b}n^2\right)\right] &= \frac{1}{q}\sum_{n=0}^{q-1}\exp\left[2\pi i\left(\frac{k}{b}n + \frac{2a}{b}n - \frac{a}{b}n^2\right)\right] \\
&= \frac{1}{q}\sum_{n=0}^{q-1}\exp\left[2\pi i\left(\frac{k}{b}n - \frac{a}{b}(n-1)^2\right)\right]\exp\left(2\pi i\frac{a}{b}\right) \\
\Longrightarrow \quad c_{k'} &= c_k\exp\left[2\pi i\left(\frac{k+a}{b}\right)\right]\,, \qquad (6.5)
\end{aligned}$$

with

$$c_0 = \frac{1}{q}\sum_{n=0}^{q-1}\exp\left(-\frac{2\pi in^2a}{b}\right)\,. \qquad (6.6)$$

The position representation $\langle q|\alpha_{\pi a/2b}\rangle$ is easily obtained by simply substituting in (3.3). Under the restrictions placed here, namely that we can only access rational times $t = a\pi/2b$ with q odd, the Fourier expansion for the propagation of a coherent state under Kerr evolution converges and is exact. The restriction we have on time-values is also rather irrelevant, since we can approximate any real number using a fraction composed of mutually prime integers. The only problem of fine tuning a and b values is that to access some time of interest we might need very large b and, since we are actually approximating Kerr evolution as a sum of b coherent states (see (6.4)), the sums might become too

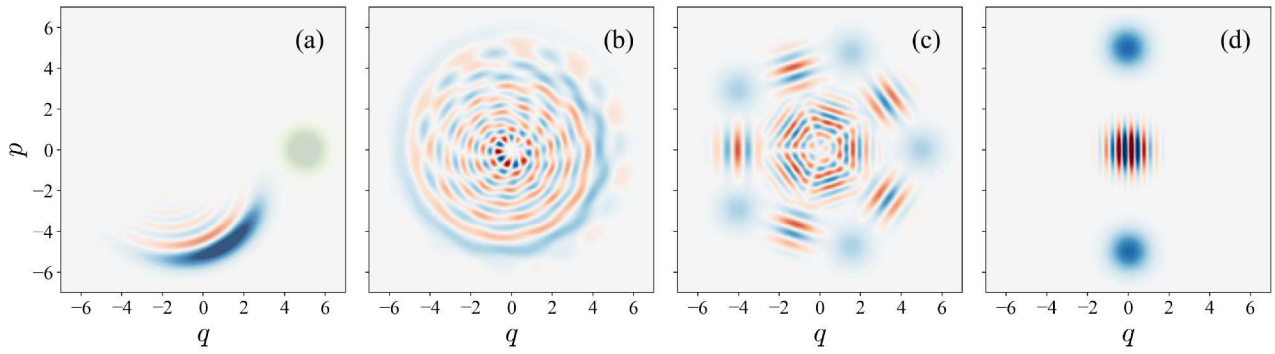

Figure 6.2: The same initial Wigner function of Fig. 6.1, shown in green in panel (a), is evolved using the Wigner transform (4.12) of (6.4) for the same time values as in Fig. 6.1, namely (a) $t = 0.013$; (b) $t = 0.071$; (c) $t = \pi/20$ and (d) $t = \pi/8$. For the short time in (a) we can clearly distinguish the classical skeleton of Fig. 6.1(a), which is harder for the larger time in (b) and impossible for (c) and (d). Following Definition 6.2.3, we can identify these latter two time-values as giving rise to the pentagonal and Schödinger cat fractional revivals.

large. Fortunately, the computers of today can effortlessly deal with b of $\mathcal{O}(10^4)$, so our time step can be taken as smaller than $\mathcal{O}(10^{-4})$.

In Definition 6.2.1 we have called a *full* revival a complete reproduction of the system's initial distribution (in our case, coherent states). However, note that the Kerr propagation given in (6.4) has several a/b combinations that will reproduce *fractions* of the initial distribution.

Example 6.2.2. For $a/b = 1/4$, the time simplifies to $t = \pi/8$. Our Fourier expansion does not converge (b is divisible by 4), but fortunately we can understand what happens calculating by hand: For this time value the system is completely described as a sum of only two coherent states and their interferences. If we consider the Fourier expansion for *e.g.* $a/b = 1000/4001 \approx 1/4$, what effectively takes place is that (6.4) becomes a sum of 4001 coherent states densely packed in the vicinity of two points. Visually, there would be basically no difference between $a/b = 0.25$ and $a/b = 0.2499$. For $a/b \approx 1/6$, $1/8$ and $1/10$, we would have coherent states distributed in a triangle, a square and a pentagon, respectively.

Definition 6.2.3. A **fractional revival** is a partial reappearance of the initial distribution.

Technically, the times we choose in order to describe propagation are able to attain fractional revivals exclusively. However, we will restrict the term to states that are *obviously* a partial reproduction, such as 2, 3 or 5 coherent states.

6.2.2 Coherent-state propagation in the Wigner representation

We are ready to bring the evolved coherent state in (6.3) to phase space and visualize its exact quantum propagation. In Fig. 6.2 we provide the Wigner functions obtained by applying (4.12) to the evolved ket (6.3), choosing the same time-values as in Fig. 6.1. The panel in Fig. 6.2(a) can be clearly interpreted as the classical backbone in Fig. 6.1(a) *plus* the oscillations caused by self-interference. The larger time-value of Fig. 6.2(b) is already challenging to trace back to Fig. 6.1(b), since interferences are so widespread that quantum-classical analogies become far-fetched. The longer times in Figs. 6.2(c) and (d) correspond to the fractional revival times, for which it is basically impossible to obtain any meaningful classical picture by comparing with Figs. 6.1(c) and (d): For this latter panel, for instance, the quantum Wigner function is completely localized around two opposing phase-space points, which interfere and create a Schrödinger's cat state; The classical Wigner function, however, is just a barely visible filament after performing several revolutions around the origin.

Can we expect to reproduce a revival pattern from a filament, *i.e.* can we provide a semiclassical method with the classical Kerr flow (6.2) and reproduce, from the filaments in Fig. 6.1, the intricate interferences and fractional revival patters of Fig. 6.2? Before attempting a semiclassical solution, we employ the theory of Subsection 4.2.3 to the quantum and classical autocorrelation functions in order to define the relevant time-scale for the problem – naturally, it will be given as a function of the Ehrenfest time.

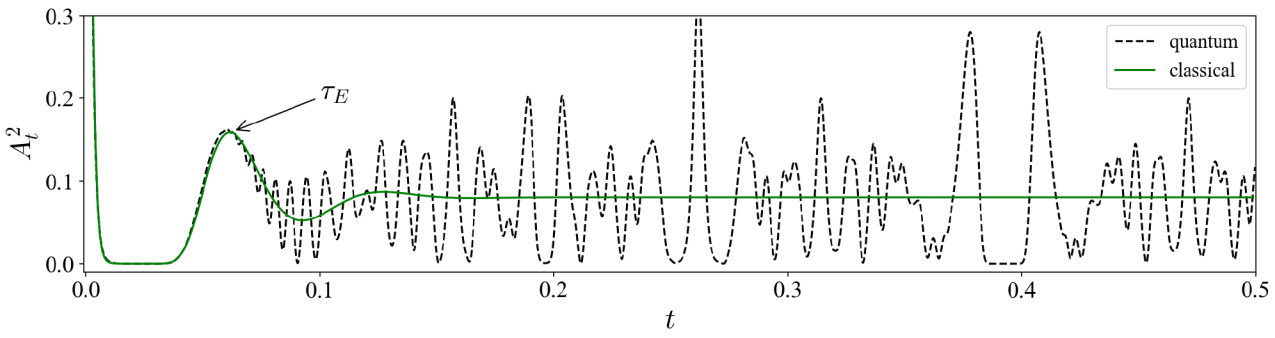

Figure 6.3: Quantum (dashed black) and classical (green) squared autocorrelation functions for the Kerr system, extracted from (4.23). The arrow points at the Ehrenfest time $\tau_E \approx 0.063$. Notice the quantum autocorrelation is reflected around $\pi/8 \approx 0.393$.

6.2.3 Autocorrelation functions and Ehrenfest time

Due to the periodicity of the Kerr system, it is possible extract the Ehrenfest time analytically. For this, notice that the frequency per orbit is given by $4(q_0^2+p_0^2)$, so the Ehrenfest time can be defined as the time it takes its center to perform a full revolution around the origin, intersecting with its starting phase-space region. Mathematically, we have

$$4(q_0^2+p_0^2)\tau_E = 2\pi \quad \Longrightarrow \quad \tau_E = \frac{\pi}{2(q_0^2+p_0^2)} = \frac{\pi}{50} \approx 0.063\,.$$

Thus, for the initial coherent state we have been propagating up to now, we expect the classical and quantum autocorrelation functions to match while $t \leq \tau_E \approx 0.063$. As we can see in Fig. 6.3, this is exactly what happens: The characteristic quantum oscillations arise immediately after τ_E, while the classical autocorrelation performs one last oscillation and stabilizes around a fixed value. We also see that we have placed the initial coherent state far away from the origin enough for the autocorrelation to really reach 0, *i.e.* the propagated state really spends some time without invading its initial domain.

It interesting to see that the cat-state revival at $t = \pi/8 \approx 0.392$ happens at exactly half the map's period, so after this fractional revival pattern the evolution is equivalent to its time reversal. This is clearly visible in Fig. 6.3, where we see that after the deep valley near $t = 0.4$ the autocorrelation function is reflected. Now that we have an Ehrenfest time available, we can also contextualize the time-values we have been using in Figs. 6.1 and 6.2: For the (a) panels, we are in the short-time regime, since $t = 0.013 \approx \tau_E/5$; For (b) we have just crossed the Ehrenfest barrier as the coherent state's center has performed a little more than one revolution around the origin; the (c) and (d) panels correspond to $t = \pi/20 \approx 2.5\tau_E$ and $t = \pi/8 \approx 6\tau_E$, respectively, considered to be *very long* times.

6.3 Semiclassical dynamics

Semiclassical propagation is about reproducing quantum dynamics from classical input, *i.e.* our objective is to reproduce Fig. 6.2 using the filaments of Fig. 6.1. Now that we possess an Ehrenfest-time scale, this appears feasible up until τ_E, but is supposed to become increasingly problematic for longer times. The possibility of reproducing fractional revival patterns from thin filaments, for instance, appears remote.

6.3.1 The monodromy matrix

By differentiating (6.2) with respect to the initial point $x_0 = (q_0, p_0)$ we obtain the monodromy matrix of (3.26):

$$\mathcal{M}_t(x) = \begin{bmatrix} (1+8pqt)\cos(\omega t) - 8q^2 t\sin(\omega t) & 8p^2 t\cos(\omega t) + (1-8pqt)\sin(\omega t) \\ -8q^2 t\cos(\omega t) - (1+8pqt)\sin(\omega t) & (1-8pqt)\cos(\omega t) - 8p^2 t\sin(\omega t) \end{bmatrix}, \tag{6.7}$$

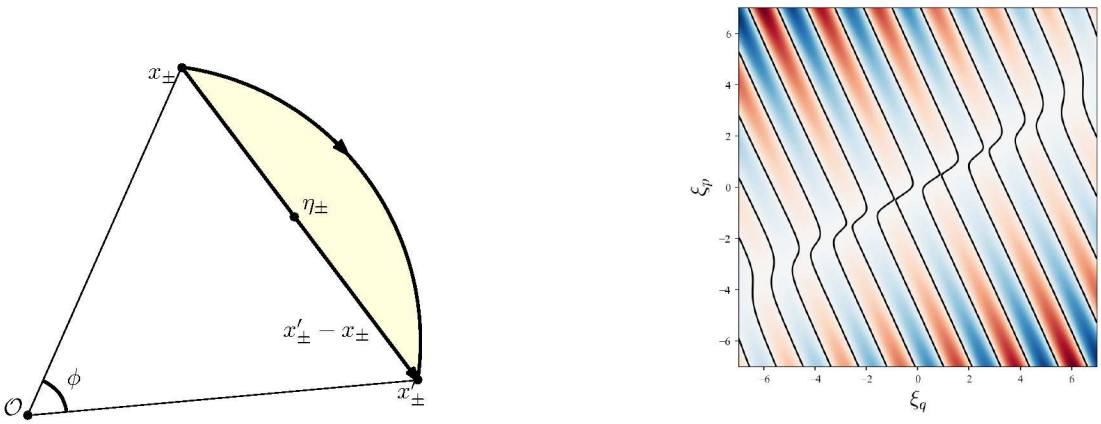

(a) Geometry of (6.9).

(b) Typical Kerr caustics.

Figure 6.4: (a) The geometric interpretation of the center generating function (6.9): It is the yellow area connecting $x_\pm$ to $x'_\pm$, limited by the chord $x_\pm - x'_\pm$ (see Fig. 1.2(b)). The area for the whole slice is simply $\phi|x_\pm|^2/2$, since $|x_\pm| = |x'_\pm|$, and the area of the extra triangle is $x_\pm \cos(\phi/2) \times x_\pm \sin(\phi/2) = x_\pm^2 \sin(\phi)/2$. For the Kerr system, $\phi = \omega_\pm t = 4(q_\pm^2 + p_\pm^2)t = 4|x_\pm|^2 t$. (b) Density plot for the determinant in (5.21) in the (ξ_q, ξ_p)-plane at $t = 0.071$ for a Wigner function evaluated at $(q, p) = (5, 2)$. The caustic submanifolds are displayed as solid black curves, being the regions where the original root-search based propagator diverges. Every time a trajectory crosses a black line, the Conley-Zehnder index changes.

where $x = (q, p)$ and $\omega = 4(q^2 + p^2)$. This matrix enters the semiclassical formula (5.23) through its determinant calculated at two distinct points, as shown in (5.21). The Conley-Zehnder indexes are then obtained from the condition

$$\begin{aligned} & \det\left[\mathcal{M}_t(x_+) + \mathcal{M}_t(x_-)\right] = 0 \\ \iff \quad & 32t^2(x_- \cdot \mathcal{J}x_+)\cos\left[\Omega t\right] + \left\{2\Omega\, t + 64t\left[(x_- \cdot \mathcal{J}x_+)\,(x_- \cdot x_+)\right]\right\}\sin\left[\Omega t\right] = -2\,, \end{aligned} \tag{6.8}$$

with $\Omega = 4(x_- - x_+)$. The condition above reflects the fact that equaling the determinant to zero is equivalent to solving $\operatorname{tr}\mathfrak{M}_t = -2$, with $\mathfrak{M}_t$ as given in Lemma 5.3.1 [dAVZ13]. Naturally, this condition needs to be solved numerically: Every time it is fulfilled, the Conley-Zehnder index changes by one.

6.3.2 The classical action

Since the orbits for the Kerr system are circles, it is easy to calculate the elements given in (5.22). As shown in Fig. 6.4, the center generating function can be obtained from basic geometry and is given by

$$S_t(\eta_\pm(x_\pm)) = x_\pm^2\left[2x_\pm^2 t - \frac{\sin(4x_\pm^2 t)}{2}\right], \tag{6.9}$$

and the energies are $H(x_\pm) = |x_\pm|^4$. The area of the quadrilateral in Fig. 5.4(b) is already explicit in (5.22), so that we have all the ingredients needed to implement (5.23). To make sure we are on the right track, we can run a little analytic test using the equations of motion and the chain rule to write[1]

$$\begin{aligned} \xi_\pm = -\mathcal{J}\left[\frac{\partial S_t(\eta_\pm(x_\pm))}{\partial \eta_\pm(x_\pm)}\right] &= -2\mathcal{J}\left[\frac{\partial \eta_\pm(x_\pm)}{\partial x_\pm}\right]^{-1}\left[\frac{\partial S_t(\eta_\pm(x_\pm))}{\partial x_\pm}\right] \\ &= -2\mathcal{J}\left[\mathcal{M}_t(x_\pm) + I\right]^{-1}\left[\frac{dS_t(\eta_\pm(x_\pm))}{dx_\pm}\right], \end{aligned}$$

[1]The order in the chain rule involves the jacobian of the center in front because it is a matrix, while the action's jacobian is a vector. We could have also used the transpose of the latter and inverted the order.

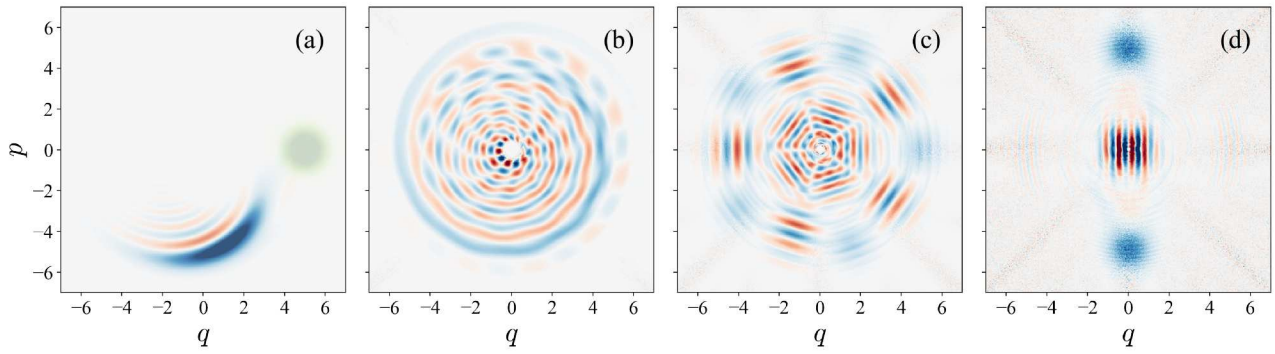

Figure 6.5: The renormalized semiclassical Wigner functions obtained from the FVR (5.23), to be compared with the exact ones in Fig. 6.2, using the same values (a) $t = 0.013$; (b) $t = 0.071$; (c) $t = \pi/20$ and (d) $t = \pi/8$. Notice the thin zero-valued regions inside the coherent states of panels (c) and (d), evincing a little of the spiraling filaments panels (c) and (d) of Fig. 6.1.

which gives the chords joining $x_\pm \longmapsto x'_\pm$ and can be obtained exactly by using (6.7) and (6.9), working as a consistency test[2]. Performing the calculations we end up with

$$\xi_\pm = \begin{pmatrix} q_\pm \cos(\omega_\pm t) + p_\pm \sin(\omega_\pm t) - q_\pm \\ p_\pm \cos(\omega_\pm t) - q_\pm \sin(\omega_\pm t) - p_\pm \end{pmatrix}, \quad \omega_\pm = 4(q_\pm^2 + p_\pm^2)\,,$$
$$\iff \quad \xi_\pm = x'_\pm - x_\pm\,,$$

as expected, and we can be absolutely sure our actions and monomodry matrices are correct.

6.3.3 FVR for coherent-state propagation

We now bring everything together and implement the FVR in (5.23) to the Kerr system. For the coherent states of interest, the characteristic function is easily obtained by substituting (3.3) into (4.11):

$$\chi_0(\xi) = \exp\left\{ix_0 \cdot J\xi - \frac{\xi\cdot\xi}{4}\right\},$$

where $x_0 = (q_0, p_0)$ is the initial coherent state's center, in our case $(5, 0)$.

The calculated Wigner functions happened to gradually lose normalization with time – this is not uncommon in the field, and semiclassical results tend to need renormalization [dLC16]. In our case, the renormalization is achieved by forcing the final Wigner function to integrate to 1, easily accomplished by transforming it using

$$\int_{\mathbb{R}^2} dx\, W(x) = C \quad \Longrightarrow \quad W(x) \longmapsto \frac{W(x)}{C}\,.$$

In the end, this works as a rescaling, since the Wigner functions are seen to lose normalization homogeneously.

The renormalized Wigner functions for the same time-values as Figs. 6.1 and 6.2 can be seen in Fig. 6.5. As expected, panels (a) and (b) are indistinguishable from their equivalents in Fig. 6.2. Panels (c) and (d) show that the FVR was also able to reproduce the revival patterns very well, although we can spot footprints of the classical filaments of Fig. 6.1: These appear as thin zero-valued regions inside the coherent states, created by destructive interferences in the semiclassical phases. These, as can be seen in the marginals of Fig. 6.6 and autocorrelation function in Fig. 6.7, do not strongly impact measurable results obtained from the Wigner functions.

Classical Geometry of Revival Patterns

The semiclassical reproduction of revival patterns using the thin filaments of Fig. 6.1 attests a precise tuning of classical trajectories. An analysis of the simplest revival, the full one at $t = \pi/4$, already

[2]These chords are the ones centered at $\eta_\pm$ in Fig. 5.4(b).

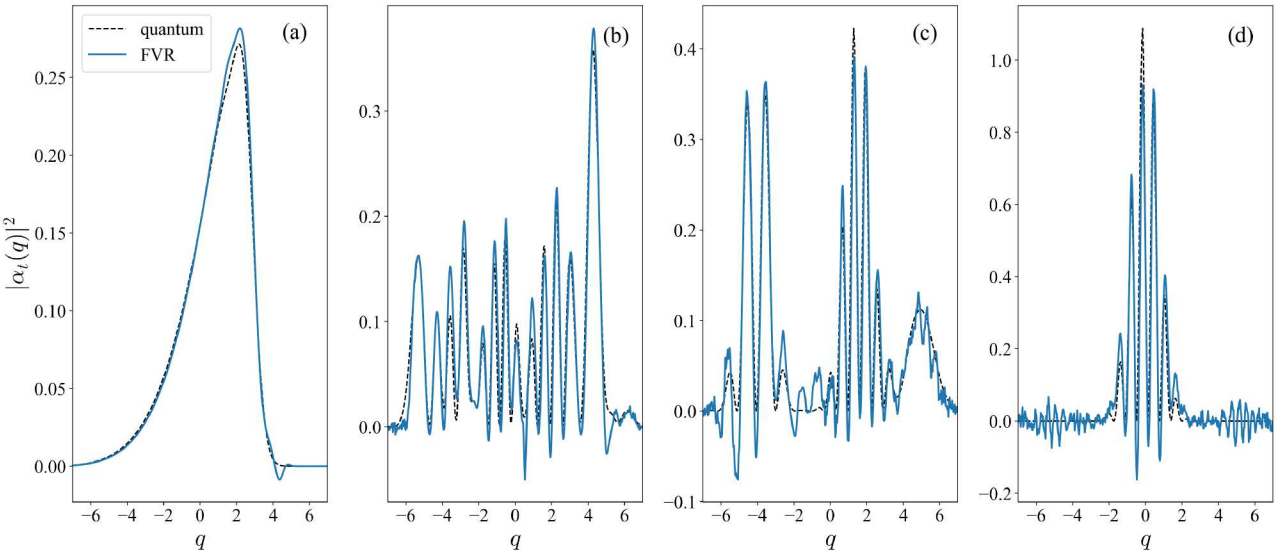

Figure 6.6: Probability marginals extracted using (4.13) from the Wigner functions in Fig. 6.5 compared with the exact ones of Fig. 6.2.

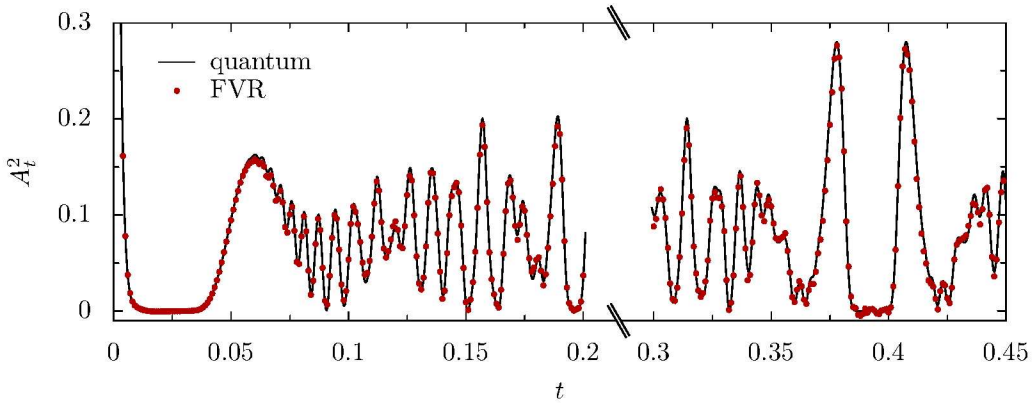

Figure 6.7: Squared autocorrelation function (4.23) obtained from the semiclassical and quantum Wigner functions.

unveils the essence of the semiclassical mechanism: Here, the final Wigner function is equal to the initial one, implying that the final chords ξ' must be backwards evolved near themselves, i.e. $\xi' \approx \xi$. Since the orbits are circles, this condition fixes contributing ξ' chords as the ones whose endpoints η'_+ and η'_- perform an integer number of complete revolutions around the origin, finishing near their initial values η_+ and η_-. In terms of the orbits' angular frequencies,

$$\omega_\pm T_{\text{rev}} = 4|\eta_\pm|^2 T_{\text{rev}} = 2\pi j_\pm \,, \tag{6.10}$$

where we define the winding numbers $j_\pm$ for $\eta_\pm$. The pairs of orbits whose radii lie in between the successive "time-quantized" values (6.10) define long chords with rapidly oscillating phases that cancel out: Their absence is responsible for the fine undulations in the revived coherent states and affects the Wigner function's normalization.

Substituting the variables in (6.10) in (5.22),

$$\widetilde{S}_t(\xi(\xi',\eta')) = \left(\frac{\pi^2}{4T_{\text{rev}}}\right)(j_+^2 - j_-^2)\,,$$

and since the winding numbers for this case are exactly the Conley-Zehnder contributions, the final phase [modulo a symplectic Fourier transform] is finally given by

$$\widetilde{S}_t(\xi(\xi',\eta')) + \frac{\hbar\pi\tilde{\sigma}}{2} = \pi(j_+ - j_-)[1 + (j_+ + j_-)]\,. \tag{6.11}$$

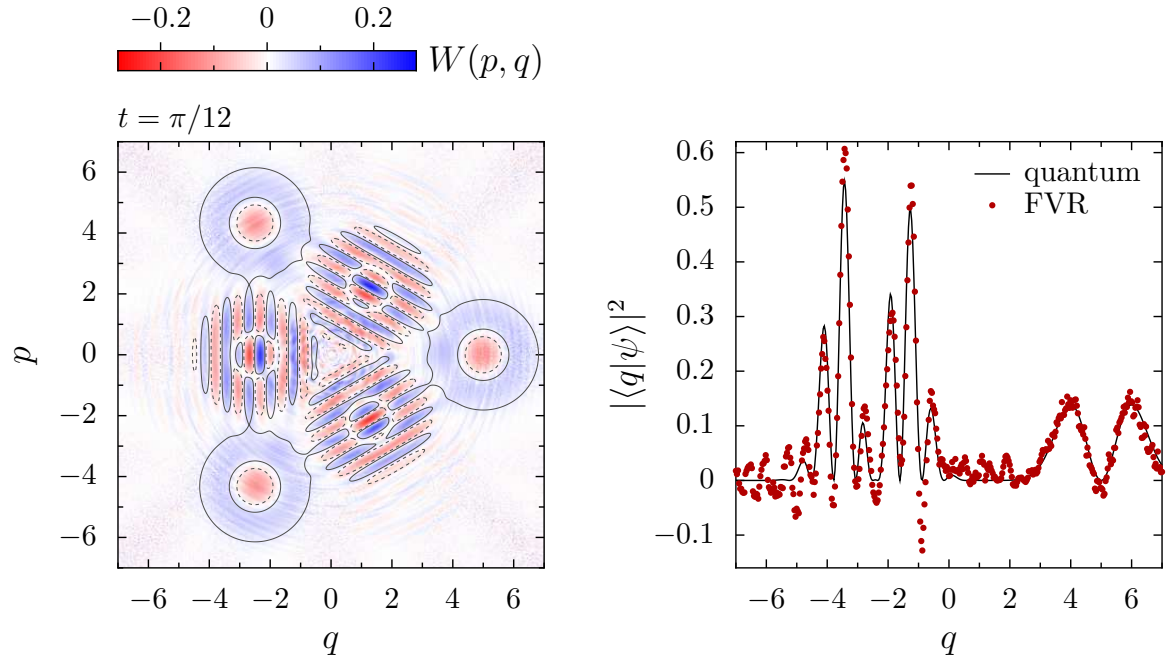

Figure 6.8: **Left:** Triangular revival recovered by the semiclassical Wigner function at $t = \pi/12$ for the displaced first excited Fock state, initially centered at $(q = 5, p = 0)$. Contour lines of the exact Wigner function are superposed, for which solid and dashed lines represent positive and negative values, respectively. **Right:** Position marginals for the exact (line) and semiclassical (points) Wigner functions on the left.

Since $j_+ - j_-$ and $j_+ + j_-$ have the same parity, the phase in (6.11) is always an even multiple of π. The relevant final chords are, therefore, selected such that the final Wigner function is localized exactly over the initial one, reproducing the complete revival as expected.

For fractional revivals with times $t = \pi/\beta$, the only difference is that the relevant final chords might perform fractional revolutions around the origin. We can express this condition as

$$\frac{\omega_\pm \pi}{\beta} = \frac{4|\eta_\pm|^2\pi}{\beta} = 2\pi(j_\pm + \alpha)\,,$$

where α is a rational number that reflects the positions of the final coherent states and thus depends on β. In contrast to the revived coherent states, the interference patterns appearing near the origin for the cat state revival ($\beta = 8$) are due exclusively to long chords, typically spanning the diameter of the classical spiral.

6.4 Propagating a non-classical state

The FVR is not restricted to the propagation of coherent states. We can, for instance, displace a SHO eigenvector $\langle q|n\rangle$, *i.e.* a Fock state, to obtain $\langle q|\hat{\mathfrak{T}}(\xi)|n\rangle$, and then evolve it using the Kerr dynamics. Since the quantum Kerr hamiltonian has the same eigenvectors as the SHO, the action of

$$\langle q|\mathfrak{T}(\xi)|n\rangle_t = \left\langle q\left|\exp\left[-(it)\,\hat{H}_{\rm Kerr}\right]\hat{\mathfrak{T}}(\xi)\right|n\right\rangle$$

can be calculated exactly: For revival times composed of a small number of superposing coherent states, such as 2 or 3, the calculations can be performed by hand. We calculated it for the triangular revival of the displaced $n = 1$ Fock state[3], with $\xi = (5, 0)$, and compared it with the FVR used to evolve the same initial state, whose characteristic function is

$$\chi_0(\xi) = \left(\frac{\xi\cdot\xi - 2}{2}\right)\exp\left\{ix_0\cdot J\xi - \frac{\xi\cdot\xi}{4}\right\}$$

[3]The final formula occupies a full page and we will not display it here.

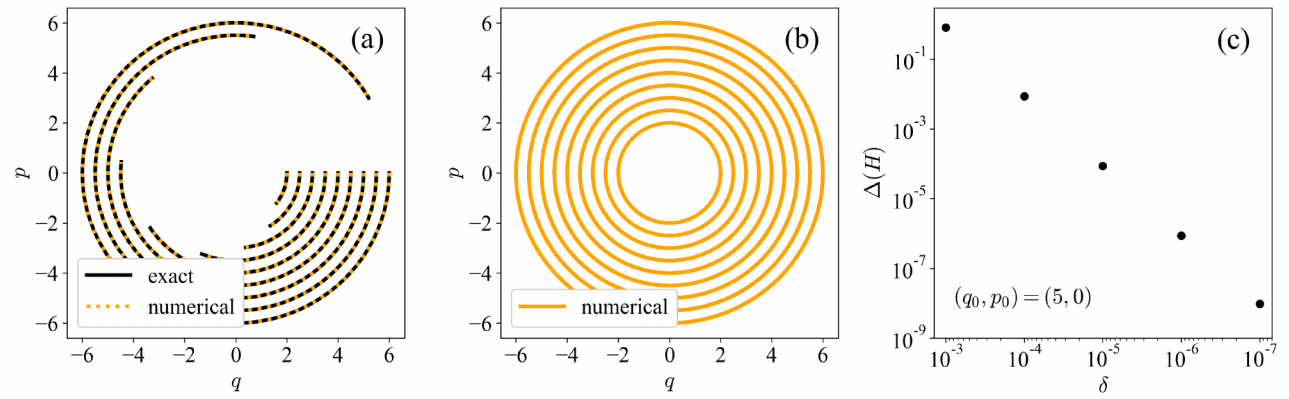

Figure 6.9: Several numerical aspects of Tao's algorithm are investigated for $\omega = 10$. In (a) we choose 6 phase-space points and propagate them exactly (black) and numerically (dashed yellow) using the SSI of Subsection 2.1.3, choosing the small time value $t = 0.04$ to show that the final times are matched. In (b) we test the algorthm's symplectic stability, *i.e.* we numerically propagate the same points in (a) for the very long time $t = 0.6$ in order to see if orbit topology changed – it did not. In (c) we propagate a single orbit with $(q_0 = 5, p_0 = 0)$ for the fixed time $t = 0.04$, but vary the iterative step δ and track how this affects the error in energy given in 6.5.1.

where x_0 is the initial center $x_0 = (5, 0)$. The results are displayed in Fig. 6.8, where we visually compare Wigner functions and use probability marginals for a more quantitative analysis. We see that even though this fractional revival happens for a time longer than $3\tau_E$, the FVR is able to achieve very good results. If we think classically, this is quite intriguing, since the final Wigner function is build upon the "classical propagation of an initially non-classical state".

6.5 Fully numerical propagation

Due to the Kerr system being non-separable and exact, we can use it to test and explore Tao's algorithm for numerically integrating the vector field of a non-separable hamiltonian, presented in Subsection 2.1.3. The Kerr system is particularly good for numerical testing because, since its hamiltonian is a fourth order polynomial in position and momentum, its orbits have numerically large energies and any inconsistency in code or algorithm will result in a divergence. We can then move on to full numerical propagation, where all elements in the calculations are obtained without reference to the system's exactness. This is a key step towards expanding our computational algorithms toward general systems.

6.5.1 Testing Tao's algorithm

Although the Kerr system can be solved using simpler SSIs due to the angular speed being conserved *per* orbit, we prefer to use it to test Tao's algorithm of Subsection 2.1.3. In Fig. 6.9 we implement and investigate several aspects of the splitting in (2.6), choosing the symbol δ to represent the kicking strength and sampling initial phase-space points ranging from $x_0 = (2, 0)$ to $x_0 = (6, 0)$. In Fig. 6.9(a) we plot the numerical flow $\bar{\rho}_\delta$ from (2.6) (dashed yellow) against the exact flow ρ_t in (6.2) (solid black), for the previously mentioned initial phase-space points. We choose the relatively short time $t = 0.04$ in order to show how well the final times match. In Fig. 6.9(b) we investigate the most important aspect of Tao's algorithm for its application in this dissertation: Its symplecticity. We evolve the same initial points of panel (a) using $\bar{\rho}_\delta$, but chose $t = 0.6$, for which the outer orbit (which has the largest errors) performs more than 50 revolutions around the origin. It was common for previous algorithms to fail this type of test [Pih14], but we clearly see that the accumulation of errors does not impact the topology of orbits obtained by Tao's prescription. In Fig. 6.9(c) we take the orbit of $x_0 = (5, 0)$ as a guinea pig for error analysis, plotting the energy error

$$\Delta(H)(x_0) = |(H \circ \rho_t - H \circ \bar{\rho}_\delta)(x_0)|$$

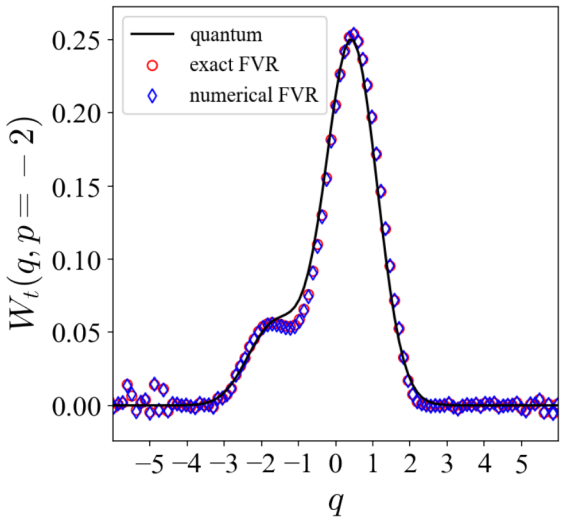

(a) $p = -2$ section of Wigner function at $t = 0.053$ for an initial coherent state centered at $(2, 0)$.

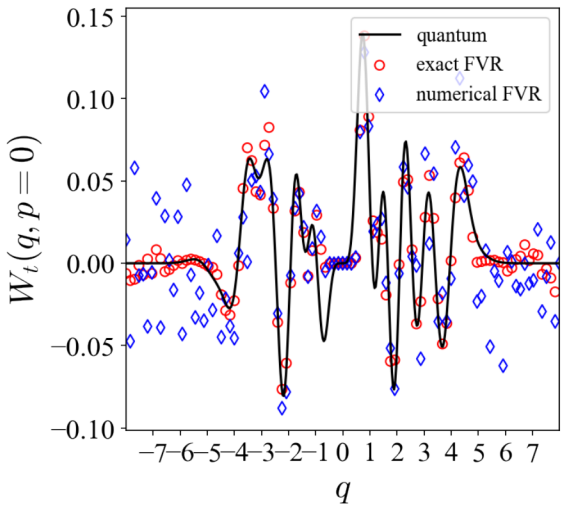

(b) $p = 0$ section of Wigner function at $t = 0.071$ for an initial coherent state centered at $(4, 0)$.

Figure 6.10: The simplest application of Tao's algorithm already gives results indistinguishable from the ones obtained using the system's exact trajectories for the short time in panel (a). For the longer time value in panel (b), however, we are close to the Ehrenfest time and the numerical Wigner function deviates from its exact correspondent, especially near the grid's extremities, due to the integration domain being too small to achieve good convergence. For both figures, the step-size in the algorithm is $\delta = 10^{-2}$. We emphasize better results could be obtained by employing a higher-order SSI.

for the same time value $t = 0.04$ of panel (a). We have somewhat arbitrarily chosen $\omega = 10$, for which the numerical integrator clearly converged, but we see that Tao's algorithm has errors slightly larger than if it were a pure Strang splitting, the dependence on ω certainly adding some error[4]. However, the energy value for $x_0 = (5, 0)$ is $q^4 = 625$, and the error we have obtained for the largest value $\delta = 10^{-3}$ was $\Delta(H)(x_0) \approx 0.82$, close to 0.1% of the energy value at this point. Since the Kerr system energies are given by a fourth order polynomial, we consider this to be a quite successful test.

6.5.2 Fully numerical FVR

The modern theory of splitting symplectic integrators, of which we only developed a small part in Section 2.1, allows us to achieve numerical propagation with machine precision – all that is needed is a powerful enough computer [RCV19]. To move on to numerical propagation, the first thing to do is to discretize time as $t = N\delta$, N being the number of steps and δ the step-size (see Section 2.1), and employ Tao's algorithm in (2.6) as described earlier. However, the flow is not the only quantity that ceases to be analytical: The amplitude of Section 5.3 also needs to be obtained numerically, which we do by finite differences, *e.g.*

$$\frac{\partial p_t(q_0, p_0)}{\partial p_0} \approx \frac{p_t(q_0, p_0 + \epsilon) - p_t(q_0, p_0)}{|\epsilon|},$$

and equivalently for the other components. By choosing ϵ small enough, such as of the order of our grid spacing, the finite difference method introduces virtually no error in our calculations. Also, since the Conley-Zehnder indexes were already calculated numerically, the procedure to obtain them remains unaltered. The action, however, must be changed: When performing the calculations using the exact flow, we had a closed expression for the center action, namely (6.9), which we employed to obtain the FVR phase of (5.22). In pursuing a completely numerical algorithm, we have to find a way to calculate the action using only our numerical flow. For this, notice that

$$-\int_{\eta_0}^{\eta_t} \xi \cdot \mathcal{J} d\eta = \int_0^t (\xi_p \cdot \dot{\eta}_q - \xi_q \cdot \dot{\eta}_p)\, dt \approx \frac{\delta}{2} \sum_{k=0}^{N} \left[\xi_{p_k} \cdot \left(\frac{\partial H(q_k, p_k)}{\partial p_k} \right) + \xi_{q_k} \cdot \left(\frac{\partial H(q_k, p_k)}{\partial q_k} \right) \right], \quad (6.12)$$

[4]For long times Tao showed that this error it of $\mathcal{O}(\omega^{-1})$. We do not strive for a better error benchmark simply because we do not need it. The algorithm is already good enough for our purposes.

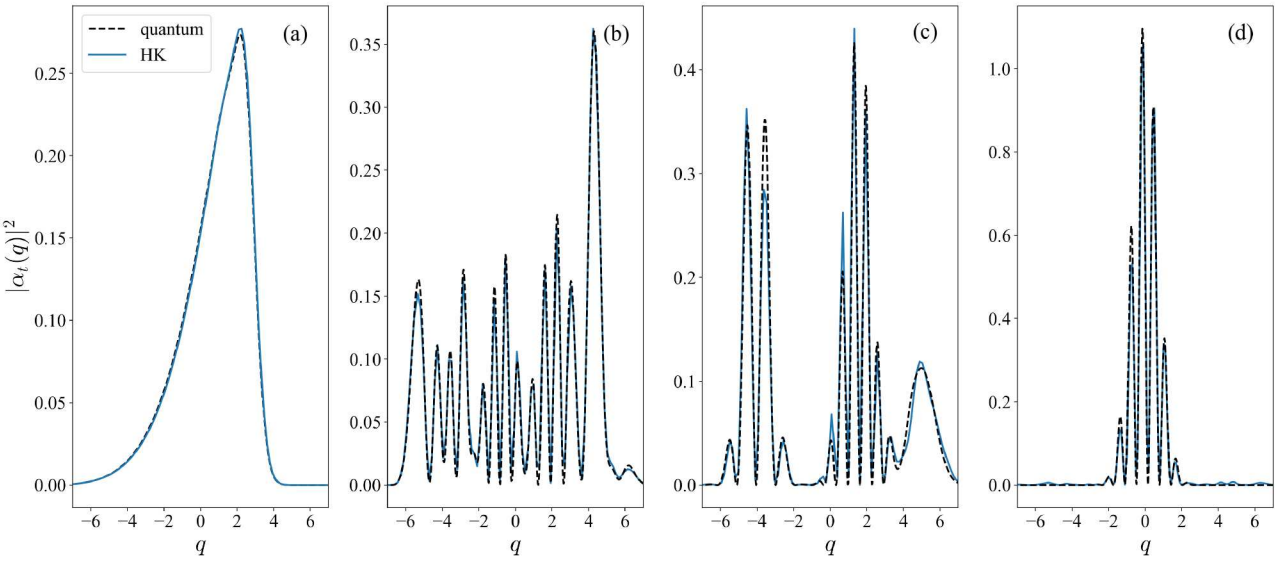

Figure 6.11: Probability marginals obtained from the fully numerical Herman-Kluk propagator for (a) $t = 0.013$; (b) $t = 0.071$; (c) $t = \pi/20$ and (d) $t = \pi/8$.

where δ is the flow's discretization step and we have substituted Hamilton's equations for the center, since

$$\dot{\eta} = \frac{d}{dt}\left(\frac{x_t + x_0}{2}\right) = \frac{\dot{x}_t}{2} = \frac{\mathcal{J}}{2}\left(\frac{dH(x_t)}{dx_t}\right).$$

The numerical expression for the action given in (6.12) depends, as required, only on the hamiltonian function and the flow. It is now possible to chose another system, not only Kerr's, to apply the theory developed in Chapter 5. For a single degree of freedom, Tao's algorithm in its simplest form already gives us sufficient precision to obtain indistinguishable results when compared to the analytical ones for short times. In Fig. 6.10 we compare numerical and exact calculations using a section of the Wigner function, meaning that we calculate $W_t(q, p)$ for a fixed momentum, so that we can plot the results one against the other and obtain quantitative comparisons.

6.5.3 The Herman-Kluk propagation of coherent states

Despite some controversy, the Herman-Kluk propagator (3.32) is still the most employed IVR in chemistry and most of physics. We then decided to implement it for the Kerr system in order to see how it fared. In principle, we expected it to not go far due to a pernicious view, unfortunately rather abundant in literature, that the HK propagator does not need us to keep track of indexes such as Maslov's or Conley-Zehnder's – if this were true, it would fail for times just after the first caustic is met. Since the Kerr system has a quite complicated caustic structure (see Fig. 6.4(b)), the estimated failure time for the HK propagator would be quite small. However, as demystified by Kay[5] [Kay94] and very well explained in [Swe11], the HK propagator does require a tracking of the proper branch of its complex amplitude and this tracking is identical to counting indexes across caustics.

The HK method, however, is not a phase-space method. The FVR of (5.23) was obtained through stationary phase approximations in phase space, and the key was to consider operators that had phase space as their domain. The HK propagator, on the other hand, lies closer to the Schrödinger picture of quantum mechanics, since it considers a form of approximate time-evolution of coherent states instead of operators – that is, it is somehow based on the Segal-Bargmann representation[6]. By the employment of wavefunctions, the HK propagator cannot be applied to open quantum systems, but for closed systems it is very easy to implement and extremely efficient. Evidently, these advantages are meaningless if the method does not work.

[5]The reference is from 1994, but people *still* get things wrong with respect to Maslov tracking for the HK propagator.
[6]The connection between the HK propagator and the Segal-Bargmann representation is provided in [MFL06].

In Fig. 6.11 we plot the probability amplitude for the Kerr system using the semiclassical wavefunction obtained via the HK propagator for the same time-values as Fig. 6.5. All the calculations are performed numerically. For this, the action entering the HK phase is just the integral of the lagrangian evaluated numerically:

$$\int_{q_0}^{q_t} p \cdot dq - \int_0^t dt\, H(q_t, p_t) = \int_0^t dt\, \left[p \cdot \dot{q} - H(q_t, p_t)\right] \approx \sum_{k=0}^{N} \left[p_k \cdot \left.\frac{\partial H(q,p)}{\partial p}\right|_{(q_k,p_k)} - H(q_k, p_k)\right] \delta\,,$$

where the propagation time has been discretized as $t = N\delta$. We use the numerical flow obtained from Tao's algorithm as well, together with the same finite-difference monodromies used for the FVR in Subsection 6.5.2. The procedure to obtain the proper branch in the amplitude is done *via* the conditions below, which must be fulfilled simultaneously:

$$\begin{cases} \Re\left[R_k(q_k, p_k)\right] & < 0 \\ \Im([R_k(q_k, p_k)] \times \Im\left[R_{k-1}(q_{k-1}, p_{k-1})\right] & < 0 \end{cases} \tag{6.13}$$

where R is the HK pre-factor

$$R_k(q_k, p_k) = \det\left\{\frac{1}{2}\left[\left(\frac{\partial p_k}{\partial p_0} + \frac{\partial q_k}{\partial q_0}\right) + i\left(\frac{\partial p_k}{\partial q_0} - \frac{\partial q_k}{\partial p_0}\right)\right]\right\}. \tag{6.14}$$

That is: When the real part of the amplitude is negative and the imaginary part crosses a branch, the Maslov index increases by +1. Formulated this way, this is equivalent to Maslov tracking [Kay94, Swe11].

6.6 Discussion

We are in a rather satisfying position: Both the FVR and the HK propagators worked. As far as we know,

1. This is the first time an integral representation in phase space has been implemented and its success, attested;

2. We have performed a very stringent test of an ubiquitous method, the HK propagator, proving it indeed works.

We must be careful about what kind of conclusions we extract from comparing Figs. 6.6 and 6.11: They do not attest an absolute supremacy of the HK propagator over the FVR, since these propagation methods are meant to do different things. Direct comparison of probability marginals is also not exactly fair to the FVR, since while basically all semiclassical propagators can approximate wavefunctions, it is only the FVR that is able to do it directly to the Wigner function. As stated earlier, in the absence of a wavefunction the HK propagator is useless, and we must resort to the FVR. However, the former is clearly extremely successful when we are interested in working with closed systems (see Appendix F); The latter, on the other hand, is completely real and might facilitate the understanding of the role played by classical structure behind semiclassical propagation. We are particularly interested in the blank regions formed in phase space by the FVR method, since they do not impact the measurable objects extrated from the Wigner function and, at the same time, emerge due to destructive interferences between classical trajectories in places they should not occur. We suspect that this might be due to some theoretically interesting mechanism, although we have not yet explored the subject in depth.

One thing we can be sure when looking at Figs. 6.6 and 6.11 is that the HK propagator is stable: It displays no oscillations and never misses from below – in fact, it never misses at all. This is due to its pre-factor never reaching zero, so that errors cannot force the result to be negative [Kay94] – The HK's domain is already the complex field, so its amplitude is naturally complex and changes of imaginary branch are expected. The FVR, on the other hand, is a real object and its pre-factor does reach zero across caustics: Although zero is better then infinite, as would happen in van Vleck

propagation, errors might result in unexpected imaginary amplitudes that render marginals negative. Of course, there might also be problems associated to the FVR's phase, which is calculated using trajectory pairs and is much more sensitive then HK's.

There are two main directions to generalize what was done in this chapter:

1. Use the FVR to approximate the Kerr system in an open environment, possibly with linear Lindblad operators to facilitate calculations;

2. Move on to chaotic systems.

The first item above is being currently investigated and will not reapper. For the rest of this thesis we shall focus on the second item, employing semicassical approximations to deal with closed systems that have chaotic classical counterparts. Due to the remarkable results obtained using the HK propagator and its high computational efficiency, it will be our standard semiclassical method from now on.

Bibliography

[AP89] I. S. Averbukh and N. F. Perelman. Fractional revivals: Universality in the long-term evolution of quantum wave packets beyond the correspondence principle dynamics. *Phys. Lett. A*, 139:449, 1989.

[Bal08] L. E. Ballentine. *Quantum Mechanics: A Modern Development*. World Scientific, 2008.

[dAVZ13] A. M. Ozorio de Almeida, R. O. Vallejos, and E. Zambrano. Initial or final values for semiclassical evolutions in the Weyl-Wigner representation. *J. Phys. A: Math. Theor*, 46:135304, 2013.

[dLC16] G. di Liberto and M. Ceotto. The importance of the pre-exponential factor in semiclassical molecular dynamics. *J. Chem. Phys.*, 145:144107, 2016.

[Kay94] K. G. Kay. Integral expressions for the semiclassical time-dependent propagator. *J. Chem. Phys.*, 100:4377, 1994.

[MFL06] E. Martín-Fierro and J. M. G. Llorente. Derivation of semiclassical asymptotic initial value representations of the quantum propagator. *Chem. Phys.*, (322):13, 2006.

[Pih14] P. Pihajoki. Explicit methods in extended phase space for inseparable hamiltonian problems. *Celest. Mech. Dyn. Astron.*, 3:211, 2014.

[RCV19] J. Roulet, S. Choi, and J. Vaníček. Efficient geometric integrators for nonadiabatic quantum dynamics. II. The diabatic representation. *J. Chem. Phys*, 150:204113, 2019.

[Swe11] D. W. H. Swenson. *Quantum Effects from Classical Trajectories: New Methodologies and Applications for Semiclassical Dynamics*. PhD dissertation, 2011.

[YS86] B. Yurke and D. Stoler. Generating quantum mechanical superpositions of macroscopically distinguishable states via amplitude dispersion. *Phys. Rev. Lett.*, 57:13, 1986.

Chapter 7

Numerical simulations: The coserf system

> It seems sometimes that through a preoccupation with science, we acquire a firmer hold over the vicissitudes of life and meet them with greater calm, but in reality we have done no more than to find a way to escape from our sorrows.
>
> Hermann Minkowski in a letter to David Hilbert

In this chapter we generalize the use of the Herman-Kluk propagator to chaotic systems by applying it to the hamiltonian maps of Chapter 2. Most discrete hamiltonian systems, however, are defined on the torus instead of the plane (such as Chirikov's standard system [Chi79]). One problem with this domain is that, unfortunately, it makes results rather cumbersome to visualize: When an initial curve is evolved and escapes outside the unit square it is brought back via the equivalence relations and evolution looks discontinuous on the plane (visualizing the system on the torus is out of the question – no one can do that!). We consider the loss of intuition a high price to pay in exchange for compact orbits, and therefore devise a map on the plane following a strategy pioneered by Berry *et al* [BBTV79], who in the early days of quantum chaos needed his evolved curves to remain bounded in order not to explode the computers of the time. Their chosen strategy was to build a map that did not grow too quickly as $(q,p) \longrightarrow \infty$. This reasoning serves as our starting point.

7.1 Classical dynamics

In this section we introduce the coserf system (actually systems), on which we focus for the rest of this dissertation. We then use them to propagate coherent states just as we did in Chapter 6, except that now we are dealing with chaotic systems and evolution is more intricate.

We start from the standard-like hamiltonian $H_\alpha(q,p) = p^2/2 + q^2/2 - \alpha\cos(q)$, which is quite interesting: It is a modification of the SHO, having at least an elliptic fixed point at the origin, but its orbits are deformed by the cosine. Its vector field $X_h = p\,\partial_q - [q + \alpha\sin(q)]\partial_q$ has a fixed point at

$$\begin{cases} p = 0 \\ q + \alpha\sin(q) = 0 \end{cases},$$

which can be numerically solved to show that, for any reasonable range of positions (*i.e.* from -40 to 40), its fixed point at the origin is the only one. We choose $\alpha = 2$ in order to achieve a significant deformation of the orbits of the SHO. The symplectic integrator map (2.3) build from $H_2(q,p) = p^2/2 + q^2/2 - 2\cos(q)$ is, for instance,

$$\begin{cases} p_i = p_{i-1} - T(q_{i-1} + 2\sin q_{i-1}) \\ q_i = q_{i-1} + Tp_i \end{cases}$$

which is quickly diverging on the plane for $T > 0.4$, so that chaos cannot be actually reached without the need to eliminate the diverging trajectories. Since the diverging variable is the momentum due

to the cosine in the potential, we can sum a function to p_i in order to force it to diverge *at least slowly*. The first function that comes to mind is a gaussian in q, since it tends to zero faster than any polynomial. This reasoning leads us to the map

$$\begin{cases} p_i = p_{i-1} - T\left[q_{i-1} + 2\sin q_{i-1} - \exp(-q_{i-1}^2)\right] \\ q_i = q_{i-1} + T p_i \end{cases}$$

which is shown (numerically) to be extremely robust with respect to T, *i.e.* chaos is easily reached and is either bounded between surviving tori or includes chaotic trajectories that diverge very slowly. This is due to an interesting property of its orbital speeds: They are not monotonically increasing with the distance from the origin (as opposed to the Kerr system) – While inner orbits have very high speeds, as we move to outer phase-space regions the orbits start slowing down. Since

$$\exp(-q^2) = \left(\frac{\sqrt{\pi}}{2}\right)\frac{d[\mathrm{erf}(q)]}{dq}\,, \qquad \mathrm{erf}(q) = \frac{2}{\sqrt{\pi}}\int_0^q \exp(-x^2)dx\,,$$

we define

Definition 7.1.1. The **coserf systems** are defined *via* the maps U_T^{FV} and U_T^{VF}, both acting on $(\mathbb{R}^2, dq\wedge dp)$, where the maps U_T^{FV} and U_T^{VF} correspond to the two possible 2-step SSIs obtained from the **coserf hamiltonian**

$$H_{\mathrm{csrf}}(q,p) = \frac{p^2}{2} + \frac{q^2}{2} - 2\cos(q) - \left(\frac{\sqrt{\pi}}{2}\right)\mathrm{erf}(q)\,, \tag{7.1}$$

namely

$$U_T^{FV} = \begin{cases} p_i = p_{i-1} - T\left[q_{i-1} + 2\sin q_{i-1} - \exp(-q_{i-1}^2)\right] \\ q_i = q_{i-1} + T p_i \end{cases} \tag{7.2}$$

$$U_T^{VF} = \begin{cases} q_i = q_{i-1} + T p_{i-1} \\ p_i = p_{i-1} - T\left[q_i + 2\sin q_i - \exp(-q_i^2)\right] \end{cases}. \tag{7.3}$$

As all SSIs, the coserf maps are 1-parameter families of symplectomorphisms with respect to the continuous variable T.

In the first row of Fig. 7.1 we display some orbits of the position-first shear (7.3) for three different values of T. In panel 7.1(a) we have $T = 0.05$ and the coserf map acts effectively as a SSI for the vector field of (7.1) and approximates its level curves – this, remember, is the original use of SSIs (see Section 2.1). In panel (b) we set $T = 0.45$ and chaotic behavior is already clearly visible in the dark, dense orbits around the stability islands formed by hamiltonian resonances. Several quasi-periodic tori are seen to survive even for this significant kicking strength around the main fixed point at origin, where position and momentum values are small enough for energy to be conserved. A careful examination shows that tori can be found actually everywhere, be it as envelopes to islands, the islands themselves, or highly deformed regular regions between chaotic seas: This is the KAM theorem in action. The perturbation strength is not strong enough to destroy all tori in the system, a fact that is strikingly depicted in 7.1(c), where we set $T = 0.7$: Here, the perturbation strength is strong enough to destroy all[1] tori outside a neighborhood of the origin, although we can clearly see some that survive around the origin.

What makes the coserf system special is that we could reach phase-space topologies such as the ones in the first row of Fig. 7.1 without paying any attention to divergences, since what usually happens is that everything blows up much earlier. Even though we are zooming on the origin and the orbits in Fig. 7.1 are actually scattered around a $(-30, 30)$ square, they remain bounded. We can actually hit

[1] Almost all, actually. The measure of the set of quasi-periodic tori fulfilling the diophantine condition tends to zero as the kicking strength is increased, meaning that the probability of us sampling initial conditions that hit a tori far away from the origin goes to zero as we increase T.

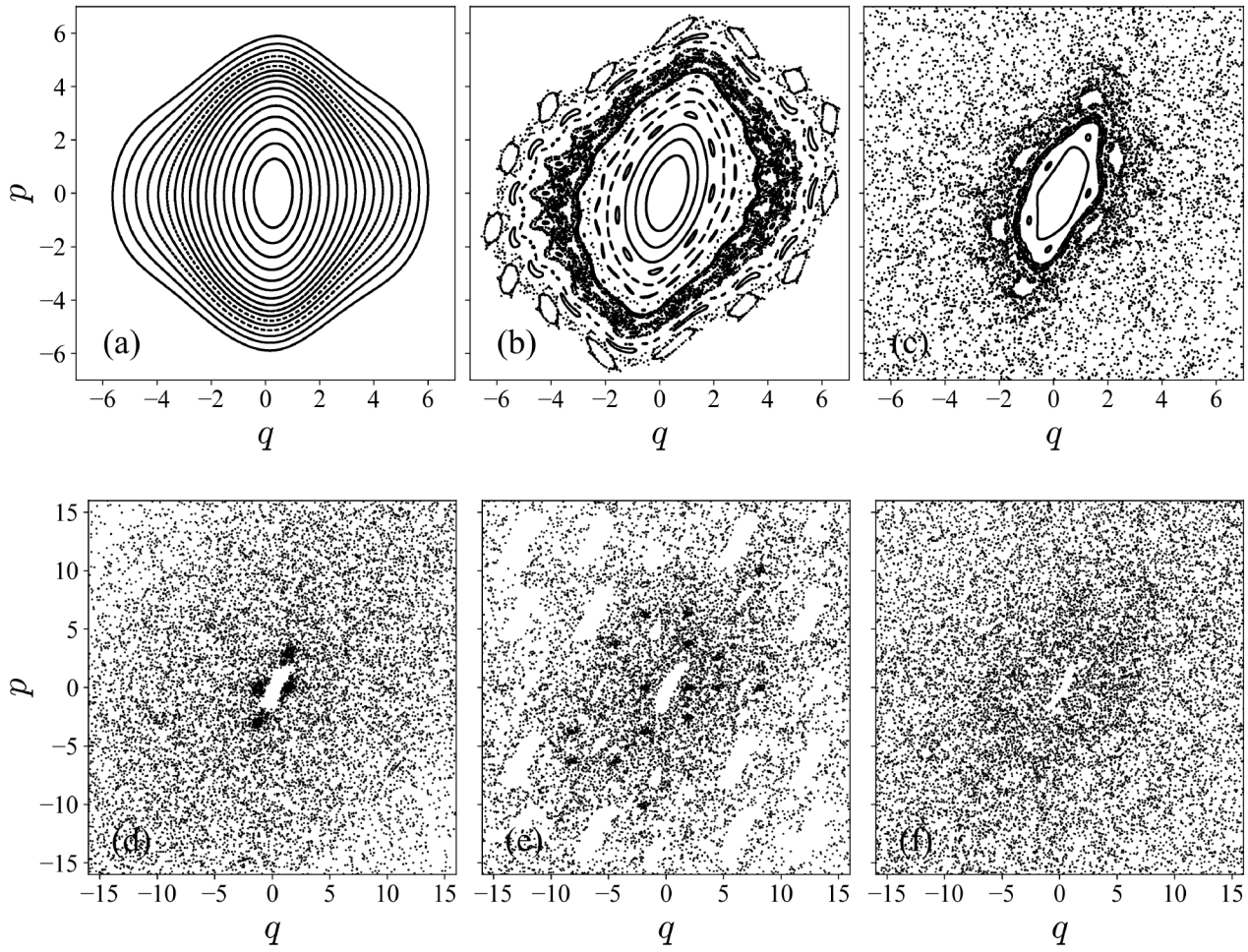

Figure 7.1: Orbits of the map (7.2) for several values of kicking strength T and the same initial phase-space points. (a) Here $T = 0.05$ and the orbits are visually identical to the level sets of (7.1), a slight deformation of the SHO. (b) For $T = 0.45$ we have mixed behavior and the regular and chaotic regions share approximately the same fraction of phase space. (c) For $T = 0.7$ chaos becomes dominant but, zooming in a neighborhood of the origin, we can still detect invariant tori. The second row zooms out and explores the persistence of tori even for large kicking strengths. Panel (d) has $T = 0.9$, where no tori can be found far from the origin. (e) Here we set $T = 1$ and tori reappear both in the neighborhood and far from the origin. (f) For $T = 1.1$ some tori still be seen.

deeper chaotic regimes, which are displayed in the second row of Fig. 7.1. We here zoom out from the origin and, as shown in panel (d), no tori appear to exist away from it. However, as we *increase* the kicking strength in panel (e), we actually have a spontaneous reappearing of small tori near the origin and large ones in the outskirts – increasing the kicking strength gave rise to new resonances. Even in panel (e), when $T > 1$ the tori can still be seen: The diophantine condition around each fixed point is simply too hard to avoid.

We now employ the position-first coserf map (7.3) to propagate the Wigner function of coherent state initially centered at $(q_0 = 2, p_0 = 0)$ using (4.22) for several kicking strengths and time values, which we display in Fig. 7.2. It's important to point out that, since Wigner functions evolve backwards, direct application of the flow U_T^{VF} in (4.22) will lead to backward time-evolution, which is what is shown in the picture. The time scale employs the Ehrenfest times obtained in the next section.

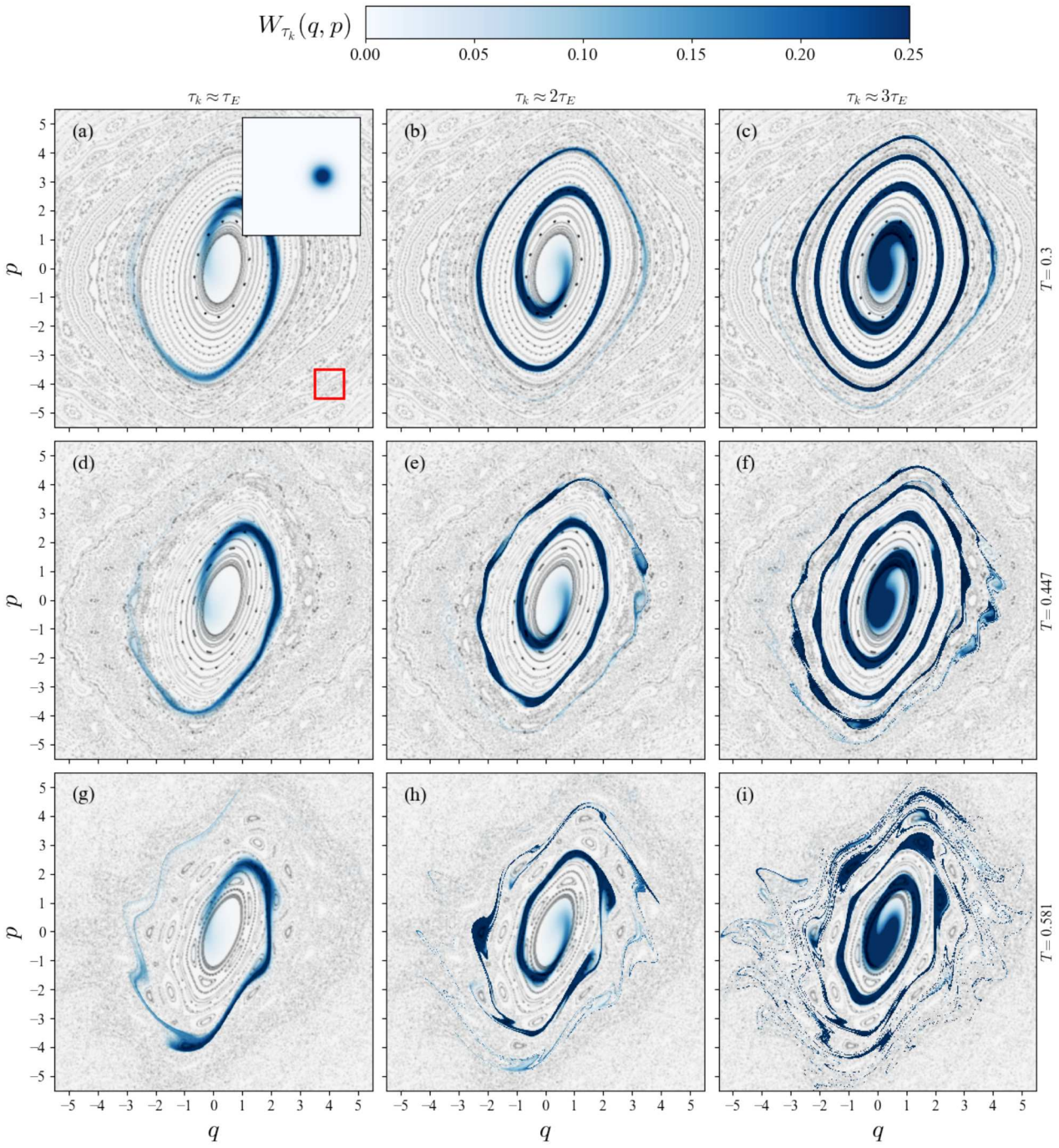

Figure 7.2: Classical propagation of the initial Wigner function in the inset of (a) by (7.3) for $T = 0.3$, $T = 0.447$ and $T = 0.581$ and discretized times near τ_E, $2\tau_E$ and $3\tau_E$. Each T value corresponds to a row, whereas each Ehrenfest time multiple corresponds to a column. The initial Wigner function is reproduced in the inset of panel (a), together with a red square of area $\hbar = 1$. We also plot the classical map as a gray background in order show the orbits along which the initial Wigner function is propagated. Notice that the regular behavior for $T = 0.3$ is gradually lost as T is increased, the extreme case being the panels for $T = 0.581$, where most of the orbits have become chaotic. The regimes for $T = 0.447$ and $T = 0.581$ have been considered problematic due to the filament developing sub-Planckian structure and being captured by stability islets [Mai00].

7.2 Quantum dynamics

Just as the Kerr system, the coserf systems are exactly quantizable by direct employment of Dirac's quantization recipe. After defining the quantum analogues of U_T^{FV} and U_T^{VF} we propagate the wavefunction of an initial coherent state and Wigner-transform it, obtaining the quantum analogue of Fig. 7.2. We then proceed to the establishment of an Ehrenfest-time scale for our model, comparing classical and quantum autocorrelation functions. As in Chapter 6, we set $\hbar = 1$.

7.2.1 Quantum maps

The flows (7.2) and (7.3) emerge as numerical solutions to Hamilton's equations and work by substituting the exponential of the vector field X_H by its decomposition $X_H = X_F + X_V$, obtained using the Baker-Hausdorff-Campbell series:

$$\exp\left(-TX_H\right) = \exp\left[-T\left(X_F + X_V\right)\right] \approx \begin{cases} \exp\left(-TX_F\right) \circ \exp\left(-TX_V\right) \\ \exp\left(-TX_V\right) \circ \exp\left(-TX_F\right) \end{cases}$$

with $X_Z(\cdot) = \{Z, \cdot\}$. Both the classical and the quantum equations of motion, however, generate flows that obey the same algebra, namely Heisenberg's algebra [Fol89], and the difficulty of transitioning between representations is the multiple possible operator orderings. For SSIs, however, there are no ordering problems, since the propagation is decomposed in terms of purely kinetic and purely potential flows, meaning that the classical flow operator above can be immediately quantized using Dirac's quantization prescription, resulting in

$$\exp\left(-it\hat{H}\right) = \exp\left[-it\left(\hat{F} + \hat{V}\right)\right] \approx \begin{cases} \exp\left(-it\hat{F}\right)\exp\left(-it\hat{V}\right) \stackrel{\text{def}}{=} \hat{U}_t^{FV} \\ \exp\left(-it\hat{V}\right)\exp\left(-it\hat{F}\right) \stackrel{\text{def}}{=} \hat{U}_t^{VF} \end{cases} .$$

Thus, quantum dynamics can also be solved using SSIs (although in this context these methods are usually called *split operator methods*). More importantly, we can exactly associate a quantum equivalent to every classical map obtained from a SSIs, each shear ordering having its particular quantized equivalent. The flow of $\hat{U}_t^{VF}$, for example, is given in position representation by

$$\begin{aligned} \langle q|\hat{U}_t^{VF}|q'\rangle &= \left\langle q\left|\exp\left(-it\hat{V}\right)\exp\left(-it\hat{F}\right)\right|q'\right\rangle = \exp\left(-itV(q)\right)\left\langle q\left|\exp\left(-it\hat{F}\right)\right|q'\right\rangle \\ &= \exp\left(-itV(q)\right)\int_{\mathbb{R}^n} dp\, \exp\left(-itF(p)\right)\langle q|p\rangle\langle p|q'\rangle \\ &= \exp\left(-itV(q)\right)\int_{\mathbb{R}^n} dp\, \exp\left(-itF(p)\right)\exp\left[-ip(q'-q)\right] . \end{aligned}$$

For the usual kinetic term $F(p) = p^2/2$ the integral above is gaussian and solvable by completing the square, resulting in [BBTV79]

$$\langle q|\hat{U}_t^{VF}|q'\rangle = \left(\frac{1}{2\pi i t}\right)^{\frac{1}{2}} \exp\left[-itV(q) + \frac{i(q-q')^2}{2t}\right] . \tag{7.4}$$

The quantum flow for the alternate order of shears is also easily found to be

$$\langle q|\hat{U}_t^{FV}|q'\rangle = \left(\frac{1}{2\pi i t}\right)^{\frac{1}{2}} \exp\left[-itV(q') + \frac{i(q-q')^2}{2t}\right] .$$

Evidently, the flows above are to be interpreted as a single iteration of kicking strength t. Just as in the classical case, we are interested in decomposing the time t as k iterations with kicking strength T, generating the discretized time $t = \tau_k = kT$. The final wavefunction corresponding is, therefore, expressed recursively as

$$\langle q|\psi_k\rangle = \int dq' \langle q|\left(\hat{U}_T\right)^k|q'\rangle\langle q'|\psi_0\rangle , \tag{7.5}$$

where $(\hat{U}_t)^k$ can be either the FV of VF shears. As an example,

$$\langle q| \left(\hat{U}_T^{VF}\right)^k |q'\rangle = \int dq_{k-1}\, dq_{k-2} \ldots dq_1\, \langle q|\hat{U}_T^{VF}|q_{k-1}\rangle\langle q_{k-2}|\hat{U}_T^{VF}|q_{k-1}\rangle \ldots \langle q_1|\hat{U}_T^{VF}|q'\rangle\,,$$

and analogously for the FV shear.

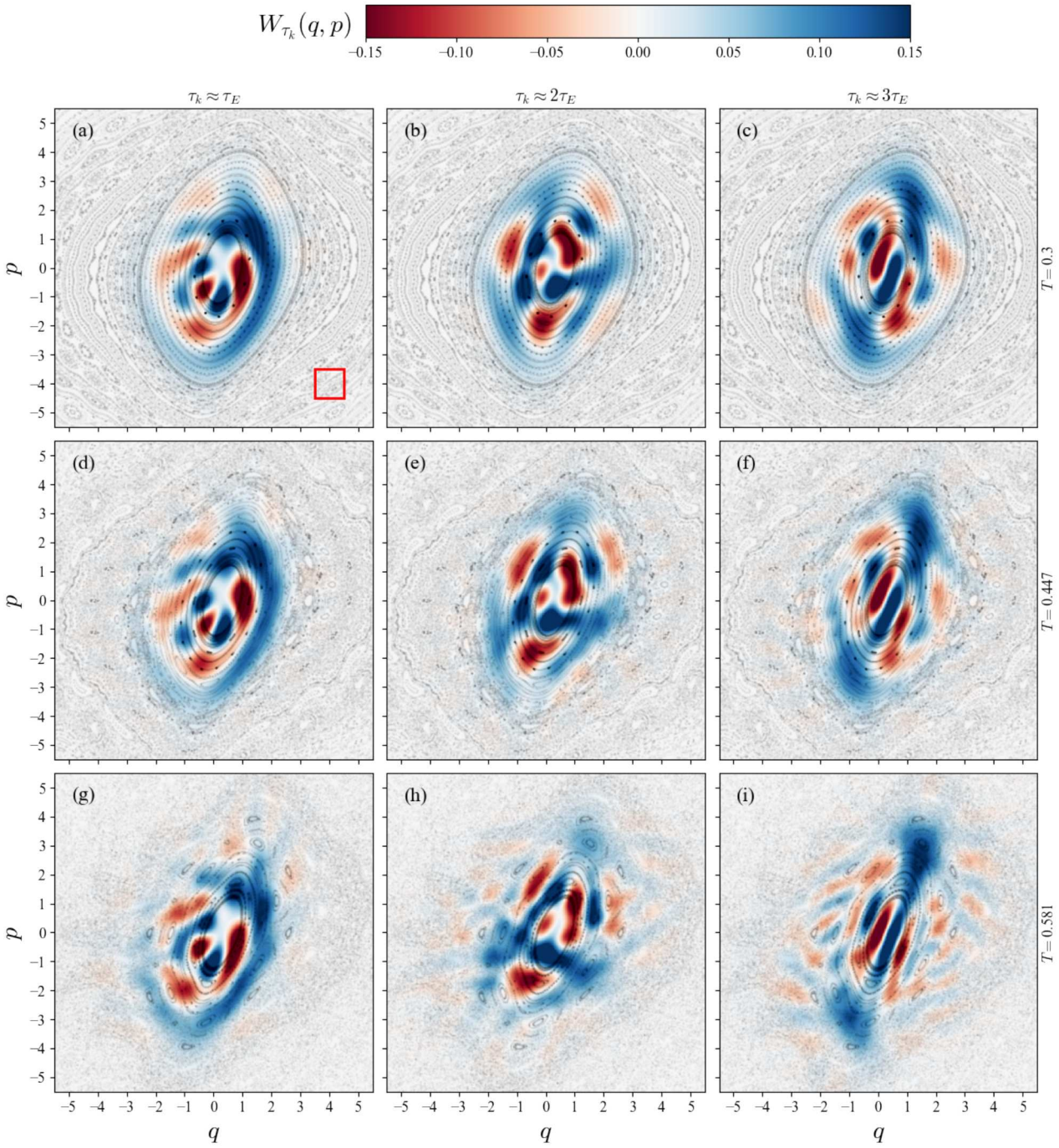

Figure 7.3: The quantum equivalent of Fig. 7.2 for the same values $T = 0.3$, $T = 0.447$ and $T = 0.581$ near the discretized times τ_E, $2\tau_E$ and $3\tau_E$. The initial Wigner function is the same as in the inset of Fig 7.2(a). The red square in (a) has area equal to $\hbar = 1$, and the classical map is still plotted as a gray background. By comparing (a), (d) and (g) with Fig. 7.2(a), 7.2(d) and 7.2(g) we notice that the quantum Wigner function has a discernible classical backbone for $\tau_k \approx \tau_E$, around which quantum interference patterns are formed. Surprisingly, for $\tau_k \approx 3\tau_E$ we have a quantum Wigner function that closely resembles a Schödinger cat state, while its classical counterpart has simply narrowed and revolved multiple times around the origin – a similar situation was observed in the Kerr system. The Wigner functions for the other T values look like deformations of the one for $T = 0.3$, vaguely reflecting the changes suffered by the classical map's orbits as T increases.

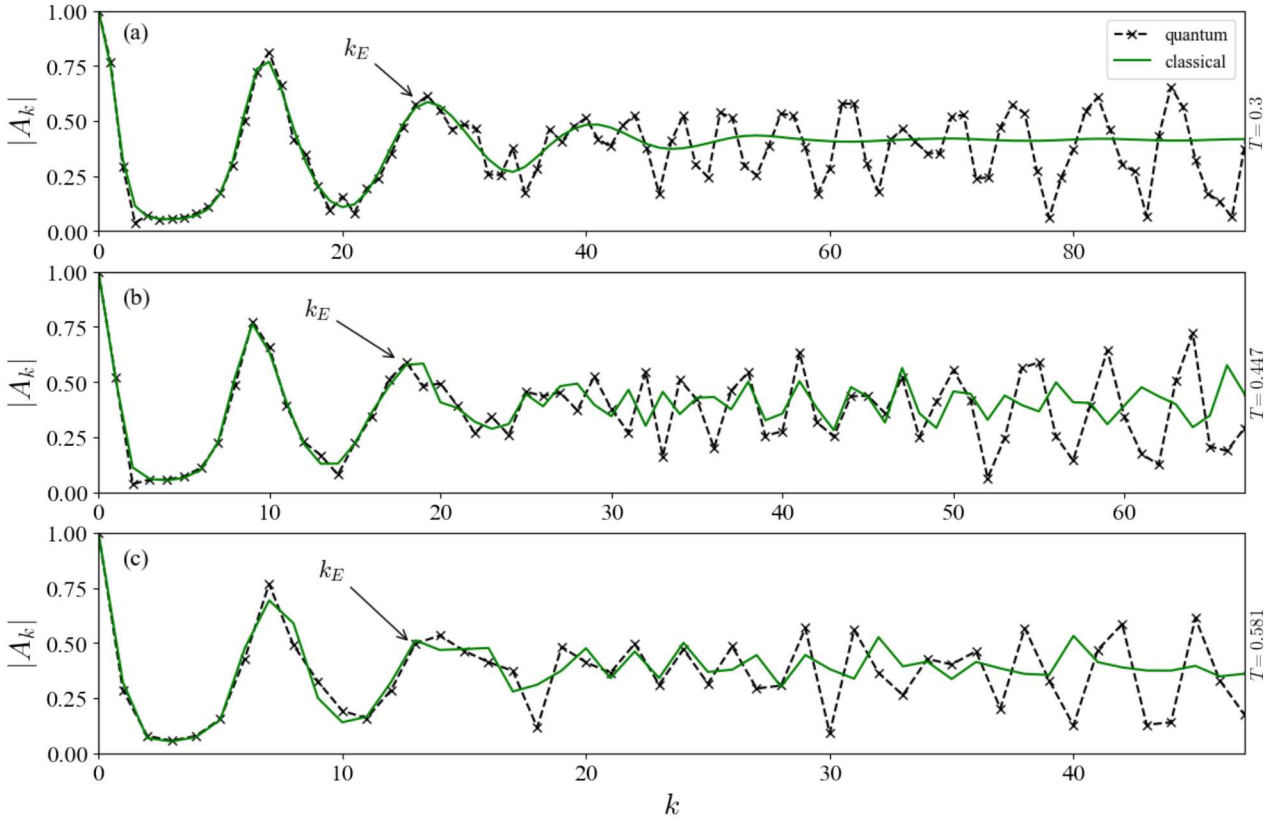

Figure 7.4: The meaning of the Ehrenfest time can be assessed through both autocorrelation function and phase-space geometry. Here we plot the quantum and classical autocorrelation functions for a coherent state initially centered at $(q = 2, p = 0)$ as a function of the kicks k for the three kicking strenghs $T = 0.3$, $T = 0.447$ and $T = 0.581$. The approximate moment at which these start to disagree is the Ehrenfest time $\tau_E = Tk_E$, where k_E is the Ehrenfest kick (arrows). For the first plot, for instance, we have $\tau_E = Tk_E \approx 0.3 \times 26 = 7.8$.

Substituting $V_{\text{coserf}}(q)$ in (7.4) and using (7.5), we can propagate the wavefunction corresponding to the initial Wigner function in the inset of Fig. 7.2(a) for the same kicking strengths and times. Instead of providing the results in terms of wavefunctions, however, it is much more geometrically appealing to use the Wigner transform of (4.12) and bring the result to phase space, which we display in Fig. 7.3.

Comparing Fig. 7.3 with Fig. 7.2, we see that the classical backbone is still visible behind quantum propagation for $\tau_k = \tau_E$, but it becomes hard or impossible to trace any connection between quantum and classical regimes as chaos becomes dominant *or* propagation times are long. We see here a mixture of the filaments already presented for the Kerr system with the "whorls and tendrils" characteristic of chaotic evolution [BBTV79]. However, for the kicking times used, even for the larger kicking strength $T = 0.581$ of Fig. 7.2(i) an inner portion of the initial state is trapped by regular orbits, while the outskirts are scattered by stability islands and chaotic seas. This phase-space portrait, however, is completely different from its quantum analogue of Fig. 7.3(i).

7.2.2 Autocorrelation functions and Ehrenfest time

Unlike the Kerr system, the Ehrenfest time for the coserf systems cannot be inferred analytically. One could naturally use its monodromy to obtain Lyapunov exponents and use them to estimate it [SVT12], but we prefer to rely on the autocorrelation functions of Subsection 4.2.3 just as we did for the Kerr system. Naturally, each kicking strength will define a different Ehrenfest time, which can be larger or smaller depending on how much chaos there is around the initial coherent state. Since the time for maps is discretized as $\tau_k = kT$, k being the number of kicks and T the kicking strength, we can also define an "Ehrenfest kick" $k_E = \tau_E/T$. In Fig. 7.4 we display the absolute value of the autocorrelation functions for the kicking strengths of Fig. 7.3 and our chosen initial coherent state with Wigner function

centered at $(q_0 = 2, p_0 = 0)$. We mark the approximate locations of our estimated Ehrenfest kicks $k_E = \tau_E/T$, *i.e.* the kick-values at which classical and quantum autocorrelation functions cease to agree.

7.3 Semiclassical dynamics

In Chapter 6 we implemented both the FVR and the HK propagators for the Kerr system, achieving remarkable results and validating both methods. The generality of the FVR propagator, however, is not necessary when the systems of interest are closed, and numerical efficiency is also very desirable. Thus, we decide to analyze the coserf system's semiclassical limit using the HK propagator. As all the routines required have already been numericized in Section 6.5, the modifications required to transport the code to the coserf systems are minimal – especially because the classical iterations are already exact. Of course, what we earlier interpreted as *time* is now a certain number of kicks with a specific kicking strength, and movement is discrete.

7.3.1 The monodromy matrix

A nice property of SSIs is that they present exact monodromy matrices. This can be seen by noticing that for each iteration we have a monodromy, and since the final iteration is the product of iterations, the final monodromy is also the product of monodromies. Consider, then, the jacobians for each iteration of ρ_i^{FV} as given in (2.3):

$$\frac{\partial(q_{i-\frac{1}{2}}, p_{i-\frac{1}{2}})}{\partial(q_{i-1}, p_{i-1})} = \begin{pmatrix} 1 & 0 \\ -TV''(q_{i-\frac{1}{2}}) & 1 \end{pmatrix}, \qquad \frac{\partial(q_i, p_i)}{\partial(q_{i-\frac{1}{2}}, p_{i-\frac{1}{2}})} = \begin{pmatrix} 1 & TF''(p_{i-\frac{1}{2}}) \\ 0 & 1 \end{pmatrix},$$

which are triangular and, by Lemma B.1.3, are symplectic. The complete monodromy is then

$$\frac{\partial(q_i, p_i)}{\partial(q_{i-\frac{1}{2}}, p_{i-\frac{1}{2}})} \frac{\partial(q_{i-\frac{1}{2}}, p_{i-\frac{1}{2}})}{\partial(q_{i-1}, p_{i-1})} = \frac{\partial(q_i, p_i)}{\partial(q_{i-1}, p_{i-1})},$$

which, being a composition of symplectic matrices, is also symplectic. Therefore, we can express the monodromy associated to N kicks as a function of the initial values (p_0, q_0) as

$$\mathcal{M}_N(p_0, q_0) = \frac{\partial(p_N, q_N)}{\partial(p_0, q_0)} = \frac{\partial(p_1, q_1)}{\partial(p_0, q_0)} \frac{\partial(p_2, q_2)}{\partial(p_1, q_1)} \cdots \frac{\partial(p_N, q_N)}{\partial(p_{N-1}, q_{N-1})}$$

$$\Rightarrow \mathcal{M}_N(p_0, q_0) = \prod_{i=1}^{N} \frac{\partial(p_i, q_i)}{\partial(p_{i-1}, q_{i-1})}, \quad \mathcal{M}_0 = I\,.$$

Such a decomposition has the further advantage that it can be computed in parallel with the equations of motion, decreasing computational cost. Using this matrix, we form the Herman-Kluk pre-factor (6.14) and calculate the Maslov indexes using the exact same procedure as in Subsection 6.5.3.

7.3.2 The classical action

The classical action corresponding to discrete maps is not obtained from an integral, but from the discretized lagrangians of Subsection 2.2.2. The actions are obtained by direct application of the theory of this subsection and care must be taken when dealing with the two possible orderings U_T^{VF} and U_T^{FV}, since they have different lagrangians (compare (2.7) and (2.8)).

7.3.3 Propagating coherent states

Propagating coherent states in the discrete case is identical to what was described in Subsection 6.5.3, except that now the flow is substituted by a map. What is required in the transition from the "continuous" to the discrete case is really *nothing*, because the continuous case was never continuous

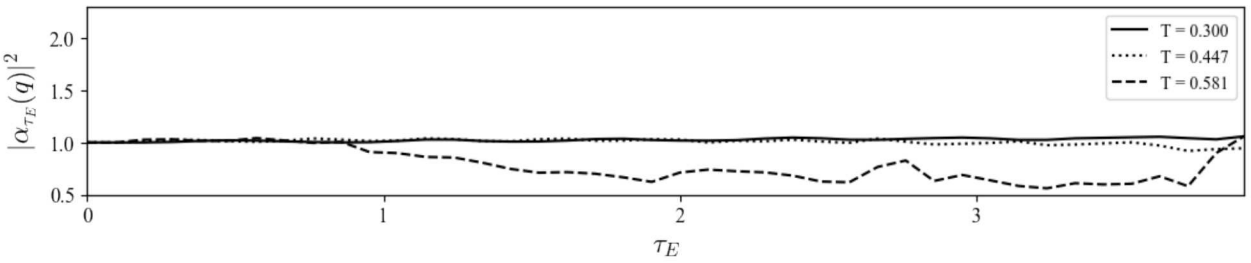

Figure 7.5: Normalizations for different kicking strengths, T, as functions of the Ehrenfest time $\tau_E = Tk_E$. Although the kicks are discrete variables, we connect the points using lines for ease of visualization. For the $T = 0.3$ (solid line), we see in Fig. 7.2 that the initial wavepacket is still confined in a regular phase-space region and normalization is not lost. For $T = 0.447$ (dotted line) we start to see deviations from unity around $\tau_k \approx 4\tau_E$. The large number of chaotic orbits for $T = 0.581$ (dashed line) causes an evident normalization loss starting at times near τ_E.

in the first place: There are no continuous variables in numerical analysis, only small iteration steps. Well, now the iteration steps are larger, and that's it! One difference with respect to Chapter 6 is that earlier the wavefunction obtained from the HK propagator did not lose normalization as it evolved, but now it does – but only for chaotic regimes. This was already known in the field and is due to the fact that, while the amplitudes of most integral representations do not diverge at 0, they do diverge along chaotic orbits due to the separation between initially close orbits increasing exponentially [Mai00, SKM98, Swe11, dLC16]. In Fig. 7.5 we plot the normalization of the semiclassical wavefunction as a function of the Ehrenfest time for the three kicking strengths we have been using up to now. As we clearly see normalization being lost, we perform a procedure analogous to that employed in Subsection 6.3.3: We define renormalized wavefunctions,

$$\int_{\mathbb{R}} dq|\alpha_k(q)|^2 = C \quad \Longrightarrow \quad \alpha_k(q) \longmapsto \bar{\alpha}_k(q) = \frac{\alpha_k(q)}{\sqrt{C}}\,,$$

a procedure we can perform for any kick k.

In Fig. 7.6 we display the Wigner transforms of the renormalized semiclassical wavefunctions outputed by the HK method. As we can see, the integrable case in the first row is indiscernible from the exact quantum case, just as for the Kerr system (see Fig. 6.11). In the second row, where we have introduced some chaos that we can consider as "weak" due to the small normalization loss it causes (see Fig. 7.5), the semiclassical approximation is still very accurate. By looking at the second row of its classical equivalent in Fig. 7.2, we see that indeed the main portion of the initial coherent state has been captured by integrable orbits – which from the first row we know provide accurate results. For the third row of Fig. 7.6, where chaos can be considered strong, the semiclassical approximation is able to reproduce the main features of its exact quantum equivalent in Fig. 7.3 until the threshold of around 6 Ehrenfest times. This is in itself quite amazing, because if we look at the normalizations of Fig. 7.5 we see that we are reproducing regimes where the semiclassical wavefunctions are coming out quite far from normalization, showing that a successfull semiclassical approximation might be attainable despite the normalization loss. As a quantitative comparison, we provide in Fig. 7.7 the position probability marginals extracted from Figs. 7.3 and 7.6.

It is also interesting to attempt a semiclassical reproduction of autocorrelation functions, since they are easier to calculate and commonly used in the field as a measure of a semiclassical approximation's success. In in Fig. 7.8 we display the quantum and semiclassical autocorrelation functions extracted from renormalized wavefunctions. For the integrable and weakly chaotic regimes of the first two rows, respectively, we see that the semiclassical approximation is excelent, but for the chaotic regime the deviations are strong after 4 Ehrenfest times and hint that we should expect poor results in this regime (as confirmed in Figs. 7.6(i) and Fig. 7.7(i)).

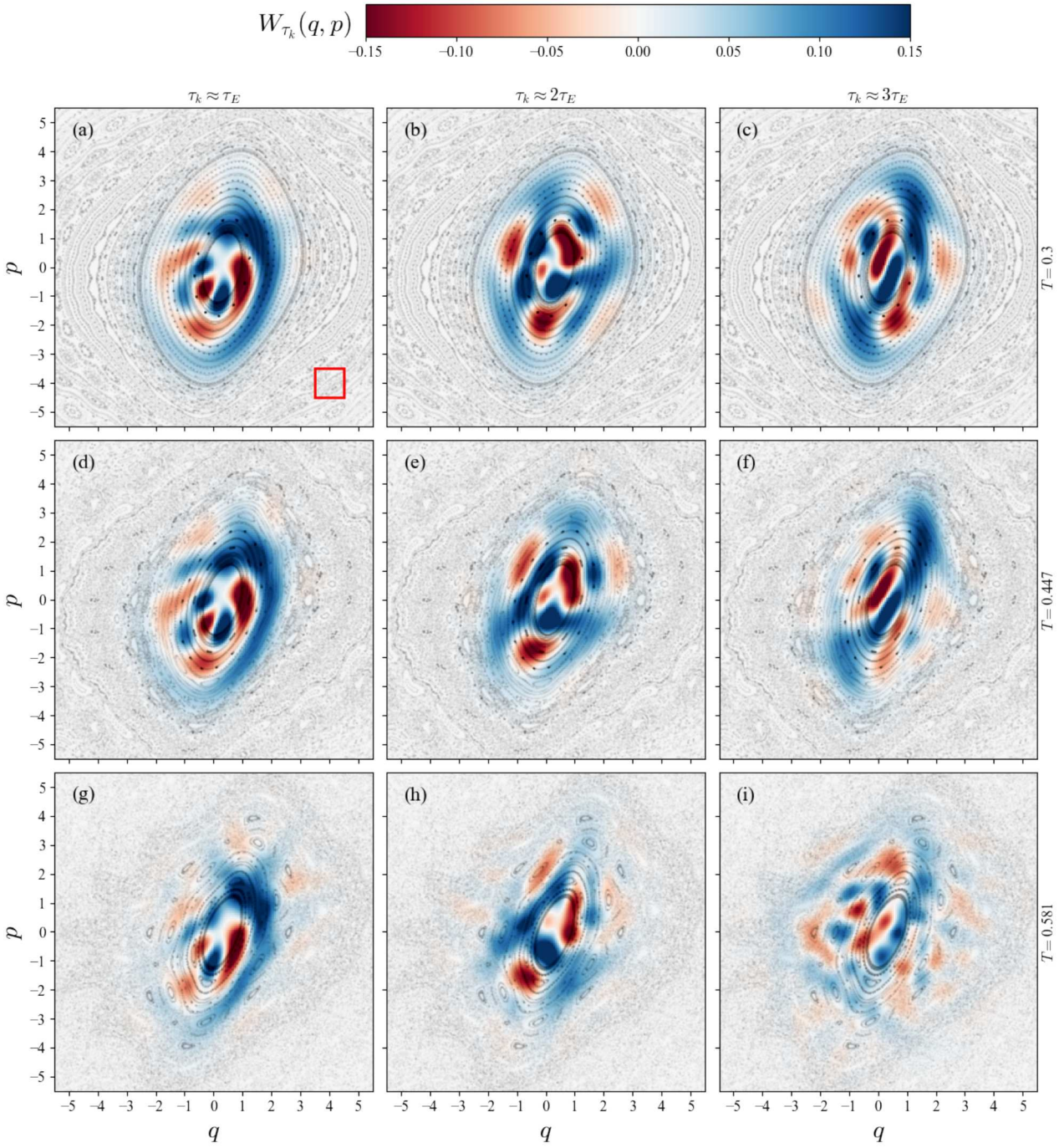

Figure 7.6: The semiclassical equivalent of Fig. 7.2 and Fig. 7.3 for the same values $T = 0.3$, $T = 0.447$ and $T = 0.581$ and discretized times τ_E, $2\tau_E$ and $3\tau_E$. The initial Wigner function is the same as in the inset of Fig 7.2**(a)**. The red square in **(a)** has area equal to $\hbar = 1$. For the completely regular case of $T = 0.3$, the semiclassical approximations and the exact quantum Wigner functions are almost indiscernible (see also Fig. 7.7). The stability islets present for $T = 0.447$ are not enough to spoil the semiclassical approximation's accuracy even for the long time $\tau_k = 3\tau_E$, for which we can see that the filament has been captured by several islands. For the extreme $T = 0.581$, the approximation finally breaks down for $\tau_k = 3\tau_E$.

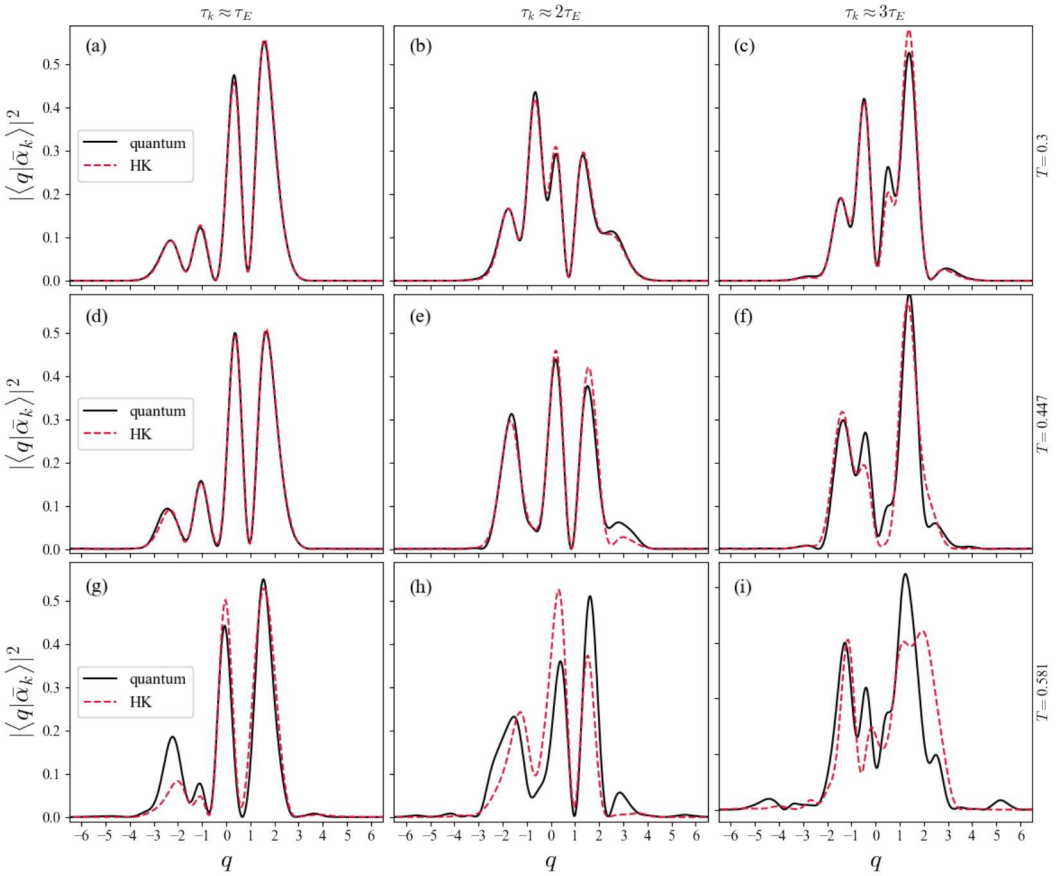

Figure 7.7: Position probability marginals obtained from the exact evolutions in Fig. 7.3 and the renormalized semiclassical Wigner functions of Fig. 7.6.

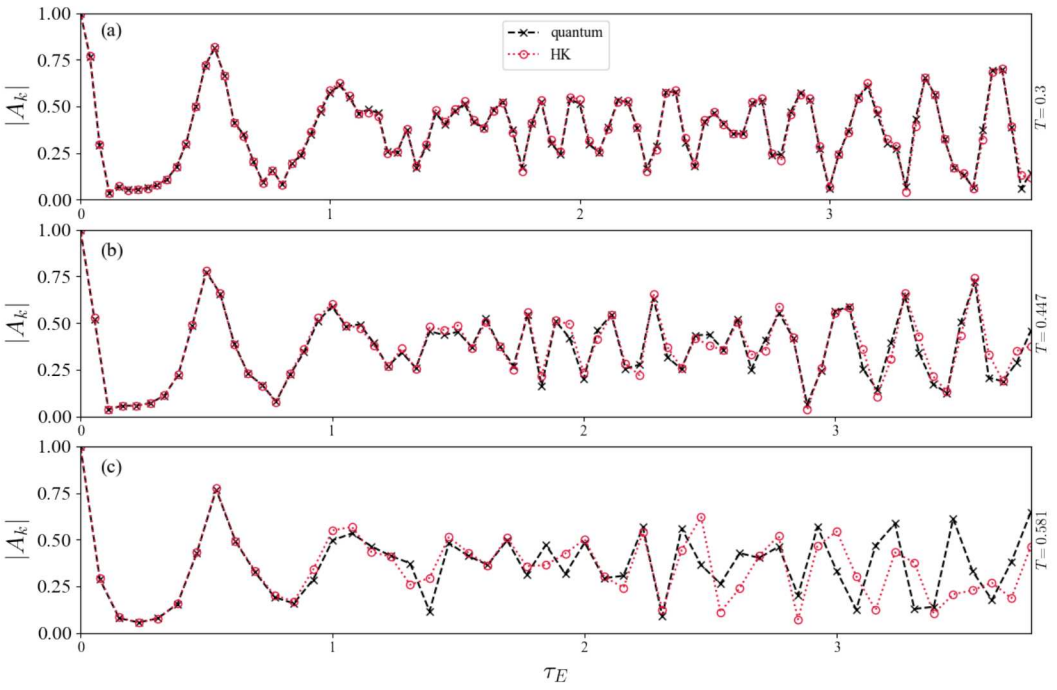

Figure 7.8: Quantum and semiclassical autocorrelation functions obtained from the wavefunctions (7.5) and by substituting the approximation (3.32) into (7.5), respectively. As in Fig. 7.5, we use the Ehrenfest time scale and the initial coherent state is centered at $(q = 2, p = 0)$. The autocorrelations are discrete entities, but we connect them using lines in order to facilitate interpreting the plots. Notice how the semiclassical autocorrelations only start to fail near the time values for which the normalizations in Fig. 7.5 also start to oscillate.

7.4 Chaos erasure: From tangles to tori

In the earlier section we presented strong numerical evidence that semiclassical propagation can be applied even for chaotic systems – which is no news by itself since the seminal work by Steven Tomsovic and Eric Heller, published in the early 1990s [TH91], even though we may have performed a more comprehensive analysis for a generally more complex system. Taking a good look at Figs. 7.2 and 7.3, however, we notice that while the system's dependence on the kicking strength T is absolutely fundamental to mold classical propagation, the impact on the quantum regime is not so strong. The emergence of islands and chaotic seas completely deforms and scatters the initial distribution, while the quantum Wigner functions appears to completely ignore both small ($\leq \hbar$) *and* large ($\geq \hbar$) classical structure formed by chaos. What happens if we simply ignore chaos altogether? The first step towards erasing chaos from a classical system is, of course, thiking about what it will be replaced with: We must find a way to map chaotic orbits into regular ones without depriving the initial system of its defining characteristics. This is when the effective hamiltonians of Subsection 2.1.1 come into play.

7.4.1 Effective trajectories

The effective hamiltonians were found to be the energies associated to the SSIs – for small kicking strengths there were conserved, and for large ones they weren't. However, as we have mentioned earlier, the kicking strength is just a parameter, not time. Thus, just as the hamiltonian maps they are extracted from, the effective hamiltonians are a *family* with respect to T and define separate vector fields and flows: For $\mathcal{H}^{VF}$, for instance, we have the Hamilton equations

$$\begin{cases} \dfrac{dq}{dt} &= \dfrac{\partial \mathcal{H}^{VF}}{\partial p} = \dfrac{\partial}{\partial p}\left[F(p)+V(q)+\dfrac{T}{2}\{V(q),F(p)\}+\mathcal{O}(\epsilon^2)\right] = F'(p)+\dfrac{TF''(p)V'(q)}{2}+\mathcal{O}(T^2) \\ \dfrac{dp}{dt} &= -\dfrac{\partial \mathcal{H}^{VF}}{\partial q} = -\dfrac{\partial}{\partial q}\left[F(p)+V(q)+\frac{T}{2}\{V(q),F(p)\}+\mathcal{O}(T^2)\right] = -V'(q)+\dfrac{TF'(p)V''(q)}{2}+\mathcal{O}(T^2) \end{cases}, \tag{7.6}$$

with a solution we shall call $\rho_t^{\mathcal{H}^{VF}}$. The kicking strength T is then seen to be a coupling constant between the initial hamiltonian vector field and a Poisson-bracket perturbation series. Since all terms in the equations above are autonomous and our system is defined on the plane, the effective system $(\mathbb{R}^2, dq\wedge dp, \rho_t^{\mathcal{H}^{VF}})$ is integrable by Corollary 2.2.7. Its flow, namely $\rho_t^{\mathcal{H}^{VF}}$, is then a perturbation of the original flow ρ_T^{VF}: For $T=0$, they are identical, and are also very close for small T. However, when we increase T enough for the map to be chaotic, the effective flow remains regular and washes away all chaos by running over the map's chaotic regions as if they were integrable: Starting with the same phase-space point x, the exact map $\rho_T^{VF}(x)$ will perform very complicated dynamics and possibly fall on chaotic seas, while $\rho_t^{\mathcal{H}^{VF}}(x)$ will be always restricted to the surface of a torus (in this case, a circle).

Effective hamiltonians have been used before in contexts such as *e.g.* chaos assisted tunneling [BSU01, LBKS10], with a system's original chaotic sets substituted by the level sets of an effective hamiltonian, and explored as normal forms for maps in [Lan15]. Notice, however, that as a perturbative series mixing position and momentum, the effective hamiltonian is not a separable function and cannot be solved by the standard SSIs: That's where Tao's algorithm, presented in Subsection 2.1.3, finds its use. We employ it to embed the effective hamiltonian into the augmented phase space and solve (7.6) for a step-size δ, which has no physical interpretation and is only an iteration parameter taken as small in order to increase the numerical integrator's accuracy. The final discretized time in the effective flow solved by Tao's algorithm will then be $t_\delta = \delta K$, K being the number of kicks, while in the original map it will be $t_T = TN$. Since these times must match, we must have $K = (T/\delta)N$, so that we immediately see that if we want a lot of accuracy in numerical integration, the number of iterations K in Tao's algorithm quickly becomes huge.

Example 7.4.1. Suppose we want to employ Tao's algorithm for $T = 0.5$ and we are interested in the very long propagation time $t = 100$, which corresponds to $N = 200$. For $\delta = 10^{-3}$, we have

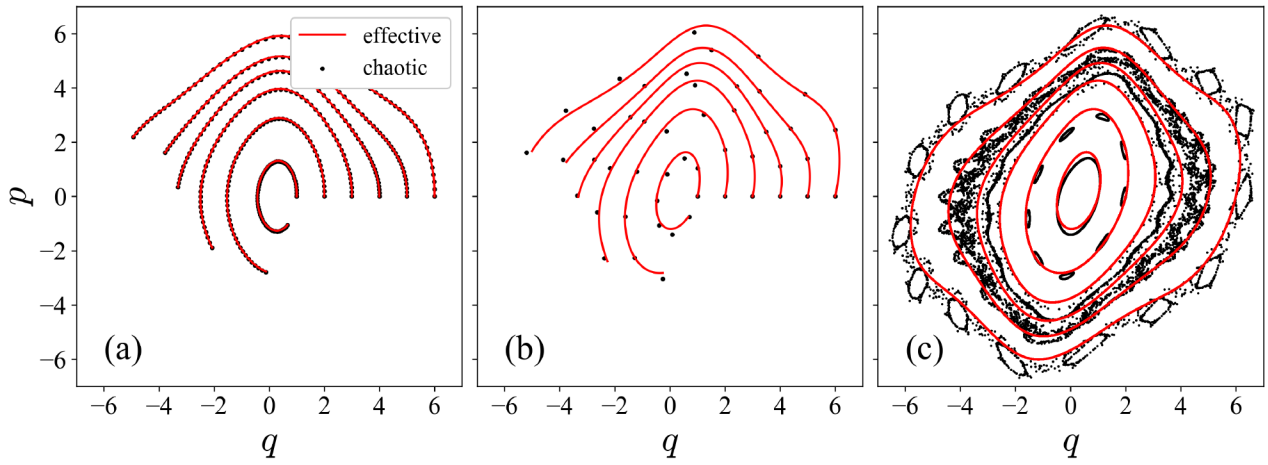

Figure 7.9: Six initial points are evolved according to the discrete dynamics of the map ρ_T^{VF} and the continuous effective flow $\rho_t^{\mathcal{H}^{VF}}$. In panel (a) we have $T = 0.05$ and $N = 5$, such that the effective flow is really nothing but a continuous approximation. For panel (b) we take $T = 0.45$ and $N = 7$, where it becomes obvious that the continuous flow is no longer an interpolation of the chaotic one. Panel (c) has the same parameters of (b) except that we iterate the map 2.000 times, showing that the chaotic trajectories biffurcate and give rise to chaotic seas and stability islands, while the effective flow runs over them as if chaos were completely absent.

$K = (T/\delta) = 10^5$. The discretized flow must then be iterated 100.000 times for 200 iterations of the original map.

We now proceed to an analysis focused on the coserf map. For the hamiltonian (7.1), Hamilton's equations for the effective hamiltonian $\mathcal{H}^{FV}$ read, up to $\mathcal{O}(T^3)$,

$$\begin{cases} \dfrac{dq}{dt} = p + \left(\dfrac{T}{2}\right)(q + 2\sin q) + \left(\dfrac{T^2}{6}\right)(p + 2p\cos q) + \left(\dfrac{T^3}{12}\right)(q + 2q\cos q + 2\sin q + 4\cos q \sin q) \\ \dfrac{dp}{dt} = -\left\{ q - \exp(-q^2) + \sin q + \left(\dfrac{T}{2}\right)(p^2 + p\cos q) + \left(\dfrac{T^2}{6}\right)[q + 2q\cos(q) - (p^2 - 2)\sin q \right. \\ \qquad \left. +2\sin(2q)] + \left(\dfrac{T^3}{12}\right) p\,[1 + 4\cos q + 4\cos(2q) - 2q\sin q] \right\}. \end{cases}$$

In Fig. 7.9 we present the effective trajectories that approximate six discrete coserf orbits for two different kicking regimes: One integrable and the other, chaotic. We fix $\delta = 10^{-2}$ in Tao's algorithm. In panel (a) we have $T = 0.05$ and $N = 60$, so $t = TN = 3$ and $K = 300$. We choose a short time in order for the comparison with the effective trajectories to be clear, especially the matching of final times. We observe the expected behavior regarding effective trajectories: In this regime the coserf map is regular and the integrable approximation can be seen as an interpolation of the map's orbits. In panel (b), however, we set $T = 0.45$ and $N = 7$, corresponding to $t = 3.15$ and $K = 315$. For this longer time chaos has settled in and we can see the effective trajectories deform, but as expected they never cease to be regular. They are no longer a "continuous" interpolation of the maps dynamics, and can be considered as completely different objects. Panel (c) is the same as (b) but for a 2.000 kicks of the coserf map, which corresponds to 90.000 iterations of Tao's algorithm! We then clearly see that the surviving invariant torus near the origin is somewhat interpolated by the effective trajectories, but the islands and chaotic regions are completely ignored by the integrable approximation as expected. It is also worthwhile to notice, once again, that Tao's algorithm remains perfectly symplectic.

7.4.2 Propagating coherent states (again)

The effective system defined in the previous subsection can be seen as a substitute to the original discrete hamiltonian system that, although following the original system's deformations, exchanges chaotic orbits by tori. We know that for large kicking strengths the effective flow does not approximate the original one: It is not really meant to be an *approximation*, but a filtering – a chaos-erasing method.

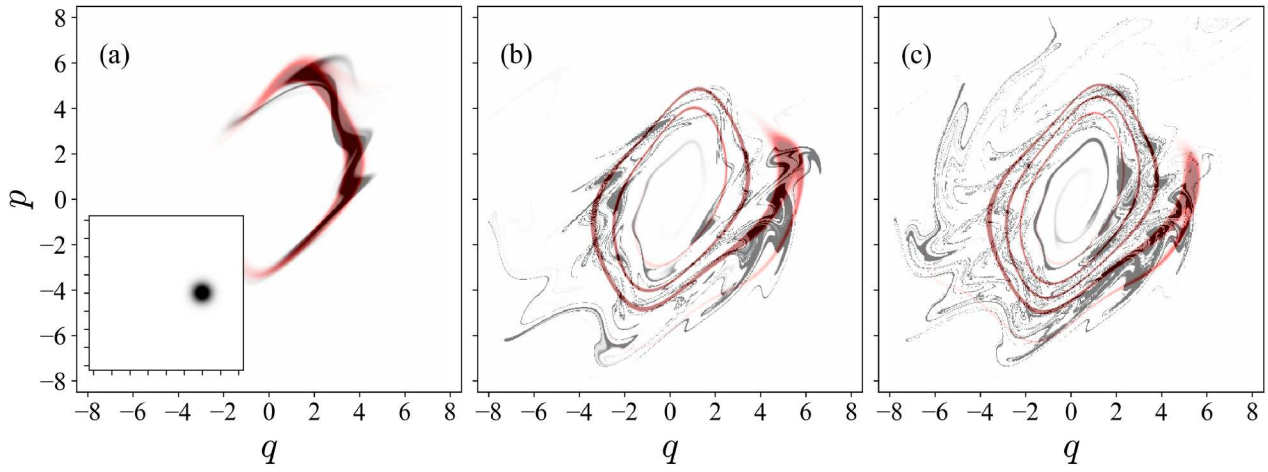

Figure 7.10: Classical propagation of the Wigner function of a coherent state initially centered at $(q = 4, p = 0)$ (shown in the inset) under the dynamics of the coserf map (7.3) and its effective flow $\rho_t^{\mathcal{H}^{VF}}$. The kicking strength is $T = 0.6$ and we used $\delta = 10^{-2}$ in Tao's algorithm, described in Subsection 2.1.3. Chaotic propagation is always shown in black, while its effective approximation is superposed in light red. Panel (a) depicts evolution for $N = 9$ in (7.3), while panels (b) and (c) use $N = 36$ and $N = 49$, respectively.

As discussed in Chapter 3, quantum mechanics is linear and, as we have stated earlier in this chapter, it does look like the quantum propagation correspoding to a chaotic map essentially ignores stability islands and chaotic seas. As is probably obvious by now, we intend to use the regular trajectories obtained from the effective hamiltonian to semiclassically approximate the coserf system instead of its exact discrete dynamics.

What can we expect from this substitution? Well, for small kicking strengths we know that the effective and the exact systems lie close to each other, so there should be no difference between using either propagation scheme – in other words, since the system is near-integrable for small kicking strengths, there are no chaotic orbits to be erased in the first place. However, as we increase the kicking strength, the effective and exact systems become completely different from the classical point of view. This is depicted in Fig. 7.10, where we classically propagate the Wigner function of an initial coherent state initially centered at $(q = 4, p = 0)$ for $T = 0.6$. We choose three different final times: (a) $N = 9$, (b) $N = 36$ and (c) $N = 49$, which are near $\tau_E/2$, $2\tau_E$ and $3\tau_E$, respectively. Taking a look at panel (a), we see that for times smaller than the Ehrenfest time there should be no stark contrast between chaotic and integrable propagation schemes, since chaos is still weak and has not yet started to strongly deform the inintial coherent state. However, as we can see in panels (b) and (c), chaotic and integrable systems become two separate entities and chaos is so dominant that the initial coherent state is deformed into a black stain. The packet propagated using regular trajectories, however, forms well-behaved red filaments that strongly resemble the Kerr system, except that after a certain phase space radius the angular speed slows down and forms a protruded horn on the right of panels (b) and (c). Notice that, interestingly, the chaotic propagation also accumulates the initial state behind these horns. In short: We expect the semiclassical propagation based on regular trajectories to approximate the quantum result well for times smaller then the Ehrenfest time, but after that it should start to fail, with the propagation based on the discrete map becoming superior[2] until it naturally fails due to chaos becoming too abundant in phase space. The initial coherent state chosen here is also intentionally placed in a very broad chaotic region, such that only a tiny portion of it is captured by regular orbits that might improve semiclassical results – the majority of orbits is chaotic, as can be seen in Fig. 7.10.

In Fig. 7.11 we display the semiclassical probability amplitudes obtained from propagating an initial coherent state centered at $(\Re(\alpha) = 4, \Im(\alpha) = 0)$ using HK propagators employing both the exact (chaotic) and the effective (regular) trajectories of Fig. 7.10, with the exact quantum result in the background. The wavefunctions obtained from chaotic trajectories, as was the case in Subsection 7.3.3, need to be renormalized and lose normalization faster than in Fig. 7.5 since we are using a

[2]Remember the quantization of hamiltonian maps is exact, so the classical system really is the exact counterpart of the quantum system, while the effective system is essentially a different thing.

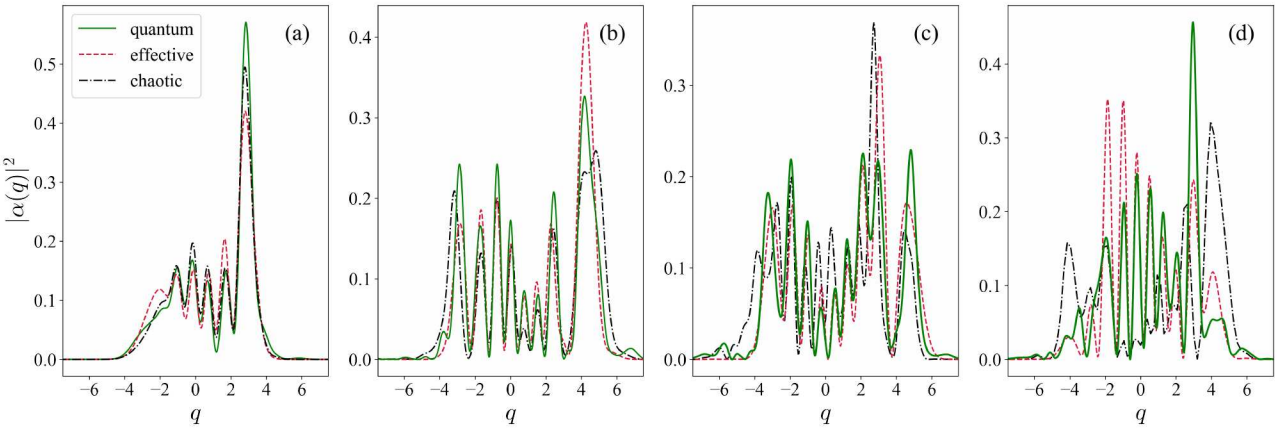

Figure 7.11: Wave densities associated to Fig. 7.10 obtained via the Herman-Kluk propagation and the exact quantum map for $T = 0.6$. The exact quantum result is displayed as a solid green line, while the semiclassical propagations using chaotic and effective trajectories are shown as black and red dashed lines, respectively. The number of kicks for the first three panels is the same as in Fig. 7.10, namely **(a)** $N = 9$, **(b)** $N = 18$ and **(c)** $N = 49$, but in **(d)** we have $N = 70$. We take $\hbar = 1$ and $\delta = 10^{-2}$.

larger kicking strength. The wavefunctions based on the regular trajectories, however, do not need to be renormalized, since as stated earlier the normalization loss is due exclusively to the presence of chaotic orbits. As can be seen in panel (a) of Fig. 7.11, both probability marginals match quite closely for $\tau_E/2$, with the one employing the system's true chaotic trajectories faring a little better. In panel (b) both propagation schemes provide reasonable results, but the one employing regular trajectories hits all the peaks very closely – this is largely unexpected! If we look at Fig. 7.10(b), we have in black an exact picture of how the coserf map classically propagates a coherent state, but the "fake" red trajectories provide a better semiclassical result. This situation becomes extreme in panel (c), where the propagation based on chaotic trajectories starts to break down, and again the propagator employing effective trajectories is superior. Exploring the absurd a little further, we performed calculations for $N = 70$, corresponding to approximately $4\tau_E$, shown in Fig. 7.11(d). This time regime is much longer than what we expect to be able to reproduce using chaotic trajectories: The plot for $N = 70$ is really just a black stain. The regular trajectories, of course, just remain regular, and to our uttermost surprise the propagator employing them hits basically all the peaks of the exact quantum result, many with reasonable amplitude.

7.5 Discussion

The results presented in Chapter 6 were largely unexpected: We did not really believe any semiclassical method would be capable of reproducing fractional revival patterns so well as the FVR and the HK did. We have actually even considered that the Kerr system's semiclassical quantization might be exact due to some unknown facet of a theorem by Duistermaat and Heckman [DH82]. The tests performed using the Herman-Kluk propagator, however, discouraged us to think along these lines: It seems that the semiclassical quantization of any integrable system is just extremely good, despite rigorous proofs currently lacking [Vor96]. The Kerr system, thus, was perhaps no exception, where the complexity of revival patterns did not superpose its integrablity. What really does spoil semiclassical propagation is strong chaos, which in the case of maps means large kicking strengths.

How is it possible that we could reproduce quantum propagation by employing a different system than its unique and exact classical analogue? Worse yet, a substitute that erases chaos? As is often the case in the field (or any field in science, really), phenomena preceed their explanations: We don't know how the results in Fig. 7.11 could be achieved. From the semiclassical point of view, what we have discovererd is that we can reproduce a quantum system by pretending that the phase space of its classical analogue is folliated by tori, when in reality the generating functions associated to the lagrangian submanifolds formed by the chaotic flow are extremely complicated. We then have a strong indicative that quantum propagation might really be *chaos-blind*: It does not really mind whether or

not you include classical chaos when propagating states (at least coherent ones).

The case of stationary states, however, requires summing over entire lagrangian submanifolds instead of trajectories. The semiclassical quantization of chaotic systems, as described in Subsection 3.4, is problematic because it involves sums over evolving lagrangian submanifolds, which in the integrable case are just invariant tori, but when the system is chaotic are complicated and open. Due to the ergodicity of these submanifolds a statistical interpretation is sometimes possible and leads to Random Matrix Theory (RMT), where it is found that quantum-chaotic systems display level repulsion: The systems have so little internal classical symmetries that their quantum eigenvalues cannot assume the same values [dA90, Gut90]. The distribution of eigenvalues in integrable systems, in contrast to time-dependent properties, is well understood: The extreme symmetry of these systems leads to severe degeneracies of the spectrum, regardless to whether the system is separable or not [BT76]. Even though we could reproduce quantum-chaotic propagation using an integrable system, the validity of such approach for the extraction of stationary properties looks, at first glance, impossible: While the chaotic system displays level repulsion, the spectrum of its effective twin should be degenerate.

The situation described above would seem hopeless except for a single detail: The coserf system, as all hamiltonian maps on the plane, cannot have its spectrum entirely modelled by RMT. This is due to its *soft* chaotic nature, defined by small tori appearing intertwined with chaotic regions: For RMT to be applied, one needs full ergodicity of classical orbits, while for EBK quantization complete integrability is required. Soft chaos, therefore, lies in an obscure region where neither of the currently available stationary formalisms is expected to work [HdA83]. Based on the numerical evidence presented here, for instance, we can be quite sure that important maps (such as Chirikov's of Example 2.2.2) can be modelled using effective regular trajectories for a significant range of kicking strengths.

Our conclusions also touch an important point regarding quantization (pure quantization, not the semiclassical one): The effective hamiltonian, when quantized, must lie very close the quantum coserf hamiltonian, which is a periodically kicked system. We are then met with a rather weird situation: The quantization of a periodically kicked system is somehow equivalent to a quantized perturbation series (at least for small kicking strengths). Naturally, this topic deserves attention by itself.

As a last observation, we consider what can go wrong when applying the method of effective hamiltonians to arbitrary systems. There are two factors that might play significant roles behind our results:

1. We are restricted to the plane;

2. The coserf map is a perturbation of an integrable system.

We start from 1.: The restriction to the plane forces the effective hamiltonian to be integrable, since it is autonomous and Corollary 2.2.7 applies. In the general case what must be considered is a Poisson-series perturbation of the form $\mathcal{H}(q,p) = F(p) + V(q) + \epsilon\{F(p), V(q)\}$. For completely separable systems, where the potential and kinetic terms themselves are separable, *e.g.* $V(q) = V(q_1)+V(q_2)+...$, the system $F+V$ is guaranteed to be integrable [Arn89]. Is $\mathcal{H}$ integrable? This is a question regarding the KAM theory of Poisson-type perturbations, and our attempted proof is still unfinished. We remind the reader that the theory of integrable perturbations is far from simple (for an example see [BBM12]).

We now move to item 2.: If our chaotic map is not obtained by perturbing an initially integrable system, then its phase space is not folliated by tori even when the kicking strength is zero. This is the case, for instance, of perturbations of general systems in high dimensional phase spaces. If the method really relies on the existence of lagrangian tori for small kicking strengths, it should not work in this case.

Despite the difficulties that might arrise when adapting our method to more complex systems, the extraction of deep and often generalizable phenomena is often achieved from the study of simple mappings, *e.g.* the famous connection between Chirikov's map and Anderson localization [GP84]. As an example of a practical use of chaos-erasure, chaotic trajectories were recently mapped into regular ones using the concept of dominant-interaction hamiltonians and were shown to be able to reproduce the spectrum characteristic of high harmonic generation[3] [ZGGR12]. We then expect our results to

[3]Their method cannot be really taken as chaos-erasing due to the switching between dominant hamiltonians reflecting the original system's chaotic nature. Here, however, chaos is entirely absent from the final trajectories.

find a place within practical calculations, but the intriguing theoretical aspects they brought up are already enough to motivate further research.

Bibliography

[Arn89] V. I. Arnold. *Mathematical Methods of Classical Mechanics*. Springer, 2nd edition, 1989.

[BBM12] A. Blasco, A. Ballesteros, and F. Musso. Integrable perturbations of hénon-heiles systems from poisson coalgebras. *AIP Conf. Proc.*, 1460:159, 2012.

[BBTV79] M. V. Berry, N. L. Balasz, M. Tabor, and A. Voros. Quantum maps. *Ann. Phys.*, 122:26, 1979.

[BSU01] O. Brodier, P. Schlagheck, and D. Ullmo. Resonance-assisted tunneling in near-integrable systems. *Phys. Rev. Lett.*, 87:064101, 2001.

[BT76] M. V. Berry and M. Tabor. Closed orbits and the regular bound spectrum. *Proc. R. Soc. Lond. A*, 349:101, 1976.

[Chi79] B. V. Chirikov. A universal instability of many-dimensional oscillator systems. *Phys. Rep.*, 52:263, 1979.

[dA90] A. M. Ozorio de Almeida. *Hamiltonian Systems: Chaos and Quantization*. Cambridge University Press, 2nd edition, 1990.

[DH82] J. J. Duistermaat and G. J. Heckman. On the variation in the cohomology of the symplectic form of the reduced phase space. *Invent. Math.*, 69:259, 1982.

[dLC16] G. di Liberto and M. Ceotto. The importance of the pre-exponential factor in semiclassical molecular dynamics. *J. Chem. Phys.*, 145:144107, 2016.

[Fol89] G. B. Folland. *Harmonic Analysis in Phase Space*. Princeton University Press, 1989.

[GP84] D. R. Grempel and R. E. Prange. Quantum dynamics of a nonintegrable system. *Phys. Rev. A*, 29:4, 1984.

[Gut90] M. Gutzwiller. *Chaos in Classical and Quantum Mechanics*. Springer-Verlag, 1990.

[HdA83] J. H. Hannay and A. M. Ozorio de Almeida. Periodic orbits and a correlation function for the semiclassical density of states. *J. Phys. A: Math. Theor.*, 17:3429, 1983.

[Lan15] G. M. Lando. *Integrable approximations of discrete dynamical systems: Classical and quantum aspects*. MSc thesis, 2015.

[LBKS10] S. Löck, A. Bäcker, R. Ketzmerick, and P. Schlagheck. Regular-to-chaotic tunneling rates: From the quantum to the semiclassical regime. *Phys. Rev. Lett.*, 104:114101, 2010.

[Mai00] N. T. Maitra. Semiclassical maps: A study of classically forbidden transitions, sub-h structure, and dynamical localization. *J. Chem. Phys.*, 112:531, 2000.

[SKM98] J. L. Schoendorff, H. J. Korsch, and N. Moiseyev. Semiclassical quantization of a system with mixed regular/chaotic dynamics. *Europhys. Lett.*, 44:290, 1998.

[SVT12] R. Schubert, R. O. Vallejos, and F. Toscano. How do wave packets spread? Time evolution on Ehrenfest time scales. *J. Phys. A: Math. Theor.*, 45:215307, 2012.

[Swe11] D. W. H. Swenson. *Quantum Effects from Classical Trajectories: New Methodologies and Applications for Semiclassical Dynamics*. PhD dissertation, 2011.

[TH91] S. Tomsovic and E. J. Heller. Semiclassical dynamics of chaotic motion: Unexpected long-time accuracy. *Phys. Rev. Lett*, 67:664, 1991.

[Vor96] A. Voros. Aspects of semiclassical theory in the presence of classical chaos. *Prog. Theo. Phys. Supp.*, 116:116, 1996.

[ZGGR12] C. Zagoya, C.-M. Goletz, F. Grossmann, and J.-M. Rost. Dominant-interaction hamiltonians for high-order-harmonic generation in laser-assisted collisions. *Phys. Rev. A*, 85:041401(R), 2012.

Appendix A

Mathematical companion

A.1 Differentiable manifolds

Let $(M, \mathcal{T})$ be a Hausdorff space equipped with a topology $\mathcal{T}$, which from now on we will omit. A *chart* is a pair $\mathcal{C} = (U, x)$ such that $x : M \supset U \longrightarrow V \subset \mathbb{R}^n$, where U and V are open sets and ϕ is a homeomorphism. We call x a *chart* or *local coordinate system* on M. Let $\mathcal{C}_1 = (U_1, \phi_1)$ and $\mathcal{C}_2 = (U_2, \phi_2)$ be charts over M such that $U_1 \cap U_2 \neq \varnothing$. This means that there is a subset of M that belongs both to the domains of ϕ_1 and ϕ_2. It is then necessary to be sure that such a subset is mapped equally, and this means to assure that $\phi_2 \circ \phi_1^{-1}$ and $\phi_1 \circ \phi_2^{-1}$ are homeomorphisms. For differentiable manifolds it is required that those compositions be actually C^k-diffeomorphisms, and we'll take $k = \infty$. The diagram below is, therefore, commutative.

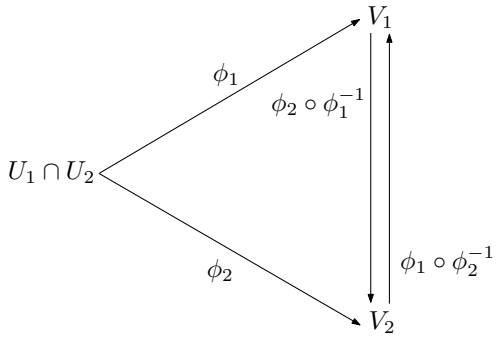

The compositions in the above diagram are called *transition functions* or *coordinate changes*.

Let us now come back to the topological space M. A Hausdorff space is said to be *second countable* if, roughly, it can be decomposed as a countable union of open sets. Let us assume this is the case. We then have $M \subseteq \bigcup_{i\in\mathbb{N}} U_i$, each U_i being an open set. By equipping each U_i with a homeomorphism ϕ_i, we are saying that each neighborhood of M is locally homeomorphic to a subset of an euclidean space. The collection of all (U_i, ϕ_i) is called an *atlas*, and of course there are many ways of covering M by open sets. Second countability, nevertheless, restricts the ways M can be covered, and we define the *maximal atlas* to be the atlas that contains all other atlases, $\mathcal{A} = \bigcup_{i\in\mathbb{N}}(U_i, \phi_i)$. Finally, we call the pair $(M, \mathcal{A})$ a *differentiable manifold* or simply *manifold*, in our context. If all the ϕ_i map on an euclidean space of dimension n, then the manifold M (we'll omit the atlas from now on) is said to be n-dimensional.

T_pM, that is, the *tangent space to M at p*, can now be defined. Pick a chart $x : U \to \mathbb{R}^n$ and let $\gamma : \mathbb{R} \supset I \to U \subseteq M$ be a curve such that $\gamma(0) = p$ and $x \circ \gamma$ is differentiable at p. Then $(x \circ \gamma)'(p)$ gives a tangent vector to M at p. There are clearly an infinity of curves that have the same derivative at p, and we form an equivalence class of such derivatives [Spi99]. T_pM is then defined as the space composed of all equivalence classes of derivatives of curves at p and easily proven to be a vector space with the same dimension as M [Spi99]. If x_i are the components of a local coordinate system at p, then

the associated basis of T_pM is proven to be $\frac{\partial}{\partial x_i}|_p$, and in this way vectors in T_pM can be obtained from curves in M, *i.e*, vectors can be seen as *operators* acting on the space of smooth functions over M. Naturally, as a vector space, T_pM has a dual space T_p^*M called *cotangent space to M at p*, whose dual basis is proven to be $dx_i(p)$. As we are considering only finite-dimensional manifolds, $T_pM \sim T_p^*M$. We can also define *tangent TM* and *cotangent bundles T^*M of M* as being the union of all tangent and cotangent spaces at all points in M.

Let $f : M \to N$ be a smooth (class C^∞) mapping from a manifold M to a manifold N. Taking $p \in M$ and $f(p) \in N$, a mapping $df_p : T_pM \to T_{f(p)}N$ is also induced by f and called its *pushforward* at p. What this function does is to associate a vector in T_pM to a vector in $T_{f(p)}N$: if $(x \circ \gamma)'(0)$ is a tangent vector to M at p in a coordinate system x, then $(y \circ f \circ \gamma)'(0)$ is a vector tangent to N at $f(p)$ in the coordinate system y (this definition is clearly coordinate free). The transpose of the pushforward is called *pullback*, and is a function $f_p^* : T_{f(p)}^*N \to T_p^*M$ defined by

$$(f^*\alpha)_p(X) = \alpha_{f(p)}(df_p(X))\,, \tag{A.1}$$

where α_p is a 1-form in T_p^*N and X is a vector in T_pN. Taking $\alpha_p \equiv d\beta_p$, then (A.1) becomes

$$(f^*d\beta)_p(X) = d\beta_{f(p)}(df_p(X)) = d(\beta \circ f)_p(X) \quad \Longleftrightarrow \quad f^*(d\beta) = d(\beta \circ f),$$

where we have omitted the point p and used the chain rule. This identification will be extensively used in this dissertation, and is easy to generalize to k-forms [Spi99].

A.2 Two lemmas involving Lie derivatives

Lemma A.2.1. (Cartan's magic formula) For the Lie derivative $\mathcal{L}_X$, we have $\mathcal{L}_X = d \circ \imath_X + \imath_X \circ d$.

Proof. Let $\omega =$ be a 1-form. Writting it using the basis dx and Einstein notation, we have $\omega = \omega_\mu dx^\mu$. Then,

$$\begin{aligned}
(d \circ i_X + i_X \circ d)\omega &= di_X\omega + i_X d\omega \\
&= d(X^\mu\omega_\mu) + i_X(\partial_\nu\omega_\mu dx^\nu \wedge dx^\mu) \\
&= dX^\mu\omega_\mu + X^\mu d\omega_\mu + \partial_\nu\omega_\mu(dx^\nu(X)dx^\mu - dx^\mu(X)dx^\nu) \\
&= (\partial_\nu X^\mu\omega_\mu + X^\mu\partial_\nu\omega_\mu)\, dx^\nu + (X^\mu\partial_\mu\omega_\nu - X^\mu\partial_\nu\omega_\mu)dx^\nu \\
&= (X^\mu\partial_\mu\omega_\nu + \omega_\mu\partial_\nu X^\mu)dx^\nu \\
&= \mathcal{L}_X\omega\,.
\end{aligned}$$

Since the Lie derivative is a derivation, this conclusion is valid for any k-form. We used 1-forms because dealing with a single index is easier. □

Lemma A.2.2. Let ρ_t be the flow of a hamiltonian H, interpreted as a 1-parameter group of diffeomorphisms. Then,

$$\frac{d}{dt}\rho_t^*\omega = \rho_t^*\mathcal{L}_{X_H}\omega\,.$$

Proof.

$$\begin{cases}
\dfrac{d}{dt}\rho_t^*\omega & = \lim_{\alpha\to 0}\left\{\dfrac{(\rho_{t+\alpha}^* - \rho_t^*)}{\alpha}\right\}\omega \\
\dfrac{d}{dt}\rho_t^*\omega\Big|_{t=0} & = \lim_{\alpha\to 0}\left\{\dfrac{(\rho_\alpha^*\omega - \omega)}{\alpha}\right\} = \mathcal{L}_{X_H}
\end{cases},$$

so

$$\frac{d}{dt}\rho_t^*\omega = \rho_t^*\frac{d}{dt}\rho_t^*\omega\Big|_{t=0} = \rho_t^*\mathcal{L}_{X_H}\,,$$

where we have used Lemma A.2.1. □

Bibliography

[Spi99] M. Spivak. *A Comprehensive Introduction to Differential Geometry, Vol. 1.* Publish or Perish, 3rd edition, 1999.

Appendix B

Linear symplectomorphisms

Linear movement is the simplest in nature. Since the flow forms a group with respect to time and arises from exponentiation, it forms a Lie group and a first order approximation to any flow is a matrix. This matrix naturally reflects several properties of the flow and, inverting this logic, presents also a way of identifying a symplectomorphism through its jacobian. We have already encountered the symplectic group $\mathrm{Sp}(n)$ in Chapter 1, and here prove some lemmas and introduce some concepts used in the main body of this dissertation about it.

B.1 Lemmas regarding Sp(n) group

Let the mapping $(q,p) \longmapsto (Q,P)$ be linear and represented by a matrix $\mathcal{M}$

$$X = \mathcal{M}x \quad \Longleftrightarrow \quad \begin{pmatrix} Q \\ P \end{pmatrix} = \mathcal{M} \begin{pmatrix} q \\ p \end{pmatrix}, \quad \mathcal{M} = \begin{pmatrix} A & B \\ C & D \end{pmatrix},$$

where the blocks A, B, C and D are in general functions of time. Naturally, $\mathcal{M}$ can be a function of anything *except* the initial points (q,p).

Lemma B.1.1. For a linear symplectomorphism, considered as a flow of a hamiltonian, there is only a single trajectory that connects arbitrary initial and final points x and X in a fixed time t.

Proof. Suppose $X = \mathcal{M}x_1 = \mathcal{M}x_2$. Then $X - X = \mathcal{M}x_1 - \mathcal{M}x_2 = \mathcal{M}(x_1 - x_2) = 0 \Longrightarrow x_1 = x_2$. □

Lemma B.1.2. Let $\mathcal{M} \in \mathrm{Sp}(n)$. Then

$$\mathcal{M} = \begin{pmatrix} A & B \\ C & D \end{pmatrix} \quad \Longrightarrow \quad \begin{cases} A^T C - C^T A = 0 \\ A^T D - C^T B = 1 \\ B^T C - D^T A = -1 \\ B^T D - D^T B = 0 \end{cases}.$$

Proof. Directly application of Proposition 1.2.4:

$$\mathcal{M}^T \mathcal{J} \mathcal{M} = \mathcal{J} \quad \Longleftrightarrow \quad \begin{pmatrix} A^T & C^T \\ B^T & D^T \end{pmatrix} \begin{pmatrix} 0 & 1 \\ -1 & 0 \end{pmatrix} \begin{pmatrix} A & B \\ C & D \end{pmatrix} = \begin{pmatrix} 0 & 1 \\ -1 & 0 \end{pmatrix}.$$

□

Lemma B.1.3. Every upper- and lower-triangular matrix is symplectic.

Proof. Again by direct application of Proposition 1.2.4, for any upper-triangular $\mathcal{A}$ we have

$$\mathcal{A} = \begin{pmatrix} I & L \\ 0 & I \end{pmatrix} \quad \Longrightarrow \quad \mathcal{A}^T \mathcal{J} \mathcal{A} = \begin{pmatrix} I & 0 \\ L & I \end{pmatrix} \begin{pmatrix} 0 & I \\ -I & 0 \end{pmatrix} \begin{pmatrix} I & L \\ 0 & I \end{pmatrix} = \begin{pmatrix} 0 & I \\ -I & 0 \end{pmatrix}.$$

The proof for lower-triangular matrices is identical. □

B.2 Position-position generating functions

As we saw in Section 1.4, there are infinite possible generating functions for $\mathcal{M} \in \mathrm{Sp}(n)$, depending on what variables we choose to represent it with. We will be mostly interested in obtaining closed expressions for the position-position generating function ("type 1 generation function" [GJS01]) $S_t^1(Q,q)$, and for the center and chord generating functions $S(\eta)$ and $\tilde{S}(\xi)$. Let us start with $S_t^1(Q,q)$. Writing the mapping in terms of initial and final momentum,

$$\begin{cases} Q = Aq + Bp \\ P = Cq + Dp \end{cases} \implies \begin{cases} p = B^{-1}Q - B^{-1}Aq \\ P = (C - DB^{-1}A)q + DB^{-1}Q \end{cases}, \tag{B.1}$$

but, from Lemma B.1.2, we have $B^T D = D^T B \implies (DB^{-1})^T = DB^{-1}$ and, using this symmetry,

$$A^T D - C^T B = 1 \implies A^T DB^{-1} - C^T = (B^{-1}) \implies (DB^{-1})^T A - C = (B^{-1})^T = DB^{-1}A - C\,;$$

Substituting in (B.1) and assuming $\mathcal{M}$ to be *free*, *i.e.* $\det B \neq 0$, then[1]

$$\begin{cases} p = B^{-1}Q - B^{-1}Aq \\ P = DB^{-1}Q - (B^{-1})^T q \end{cases},$$

and, as we saw in Section 1.4, we must have

$$\begin{aligned} \begin{cases} p = -\dfrac{\partial S_t^1(q,Q)}{\partial q} \\ P = \dfrac{\partial S_t^1(q,Q)}{\partial Q} \end{cases} &\implies \begin{cases} \dfrac{\partial S_t^1(q,Q)}{\partial q} = B^{-1}Aq - B^{-1}Q \\ \dfrac{\partial S_t^1(q,Q)}{\partial Q} = DB^{-1}Q - (B^{-1})^T q \end{cases} \\ &\implies S_t^1(q,Q) = \frac{Q\cdot(DB^{-1})Q}{2} + \frac{q\cdot(B^{-1}A)q}{2} - Q\cdot(B^{-1})^T q \\ &\qquad = \begin{pmatrix} q \\ Q \end{pmatrix} \cdot \begin{pmatrix} B^{-1}A & -B^{-1} \\ -(B^{-1})^T & DB^{-1} \end{pmatrix} \begin{pmatrix} q \\ Q \end{pmatrix}. \end{aligned}$$

We now prove an important lemma regarding the mixed derivatives of $S_t^1(q,Q)$.

Lemma B.2.1. Let

$$\mathcal{M} = \begin{pmatrix} A & B \\ C & D \end{pmatrix}$$

be a free symplectic matrix and

$$S_t^1(q,Q) = \begin{pmatrix} q \\ Q \end{pmatrix} \cdot \begin{pmatrix} \alpha & -\beta \\ -\beta & \gamma \end{pmatrix} \begin{pmatrix} q \\ Q \end{pmatrix}, \quad \text{where} \quad \alpha = B^{-1}A\,, \quad \beta = DB^{-1}\,, \quad \gamma = B^{-1}\,.$$

Then,

$$\det(\mathcal{M} - I) = (-1)^n \det\left(\gamma^{-1}\right) \det\left(\alpha + \beta - \gamma - \gamma^T\right)$$

.

Proof. Since $\det B \neq 0$ the block B is invertible and we can factorize $\mathcal{S} - I$ as

$$\begin{pmatrix} A - I & B \\ C & D - I \end{pmatrix} = \begin{pmatrix} 0 & B \\ I & D - I \end{pmatrix} \begin{pmatrix} C - (D-I)B^{-1}(A-I) & 0 \\ B^{-1}(A-I) & I \end{pmatrix};$$

hence,

$$\det(\mathcal{S} - I) = \det(-B)\det\left(C - (D-I)B^{-1}(A-I)\right) = (-1)^n \det B \det\left(C - (D-I)B^{-1}(A-I)\right).$$

Now, using $(B^{-1})^T = DB^{-1}A - C$,

$$C - (D-I)B^{-1}(A-I) = B^{-1}A + DB^{-1} - B^{-1} - (B^{-1})^T = \alpha + \beta - \gamma - \gamma^T\,,$$

and since $\gamma = B^{-1}$, the lemma follows. □

[1] This assumption is not restrictive because, since $\det \mathcal{M} \neq 0$, there will always be two blocks with non-vanishing determinants that we can use to parametrize $\mathcal{M}$. Every symplectic matrix can, therefore, be written as a product of at most two free matrices [dG06].

B.3 Center and chord generating functions

In the case of centers and chords, two particular matrix parametrizations occur very naturally – we can extract them directly from equations (1.19). Start with the general quadratic generating functions for linear symplectomorphisms

$$\begin{cases} S(\eta) &= \eta \cdot \mathcal{B}\eta \\ \widetilde{S}(\xi) &= \xi \cdot \widetilde{\mathcal{B}}\xi/4 \end{cases},$$

Using the chord equation in (1.19) and the quadratic form $S(\eta)$ above,

$$\begin{aligned} \xi &= -2\mathcal{J}\mathcal{B}\eta \\ \Leftrightarrow X - x &= -J\mathcal{B}\,(x+X) \\ \Leftrightarrow (I+J\mathcal{B})\,X &= (I-J\mathcal{B})\,x \\ \Rightarrow X &= (I+J\mathcal{B})^{-1}(I-J\mathcal{B})\,x\,; \end{aligned}$$

the same reasoning applied to the center equation in (1.19) leads to

$$X = -(I-J\widetilde{\mathcal{B}})^{-1}(I+J\widetilde{\mathcal{B}})x\,.$$

Since $X = \mathcal{M}x$, we have

$$\begin{aligned} \mathcal{M} &= (I+J\mathcal{B})^{-1}(I-J\mathcal{B})\,, \quad \text{for centers} \\ \mathcal{M} &= -(I-J\widetilde{\mathcal{B}})^{-1}(I+J\widetilde{\mathcal{B}})\,, \quad \text{for chords.} \end{aligned}$$

Solving the equations above for $\mathcal{B}$ and $\widetilde{\mathcal{B}}$ gives us the well-known Cayley parametrizations [Hel08]

$$\begin{cases} \mathcal{B} &= J\,(I+\mathcal{M})^{-1}(I-\mathcal{M}) \\ \widetilde{\mathcal{B}} &= J\,(\mathcal{M}-I)^{-1}(\mathcal{M}+I) \end{cases}. \tag{B.2}$$

B.4 Linear complexification

We now introduce a particular linear transformation that is not a symplectic, but can effectively be treated as if it were. It is an example of what is sometimes called *symplectomorphism with a multiplier*, where $\mathcal{M}^*\omega = \alpha\omega$, $\alpha \in \mathbb{C}^n$, whereas the definition of "pure" symplectomorphism has $\alpha = 1$.

We start by noticing that, by considering the symplectomorphism $\mathcal{M}_t$ to have emerged as the flow associated to a hamiltonian function $H(x)$, the linearity of the flow implies that the hamiltonian is a quadratic form:

$$H(x) = x \cdot \mathcal{A}x \quad \Longrightarrow \quad \dot{x} = Ax \quad \Longrightarrow \quad \rho_t(x_0) = \mathcal{M}_t x_0\,, \quad \mathcal{M}_t = \exp(t\mathcal{A})\,.$$

We now proceed to the

Definition B.4.1. The transformation

$$\begin{aligned} &\mathcal{C} : \mathbb{R}^{2n} \longrightarrow \mathbb{C}^{2n} \\ &\begin{pmatrix} q \\ p \end{pmatrix} \longmapsto \begin{pmatrix} z \\ z^* \end{pmatrix} = \frac{1}{\sqrt{2}} \begin{pmatrix} p - iq \\ p + iq \end{pmatrix} = \frac{1}{\sqrt{2}} \begin{pmatrix} -iI_{n\times n} & I_{n\times n} \\ iI_{n\times n} & I_{n\times n} \end{pmatrix} \begin{pmatrix} q \\ p \end{pmatrix} \end{aligned}$$

is the **linear complexification** of phase-space variables.

It is easy to see the transformation above is a symplectomorphism with multiplier $-i$:

$$\mathcal{C}^T\mathcal{J}\mathcal{C} = \frac{1}{2}\begin{pmatrix} -iI & iI \\ I & I \end{pmatrix}\begin{pmatrix} 0 & I \\ -I & 0 \end{pmatrix}\begin{pmatrix} -iI & I \\ iI & I \end{pmatrix} = \frac{1}{2}\begin{pmatrix} -iI & -iI \\ -I & I \end{pmatrix}\begin{pmatrix} -iI & I \\ iI & I \end{pmatrix} = \begin{pmatrix} 0 & -iI \\ iI & 0 \end{pmatrix} = -i\mathcal{J}\,,$$

so that the transformed canonical form is given by $dq \wedge dp = (C^*)^{-1}(-idz^* \wedge dz)$. We also have

$$\frac{\partial}{\partial z} = \frac{1}{\sqrt{2}}\left(\frac{\partial}{\partial p} + i\frac{\partial}{\partial q}\right), \quad \frac{\partial}{\partial z^*} = \frac{1}{\sqrt{2}}\left(\frac{\partial}{\partial p} - i\frac{\partial}{\partial q}\right),$$

where the signs are exchanged in order for $\partial_z z = \partial_{z^*} z^* = I$. Therefore, from (1.3),

$$\begin{cases} \dot{q} = \dfrac{\partial H(q,p)}{\partial p} \\ \dot{p} = -\dfrac{\partial H(q,p)}{\partial q} \end{cases} \implies \begin{cases} \dfrac{d}{dt}\left(\dfrac{p - iq}{\sqrt{2}}\right) = \dfrac{-i}{\sqrt{2}}\left(\dfrac{\partial}{\partial p} - i\dfrac{\partial}{\partial q}\right) H(q,p) \\ \dfrac{d}{dt}\left(\dfrac{p + iq}{\sqrt{2}}\right) = \dfrac{i}{\sqrt{2}}\left(\dfrac{\partial}{\partial p} + i\dfrac{\partial}{\partial q}\right) H(q,p) \end{cases} \iff \begin{cases} \dot{z} = -i\left(\dfrac{\partial H(z,z^*)}{\partial z^*}\right) \\ \dot{z}^* = i\left(\dfrac{\partial H(z,z^*)}{\partial z}\right) \end{cases},$$

which are the complexified form of Hamilton's equations, abbreviated as $\dot{Z} = -i\mathcal{J}dH(Z)/dZ$, with $Z \in \mathbb{C}^{2n}$. Notice this form is completely general and not at all restricted to quadratic hamiltonians, but the SHO acquires a particularly simple expression when complexified: It just $|z|^2$. It's also worthwhile mentioning that any mapping that goes from $\mathbb{R}^{2n}$ to $\mathbb{C}^{2n}$ is at most an immersion, since $\mathbb{R}^{2n} \sim \mathbb{C}^n$. This means that we can perform all calculations in some complex coordinates u and v as if there were independent, but the underlying structure fixes $v = u^*$.

Bibliography

[dG06] M. de Gosson. *Symplectic Geometry and Quantum Mechanics*. Birkhauser, 2006.

[GJS01] H. Goldstein, C. P. Poole Jr, and J. L. Safko. *Classical Mechanics*. Addison-Wesley, 3rd edition, 2001.

[Hel08] G. Helmberg. *Introduction to Spectral Theory in Hilbert Space*. Dover, 2008.

Appendix C

An extended discussion on quantum theory

Quantum mechanics was borne out of several experimental facts that departed strongly from the behavior predicted by classical mechanics. Suddenly, the outcome of measurements of several systems prepared in the same initial state could not be generally predicted and behaved stochastically. A description in terms of a probabilistic theory was then necessary where the focus was shifted from predicting an experimental outcome to establishing the probability of its occurrence. The dominant interpretation of the theory also implies that physical properties do not really have fixed values until they're measured, the whole system magically collapsing to a single state. As could be fathomed from experiment, measurements were also not generally commutative, so that observable variables could not be described by functions over manifolds. Somehow, though, everything needs to approach classical theory as the system's size is increased, meaning that the failure to commute should be a function of a very small parameter with respect to the classical world. A description in terms of two entities $\hat{A}$ and $\hat{B}$ associated to two separate measurements should therefore fail to commute proportionally to a small constant $\hbar$:

$$\hat{A}\hat{B} - \hat{B}\hat{A} = [\hat{A}, \hat{B}] \propto \hbar \,.$$

Since the hamiltonian fields associated to position and momentum do not commute, a clear analogy with classical variables emerges:

$$[X_q, X_p] = \{q, p\} = 1 \quad ,$$

This is a fundamental connection between classical and quantum mechanics and is the starting point of most *quantization* procedures, which are recipes for associating classical systems to their quantum equivalents. Notice that, since all $f \in C^\infty(X)$ are commutative for any X, it is very natural to associate $\hat{A}$ and $\hat{B}$ with *operators* acting on a particular space. Obviously, these do not need to have a faithful matrix representation, but one is sure to exist at least for the finite-dimensional case.

C.1 Finite quantum mechanics

Quantum evolution is governed by linear differential equations. This is the source of the most striking differences between classical and quantum motion, since it is this linearity that allows for state superposition and quantum interference and, simultaneously, makes quantum chaos impossible. While the mathematics of classical mechanics were rather simple but the dynamical behavior was generally quite complex due to non-linearities, the mathematical background of quantum mechanics is more involved but the output dynamics is unexpectedly simpler than its classical counterpart.

Mathematical background

Having established that quantum observables must be non-commutative, a further aspect that should be considered is: Since our observables are now described by operators instead of functions, what do

we effectively measure in the lab? We start by noticing that the number of possible outputs associated to an operator must be invariant with dimension: A measurement with n outcomes must be associated to an operator with n possible outputs. Thus, n needs to be described by an invariant and the only invariant in the vector-space category is dimension. A measurement experimentally associated with n possible outputs is then postulated to be described by an operator acting on $\mathbb{R}^n$ and belonging to $\mathbb{R}^{n\times n}$. Also, systems can be prepared in several different states and these provide different sets of measurements for the same operator, thus the operators' domain needs to be the space of initial states – which, by the earlier reasoning, should be n-dimensional. Mathematically, one has this set of initial *kets* $\{|\psi_{i\leq n}\rangle\}$, and some operator $\hat{U}$ that acts on it. For $n<\infty$ the operator $\hat{U}$ has a faithful matrix representation and $|\psi_i\rangle\in V$, with $\dim(V)=n$, and $\mathrm{Mat}(n)\ni\hat{U}:V\longrightarrow V$.

What information do we extract from $\hat{U}$ when we measure it? If $\hat{U}$ is expected to describe an event with n possible outcomes, there must be n scalar quantities associated to it. The only guaranteed quantity to satisfy this requisite are the eigenvalues of $\hat{U}$. If we denote the set of eigenvectors of $\hat{U}$ by $\{|u_{i\leq n}\rangle\}$ with *distinct* eigenvalues $u_{i\leq n}$, we can always decompose any $|\psi\rangle$ as

$$|\psi\rangle=\sum_{i\leq n}c_i|u_i\rangle\,,\quad\text{where}\quad\hat{U}|u_i\rangle=u_i|u_i\rangle\,.$$

The simples way to force the eigenvectors of $\hat{U}$ to be always capable of forming a basis is to force $\hat{U}$ to be self-adjoint[1], so from now on we know $\hat{U}^\dagger=\hat{U}$.

Being a vector space, the space of kets V is isomorphic to its dual V^* and there is a unique *bra* $V^*\ni\langle\psi|:V\longrightarrow\mathbb{R}$ such that $\langle\psi|\psi\rangle=|\psi|^2$, where the action of an linear functional over V is naturally described in terms of the induced conjugate-symmetric inner-product in $V\times V$ defined as

$$\begin{aligned}(\,,\,):V\times V&\longrightarrow\mathbb{R}\\(|\psi\rangle,|\phi\rangle)&\longmapsto(\psi,\phi)=\langle\psi|\phi\rangle=(\langle\phi|\psi\rangle)^*\,,\end{aligned}$$

such that, choosing a basis $\{|a_i\rangle\}$ for $|\psi\rangle$ and $|\phi\rangle$, we have

$$\left(\sum_{i\leq n}c_i|a_i\rangle,\sum_{j\leq n}d_j|a_j\rangle\right)=\sum_{i\leq n}c_id_i^*\,.$$

Therefore, we can take $\{|u_{i\leq n}\rangle\}$ to be normalized and write

$$\hat{U}|\psi\rangle=\sum_{i\leq n}c_iu_i|u_i\rangle\quad\Longrightarrow\quad(\psi,U\psi)=(\hat{U}^\dagger\psi,\psi)=\langle\psi|\hat{U}|\psi\rangle=\langle\psi|\hat{U}^\dagger|\psi\rangle=\sum_{i\leq n}u_i|c_i|^2\,.$$

Notice that if $\hat{U}=\hat{I}$ we recover the invariant norm of $|\psi\rangle$, but otherwise we obtain information of $\hat{U}$ through its eigenvalues using the inner product above. Indeed, we obtain *all* information we want from $\hat{U}$, so it makes sense to identify eigenvalues as measurement outcomes and the inner products as measurements themselves. These inner products, however, have the exact form of a mean value of u_i with probability density function $|c_i|^2$ as long as we fix

$$\langle\psi|\psi\rangle=\sum_{i\leq n}|c_i|^2=1\,,$$

so that c_i represent amplitudes and a probabilistic component is naturally introduced in the theory by imposing normalization. This is the first restriction we place on the space of states V, from which we take only the subset of all normalized states. The dimension is the only vector space invariant and the subspace of normalizable vectors of V would at first glance appear isomorphic to V, but this is

[1]The fact that $\hat{U}$ must be self-adjoint was fixed much earlier by postulating that it should always have n linearly independent eigenvectors associated to n different eigenvalues so that they can be used as a basis for V – self-adjoint operators are guaranteed to fulfill this requisite. Strictly speaking, however, self-adjointness is sufficient but not necessary, and formulations of quantum mechanics in terms of PT-symmetric operators have attained a considerable degree os success in the past years. In fact, some measurements that appear in quantum optics can only be described in terms of PT-symmetric operators [BBJ03].

not true: the zero vector is not normalizable. Our final space is, therefore, not isomorphic to V, but to the projectivization[2]

$$\mathbb{P}(V) = \{[x] \in V/\{0\} : x,\, y \in [x] \iff x = \alpha y\}\,.$$

The equivalence relation is naturally required by state vectors due to the normalization requisite, from which the factor α can be easily obtained:

$$|\psi|^2 = 1 \quad \iff \quad |\alpha|^2|\psi|^2 = 1 \quad \implies \quad |\alpha|^2 = 1 \quad \implies \quad \alpha = e^{is}\,, \quad s \in \mathbb{R}\,,$$

which is just a global phase factor.

The Schrödiger picture

Let us now consider the operators associated to time-evolution, which we shall call $\hat{U}_t : \mathbb{R} \times \mathbb{P}(V) \longrightarrow \mathbb{P}(V)$. Their action is taking an initial state $|\psi_0\rangle$ to the final state $|\psi_t\rangle = \hat{U}_t|\psi_0\rangle$. We don't know how $\hat{U}_t$ depends on time yet. Suppose, however, that we take one of its eigenvectors:

$$\hat{U}_t|\lambda\rangle = \lambda|\lambda\rangle \quad \implies \quad \langle\lambda|\hat{U}_t^\dagger\hat{U}_t|\lambda\rangle = |\lambda|^2\langle\lambda|\lambda\rangle = |\lambda|^2 = 1\,,$$

since we must have $|\lambda\rangle \in \mathbb{P}(V)$. This amounts to evolving an initial state that is stationary under the action of $\hat{U}_t$, from which we obviously expect that the measured quantities λ and their probability distribution does not change. We then immediately have $\hat{U}_t \in U(n)$ and the quite obvious

Proposition C.1.1. For unitary the operator $\hat{U}_t \in U(n)$, we have

$$\text{i)} \quad \hat{U}_{t_1+t_2} = \hat{U}_{t_1}\hat{U}_{t_2} = \hat{U}_{t_2}\hat{U}_{t_1}$$
$$\text{ii)} \quad \hat{U}_{t_1}^\dagger = \hat{U}_{-t_1}\,.$$

Proof. To prove i):

$$\hat{U}_{t_1}|\psi_0\rangle = |\psi_{t_1}\rangle \quad \iff \quad \hat{U}_{t_2}\hat{U}_{t_1}|\psi_0\rangle = \hat{U}_{t_2}|\psi_{t_1}\rangle = |\psi_{t_1+t_2}\rangle = \hat{U}_{t_1+t_2}|\psi_0\rangle = \hat{U}_{t_2+t_1}|\psi_0\rangle$$

The statement in ii) is trivially proved by substituting $t_2 = -t_1$. □

What we have shown is that the evolution operators $\hat{U}_t$ form a unitary, one-parameter group that acts on the complex projective space $\mathbb{P}(V)$. We now completely characterize such operators by means of a very simple representation lemma found ubiquitously in Lie group theory.

Proposition C.1.2. Every unitary operator $\hat{U}_t \in U(n)$ depending smoothly on t admits a unique representation in terms of the exponential of an associated self-adjoint operator $\hat{K}$, given by

$$\hat{U}_t = \exp(-it\alpha\hat{K})\,. \tag{C.1}$$

Proof. Smooth dependence on t is fundamental for time-propagation to be continuous – the unitary operators considered do not form only a group, but a Lie group. This implies, of course, that $\hat{U}_t$ can be expanded as a Taylor series in t:

$$\hat{U}_t = I - \left.\frac{d\hat{U}_t}{dt}\right|_{t=0} t + \mathcal{O}(t^2) \quad \iff \quad \hat{U}_t^\dagger\hat{U} = I - t\left[\frac{d\hat{U}_t}{dt} + \frac{d\hat{U}_t^\dagger}{dt}\right]_{t=0} + \mathcal{O}(t^2)\,, \tag{C.2}$$

but since $\hat{U}_t^\dagger\hat{U}_t = \hat{I}$, the $\mathcal{O}(t)$ term must vanish. The adoption

$$\frac{d\hat{U}_t}{dt} \stackrel{\text{def}}{=} -i\alpha\hat{K}\,, \quad \hat{K} = \hat{K}^\dagger\,, \quad \alpha \in \mathbb{R}\,, \tag{C.3}$$

[2]The projectivization of an n-dimensional vector space is isomorphic to the complex projective space $\mathbb{CP}^{n-1}$. The space $\mathbb{CP}^1$, for example, is known in physics literature as the *Bloch sphere*.

clearly cancels the term inside square brackets in (C.2). Take now property i) in Proposition C.1.1 and differentiate it with respect to t_2:

$$\hat{U}_{t_1+t_2} = \hat{U}_{t_1}\hat{U}_{t_2} \quad \Longleftrightarrow \quad \left.\frac{\partial \hat{U}_{t_1+t_2}}{\partial t_2}\right|_{t_2=0} = \hat{U}_{t_1}\left(\frac{\partial \hat{U}_{t_2}}{\partial t_2}\right)_{t_2=0} = -i\alpha\hat{K}\hat{U}_{t_1} \quad \Longleftrightarrow \quad \left.\frac{\partial \hat{U}_t}{\partial t}\right|_{t=t_1} = -i\alpha\hat{K}\hat{U}_{t_1}\,,$$

where we have employed (C.3). The group condition forces $\hat{U}(0) = \hat{I}$, so that the equation above has the unique solution given in (C.1). The operator $\hat{K}$ is called the *generator* of the family $\hat{U}_t$. □

We can then employ the exponential form of $\hat{U}_t$ and write

$$\hat{U}_t = \exp(-i\alpha t\hat{H}) \quad \Longrightarrow \quad \left(\frac{d\hat{U}_t}{dt}\right)|\psi_0\rangle = \frac{\partial|\psi_t\rangle}{\partial t} \quad \Longleftrightarrow \quad -i\alpha\hat{H}|\psi_t\rangle = \frac{\partial|\psi_t\rangle}{\partial t}\,.$$

This is a linear, first order partial differential equation in $|\psi_t\rangle$, so that

$$\frac{i}{\alpha}\frac{\partial|\psi_t\rangle}{\partial t} = \hat{H}|\psi_t\rangle\,, \qquad |\psi_t\rangle = \exp(-i\alpha\, t\hat{H})|\psi_0\rangle\,. \tag{C.4}$$

We now collect some results obtained previously. As stated in the introduction, observables do not commute by a factor proportional to a small quantity, which we called $\hbar$. We now know, however, that quantum theory should be described by self-adjoint operators, such that the commutator presented in the introduction should therefore be expanded to

$$[\hat{A},\hat{B}] \propto \hbar \quad \longmapsto \quad [\hat{A},\hat{B}] = \hbar\,\hat{C}\,, \tag{C.5}$$

since the product of operators is a new operator. We also absorb any multiplication constants into $\hbar$ in order to write an equality. We run into the no-go

Proposition C.1.3. The operator $\hat{C}$ in (C.5) is not self-adjoint.

Proof. Self-adjointness of $\hat{C}$ would imply $[\hat{A},\hat{B}]^\dagger = \hbar\,\hat{C}^\dagger$, but

$$[\hat{A},\hat{B}]^\dagger = \left(\hat{A}\hat{B} - \hat{B}\hat{A}\right)^\dagger = \hat{B}^\dagger\hat{A}^\dagger - \hat{A}^\dagger\hat{B}^\dagger = \hat{B}\hat{A} - \hat{A}\hat{B} = -[\hat{A},\hat{B}] \propto -\hbar\,\hat{C} \neq \hbar\hat{C}^\dagger$$

□

Corollary C.1.4. The substitution $\hat{C} \longmapsto i\hat{C}$ solves the self-adjointness problem.

Proof.

$$\begin{aligned} [\hat{A},\hat{B}] = i\hbar\,\hat{C} \quad &\Longleftrightarrow \quad [\hat{A},\hat{B}]^\dagger = -i\hbar\,\hat{C}^\dagger \\ \hat{A}\hat{B} - \hat{B}\hat{A} = i\hbar\hat{C} \quad &\Longleftrightarrow \quad \hat{B}\hat{A} - \hat{A}\hat{B} = -i\hbar\hat{C} \end{aligned}$$

so that everything fits for $\hat{C} = \hat{C}^\dagger$. □

Due to the corollary above, we subsequently modify (C.5) to

$$[\hat{A},\hat{B}] = i\hbar\hat{C}\,, \tag{C.6}$$

guaranteeing that the operator ring is closed with respect to conjugate-transposition. Interestingly, this commutation relation is deeply connected to the standard deviation of general observables. To see this we start by defining the operator $\hat{A}' = \hat{A} - \langle\hat{A}\rangle_\psi\hat{I}$, identified with the standard deviation by

$$\langle\hat{A}'\rangle_\psi = \langle\psi|\hat{A} - \langle\hat{A}\rangle_\psi\hat{I}|\psi\rangle = \langle\hat{A}\rangle_\psi - \langle\hat{A}\rangle_\psi^2 = \sigma_\psi^2(\hat{A})\,.$$

By the Schwartz inequality,

$$\sigma_\psi^2(\hat{A})\,\sigma_\psi^2(\hat{B}) = |\langle\psi|\hat{A}'|\psi\rangle||\langle\psi|\hat{B}'|\psi\rangle| \geq |\langle\psi|\hat{A}'\hat{B}'|\psi\rangle|^2$$
$$\geq \left|\Im\left(\langle\psi|\hat{A}'\hat{B}'|\psi\rangle\right)\right|^2 = \frac{1}{4}|\langle\psi|\hat{A}'\hat{B}'|\psi\rangle - \langle\psi|\hat{B}'\hat{A}'|\psi\rangle|^2\,,$$
$$\implies \quad \sigma_\psi^2(\hat{A})\,\sigma_\psi^2(\hat{B}) \geq \frac{|\langle\psi|[\hat{A}',\hat{B}']|\psi\rangle|^2}{4}\,.$$

But

$$[\hat{A}',\hat{B}'] = (\hat{A} - \langle\hat{A}\rangle_\psi\hat{I})(\hat{B} - \langle\hat{B}\rangle_\psi\hat{I}) - (\hat{B} - \langle\hat{B}\rangle_\psi\hat{I})(\hat{A} - \langle\hat{A}\rangle_\psi\hat{I}) = [\hat{A},\hat{B}] = i\hbar\hat{C}\,,$$

where we employed (C.6). Therefore:

$$\sigma_\psi(\hat{A})\,\sigma_\psi(\hat{B}) \geq \frac{\hbar}{2}|\langle\sigma_\psi(\hat{C})\rangle|\,,$$

The inequality in (C.6) is the well-known *Heisenberg's uncertainty principle*. It states that, in quantum mechanics, there are variables which we simply cannot measure at the same time, since the better we know the value of the observable $\hat{A}$ the less we know the value of $\hat{B}$. This happens exactly when the commutator of $\hat{A}$ and $\hat{B}$ does not vanish, otherwise there is no problem in obtaining a complete and simultaneous knowledge of them. Non-commuting variables are often called *conjugate*.

One missing piece remains: What is α in (C.4)? Start by writing the commutator of an arbitrary operator $\hat{W}$ conjugate to $\hat{H}$,

$$[\hat{W},\hat{H}] = i\hbar\hat{Z}\,.$$

Since

$$\frac{i}{\alpha}\frac{\partial|\psi\rangle}{\partial t} - \hat{H}|\psi\rangle = 0 \quad\iff\quad \left(\frac{i}{\alpha}\frac{\partial}{\partial t} - \hat{H}\right)|\psi\rangle = 0 \quad\implies\quad \hat{H} = \frac{i}{\alpha}\frac{\partial}{\partial t},$$

we have

$$[\hat{W},\hat{H}] = i\hbar\hat{Z} \quad\iff\quad \left[\hat{W},\frac{i}{\alpha}\frac{\partial}{\partial t}\right]|\psi\rangle = i\hbar\hat{Z}|\psi\rangle \quad\iff\quad \left[\frac{1}{\alpha}\frac{\partial\hat{W}}{\partial t} - \hbar\hat{Z}\right] = 0$$

strongly suggesting that $\alpha = 1/\hbar$ by dimensional considerations. Then, (C.4) becomes the *Schrödinger equation*

$$i\hbar\frac{\partial|\psi_t\rangle}{\partial t} = \hat{H}|\psi_t\rangle\,, \quad \hat{H} = \hat{H}^\dagger\,, \quad |\psi_{t\in\mathbb{R}}\rangle \in \mathbb{P}(V)\,,$$

with solution [for time-independent hamiltonian operators]

$$U(n) \ni \hat{U}_t : \mathbb{R}\times\mathbb{P}(V) \longrightarrow \mathbb{P}(V)$$
$$|\psi_t\rangle \longmapsto \hat{U}_t|\psi_0\rangle = \exp\left(-\frac{it\hat{H}}{\hbar}\right)|\psi_0\rangle\,.$$

The Heisenberg picture

The Heisenberg picture of quantum mechanics can be easily derived from Schrödinger's by placing time-dependence on the operators instead of on the kets. The expectation value of some observable $\hat{A}$ calculated in a state $|\psi_t\rangle$ in the Schrödinger representation,

$$\langle\hat{A}\rangle_{\psi_t} = \langle\psi_t|\hat{A}|\psi_t\rangle\,,$$

with its time-dependence expressed explicitly, reads

$$|\psi_t\rangle = \hat{U}_t|\psi_0\rangle \quad\implies\quad \langle\hat{A}\rangle_{\psi_t} = \langle\psi_0|\hat{U}_t^\dagger\hat{A}\hat{U}_t|\psi_0\rangle\,,$$

implying that operators evolve as

$$\hat{A}_t = \hat{U}_t^\dagger \hat{A} \hat{U}_t \,. \tag{C.7}$$

We can proceed to obtain an evolution law based on the derivative of the above with respect to time:

$$\begin{aligned}
\frac{d\hat{A}_t}{dt} &= \left(\frac{d\hat{U}_t^\dagger}{dt}\right)\hat{A}\hat{U}_t + \hat{U}_t^\dagger\left(\frac{\partial\hat{A}}{\partial t}\right)\hat{U}_t + \hat{U}_t^\dagger\hat{A}\left(\frac{d\hat{U}_t}{dt}\right) \\
&= \left(\frac{i\hat{H}_t}{\hbar}\right)\hat{U}_t^\dagger\hat{A}\hat{U}_t + \hat{U}_t^\dagger\left(\frac{\partial\hat{A}}{\partial t}\right)\hat{U}_t - \hat{U}_t^\dagger\hat{A}\hat{U}_t\left(\frac{i\hat{H}_t}{\hbar}\right) \\
&= \left(\frac{i}{\hbar}\right)\hat{U}_t^\dagger\hat{H}_t\hat{U}_t\hat{U}_t^\dagger\hat{A}\hat{U}_t - \hat{U}_t^\dagger\hat{A}\hat{U}_t\hat{U}_t^\dagger\hat{H}_t\hat{U}_t\left(\frac{i}{\hbar}\right) + \hat{U}_t^\dagger\left(\frac{\partial\hat{A}}{\partial t}\right)\hat{U}_t \\
&= \frac{i}{\hbar}[\hat{H}_t, \hat{A}_t] + \frac{\partial\hat{A}}{\partial t}\,,
\end{aligned}$$

where we have employed the evolution operator expressed in terms of is Hermitian generator. For a hamiltonian operator that is not a function of time, we have the [time-independent] **Heisenberg's equation**

$$-i\hbar\left(\frac{d\hat{A}_t}{dt}\right) = [\hat{H}, \hat{A}_t]\,.$$

Notice how Heisenberg's equation is similar to the Liouville equation 1.6, implying the naïve *canonical quantization* procedure that associates classical observables to quantum operators by

$$\begin{cases} f & \longmapsto & \hat{f} \\ \{\cdot,\cdot\} & \longmapsto & \dfrac{1}{i\hbar}[\cdot,\cdot] \end{cases}.$$

A special type of operators, called *projectors*, can be expressed in terms of arbitrary bras and kets: If $|\psi\rangle \in V$ and $\langle\psi| \in V^*$, the dyadic product $|\psi\rangle\langle\psi|$ acts on the left as $V \longrightarrow V$ and on the right as $V^* \longrightarrow V^*$. It clearly provides a complete characterization of $|\psi\rangle$. Since projectors in the Schödinger picture evolve as

$$\hat{\beta} = |\psi_t\rangle\langle\psi_t| = \hat{U}_t|\psi_0\rangle\langle\psi_0|\hat{U}_t^\dagger\,,$$

that is, *backwards* when compared to Heisenberg evolution (C.7), time-differentiation easily results in the dynamical equation

$$i\hbar\left(\frac{\partial\hat{\beta}}{\partial t}\right) = [\hat{H}, \hat{\beta}]\,,$$

which is the *von Neumann equation*. Its most important use is related to the projector

$$\hat{\varrho} = |\Psi\rangle\langle\Psi| = \sum_{i\in\mathbb{N}} |\lambda_i|^2 |\psi_i\rangle\langle\psi_i|\,, \quad |\psi_i\rangle \in V\,, \quad \sum_{i\in\mathbb{N}} |\lambda_i|^2 = 1\,, \quad \langle\psi_i|\psi_j\rangle = \delta_{ij}\,,$$

where $|\Psi\rangle$ is used in order to imply that our system is entirely characterized by this state vector. The projector $\hat{\varrho}$ is known as the *density operator*. It is easy to see that the unitarity of $|\Psi\rangle$ implies $\hat{\varrho}^2 = \hat{\varrho}$, and that the expectation value of an operator is expressed quite succinctly as

$$\langle\Psi|\hat{A}|\Psi\rangle = \sum_{i\in\mathbb{N}} |\lambda_i|^2 \langle\psi_i|\hat{A}|\psi_i\rangle = \mathrm{tr}\left(\sum_{i\in\mathbb{N}} |\lambda_i|^2 |\psi_i\rangle\langle\psi_i|\hat{A}\right) = \mathrm{tr}(\hat{\varrho}\hat{A})\,.$$

By using projectors we can also write any self-adjoint operator in a specific form called its *spectral decomposition*, which is much more general than bras and kets [Mor16, Hel08]. For this, let $\{|a_{i\leq n}\rangle\}$

and $\{a_{i\leq n}\}$ be the eigenvectors and eigenvalues of $\hat{A}$, respectively. Then, since the set of eigenvectors is linearly independent, we have

$$|a_i\rangle\langle a_j| = \hat{I}\delta_{ij} \quad \Longrightarrow \sum_{i\leq n} |a_i\rangle\langle a_i| = \hat{I}\,.$$

This implies

$$\hat{A}\left(\sum_{i\leq n} |a_i\rangle\langle a_i| = \hat{I}\right) \quad \Longrightarrow \quad \sum_{i\leq n} a_i|a_i\rangle\langle a_i| = \hat{A}\,.$$

The name "spectral decomposition" clearly stems in the fact that we are representing an operator as a function of its spectrum, defined in the finite-dimensional case as the set of points $\{s_{i\leq n}\}$ for which $\det(\hat{A} - s_i\hat{I}) = 0$, coinciding with the eigenvalues of $\hat{A}$. A function of an operator is then defined as

$$f(\hat{A}) = \sum_{i\leq n} f(a_i)|a_i\rangle\langle a_i|\,, \quad f \in C^\infty(\mathbb{C}^n)\,.$$

C.2 Transitioning to function spaces

Let $|\psi\rangle \in V$. There is no name for a vector such that $|\psi|^2 < \infty$, since this is never false. However, if $n = \infty$ the whole field of functional analysis is proof that the matter becomes much more intricate. Infinite-dimensional quantum mechanics is, however, everything we are actually concerned about in this thesis, so we spare some time to enumerate some details.

Mathematical background

In order to extend the interpretation developed for the finite to the infinite case, several subtleties need to be accounted for. To make sense of the probabilistic component of the theory, for instance, quantum mechanics requires the huge simplification provided by Hilbert spaces, which are complete vector spaces $\mathfrak{H}$ equipped with an inner product-induced norm. There was no need to mention such special spaces earlier, since every finite-dimensional vector space is a Hilbert space, but in infinite dimensional theory these are a major simplification when compared to general Banach spaces:

1. An infinite-dimensional basis of orthogonal vectors exists is normalizable by Gram-Schmidt ([BPT15], theorem 5.3.10);
2. For separable[3] $\mathfrak{H}$, the orthonormal bases are countable ([BPT15], theorem 5.4.3);
3. Separable Hilbert space $\mathfrak{H}$ is reflexive, *i.e.* they are isomorphic to their dual $\mathfrak{H}^*$ ([Hel08], theorem 10.1);
4. Every element in $\mathfrak{H}^*$ can be uniquely written as an inner-product contraction (Riesz representation's theorem, item (c) of theorem 10.1 in [Hel08]);

and others. Since this is intermediate functional analysis material, the proofs involve several auxiliary lemmas and theorems such as Banach-Steinhaus' and closed graph's, so we refer to [BPT15, Hel08] for proofs. The main point here is that infinite dimensional Hilbert spaces are as close as one can get from finite-dimensional behavior. The most important Hilbert space in quantum theory (actually, pretty much the only) emerges due to our need to interpret the norm $|f|^2$ as a continuous probability density function. We then draw the analogy

$$\left(\sum_{i\leq n} |f|^2 = 1\right) \longmapsto \left(\int_A d\mu(x)|f(x)|^2 = 1\right)\,,$$

[3] A space is separable if it contains a countable dense subset, *e.g.* $\mathbb{R}$ is separable because $\mathbb{Q}$ is dense in $\mathbb{R}$. All spaces in this thesis are separable.

together with

$$\left((\psi,\phi)=\langle\psi|\phi\rangle=\sum_{i\leq n}a_i b_i^*\right)\longmapsto\left((f,g)=\langle f|g\rangle=\int_A d\mu(x)f(x)g^*(x)\right). \tag{C.8}$$

The inner product on the right hand side of the equation above is ubiquitous in functional analysis. We then define the *space of absolutely square integrable functions*

$$\mathfrak{L}_2(A)=\left\{f\in C^\infty(A):\int_A dx\,|f(x)|^2<\infty\right\},$$

where dx is the n-dimensional Lebesgue measure over A, which should also be substituted in the inner product in (C.8). It is standard in measure theory courses to prove that $\mathfrak{L}_2$, with inner product in (C.8), is a Hilbert space (it is the *only* $\mathfrak{L}_p$ to be so) [Bar95, BPT15]. We then have all prerequisites needed to interpreted the absolute value squared as a probability distribution on an infinite-dimensional Hilbert space. The domain A we will be most interested in is the particularly problematic $\mathbb{R}^n$, and we also bring back the fact that we need to exclude non-normalizable functions from $\mathfrak{L}_2(\mathbb{R}^n)$ and employ the same equivalence classes as used in the finite-dimensional case – this leaves us with the *projective Hilbert space of absolutely square integrable functions*

$$\mathbb{P}[\mathfrak{L}_2(\mathbb{R}^n)]=\{[f]\in\mathfrak{L}_2(\mathbb{R}^n)/\{0\}:f\sim g\iff f=e^{is}g\quad\text{almost everywhere}\},$$

which we shall refer to simply as $\mathfrak{H}$.

Now that we are free to pick infinite-dimensional operators, we would like to keep using Dirac's elegant notation also in the infinite dimensional case, since it beautifully allows us to ignore all the mathematical difficulties involved in quantum mechanics and confuses us into believing everything is alright. However, to employ *e.g.* the position representation as is it is used in physics, which for a single degree of freedom reads

$$\langle q|\hat{q}|f\rangle=q\langle q|f\rangle\,,\quad\langle q|\hat{p}|f\rangle=-i\hbar\,d_q\langle q|f\rangle\quad\iff\quad\hat{q}f(q)=qf(q)\,,\quad\hat{p}f(q)=-i\hbar f'(q)\,,$$

we immediately run into a very obvious problem: Can we guarantee $f(q)\in\mathfrak{H}$ after the application of $\hat{q}$? We clearly can't, since the fact that $f(q)$ is square integrable does not imply that $qf(q)$ is also square integrable. We must then define a domain $\mathcal{D}(q)$ in which the position operator makes sense,

$$\mathcal{D}(q)=\left\{f(q)\in\mathfrak{H}\,:\,qf(q)\in\mathfrak{H}\quad\iff\quad\int_{\mathbb{R}}dq\,|qf(q)|^2<\infty\right\},$$

where clearly $\mathcal{D}(q)\subset\mathfrak{H}$, since $f(q)$ is square integrable by definition. In the exactly same way, for the momentum we have

$$\mathcal{D}(p)=\left\{f(q)\in\mathfrak{H}\,:\,f'(q)\in\mathfrak{H}\quad\iff\quad\int_{\mathbb{R}}dq\,|f'(q)|^2<\infty\right\}.$$

As we can see, we cannot guarantee that a function will remain square integrable after the application of *any* combination of positions to it. This is in severe contrast to the finite dimensional case, since all matrices are bounded operators and we have no reason to even suspect that something might go wrong after applying them to our states. There is, however, a remarkable exception to this rule: Notice that

$$\begin{aligned}
\mathcal{D}(q\,p)&=\left\{f(q)\in\mathfrak{H}\,:\,qf'(q)\in\mathfrak{H}\quad\iff\quad\int_{\mathbb{R}}dq\,|qf'(q)|^2<\infty\right\}\\
\mathcal{D}(p\,q)&=\left\{f(q)\in\mathfrak{H}\,:\,[qf(q)]'\in\mathfrak{H}\quad\iff\quad\int_{\mathbb{R}}dq\,|qf'(q)+f(q)|^2<\infty\right\}\\
\implies\quad\bar{\mathcal{D}}(q\,p-p\,q)&=\left\{f(q)\in\mathfrak{H}\,:\,qf'(q)\in\mathfrak{H}\quad\iff\quad\int_{\mathbb{R}}dq\,|f(q)|^2<\infty\right\}\\
&\overset{!}{=}\mathfrak{H}\,,
\end{aligned}$$

where the bar represents the closure of a set. We then arrive at an incredible fact: The invariant subspace generated by the commutator of position and momentum is our initial $\mathfrak{H}$ – especially if one

considers that Lebesgue integration will naturally ignore the closure[4]. In the general case, however, we must define a space where it makes sense to talk about all possible applications of position and momentum, namely

$$\Phi = \bigcap_{\substack{m,n=0 \\ A,B=Q,P}} \mathcal{D}(A^n B^m)\,, \tag{C.9}$$

which is a small space when compared to $\mathfrak{H}$, known as the *maximal invariant subspace generated by* $\hat{q}$ *and* $\hat{p}$: Here, and only here, we can be sure $A\Phi \subset \Phi$, with $A = q, p$, such that all quantities like expectation values and standard deviations have a meaning. Notice that the elements of Φ are smooth and very well behaved when compared to the ones in $\mathfrak{H}$.

What happens to functions such as q, p or $\exp(-iqp/\hbar)$, which are clearly not in Φ nor in $\mathfrak{H}$? In order to keep using Dirac's bra-ket notation, we must provide them with a meaning. We then run into a technical problem of great importance: We can only guarantee $\mathfrak{H} \sim \mathfrak{H}^*$ if it is the projectivization of the whole $\mathfrak{L}_2$, otherwise we no longer have the safety net of Riesz representation theorem. As Φ is not a Hilbert space, its dual Φ' will no longer be isomorphic to it, so we can form the *Gel'fand triple* $(\Phi, \mathfrak{H}, \Phi')$, made of:

1. A dense subspace $\Phi \subset \mathfrak{H}$ where position and momentum operators have meaning;
2. The projectivization of the space of square integrable functions $\mathfrak{L}_2(\mathbb{R})$;
3. The dual Φ', whose elements act as linear functionals on Φ.

In physics, the dual Φ' is the vector space where general bras live, including the ones obtained from position and momentum eigenvectors – for which we haven't defined a set yet. Thus, let us define the associate triple $(\Phi, \mathfrak{H}, \Phi^\times)$, where $\Phi^\times$ is the space of anti-linear functionals over Φ: This is the space whose points are general kets, since they act as anti-linear functionals over Φ through the inner product of $\mathfrak{H}$. In the language of Schwartz distributions, Φ is the space of test functions and $\Phi^\times$ is the space of distributions [dlM01]. Then, every contraction of kets and bras involving position and momentum eigenvectors must be interpreted as the kernel of an integral operator, namely a weak derivative over Φ, and Dirac's notation makes complete sense: We can write $|q\rangle$ and still be able to sleep at night. It is enough to remember that general kets and bras are *not* directly linked to observables, but can still be contracted into kernels.

A note on the Segal-Bargmann representation

We now include some words on the Segal-Bargmann representation, where coherent states are used as a basis:

$$\psi(q) \longrightarrow \int dq\, \alpha(q)\psi(q)\,, \qquad \alpha(q) \propto \exp\left\{-\frac{[q-\Re(\alpha)]^2}{2} + \frac{i\Im(\alpha)}{\hbar}[q-\Re(\alpha)]\right\}.$$

Notice that, in the position representation, we impose the normalization condition

$$\langle\psi|\psi\rangle = 1 \quad \Longrightarrow \quad \int_{\mathbb{R}} dq\, |\psi(q)|^2 < \infty\,,$$

but if we choose to represent $|\psi\rangle$ using coherent states,

$$\begin{aligned} \langle\psi|\psi\rangle = 1 \quad \Longrightarrow \quad \int_{\mathbb{C}} d\alpha\, |\psi(\alpha)|^2 < \infty \quad &\Longleftrightarrow \quad \int_{\mathbb{R}} dq\, |\psi(q)|^2 |\alpha(q)|^2 < \infty \\ &\Longleftrightarrow \quad \int_{\mathbb{R}} dq\, |\psi(q)|^2 \exp\left\{-[q-\Re(\alpha)]^2\right\} < \infty\,. \end{aligned} \tag{C.10}$$

As can be seen above, the Segal-Bargmann representation induces an inner product that includes a gaussian smoothing on the probability amplitude $|\psi(q)|^2$, such that functions that didn't belong to $\mathfrak{H}$

[4] Or, in other words, $[\hat{q}, \hat{p}] = i\hbar\hat{I}$. Notice proportionality to $\hat{I}$ is only possible due to dimension being infinite.

generally belong to the *Bargmann space*, composed of the elements whose *Bargmann transform* fulfills (C.10). In particular, the gaussian smoothing of Wigner functions represented in Segal-Bargmann space is known as the *Husimi function* [dA98]. Notice that, since the gaussians converge faster than any polynomial diverges, the Bargmann space at least contains the maximal invariant space in (C.9) [Fol89]. It is also easy to establish a mapping between the Bargmann space and the *Fock-Bargmann space*, which arises by expanding states in terms of the eigenvectors of the simple harmonic oscillator [Fol89]. These Fock states $|n\rangle$ are a nice way to understand quantum mechanics from a mathematical point of view, since they form a countable orthonormal basis, which really belong in a Hilbert space setting.

Bibliography

[Bar95] R. G. Bartle. *The Elements of Integration and Lebesgue Measure*. Wiley-Interscience, 1st edition, 1995.

[BBJ03] C. M. Bender, D. C. Brody, and H. F. Jones. Must a hamiltonian be hermitian? *Am. J. Phys*, 71:1095, 2003.

[BPT15] G. Botelho, D. Pellegrino, and E. Teixeira. *Fundamentos de Análise Funcional*. SBM, 2nd edition, 2015.

[dA98] A. M. Ozorio de Almeida. The Weyl representation in classical and quantum mechanics. *Phys. Rep.*, 295:265, 1998.

[dlM01] R. de la Madrid. *The role of the rigged Hilbert space in Quantum Mechanics*. draft, 2001.

[Fol89] G. B. Folland. *Harmonic Analysis in Phase Space*. Princeton University Press, 1989.

[Hel08] G. Helmberg. *Introduction to Spectral Theory in Hilbert Space*. Dover, 2008.

[Mor16] V. Moretti. *Mathematical Foundations of Quantum Mechanics: An Advanced Short Course*. draft, 2016.

Appendix D

Stationary phase approximations

As stated several times in the main body of this dissertation, it doesn't take much for the action to become much larger than $\hbar$ – it is then not surprising that including first order corrections in $\hbar$ already allows for very good agreement with experimental data. As we always deal with highly oscillatory integrals, we are led to consider an expansion around the extrema of the action, *i.e.* its critical points x_0 where $S'(x_0) = 0$, since these define the regions where $S(x_0) \approx \hbar \approx 0$:

$$S(x) \approx S(x_0) + \left(\frac{1}{2}\right) S''(x_0)(x - x_0)^2 \,,$$

Since away from these regions the integrals tend to zero. Thus, integrals of the type

$$I = \int dx\, A(x) \exp\left[ikS(x)\right] \,, \qquad k = 1/\hbar \,,$$

can be approximated near a fixed point x_0 by

$$\begin{aligned} I(x_0) &\approx \int dx\, A(x) \exp\left\{ik\left[S(x_0) + \left(\frac{1}{2}\right) S''(x_0)(x - x_0)^2\right]\right\} \\ &= \exp\left[ikS(x_0)\right] \int dx A(x) \exp\left\{\left(\frac{ik}{2}\right) S''(x_0)(x - x_0)^2\right\} \,. \end{aligned}$$

The amplitude $A(x)$, however, does not depend on $\hbar$ or any other quantity as tiny as $\hbar$, so it is quite safe to assume the exponential above oscillates much more quickly than any oscillations performed by $A(x)$, and we can move it outside the integral[1] to obtain

$$I(x_0) = A(x_0) \exp\left[ikS(x_0)\right] \int dx\, \exp\left\{\left(\frac{ik}{2}\right) S''(x_0)(x - x_0)^2\right\} \,.$$

Assume now that the hessian $S''(x_0)$ does not vanish, *i.e.* that we stay away from caustics. Then the integral above is just a simple Fresnel integral [GS90], with

$$\int dx\, \exp\left\{\left(\frac{ik}{2}\right) S''(x_0)(x - x_0)^2\right\} = \left(\frac{2\pi}{s \det\left[S''(x_0)\right]}\right)^{\frac{n}{2}} \exp\left\{\frac{i\pi}{4} \text{sign}\left[S''(x_0)\right]\right\} \,.$$

Evidently, all critical points of S enter the integral and we have $i = \sum_{\text{all } x_0} I(x_0)$, so

$$I \approx \left(\frac{1}{2\pi\hbar}\right)^{-\frac{n}{2}} \sum_{\Sigma} \left|\det S''(x_0)\right|^{-\frac{n}{2}} A(x_0) \exp\left\{\frac{i}{\hbar}\left[S(x_0) + \frac{\pi}{4} \text{sign}\left(S''(x_0)\right)\right]\right\} \,,$$

where Σ is the critical set $\Sigma = \{x_0 \,:\, S'(x_0) = 0\}$. For a proof that its error is of $\mathcal{O}(\hbar^{\frac{n}{2}})$ see [GS90, GS12].

Bibliography

[GS90] V. Guillemin and S. Sternberg. *Geometric Asymptotics.* AMS, 1990.
[GS12] V. Guillemin and S. Sternberg. *Semi-classical analysis.* draft, 2012.

[1] This argument can be made rigorous by using the Riemann-Lebesgue lemma, which is actually overkill, since it concerns integrands that oscillate slower than this one.

Appendix E

Weyl-Wigner symbols for linear flows

We here provide the complete calculations of the Weyl-Wigner symbols for linear flows, *i.e.* we fill-in the steps leading from (5.4) to (5.5) and (5.6).

In Appendix B.2 we have shown that, for the linear flow

$$x' = \mathcal{M}_t x \quad \Longleftrightarrow \quad \begin{pmatrix} q' \\ p' \end{pmatrix} = \begin{pmatrix} A_t & B_t \\ C_t & D_t \end{pmatrix} \begin{pmatrix} q \\ p \end{pmatrix},$$

the position-position generating function assumes the form

$$S_t(q,q') = \frac{q\cdot\alpha_t q}{2} + \frac{q'\cdot\beta_t q'}{2} - \frac{q\cdot\gamma_t q'}{2} - \frac{q\cdot\gamma_t^T q'}{2}, \quad \text{where} \quad \alpha_t = B_t^{-1}A_t, \quad \beta_t = D_t B_t^{-1}, \quad \gamma_t = B_t^{-1}. \tag{E.1}$$

Substituting $S_t(q,q')$ in (5.4) and noticing that $\partial^2_{qq'}S_t = -\gamma_t$ and that $\det(-\gamma_t) = (-1)^n \det\gamma_t$,

$$\begin{aligned}
\tilde{U}_t(\xi) &= \left(\frac{1}{2\pi i\hbar}\right)^{\frac{n}{2}} \exp\left(\frac{i\xi_q\xi_p}{2\hbar}\right) \int dq\, \exp\left(\frac{iq\cdot\xi_p}{\hbar}\right) \mathcal{K}_t^{\mathrm{v}\mathrm{V}}(q, q-\xi_q) \\
&= \left(\frac{1}{2\pi i\hbar}\right)^{\frac{n}{2}} \exp\left(\frac{i\xi_q\xi_p}{2\hbar}\right) \sqrt{|(-1)^n \det\gamma_t|} \int dq \exp\left(\frac{iq\cdot\xi_p}{\hbar}\right) \\
&\qquad \times \exp\left[\frac{i}{\hbar}\begin{pmatrix} q \\ q-\xi_q \end{pmatrix} \cdot \begin{pmatrix} \alpha_t & -\gamma_t \\ -\gamma_t^T & \beta_t \end{pmatrix} \begin{pmatrix} q \\ q-\xi_q \end{pmatrix}\right] \\
&= \left|\frac{(-1)^n \det\gamma_t}{\det\left(\gamma_t + \gamma_t^T - \alpha_t - \beta_t\right)}\right|^{\frac{1}{2}} \exp\left\{\frac{i}{\hbar}\left[\frac{\xi_p + (\beta_t - \alpha_t)\xi_p\xi_q + (\gamma_t^2 - \alpha_t\beta_t)\xi_q}{2(\gamma_t + \gamma_t^T) - 2(\alpha_t + \beta_t)}\right]\right\}.
\end{aligned}$$

The amplitude above is recognizable from Lemma B.2.1, where we prove that

$$\frac{(-1)^n \det\gamma_t}{\det\left(\gamma_t + \gamma_t^T - \alpha_t - \beta_t\right)} = \frac{1}{\det\left(\mathcal{M}_t - I\right)};$$

also, by substituting the values for α, β and γ given in (E.1) in the phase,

$$\begin{aligned}
\frac{\xi_p + (\beta_t - \alpha_t)\xi_p\xi_q + (\gamma_t^2 - \alpha_t\beta_t)\xi_q}{2(\gamma_t + \gamma_t^T) - 2(\alpha + \beta)} &= \frac{C_t\xi_q^2 + (D_t - A_t)\xi_p\xi_q - B_t^2\xi_p^2}{A_t + D_t - 4} \\
&= \frac{1}{4}\begin{pmatrix} \xi_q \\ \xi_p \end{pmatrix} \cdot \left\{ J\left[\mathcal{M}_t - I\right]^{-1}\left[I + \mathcal{M}_t\right] \begin{pmatrix} \xi_q \\ \xi_p \end{pmatrix}\right\},
\end{aligned}$$

where we have used Lemma B.1.2 and the fact that, since $\mathcal{M}$ in symplectic, $\det\mathcal{M} = A_tD_t - B_tC_t = 1$. Upon the identification of the phase as the *Cayley parametrization* in (B.2), the final result for short times can thus be written as

$$\widetilde{U}_t(\xi) = \left|\det\left(\mathcal{M}_t - I\right)\right|^{-\frac{1}{2}} \exp\left\{\frac{i}{\hbar}\left[\widetilde{S}_t(\xi) + \frac{\hbar\pi\widetilde{\alpha}}{4}\right]\right\},$$

where we have included a signature in the phase that would have naturally arisen if we had started with $U_t(\eta)$ (see Section 3.2.3). To obtain the Wigner symbol we use the symplectic Fourier transform (4.9), and the result is now obtained in terms of the center generating function in (B.2):

$$\begin{aligned} U_t(\eta) &= \left(\frac{1}{2\pi\hbar}\right)^{\frac{n}{2}} \int d\xi \exp\left[\frac{i}{\hbar}\left(\xi\cdot\mathcal{J}\eta\right)\right] \widetilde{U}_t(\xi) \\ &= \left(\frac{1}{2\pi\hbar}\right)^{\frac{n}{2}} |\det\left(\mathcal{M}_t - I\right)|^{-\frac{1}{2}} \int d\xi \exp\left\{\frac{i}{\hbar}\left[\widetilde{S}_t(\xi) + \xi\cdot\mathcal{J}\eta\right]\right\} . \end{aligned}$$

Even though the integral above is gaussian due to $\widetilde{S}(\xi)$ being a quadratic form, it is enlightening to evaluate it using the stationary phase approximation, which is exact for the quadratic case but brings to surface important considerations regarding long times. The reason is that the SPA requires a sum over the fixed points of the phase, namely the trajectories fulfilling

$$\frac{\partial}{\partial\xi}\left(\widetilde{S}_t(\xi) + \xi\cdot\mathcal{J}\eta\right) \quad\Longrightarrow\quad \left.\frac{\partial\widetilde{S}_t(\xi)}{\partial\xi}\right|_{\xi=\xi^{(j)}} = -\mathcal{J}\eta \quad\Longleftrightarrow\quad \mathfrak{n}(\xi^{(j)}) = -2\widetilde{B}^{-1}\mathcal{J}\eta\,, \tag{E.2}$$

where $\mathfrak{n} \stackrel{\text{def}}{=} \partial_\xi \widetilde{S}(\xi)$, which in the quadratic case resumes to a single one due to the root-search equation being linear in ξ (see Lemma B.1.1). The signature of $\widetilde{S}_t(\xi)$ also pops up and we obtain

$$U_t(\eta) = \left(\frac{1}{2\pi\hbar}\right)^{\frac{n}{2}} |\det\left(\mathcal{M}_t - I\right)|^{-\frac{1}{2}} \left|\det\left(\frac{\partial^2\widetilde{S}_t(\xi)}{\partial\xi^2}\right)\right|^{-\frac{1}{2}} \exp\left\{\frac{i}{\hbar}\left[\widetilde{S}_t(\xi) + \xi\cdot\mathcal{J}\eta + \frac{i\pi\alpha}{4}\right]\right\} ,$$

where

$$\alpha = \operatorname{sign}\left\{\left(\frac{\partial^2\widetilde{S}_t(\xi)}{\partial\xi^2}\right)\right\} .$$

The amplitude can be explicitly written using (E.2) and (B.2):

$$\frac{\partial^2\widetilde{S}_t(\xi)}{\partial\xi^2} = \frac{\partial^2}{\partial\xi^2}\left[\frac{\xi\cdot\mathcal{B}_t\xi}{4}\right] = \frac{\mathcal{B}_t}{2} = \frac{\mathcal{J}}{2}\left(\mathcal{M}_t - I\right)^{-1}\left(\mathcal{M}_t + I\right) ,$$

which, since all matrices are even-dimensional, implies

$$\left|\det\left(\mathcal{M}_t - I\right)\det\left(\frac{\partial^2\widetilde{S}_t(\xi)}{\partial\xi^2}\right)\right|^{-\frac{1}{2}} = \left|\frac{\det\left(\mathcal{M}_t - I\right)\det\left(\mathcal{M}_t + I\right)}{2^{2n}\det\left[\left(\mathcal{M}_t - I\right)\right]}\right|^{-\frac{1}{2}} = 2^n\left|\det\left(I + \mathcal{M}_t\right)\right|^{-\frac{1}{2}} .$$

The final short-time propagation in the Wigner representation is, therefore,

$$U_t(\eta) = 2^n|\det\left(I + \mathcal{M}_t\right)|^{-\frac{1}{2}} \exp\left\{\frac{i}{\hbar}\left[S_t(\eta) + \frac{i\pi\alpha}{4}\right]\right\} .$$

Appendix F

Computational and numerical details

We here provide a brief account of the computational aspects in this dissertation. We have used three computer languages for calculations: Python, Julia and Mathematica. We will focus on Python, which is more well-known, although many numerical calculations were actually performed in Julia. We omit all considerations regarding Mathematica, which was only used for some algebraic manipulations and cross-checking.

Some facts about Python

Python is an interpreted language: A great effort is done by the Python community in making the interpreter smarter and faster, so that it can efficiently simplify the input code before it is effectively compiled, sometimes even ignoring chucks of useless code that might have slipped the programmer's hands. This results in almost all *built-in* functions being more efficient than raw code, together with a preference for some algorithms instead of others. For example, there is no distinction between input type for Python functions, such that a function defined to act on an integer can be applied with no modification to a list, a matrix, or any kind of tensor. This is usually stated as saying that functions in Python are actually *generalized functions*, rendering them extremely easy to use, but since the interpreter needs to compensate such arbitrariness by identifying and passing which kind of object the functions are actually acting on instead of the programmer, it can also be a slow process.

A similar situation is encountered when dealing with "for" loops, which in Python should almost never be explicitly written – instead, one uses the concept of *vectorization*, employing generalized functions to a list instead of an atomic function in a loop. While this may look be nice for those running simple codes, it is sometimes not a desirable characteristic at least because:

- Lists occupy memory: one can be absolutely sure a 1990s computer can run any "for" loop in *e.g.* C, although it might take forever; in Python, however, one can only immediately apply vectorization if the computer is able to create the tensor on which we intend to apply a generalized function. If this tensor is huge, the computer will crash due to memory overflow;
- Generalized functions are slow: Compensating the programmer's incompetence with a very smart interpreter can be a great advantage in many situations, but not all of them – sometimes it is just better to train the user.

Several Python packages, such as *Numba*, were developed in order to correct problems such as the ones listed above, and in the hands of an experienced Python programmer numerical programming (done with the package *Numpy*) can be quite efficient. The same programmer, however, would achieve faster results in almost any compiled language, but for these languages code development is just too slow. The advantage of the Python language is really its simplicity, but when one finds an efficient algorithm and is interested in speed, it usually needs to be translated to Fortran or C – which is not so easy since Python uses built-in functions so much. This need of using one language for code development and another one for efficiency is the famous *two language problem* of scientific programming.

Python is also very nice for scientific purposes due to being *dynamically typed*, such that we can actually write theory in LaTeX and perform calculations simultaneously in a same environment (such as in a *Jupyter Notebook*). The defined variables are stored and can be used in further calculations, and cells can be compiled one at a time. A multi-paradigmatic language, Python also allows for both procedural and object-oriented programming, accommodating both sets of programmers instead of adding to the controversy over which paradigm is best.

Some facts about Julia

Julia is a compiled language, but it is rather different from C, Fortran, and most older languages. For instance, just as Python, Julia is *garbage-collected*, meaning that the compiler automatically looks for unused memory sections and reuses them in further calculations. This is in strong contrast with the compiler in C, which is "stupid", *i.e.* the programmers themselves need to think about each memory allocation and address. Garbage-collection consumes time and can be less efficient than a well-devised manipulation of pointers and memory in a low level language such as C – the problem is that training someone to learn how to efficiently manipulate memory in C can take a lifetime, and the excess of pointers and pointers to pointers and pointers to pointers to pointers can render C code unintelligible. It is somewhat commonplace between programmers that garbage-collection is a good idea.

Unlike Python, however, functions in Julia are not generalized, although one can modify them to be. Such a modification renders them pretty much as slow as in Python and is usually avoided. Instead, the Julia compiler uses the concept of *multiple dispatch*, meaning that it actually builds different functions to deal with different data structures – the programmer can also help by providing as much information about the input/output as possible. Although this might look stupid, it is similar to what the interpreter in Python is doing behind the stage, but Python creates general methods and multiple dispatch is much more efficient by being run-time based. Also, Julia *loves* "for" loops: Stacked "for"s are a reality in Julia just as they are in C, and might be hard to get used to in the beginning[1]. Again, stacked "for"s might look stupid, but are once more what the Python interpreter is effectively doing when we use vectorization – except that it is also allocating a lot of memory, while loops allocate almost nothing.

In even starker contrast with other compiled languages, Julia can also by dynamically typed. The *Jupyter* environment mentioned earlier can be modified to run on a Julia kernel, so that it can be used just as Python for scientific projects. The ubiquitous MatPlotLib package for scientific plotting, well-known to Python users, has also been translated to Julia, so people migrating from Python should already feel at home with respect to data visualization.

The Julia language was developed with scientific computing in mind. It can be as fast as C, but it is also almost as high-level as Python, so code development is easy. One can say that Julia allows for the programmer to use all his/her knowledge and that knowledge pays off, but if the programmer is lazy the compiler will do its best to compensate for his/her ignorance (which is Python's leitmotif). As of today, and at least for scientific computing, it can be said that the Julia language is the closest we have ever gotten to solving the two language problem.

F.1 Numerical discretization

There are no continuous objects in numerical analysis. Everything is effectively discrete:

- continuous functions are functions for which the spacing between points in the image is small when compared to some parameter of interest,
- derivatives are finite differences,
- integrals are sums,

[1] Especially because the Julia indexing, just as Matlab's, moves faster on the left, while in C and Python the fastest index is always on the right.

etc. This can be resumed as: Objects in calculus that are obtained as limits of something going to zero are really calculated as this something not approaching zero, but a small value instead. The grids we use for calculations are, thus, tensors whose dimension depends on what we are calculating. There is a huge difference, however, between how we deal with grids in Python and Julia.

Grid manipulation

Grids in Python are simple. Importing numpy as `np`, we can form grids as[2]

```
np.arange(-3,4,1)                              # this is 1D grid
>> array([-3,-2,-1,0, 1, 2, 3])

np.mgrid[-3:4:1, -10:11:dx]                    # this is a 2D grid
>> array([[[-3, -3, -3, -3, -3, -3, -3],
[-2, -2, -2, -2, -2, -2, -2],
[-1, -1, -1, -1, -1, -1, -1],
[ 0,  0,  0,  0,  0,  0,  0],
[ 1,  1,  1,  1,  1,  1,  1],
[ 2,  2,  2,  2,  2,  2,  2],
[ 3,  3,  3,  3,  3,  3,  3]],

[[-3, -2, -1,  0,  1,  2,  3],
[-3, -2, -1,  0,  1,  2,  3],
[-3, -2, -1,  0,  1,  2,  3],
[-3, -2, -1,  0,  1,  2,  3],
[-3, -2, -1,  0,  1,  2,  3],
[-3, -2, -1,  0,  1,  2,  3],
[-3, -2, -1,  0,  1,  2,  3]]])
```

The first grid is the set $(-3, 3)$, with spacing between elements given by 1; the second grid is composed of two 7×7 matrices, each representing an axis, which include all possible (x, y) tuples that form a 2-dimensional grid, so we can identify the first with y components and the second with x components.

When we talk about propagating and applying functions to grids in Python, these are the types of grids we are using as input. In Python, defining and applying a function to a grid is done, for instance, as

```
grid=np.mgrid[-1:2:1, -1:2:1]              # defines the input
def f(x):                                  # defines a function
   return np.cos(x)

f(grid)                                    # applies function to input
>> [[[0.54030231 0.54030231 0.54030231]
[1.         1.         1.        ]
[0.54030231 0.54030231 0.54030231]]

[[0.54030231 1.         0.54030231]
[0.54030231 1.         0.54030231]
[0.54030231 1.         0.54030231]]]
```

The classical flow for the Kerr system, presented in Chapter 6, is nothing but a function as the above, since the equations of motion are exact.

[2]Notice that Python "eats" the last element. The notation >> symbolizes output.

Numerical integration

Wigner functions, classical actions and Fourier transforms are all integrals. To perform them numerically, we simply discretize them as Riemann sums. Nowhere in this dissertation a more elaborate integration algorithm was used. As an example, take the numerical classical actions of (6.12). These are evaluated simply by

```
def numerical_actions(path):
   p , q = path[0], path[1]
   xi_p, xi_q = p - p[0], q - q[0]                    # chords
   A = 4*q*(q**2+p**2)                                # derivative of H wrt q
   B = 4*p*(q**2+p**2)                                # derivative of H wrt p
   return (1/2)*np.sum(xi_q*A + xi_p*B, axis=0)*T
```

where the input `path` is just the orbit we wish to evaluate the action for. This orbit was already calculated using, for instance, the SSIs for Subsection F.2.

F.2 Classical dynamics

For computing the classical dynamics of maps and coherent states, we simply define functions over the grids of Section F.1. The exact evolution for the Kerr system, for instance, is given by

```
def init(t, p, q):
   phasespaceradius2 = p**2+q**2
   angle = 4*phasespaceradius2*t
   cosine = np.cos(angle)
   sine = np.sin(angle)
   pi = p*cosine+q*sine
   qi = -p*sine+q*cosine
   return pi, qi
```

where the equations need to be time-reversed because classical probability distributions evolve backwards (see *e.g.* (4.22)). Using this exact evolution, Fig. 6.1 can be reproduced using

```
def coherent_evolution(x, kick, alpha, T):
   P, Q = init(t, p, q)
   return (1/(np.pi))*np.exp(-(Q - alpha.real)**2 - (P - alpha.imag)**2)
```

easily recognizable as an implementation of (4.22). The classical evolution of maps is equally obvious, employing SSIs instead of `init`, and is described in the following.

Splitting symplectic integrators

The implementation of SSIs is trivial. For instance, (2.4) can be easily implemented as

```
def SSI(V_pr, x, kick, T):                                          1.
   path = np.zeros(shape = np.hstack((kick+1, np.asarray(x).shape)))  2.
   P, Q = path[:,0], path[:,1]                                      3.
   P[0], Q[0] = x                                                   4.

   for n in range(1,kick+1):                                        5.
       X0, Y0 = Q[n-1], P[n-1]                                      6.
       X1 = X0 + T*Y0                                               7.
       Y1 = Y0 - T*V_pr(X1)                                         7.
       Q[n], P[n] = X1, Y1                                          8.

   return path                                                      9.
```

where[3]

1. Calls the SSI, whose input is given by the derivative of the potential energy `V_pr` (we assume $F(p) = p^2/2$), the initial grid to be propagated `x`, the number of iterations `kicks` and the kicking strength `T`;
2. Builds a tensor of zeros, to be later filed with the orbit of `x`;
3. Defines the momentum and position components of the orbit above;
4. Sets the initial grid to be propagated as `x`;
5. Iterates over kicks;
6. Each element for a present kick `n` equals the element for kick `n-1`;
7. Direct implementation of (2.4);
8. Defines the element at kick `n`.
9. Returns result.

The iteration of any initial grid using the SSI above results in figures like Fig. 7.1. Tao's algorithm for integrating non-separable hamiltonians is a combination of several SSIs as the one above, except that grids are now 4-dimensional and occupy too much space to be reproduced here, but after the example above is understood the implementation of Tao's algorithm is straightforward.

F.3 Quantum dynamics

Quantum propagation is slightly more complicated than its classical counterpart in the earlier section, although in the end it is nothing but the direct implementation of the formulas developed in the main body of this dissertation.

The Kerr system

The quantum propagation of a coherent state under the Kerr hamiltonian was presented in Section 7.2, its final result being (6.4). In Python, we use object-orientation and implement evolution as a class. The class initializes with

```
def __init__(self, p, q, alpha, x0, npts):
```

where `p` and `q` are not momentum and position, but the a and b mutually prime integers that multiply the revival time in Definition 6.2.1. The class also takes the center of the initial coherent state as input, namely `alpha`, the number of points in the grid `npts` and `x0` to define its boundaries, given by `-x0` and `x0`. We now proceed and enumerate each of its components.

Naturally, we need a coherent state, given by

```
def gaussian(self, x, ar):
   return np.pi**(-.25)*np.exp(-0.5*(x - np.sqrt(2)*ar.real)**2
   + 1j*ar.imag*(np.sqrt(2)*x - ar.real))
```

The c_0 and c_k in (6.5) and (6.6) are implemented as

```
def get_c0(self):
   nvals  = np.arange(self.q)
   phases = np.exp(-2j*np.pi*self.p*nvals**2/self.q)
   return np.sum(phases)/self.q
```

[3]We remind the reader that in Python all variables can be grids.

```
def generate_ck(self):
   self.coeffs = np.ndarray(shape=(self.q,), dtype=np.complex128)
   k = 0
   self.coeffs[0] = self.get_c0()
   for _ in range(self.q-1):
   knew = (k+2*self.p) % self.q
   self.coeffs[knew] = self.coeffs[k]*np.exp(2j*np.pi*(k+self.p)/self.q)
   k = knew
```

culminating in

```
def generate_alphas(self):
   self.alphas = self.alpha*np.exp(-2j*np.pi*np.arange(self.p, self.p+self.q)/self.q)
```

which builds the big coherent states in (6.4). After generating the Fourier coefficients, the wavefunction is trivial:

```
def wavefunction(self, x):
   self.generate_ck()
   self.generate_alphas()
   self.coeffs = self.coeffs[:, np.newaxis]
   self.alphas = self.alphas[:, np.newaxis]
   psi = np.sum(self.coeffs*self.gaussian(x, self.alphas), axis=0)
   return psi*np.exp(-0.5j*np.pi*self.p/self.q)
```

and the only thing missing is the Wigner transform, which will be described in Section F.3.

The coserf system

The quantum coserf system is considerably simpler than the Kerr system. Although implementing it is as a class using object-orientation in Python, the calculations essentially resume to the recursive loop

```
for n in range(1,self.kick+1):
   A = np.sqrt(1/(2*self.T*pi))*np.exp(-1j*self.V(q)*self.T)*exp(-1j*pi/4)
   B = np.exp(1j*(q-q[:,np.newaxis])**2/(2*self.T))*psi_prime[n-1]
   psi_prime[n] = A*np.sum(B,axis=1)*self.dx
```

which is the exact Pythonic equivalent of (7.4) substituted in (7.5), `psi_prime[0]` representing the initial coherent state.

Wigner transforms of wavefunctions

The Wigner transform of (4.12) has been implemented using several tricks throughout the years, many of them based on identifications with the Fast Fourier Transform (FFT) as long as one sets grid spacing to be equal to

```
dx = np.sqrt(np.pi/(2*npts))
```

otherwise such identification is not possible. The advantage of using FFTs is that, as the name says, they are fast: A culmination of several symmetry-searching algorithms, the FFTs in Python are especially fast – even if compared with compiled languages. The problem is that, by fixing the grid spacing, the endpoints of the grid must remain free in order to render the algorithm really efficient, which can lead to huge grids being generated even though we are interested in a Wigner function that occupies a tiny phase-space portion. This can be resumed as: The FFT does not allow us to focus on the Wigner function, but does allow us to use monstrous grid sizes.

We have used all sorts of Wigner-transform algorithms in this dissertation, including FFTs, tricks with `np.lib.stride_tricks.as_strided` and simple direct implementation. We will not go into the

details of the first two methods mentioned, because their advantage over direct implementation is efficiency only: What takes 15min to calculate by direct implementation can take 12ms using `strides` or `np.fft.fft`. For the direct Wigner function, the transform is given simply by

```
def wigner(self):
       gamma = np.arange(-self.x0, self.x0 + self.dx/2, self.dx)[:, np.newaxis]# (1.)
       grid_p = np.arange(-self.x0, self.x0 + self.dx/2,
             self.dx)[:, np.newaxis, np.newaxis]                               # (2.)
       R = np.conjugate(self.wavefunction(self.grid_q - gamma/2))              # (3.)
       L = self.wavefunction(self.grid_q + gamma/2)                            # (4.)
       W = (self.dx/np.pi)*np.sum(R*L*np.exp(-1j*gamma*grid_p),axis=1)         # (5.)
       return W.real
```

The marked lines have the following function in implementing (4.12)):

1. Defines the γ grid;
2. Defines the p grid;
3. Calculates the wavefunction displaced by $-\gamma/2$ and takes conjugate;
4. Calculates the wavefunction displaced by $+\gamma/2$;
5. Integrate with respect to the p grid (`axis=1`) using Riemann sum.

F.4 Semiclassical dynamics

The calculations in semiclassical dynamics are much more intricate than the ones in the classical and quantum sections of this appendix. We will not explicitly include them here, but rather describe what is done using some code snippets when necessary.

The Kerr system

The FVR for Kerr evolution starts with a chord grid, from which we extract the initial phase-space points that we employ for backward-propagation. The Wigner function is calculated as a sum of slices, meaning that the complete $W(q,p)$ is obtained as a union of $W(q,p_1) \cup W(q,p_2) \cup W(q,p_3)$..., each slice as the ones displayed in Fig. 6.10.

Defining variables

We first show in detail how to form all variables defined in the enumeration of Subsection 5.2.3. Naturally, everything in this section happens inside a class with

```
def __init__(self, alpha, t, evaluation_grid, integration_grid):

   self.alpha = alpha                                  # center of initial state
   self.t = t                                          # evaluation time

   self.a_i, self.b_i, self.npts_i = evaluation_grid  # evaluation grid limits
   self.dx_i = abs(self.a_i-self.b_i)/self.npts_i     # evaluation grid spacing
   self.l = self.npts_i                                # evaluation grid size

   self.a_g, self.b_g, self.npts_g = integration_grid # integration grid
   self.dx_g = abs(self.a_g-self.b_g)/self.npts_g     # is made of chords!
   self.Xi_p, self.Xi_q = np.mgrid[self.a_g:self.b_g
      +self.dx_g:self.dx_g,self.a_g:self.b_g
         +self.dx_g:self.dx_g]                         # this is a chord grid!
```

Then, the variables used by the semiclassical Wigner function, following strictly the instructions of Subsection 5.2.3, are defined as

```
for n in range(self.l):
   eta_p, eta_q = p0, n*self.dx_i+self.a_i                  # final center grid

   Xp_p, Xq_p = eta_p + self.Xi_p/2, eta_q + self.Xi_q/2    # final x+ grid
   Xp_m, Xq_m = eta_p - self.Xi_p/2, eta_q - self.Xi_q/2    # final x- grid

   xp_p, xq_p = self.init(self.t, Xp_p, Xq_p)               # initial x+ grid
   xp_m, xq_m = self.init(self.t, Xp_m, Xq_m)               # initial x- grid
```

All functions required by the FVR and described in Section 5.3 are easily implemented in terms of the variables above.

The Conley-Zehnder indexes

Obtaining the Conley-Zehnder indexes for the Kerr system is done by solving (6.8). Since the left hand side of this equation is periodic and we don't really need to find the zeros, only how many of them were crossed during time-evolution, the strategy chosen was to use the trace's period. Start by equating the left hand side of (6.8) to zero, writing this in the simplified form

$$A\cos(\Omega t) + B\sin(\Omega t) = 0 \quad \Longrightarrow \quad \phi \overset{\text{def}}{=} \frac{1}{2\pi}\left[\Omega t - \arctan\left(\frac{A}{B}\right)\right],$$

where ϕ is rounded in order to be an integer. In practice, `np.floor`(ϕ) represents the number of periods realized by the left hand side of (6.8). Then, start with $\widetilde{\sigma} = 2\phi$, since each period has two zeros, and map the intermediate zero through

$$\begin{cases} A\cos(\Omega t) + B\sin(\Omega t) <= -2 & , \quad \widetilde{\sigma} = \widetilde{\sigma} + 1 \\ \phi < \texttt{np.floor}(\phi) \text{and} A\cos(\Omega t) + B\sin(\Omega t) \text{and} > -2 & , \quad \widetilde{\sigma} = \widetilde{\sigma} + 2 \end{cases},$$

where the first case represents us falling in the middle of a period of $A\cos(\Omega t) + B\sin(\Omega t)$, so that the index increases by 1, while in the second we have passed a full period and the index increases by 2. This is implemented in Python as

```
def cz_index(self, t, P, Q, p, q): #
   A = 2*(1+32*t**2*(P*q-p*Q)**2)
   B = 8*t*(P**2+Q**2-p**2-q**2+8*t*(P*q-p*Q)*(P*p+q*Q))
   omega = 4*(q**2+p**2-Q**2-P**2)

   trM = A*np.cos(omega*t)+B*np.sin(omega*t)
   phi = abs(omega*t-np.arctan2(B, A))/(2*np.pi)

   pre_maslov = 2*np.floor(phi)
   mid_maslov = np.where(trM <= -2, pre_maslov+1, pre_maslov)
   end_maslov = np.where((phi < np.round(phi))&(trM > -2), mid_maslov+2, mid_maslov)

   return end_maslov
```

where we later use the signs of the actions to decide whether of not the Conley-Zehnder indexes are positive or negative.

The coserf system

The coserf system used the Herman-Kluk propagator and was implemented almost entirely in Julia. From what was presented up to now, it is quite clear that implementing the HK propagator is trivial: Everything we need to do is to use a discretized lagrangian in the action and a procedure to calculate the Maslov indexes. Since the coserf system is composed of a discrete map, all that needs to be done is to directly implement the conditions (6.13).

Effective dynamics

The procedure required for effective trajectories is exactly the same as for discrete or continuous ones, except that we now use Tao's algorithm to calculate the flow.

F.5 Settings for all figures

All figures were calculated using a personal computer with 8gb of RAM and i7-7500U processor running the Linux OS (Mint 18.3). We did not use any optimization procedure, such as selecting only a particular set of chords or trajectories. Everything was obtained by direct implementation. We now present all grid sizes and computation times required for each of them individually.

The Kerr system

For the Kerr system, the evaluation and integration grids are different: We evaluate at the points we want to see, and integrate over larger grids to attain better results. Integration grids are all $(-10, 10)$. The autocorrelation could have also been extracted directly without the need to calculate hundreds of Wigner functions, but since the cluster was at our disposal, we used it.

Figure	grid size	elapsed time	comments
6.1	2000 x 2000	1min each	
6.2	401 by 401	2s each	b taken as 15711
6.3	1000 x 1000 (class) + 401 x 401 (quan)	sum of times	around 8 min
6.5	1001 x 1001 (eval) 2001 x 2001 (integ)	26h	
6.6	doesn't apply	doesn't apply	extracted from 6.5
6.7	1001 x 1001 (eval) 2001 x 2001 (integ)	?	ran on cluster at U. Augsburg
6.8	1001 x 1001 (eval) 2001 x 2001 (integ)	26h	
6.9	101 x 101 (eval=integ)	1min/16min	exact/numerical
6.10	101 x 101 (eval=integ)	1min/16min	exact/numerical
6.11	101 x 101	0.3s	compare with 6.5

The coserf system

Autocorrelations were also obtained from wavefunctions. Integration and evaluation grids are the same, equal to $(-4\pi, 4\pi)$. We represent "chaotic" by *ch* and "effective" by *eff*.

Figure	grid size	elapsed time	comments
7.1	doesn't apply	μs	computationally trivial
7.2	2000 x 2000	3min each	
7.3	2^{12}	ms/4min	wavefunctions/Wigner transf.
7.4	doesn't apply	doesn't apply	calculated from the above
7.5	250 x 250	sum of times	several days
7.6	501 x 501	8h	
7.7	doesn't apply	doesn't apply	extracted from 7.6
7.8	250 x 250 (semiclass)	sum of times	several days
7.9	doesn't apply	μs	
7.10	2000 x 2000 (ch) 501 x 501 (eff)	2min (ch) 17min (eff)	
7.11	501 x 501	6h/8h	chaotic/effective

The times in 7.11 might look surprising, since the effective flow needs thousands iterations and the exact chaotic flow, only a few. However, the chaotic flow was implemented in Python and the effective in Julia – here resides the difference.